



# **Optimal design of a CO<sub>2</sub> capture unit with assessment of solvent degradation**

*Grégoire Léonard*

*Mai 2013*



Thèse présentée en vue de l'obtention du grade de  
Docteur en Sciences de l'Ingénieur



## Summary

In response to increasing environmental concerns and globally growing energy demand, CO<sub>2</sub> capture, re-use and storage technologies have been proposed to reduce the emissions of carbon dioxide resulting from fossil fuel combustion. In the present thesis, the post-combustion CO<sub>2</sub> capture with amine solvents is studied for the case of fossil fuel-fired power plants. This technology treats the flue gas after the combustion so that operating power plants can be retrofitted to rapidly reduce their CO<sub>2</sub> emissions. However, different drawbacks still limit the development of this technology. At the operational level, the two main drawbacks are the high energy requirement for desorbing CO<sub>2</sub> (leading to a decrease by about 30% of the power plant efficiency) and the environmental impact related to the emissions of amine solvent and its degradation products to the atmosphere. The main originality of the present work is to simultaneously consider both aspects within a global model of the CO<sub>2</sub> capture process assessing solvent degradation. The purpose of this model is to gain a better understanding of the influence of process operating conditions on solvent degradation. Consequently, solvent degradation may be considered more accurately during the design of CO<sub>2</sub> capture units, which is particularly relevant for the large-scale deployment of the CO<sub>2</sub> capture technology.

The study has been performed in two phases. In the first phase, experimental data about oxidative and thermal degradation of the solvent have been obtained by using newly-developed test benches. The influence of process operating parameters on solvent degradation and on the formation of degradation products has been quantified by appropriate analytical techniques. It results from this study that the main solvent degradation mechanism is the oxidative degradation. This is the case in laboratory conditions as well as in industrial CO<sub>2</sub> capture pilots for which degraded solvent samples could be obtained thanks to the collaboration with our industrial partner Laborelec. Lab experiments show that this type of degradation is enhanced when whether the O<sub>2</sub> concentration in the flue gas, the gas-liquid contact or the temperature are increased. Moreover, it appears that the presence of dissolved metals in the solvent catalyzes the oxidative degradation. On the contrary, the presence of CO<sub>2</sub> reduces the rate of oxidative degradation. Adding degradation inhibitors also reduces the oxidative degradation, more or less successfully depending on the tested inhibitor. Regarding thermal degradation, significant degradation is only observed in the presence of CO<sub>2</sub> and at a high temperature (140°C). Moreover, thermal degradation is not influenced by the presence of dissolved metals, but some degradation inhibitors have a negative influence on the solvent thermal stability.

The second phase has consisted in developing a model of the CO<sub>2</sub> capture process using the Aspen Plus software package. This kind of model allows the evaluation of the process energy requirement. The main innovation of this thesis was to propose a kinetics model for the oxidative and the thermal degradations based on the results of the experimental study, and to include it into a global process model. This last model has led to the identification of oxidative degradation in the absorber as the major cause of solvent loss in the process, which is in agreement with results reported in CO<sub>2</sub> capture pilot plants. The emission of ammonia (main oxidative degradation product of the amine solvent) has also been confirmed to be one of the main environmental issues of the CO<sub>2</sub> capture process. Furthermore, this model is used to evaluate the influence of operating conditions both on the process energy requirement and on its environmental impact. The largest energy savings are observed when increasing the stripper pressure and the solvent concentration, while the most significant increases of the solvent consumption are due to the increased oxygen concentration in the flue gas and to the

higher solvent concentration. Two process improvements have also been tested (absorber intercooling and lean vapor compression), leading to a significant decrease of the total process energy requirement with low influence on solvent degradation. Thanks to this global process model, optimum operating conditions have been proposed for CO<sub>2</sub> capture, reducing the process energy requirement by 12% at equivalent solvent consumption rate.

However, the solvent consumption rate is under-predicted by the model in comparison to pilot plant studies. Thus, different perspectives are proposed to improve the model, among others by considering the effect of dissolved metals and flue gas contaminants like SO<sub>x</sub> and NO<sub>x</sub> in the degradation kinetics.

Finally, this kind of model represents an important step for the consideration of solvent degradation during the design of CO<sub>2</sub> capture plants. It could and should be used for the development of CO<sub>2</sub> capture units to consider not only the process energy penalty, but also its environmental penalty which is particularly relevant for large-scale applications. Moreover, this methodology has been developed for an aqueous solution of monoethanolamine (MEA), the benchmark solvent for CO<sub>2</sub> capture. In future developments, it may be applied to alternative promising solvents to further improve the CO<sub>2</sub> capture process.

## Résumé

En réponse à la prise de conscience des problématiques environnementales et à la demande croissante en énergie, les techniques de capture, utilisation et stockage du CO<sub>2</sub> ont été proposées pour réduire les émissions de CO<sub>2</sub> résultant de la combustion de ressources fossiles. Dans cette thèse, la capture post-combustion du CO<sub>2</sub> au moyen de solvants aminés a été étudiée pour le cas des centrales électriques au charbon et au gaz naturel. Cette technologie traite les gaz de combustion, permettant ainsi d'équiper des centrales existantes afin de rapidement diminuer leurs émissions de CO<sub>2</sub>. Cependant, différents freins limitent encore le développement de cette technique. Au niveau opératoire, les deux principaux désavantages sont un besoin énergétique élevé pour la désorption du CO<sub>2</sub> (entraînant une diminution de près de 30% du rendement de la centrale) et un impact environnemental lié aux émissions du solvant aminé et de ses produits de dégradation dans l'atmosphère. La principale originalité de ce travail est de considérer simultanément ces deux aspects au sein d'un modèle global du procédé de capture du CO<sub>2</sub> incluant la dégradation des solvants. L'utilité de ce modèle est d'apporter une meilleure compréhension de l'influence des conditions opératoires du procédé sur la dégradation du solvant. Ainsi, celle-ci pourrait mieux être prise en compte lors du design d'unités de capture du CO<sub>2</sub>, ce qui est particulièrement pertinent pour le déploiement à grande échelle de la technologie de capture du CO<sub>2</sub>.

Cette étude a été menée en deux étapes. Dans la première étape, des données expérimentales sur la dégradation oxydative et thermique des solvants ont été obtenues sur des bancs d'essais développés dans le cadre de cette thèse. L'influence des paramètres opératoires sur la dégradation des solvants et sur la formation de produits de dégradation a été quantifiée par des techniques analytiques appropriées. Il ressort de cette étude que le principal mécanisme de dégradation des solvants est la dégradation oxydative, que ce soit dans les conditions du laboratoire ou dans des pilotes industriels de capture du CO<sub>2</sub> pour lesquels des échantillons de solvant dégradés ont pu être obtenus grâce à la collaboration avec Laborelec, partenaire industriel de cette thèse. Les tests en laboratoire montrent que ce type de dégradation est accéléré lorsque la teneur en O<sub>2</sub> des gaz de combustion, le contact gaz-liquide ou la température sont augmentés. De plus, il apparaît que la présence de métaux dissous dans le solvant catalyse la dégradation oxydative. Au contraire, la présence de CO<sub>2</sub> diminue le taux de dégradation oxydative. L'ajout d'inhibiteurs de dégradation oxydative diminue également ce type de dégradation avec plus ou moins de succès selon l'inhibiteur testé. En ce qui concerne la dégradation thermique, elle n'intervient de façon significative qu'en présence de CO<sub>2</sub> et à haute température (140°C). De plus, la dégradation thermique n'est pas influencée par la présence de métaux, mais certains inhibiteurs de dégradation oxydative ont une influence négative sur la stabilité thermique du solvant.

La seconde étape a consisté à développer un modèle du procédé de capture du CO<sub>2</sub> au moyen du logiciel de simulation Aspen Plus. Ce type de modèle permet d'évaluer le besoin énergétique du procédé. La principale innovation de cette thèse a été de proposer une cinétique de dégradation oxydative et thermique du solvant sur base des résultats de l'étude expérimentale, et d'inclure cette cinétique dans le modèle du procédé. La dégradation oxydative du solvant se produisant dans l'absorbeur a été identifiée comme la principale contribution à la consommation de solvant, confirmant les résultats observés dans des installations pilotes de capture du CO<sub>2</sub>. Il est également montré que l'émission d'ammoniac (principal produit de la dégradation oxydative du solvant aminé) constitue un des plus grands défis environnementaux du procédé de capture. De plus, le modèle résultant a permis d'évaluer l'influence des conditions opératoires à la fois sur le besoin énergétique du procédé

et sur son impact environnemental. Les réductions les plus importantes des besoins énergétiques du procédé ont été obtenues en augmentant la pression de régénération et la concentration du solvant. Les augmentations les plus prononcées de la consommation de solvant sont dues à l'augmentation de la concentration en oxygène dans les gaz de fumée et à l'augmentation de la concentration de solvant. Deux modifications de procédé ont également été étudiées (refroidissement intermédiaire dans l'absorbeur et compression de vapeur pauvre), réduisant significativement le besoin énergétique du procédé tout en montrant peu d'influence sur la consommation de solvant. Grâce à ce modèle, des conditions opératoires optimales ont été proposées, permettant de réduire le besoin énergétique du procédé de 12% à consommation de solvant égale.

Cependant, le modèle sous-estime la consommation de solvant observée dans les installations pilotes. En conséquence, différentes pistes d'amélioration sont proposées, considérant notamment l'effet des métaux dissous et des impuretés présentes dans les gaz de combustion ( $\text{NO}_x$  et  $\text{SO}_x$ ) dans le modèle.

Enfin, ce type de modèle représente un pas important vers la prise en compte de la dégradation des solvants lors du dimensionnement d'unités de capture du  $\text{CO}_2$ . Ce type de modèle pourrait et devrait être utilisé lors du développement d'installations de capture du  $\text{CO}_2$  en vue de considérer non seulement l'impact énergétique de l'installation sur la centrale, mais également son impact environnemental qui s'avère particulièrement important dans le cas d'applications à grande échelle. De plus, cette méthodologie développée pour une solution aqueuse de monoéthanolamine (MEA, le solvant de référence pour la capture de  $\text{CO}_2$ ) pourrait également être appliquée à d'autres solvants prometteurs afin d'encore améliorer la technologie de capture post-combustion du  $\text{CO}_2$ .

## Acknowledgements

First of all, I would like to sincerely thank Professor Georges Heyen for giving me the opportunity to learn and to evolve as a member of the Laboratory for Analysis and Synthesis of Chemical Systems. His advices have always been judicious and he was always available to answer my questions, and I am very grateful for that.

I also thank Professor Dominique Toye for welcoming me in her team at the experimental hall for applied chemistry. I am also very grateful for the constructive discussions that have guided the realization of this work and improved its quality.

I also want to thank the other members of the thesis committee for their interest and participation to the evaluation of this work: Professor Diane Thomas from the University of Mons, Mrs Marie-Laure Thielens from Laborelec and Doctor Ludovic Raynal from the IFP Energies Nouvelles, as well as Professor Pierre Dewallef, Professor Angélique Léonard and Professor Michel Crine from the University of Liège.

I am very grateful to the Belgian FRIA-FNRS for the financial support of this PhD Thesis during four years, giving me the opportunity to develop the present research project.

I also address a special thanks to the company Laborelec who partially funded this work and provided technical support. I especially thank you Hélène Lepaumier, for the relevant advices and the enthusiastic discussions about solvent degradation, Frédéric Mercier, Han Huynh, Fabrice Blandina, and Philippe Demlenne for the nice collaboration and the enriching exchanges.

Then, I also sincerely thank Ms Ségolène Belletante, student at the INP Ensiacet Toulouse, Ms Marion Bascougnano, formerly student at the IUT Paul Cézanne Aix- Marseille, and Mr Bruno Cabeza Mogador, formerly student at the University of Liège, for their participation to this PhD thesis. Without their support, it would have been impossible to obtain all the experimental and modeling results presented in this work. Their support and their motivation in this research project have been considerably appreciated.

I also thank the PhD students met during the time of this work and that have contributed to its achievement. I especially thank Lionel Dubois from the University of Mons for the enthusiastic collaboration and the constant availability, as well as Alexander Voice from the University of Texas at Austin, for the enriching discussions and the sending of inhibited amine solvents that have been tested in this work.

Many thanks are addressed to the people of the Chemical Engineering Department that have contributed to make this work possible by their helpful technical advices, and to the whole department staff for the nice working atmosphere during this research project.

Finally, my last thanks go to my family, to my parents that have always supported and encouraged my choices, and to Séverine for her patience and her love.





# Table of content

|                         |            |
|-------------------------|------------|
| <b>Summary</b>          | <b>III</b> |
| <b>Résumé</b>           | <b>V</b>   |
| <b>Acknowledgements</b> | <b>VII</b> |

## Chapter I: Introduction

|   |           |
|---|-----------|
| <b>1. General context</b>   | <b>3</b>  |
| <b>2. Carbon capture and storage</b>  | <b>5</b>  |
| 2.1 Basic techniques for CO <sub>2</sub> capture                            | 5         |
| 2.2 CO <sub>2</sub> capture processes                                       | 8         |
| 2.3 Transport, utilization and storage                                      | 13        |
| <b>3. Post-combustion capture with amine solvents</b>                       | <b>17</b> |
| 3.1 Process description   | 17        |
| 3.2 Main post-combustion capture projects                                   | 18        |
| 3.3 Advantages and drawbacks of post-combustion capture with amine solvents | 20        |
| <b>4. Objectives</b>  | <b>22</b> |

## Chapter II: Experimental study of amine solvent degradation

|  |           |
|--|-----------|
| <b>1. Introduction</b>                           | <b>25</b> |
| <b>2. State of the art</b>                       | <b>27</b> |
| 2.1 Degradation mechanisms                       | 27        |
| 2.2 Main studies published about MEA degradation | 32        |
| 2.3 Influence of dissolved metals                | 37        |
| 2.4 Possible answers to amine degradation        | 39        |
| <b>3. Experimental methods</b>                   | <b>46</b> |
| 3.1 Semi-batch degradation test rig              | 46        |
| 3.2 Batch degradation cylinders                  | 49        |
| 3.3 Analytical methods                           | 49        |
| <b>4. Semi-batch experiments</b>                 | <b>62</b> |
| 4.1 Base case definition                         | 62        |

|  |           |
|--|-----------|
| 4.2 Evaluation of the experimental error | 63        |
| 4.3 Influence of the gas feed            | 66        |
| 4.4 Influence of the agitation rate      | 70        |
| 4.5 Influence of the temperature         | 74        |
| 4.6 Influence of the test duration       | 78        |
| 4.7 Influence of additives               | 79        |
| <b>5. Batch Experiments</b>              | <b>84</b> |
| 5.1 Influence of CO <sub>2</sub>         | 84        |
| 5.2 Influence of temperature             | 86        |
| 5.3 Influence of degradation inhibitors  | 88        |
| <b>6. Conclusions</b>                    | <b>91</b> |

### Chapter III: Simulation of the CO<sub>2</sub> capture process

|  |            |
|--|------------|
| <b>1. Introduction</b>   | <b>94</b>  |
| <b>2. State of the art</b>                                       | <b>96</b>  |
| 2.1 Thermodynamic model  | 96         |
| 2.2 Reactive absorption  | 100        |
| 2.3 Main modeling studies about CO <sub>2</sub> capture with MEA | 112        |
| <b>3. Model construction</b>                                     | <b>126</b> |
| 3.1 Mobile Pilot Unit models                                     | 127        |
| 3.2 Dynamic model  | 131        |
| 3.2 Degradation model  | 1315       |
| <b>4. Simulation results</b>                                     | <b>146</b> |
| 4.1 Equilibrium and rate-based model comparison                  | 146        |
| 4.2 Dynamic modeling   | 150        |
| 4.3 Degradation modeling   | 154        |
| <b>5. Conclusions</b>  | <b>164</b> |

### Chapter IV: Conclusions and perspectives

|                        |            |
|------------------------|------------|
| <b>1. Conclusions</b>  | <b>167</b> |
| <b>2. Perspectives</b> | <b>169</b> |

|  |            |
|--|------------|
| <b>Bibliography</b>  | <b>171</b> |
| <b>Figure index</b>  | <b>189</b> |
| <b>Table index</b>   | <b>194</b> |
| <b>Abbreviation list</b>   | <b>196</b> |
| <b>Appendices</b>  | <b>198</b> |
| <i>Appendix 1: Influence of dissolved metals on MEA degradation</i>        | 199        |
| <i>Appendix 2: Influence of degradation inhibitors for the MEA solvent</i> | 209        |
| <i>Appendix 3: Risk analysis for the degradation test rig.</i>             | 218        |
| <i>Appendix 4: Error analysis</i>  | 229        |
| <i>Appendix 5: Experimental results</i>                                    | 231        |
| <b>List of publications</b>  | <b>244</b> |

# Chapter I

## Introduction

*“To believe with certainty, we must begin by doubting”  
Polish quote*

## 1. General context

One of the biggest challenges our modern society has to face is the preservation of the environment combined with a growing world energy demand driven by the fast increase of the world population and the expectation of a higher standard of living. To face these challenges, it is necessary to re-evaluate and improve our way of dealing with energy. Reducing energy wastes on the production side as well as on the end-use side and promoting renewable energies are the best solutions towards sustainable energy systems. A third solution that could be rapidly applied at a large scale is to reduce the impact of the energy transformation steps on the environment. This can be accomplished by reducing the amount of emitted greenhouse gases, especially CO<sub>2</sub> which is the most widely produced greenhouse gas.

Worldwide, electricity is the fastest-growing form of end-use energy. Figure 1.1 shows that the electricity generation is clearly growing faster than the total energy consumption compared to the 1990 reference. This gap between both curves is largely due to non-OECD countries and it is supposed to continuously increase in the near-future (IEO, 2011).

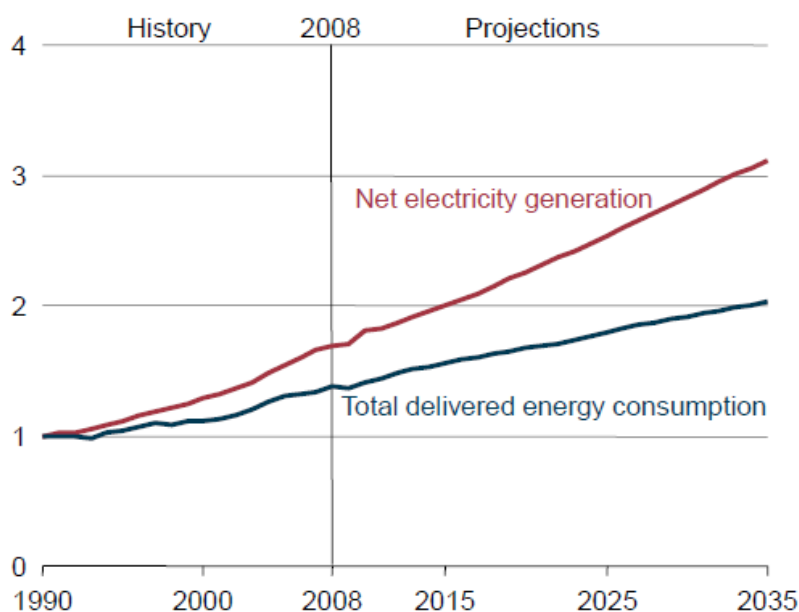


**Figure 1.1: growth in world energy generation and total delivered energy consumption, 1990-2035 (index 1990=1) (IEO, 2011).**

Moreover, coal is the most-used fuel for electricity generation and it will remain so for at least 20 years as shown in figure 1.2. This increase of the coal consumption is mainly due to non-OECD countries (IEO, 2011). In the same time, coal has the largest carbon content among all fossil fuels, so that its CO<sub>2</sub> emissions are proportionally higher. Coal-fired power plants are then large and stationary CO<sub>2</sub> sources, which facilitates CO<sub>2</sub> capture<sup>1</sup>.

<sup>1</sup> In comparison, CO<sub>2</sub> emissions from the transportation sector are due to many small and mobile sources. They are thus more difficult to capture. On the contrary, natural gas-fired power plants are also large and stationary CO<sub>2</sub> sources even if the CO<sub>2</sub> concentration in the plant flue gas is lower. Thus CO<sub>2</sub> capture can be implemented in natural gas-fired power plants as well.

As a consequence, it is particularly relevant to reduce the CO<sub>2</sub> emissions of coal-fired power plants. This can be achieved using three main solutions: continuous improvement of energy efficiency, biomass co-combustion and carbon capture and storage. The present work focuses on the CO<sub>2</sub> capture process in coal power plants.

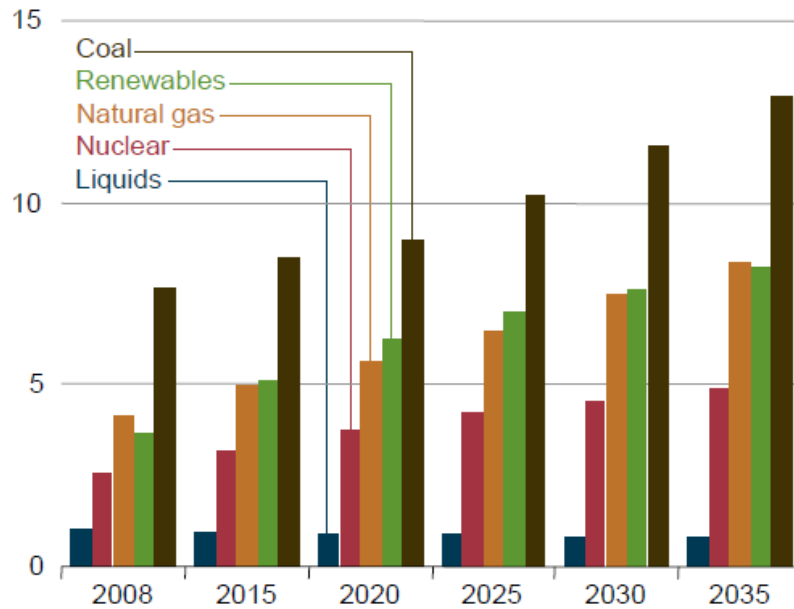


**Figure 1.2: world net electricity generation by fuel in trillion kWh, 2008-2035 (IEO, 2011)**

## 2. Carbon capture and storage

The goal of carbon capture and storage (CCS) is to capture the carbon dioxide where it is emitted, to transport it and to store it in geological formations. The captured CO<sub>2</sub> remains underground and does not contribute anymore to the greenhouse gas effect. An alternative solution to geological storage is the valorization of the captured CO<sub>2</sub>.

CCS simultaneously faces the reduction of CO<sub>2</sub> emissions and the large use of fossil fuels worldwide. One of its main advantages is that it can be rapidly implemented to mitigate anthropogenic CO<sub>2</sub> emissions to the atmosphere. It is thus a key technology for keeping the CO<sub>2</sub> concentration in the atmosphere by 450 ppm, so that the global temperature rise can be limited to 2°C (WEO, 2012). This technology can help to perform the transition from our carbon-based society with its greenhouse gases emissions concerns towards a society based on sustainable energy systems. However, long-term use of CCS is not recommended due to its high energy cost and to the limited availability of fossil fuels (Piessens et al., 2010).

In the present section, some techniques for capturing CO<sub>2</sub> from a flue gas stream are briefly presented. Three main processes using these techniques are described. Some insight is also given into transport, valorization and storage of CO<sub>2</sub>.

### 2.1 Basic techniques for CO<sub>2</sub> capture

The main techniques for CO<sub>2</sub> capture are presented in this section. They are techniques for isolating the carbon dioxide present in a gas stream. In the case of a fossil fuel-fired power plant, CO<sub>2</sub> is captured from a flue gas stream containing mainly nitrogen, water and oxygen, which are environmentally harmless.

#### *Chemical absorption*

The most used CO<sub>2</sub> separation technique is the chemical absorption, also called reactive absorption. This is the preferred technique when the CO<sub>2</sub> partial pressure is low, independently of the process pressure. A chemical reaction takes place between CO<sub>2</sub> and the chemical solvent at moderate or low temperature. This reaction can be reversed by increasing the temperature. However, the high energy requirement for the solvent regeneration is the main drawback of this technique.

Many characteristics must be evaluated when looking for an optimal chemical solvent. Among others, the ideal solvent has a low CO<sub>2</sub> absorption enthalpy, so that its regeneration requires less energy. Its reaction with CO<sub>2</sub> is rapid and its CO<sub>2</sub> loading capacity important. Furthermore, the ideal solvent is not toxic or corrosive and it does not degrade in the conditions of the capture process. In the same time, it degrades to harmless products in case of leakage to the environment. Its vapor pressure is low to prevent evaporation losses. Last but not least, it is also cheap and industrially available.

The most widely used solvents for CO<sub>2</sub> capture are aqueous amine solutions. These amines can be primary, secondary, or tertiary amines, depending on the number of hydrogen atoms bonded to nitrogen. Figure 1.3 represents some typically used solvents like alkanolamines, i.e. amines with at least an alcohol group: monoethanolamine (MEA), diethanolamine (DEA) and methyldiethanolamine (MDEA) (Jamal et al., 2006). Diamines like piperazine (PZ) (Rochelle

et al., 2011) or ethylenediamine (EDA) are also represented, as well as a sterically hindered amine, 2-amino-2-methylpropanol (AMP).

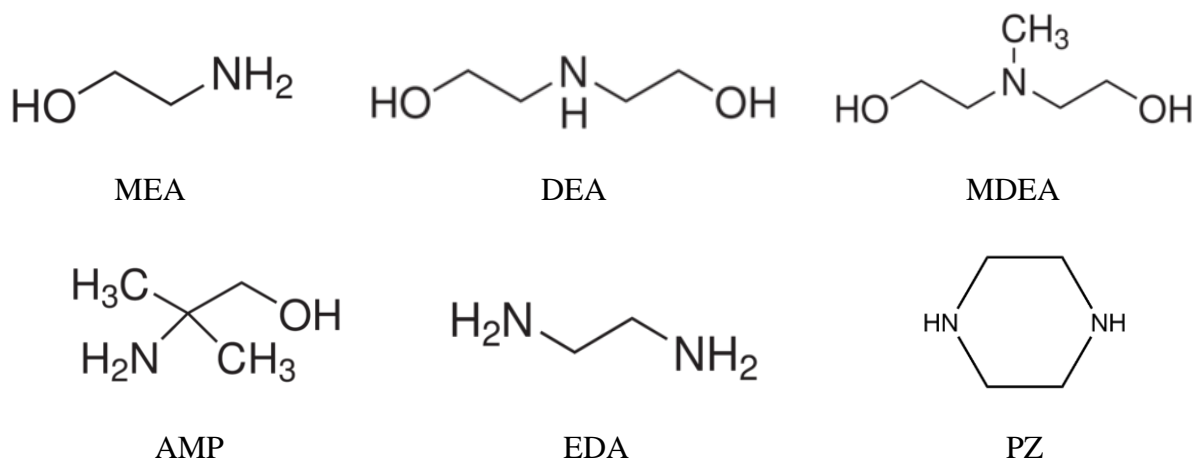


**Figure 1.3: typically used alkanolamines for chemical absorption of CO<sub>2</sub>**

Many alternatives to conventional amine solvents have been proposed in the last decade. Among them, chilled ammonia (Ciferno et al., 2005) and potassium carbonate (K<sub>2</sub>CO<sub>3</sub>) (Rochelle et al., 2003) have been widely studied. New generations of chemical solvents have been developed, including amino-acids (Jockenhövel et al., 2009a) and ionic liquids (Heldebrant et al., 2009). Demixing solvents seem to be another promising alternative, taking advantage of the phase separation between a CO<sub>2</sub> rich loaded amine and a CO<sub>2</sub> lean loaded one (Raynal et al., 2011). However, due to the numerous properties that an ideal solvent should possess, research in this field is still on-going.

### ***Physical absorption***

An alternative to the chemical absorption is the physical absorption. Carbon dioxide does not chemically react with the solvent, but is only dissolved into it. As represented in figure 1.4, the CO<sub>2</sub> loading in the solvent solution is following Henry's law and is thus proportional to the CO<sub>2</sub> partial pressure in the gas. This was not the case for the reactive absorption due to the chemical reaction. As a consequence, physical absorption is less relevant than chemical absorption at low CO<sub>2</sub> partial pressures. However, for a higher CO<sub>2</sub> content at moderate pressure (typically 35%-40% CO<sub>2</sub> in a stream at 20 bar), the physical absorption is preferred. Typical physical solvents are cold methanol (Rectisol process) or dimethylether of polyethylene glycol (Selexol process) (Figuerola et al., 2008).



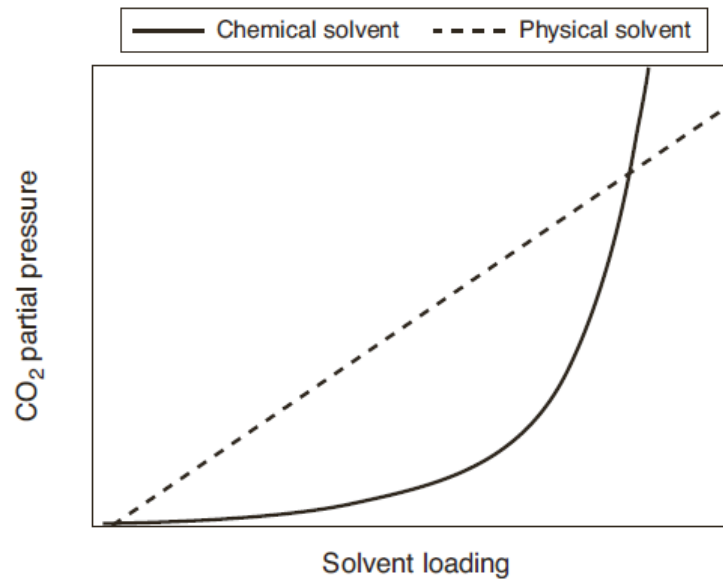


**Figure 1.4: comparison between chemical and physical absorption (Bailey and Feron, 2005)**

### *Emerging alternatives*

Some alternative CO<sub>2</sub> capture techniques have demonstrated interesting results in comparison with conventional absorption but are still in development. Some of them are already commercially available for other gas separation applications, but need to be adapted to CO<sub>2</sub> capture from flue gas.

- Adsorption: reversible pressure or temperature driven adsorption onto solid sorbents like zeolites or activated carbons. This technique is commercially available for CO<sub>2</sub> separation from natural gas. However, due to the low capacity and selectivity of adsorbents, it is not mature for large scale CO<sub>2</sub> capture so far (CO<sub>2</sub> capture project, 2008).
- Membranes: CO<sub>2</sub>-permeable membranes are commercially used for CO<sub>2</sub> separation from natural gas at high pressures and CO<sub>2</sub> concentrations. However, they are not adapted to low CO<sub>2</sub> partial pressures as the driving force is too low for gas separation. Moreover, it is more difficult to achieve high capture levels with membranes (Bailey and Feron, 2005).
- Cryogenic separation: the condensation of CO<sub>2</sub> at low temperature is commercially used for streams containing more than 90% CO<sub>2</sub>. However, the high energy penalty in case of more dilute CO<sub>2</sub> streams makes it unsuitable to CO<sub>2</sub> capture from flue gas (CO<sub>2</sub> capture project, 2008).
- Biotechnologies: micro-organisms absorb CO<sub>2</sub> during their growth. Recently, many studies have highlighted the high potential of microalgae to fix CO<sub>2</sub> in comparison to terrestrial plants. These microalgae can be further valorized as biomass and biodiesel. However, the energy input required for cultivating microalgae and for transforming them into valuable products is still very high (Lam et al., 2012).

## 2.2 CO<sub>2</sub> capture processes

Using the techniques described in section 2.1, there are three main process configurations for capturing CO<sub>2</sub> in power plants: post-combustion capture, pre-combustion capture and oxyfuel combustion. Additionally, industrial CO<sub>2</sub> emitters may develop their own capture method based on their specific process. These methods are summarized in figure 1.5 and are briefly described in this section.

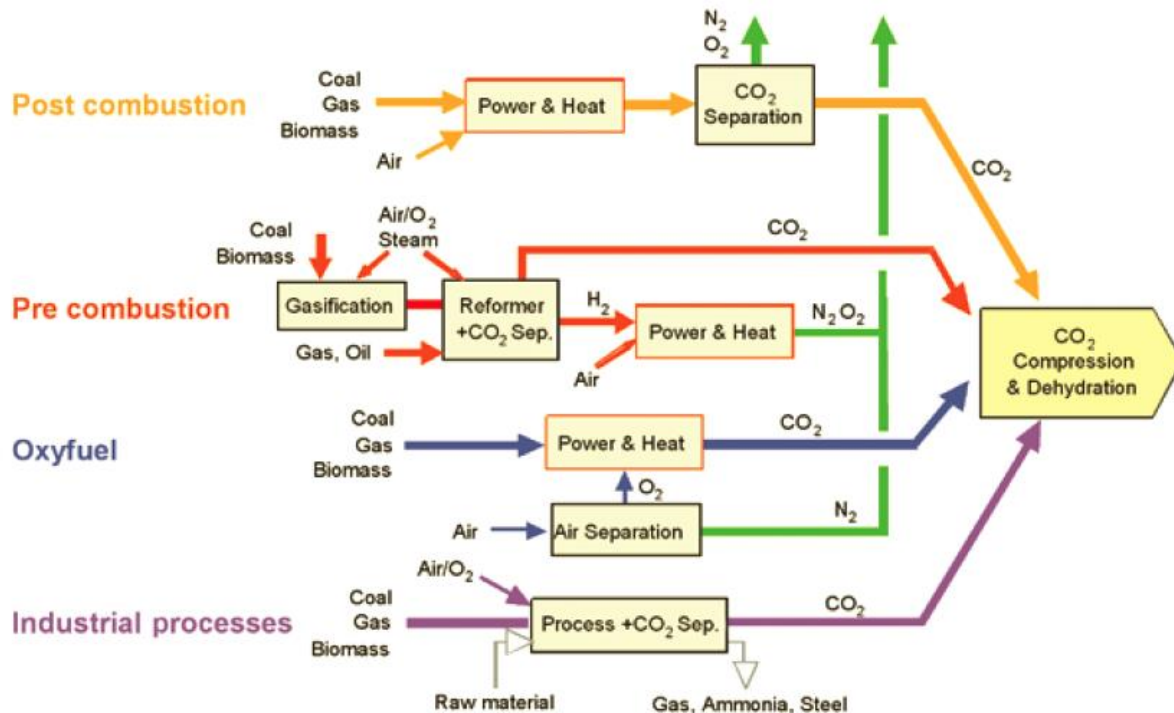
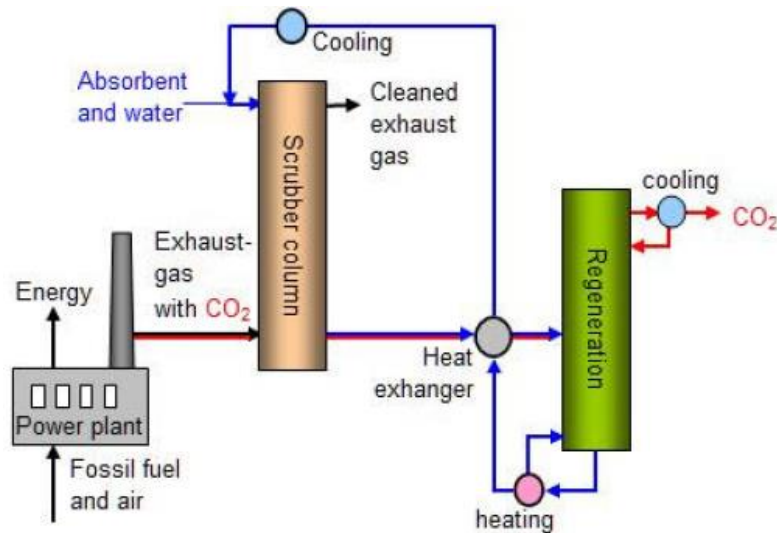


Figure 1.5: different methods for CO<sub>2</sub> capture (IPCC, 2005)

### Post-combustion capture

In the post-combustion CO<sub>2</sub> capture, CO<sub>2</sub> is separated from the flue gas resulting from the fuel combustion. Typical CO<sub>2</sub> concentrations in the flue gas vary between 3% and 15% depending on the fuel type, the main flue gas component being N<sub>2</sub> brought with the combustion air. At such CO<sub>2</sub> concentrations, the most used capture technique is the solvent loop with chemical absorption and regeneration as represented in figure 1.6. Typical post-combustion units can capture 85%-95% of the CO<sub>2</sub> present in the flue gas (IPCC, 2005). This process is described in details in the third section of this chapter.

The main advantage of the post-combustion capture is the possibility of retrofitting existing power plants by adding an end-of-pipe flue gas cleaning step. Moreover, this process is already a commercial technology for particular industrial applications like CO<sub>2</sub> production for the food and beverage industry. However, the high energy penalty for solvent regeneration is still an important drawback of this process. Other main drawbacks are the cost of the CO<sub>2</sub> capture plant, the secondary emissions of solvent degradation products and the corrosive effect of concentrated amines (IPCC, 2005). Finally, the captured CO<sub>2</sub> has a pressure close to atmospheric so that it must be compressed before transport and storage, inducing additional compression costs (Figueroa et al., 2008).



**Figure 1.6: simplified flowsheet of the post-combustion capture (Bellona, 2007)**

### *Pre-combustion capture*

The second way for reducing CO<sub>2</sub> emissions is to prevent the production of carbon dioxide during the combustion. Using steam reforming or gasification processes, the carbonated fuel is converted into CO<sub>2</sub> and H<sub>2</sub>. CO<sub>2</sub> is captured and hydrogen can be valorized as a chemical or burned to produce electricity as represented in figure 1.7. If the gasification and the electricity generation from H<sub>2</sub> take place in the same process cycle using gas and steam turbines, then the process is called integrated gasification combined cycle (IGCC).

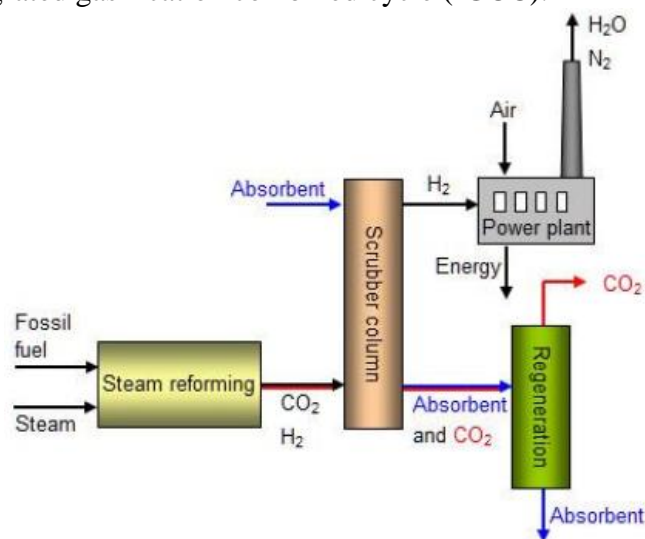


**Figure 1.7: simplified flowsheet of the pre-combustion capture (Bellona, 2007)**

Because the CO<sub>2</sub> content of the produced CO<sub>2</sub>/H<sub>2</sub> gas reaches up to 60%, the separation between H<sub>2</sub> and CO<sub>2</sub> is often performed by physical absorption (IPCC, 2005). Moreover, the high pressure of the CO<sub>2</sub>/H<sub>2</sub> gas stream induces the production of CO<sub>2</sub> at high pressure, reducing the compression costs. This method is also interesting for broadening the use of hydrogen as an energy carrier for mobile as well as stationary applications.

The pre-combustion process is already used in some industrial applications like the H<sub>2</sub> production for ammonia synthesis. However, the retrofitting of existing power plants with

pre-combustion capture is not applicable (Figuroa et al., 2008) and developing gas turbines for electricity generation from  $H_2$  still remains an important challenge (Bellona, 2013).

### *Oxyfuel combustion*

In the oxyfuel combustion process represented in figure 1.8, the combustion of the fossil fuel occurs with oxygen instead of air. Thus, the main gaseous products of the coal combustion are  $CO_2$  and water. Since water can be easily condensed, the oxyfuel combustion produces a flue gas stream composed of  $CO_2$  only, so that no gas separation step is required for the flue gas. This technology can also be used for retrofitting existing power plants.

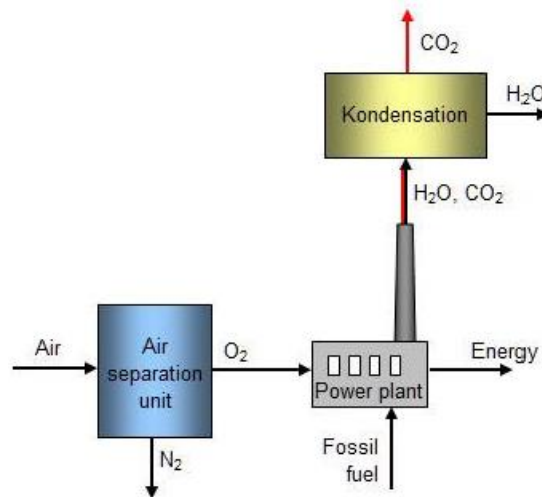


**Figure 1.8: simplified flowsheet of the  $CO_2$  capture by oxyfuel combustion (Bellona, 2007)**

However, a separation step is still required for an air-separation unit, which is the main disadvantage of oxyfuel combustion. The most mature method for air separation is the cryogenic air distillation but it requires a lot of energy for cooling the air down to its liquefaction temperature. The use of pure oxygen also implies major challenges regarding safety and material compatibility with  $O_2$ . Furthermore, part of the  $CO_2$  is cooled and recycled to the combustion chamber to limit the combustion temperature, decreasing the process efficiency.

A particular case of oxyfuel combustion is called chemical looping, which is a catalyzed combustion with oxygen. It is not always considered as an oxyfuel process since it does not require any air-separation unit. However, the fuel combustion implies oxygen instead of air. Its principle is represented in figure 1.9. In a first reactor, a metal is oxidized with air at temperatures varying between 700 and 900°C, according to the metal. The resulting metal oxide is fed to a second reactor where it reacts with some carbonated fuel at temperatures around 900°C. A combustion reaction takes place in which the fuel is oxidized and the metal oxide is reduced. As for conventional oxyfuel combustion, the flue gas contains only  $CO_2$  and water, so that  $CO_2$  can be recovered after water condensation. The reaction taking place in the metal oxidation reactor is exothermic, so that the released heat is partially used for electricity generation and partially recycled to the second reactor with the metal oxide. Indeed, the reaction in the second reactor is endothermic and requires a heat source.

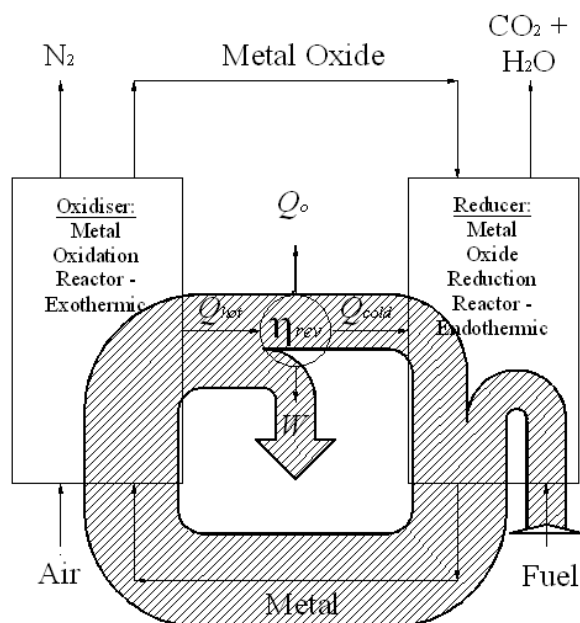


**Figure 1.9: simplified flowsheet of a chemical looping process (McGlashan, 2010)**

This technology is still under development. Important challenges are the identification of suitable metals to act as oxygen carrier and the handling of solid streams (Figuerola et al., 2008). Furthermore, the reaction kinetics of the metal oxide reduction is sometimes limiting, which is one of the main disadvantages of this method.

### *Comparison of the main CO<sub>2</sub> capture processes*

The impacts of the three main CO<sub>2</sub> capture processes on the plant efficiency have been compared by Rubin et al. (2012). They are presented in table 1.1.

**Table 1.1: impact of the CO<sub>2</sub> capture method on the power plant efficiency**

| CO <sub>2</sub> capture method and power plant                     | Net plant efficiency with no CCS | Net plant efficiency with CCS | Additional energy input per net kWh output |
|--|----------------------------------|-------------------------------|--|
| Existing subcritical coal power plant with post combustion capture | 33%                              | 23%                           | 43%  |
| New supercritical coal power plant with post-combustion capture    | 40%                              | 31%                           | 29%  |
| New supercritical coal power plant with oxy-combustion             | 40%                              | 32%                           | 25%  |
| New IGCC with pre-combustion capture                               | 40%                              | 33%                           | 21%  |
| New natural gas combined cycle with post-combustion capture        | 50%                              | 43%                           | 16%  |

The lowest energy penalty on solid fuel power plants is achieved for IGCC power plants (pre-combustion CO<sub>2</sub> capture). Oxyfuel combustion also shows good results. Post-combustion capture plants show a higher energy penalty for coal-fired power plants, but lead to competitive energy penalties in the case of natural gas combined cycles.

However, the methods should not be compared only on their respective energy penalty. For instance, post-combustion capture is currently the most adapted method for retrofitting existing power plants. As a conclusion, all methods have their pros and cons, so that the best method will depend on the practical application.

### *CO<sub>2</sub> capture in industrial processes*

Besides classical methods, some industries have already developed their own CO<sub>2</sub> capture method, based on their specific process. In some cases, the CO<sub>2</sub> capture process is still under development. The most significant examples are briefly described below:

- Natural gas sweetening: in order to preserve natural gas pipelines from corrosion, the CO<sub>2</sub> content in the gas must not exceed 2%. Depending on the initial CO<sub>2</sub> content, separation membranes, physical or chemical absorption processes are applied. Natural gas sweetening is already a commercially available technology (IPCC, 2005).
- Ammonia synthesis: this process is similar to pre-combustion capture with the difference that it is already commercially available. In ammonia plants, H<sub>2</sub> and N<sub>2</sub> react to form ammonia. Hydrogen is produced by steam reforming or gasification, depending on the fuel (light hydrocarbons or coal respectively). In order to purify the produced syngas, the CO<sub>2</sub> is generally captured by absorption. Carbon dioxide is then a by-product of the ammonia synthesis so that urea production plants – large CO<sub>2</sub> consumers – are usually associated with ammonia production plants (IPCC, 2005).
- Steel production: in 2008, the iron and steel industry accounted for 14% of the total industrial energy consumption (IEO, 2011). However, few large CO<sub>2</sub> capture projects have been identified in the steel industry. One of them is the project ULCOS in France (ULCOS, 2013). In the steel industry, the major part of the CO<sub>2</sub> production is not due to combustion, but to the reaction of iron ores with a reducing gas, usually carbon monoxide. The most promising method to cut down CO<sub>2</sub> emissions consists in capturing CO<sub>2</sub> from the gas exiting the blast furnace by vacuum pressure swing adsorption. The other components of the gas stream (CO and H<sub>2</sub>) are recycled to the furnace. Moreover, the furnace can be operated with oxygen instead of air, so that the CO<sub>2</sub> content of the flue gas is increased (Zuo and Hirsch, 2008).
- Cement production: cement production plants are also large energy consumers. In cement plants, the CO<sub>2</sub> concentration in the flue gas varies between 15% and 30%. The post-combustion capture is the most adapted process for retrofitting existing plants, but it implies higher costs than in power plants due to the additional flue gas cleaning steps. Consequently, the oxyfuel process is more adapted for a new cement production plant (Barker et al., 2009). A third route for CO<sub>2</sub> capture has been proposed, using a calcium looping cycle (Abanades et al., 2004) as represented in figure 1.10. This alternative technology takes place at high temperatures (carbonatation around 650°C, calcination around 900°C) but seems nevertheless promising, with a very low energy penalty compared to conventional capture methods (Bosoaga et al., 2009).

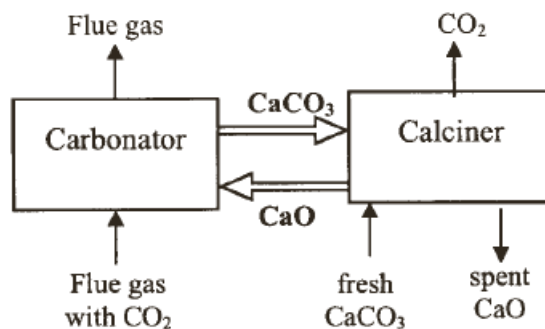


**Figure 1.10: calcium looping cycle for CO<sub>2</sub> capture (Abanades et al., 2004)**

These examples prove that carbon capture technologies do not belong to the only power generation sector and that they can be applied to all stationary processes emitting significant amounts of CO<sub>2</sub>.

### 2.3 Transport, utilization and storage

In this section, the different steps taking place after the CO<sub>2</sub> capture are briefly described. Some insight is given into the main CO<sub>2</sub> transport techniques. Different routes for CO<sub>2</sub> valorization are also described and basic considerations regarding CO<sub>2</sub> storage are presented.

#### *CO<sub>2</sub> transport*

There are two main possibilities for CO<sub>2</sub> transport: pipeline and ship transport. For small distances (lower than 500-1000 km) as well as for the transport of large amounts of CO<sub>2</sub>, pipeline transport is preferred (ZEP, 2011). Pipeline transport of CO<sub>2</sub> is similar to natural gas transport. In both onshore and offshore pipelines, it is important that CO<sub>2</sub> remains dense, which means either liquid or supercritical<sup>2</sup>. Therefore, the captured CO<sub>2</sub> is compressed to a pressure of about 100 bar (ZERO, 2013a). At this pressure, CO<sub>2</sub> is a liquid at ambient temperature and a dense supercritical fluid above the critical temperature, i.e. 31.3°C. Free water and oxygen must be removed to prevent corrosion in the pipes. In the United States, a 2500 km long pipeline network has been developed since 1972 and is currently transporting about 50 Mt CO<sub>2</sub> per year, mainly for enhanced oil recovery applications (IPCC, 2005).

In case of ship transport, the CO<sub>2</sub> is cooled down to -30°C at 20 bar in a liquefaction unit. Ship transport of CO<sub>2</sub> is similar to LPG and LNG transport and it is already commercially available at a relatively small scale for the food and beverage industry. For transporting larger amounts of CO<sub>2</sub> as it should be the case in future CCS projects, the transport conditions will certainly be similar to those of semi-refrigerated LPG carriers, i.e. -50°C and 6.5 bar (ZEP, 2011). To give an idea, the leading company in the field of CO<sub>2</sub> transport by ship is the Yara Company, with four small CO<sub>2</sub> carrier boats in operation and a delivering capacity of 400,000 tonnes CO<sub>2</sub> per year (Engebo et al., 2012). Thus ship transport of CO<sub>2</sub> remains marginal in comparison to pipeline transport.

#### *CO<sub>2</sub> utilization*

The initial objective of CCS technologies is to capture CO<sub>2</sub> and to store it underground in order to limit its effect as greenhouse gas. However, capturing CO<sub>2</sub> is expensive so that

<sup>2</sup> The critical point of CO<sub>2</sub> is T<sub>C</sub> = 31.3°C, P<sub>C</sub> = 73.87 bar.

valorizing it as a by-product instead of considering it as a waste would certainly be useful for the development of large scale CO<sub>2</sub> capture. Figure 1.11 presents the main utilizations that have been identified for CO<sub>2</sub>. Some of these utilizations release the CO<sub>2</sub> to the environment during their application, so that they cannot be considered as long-term storage options. However, they still contribute to the decrease of CO<sub>2</sub> emissions since they continuously immobilize new amounts of CO<sub>2</sub>.

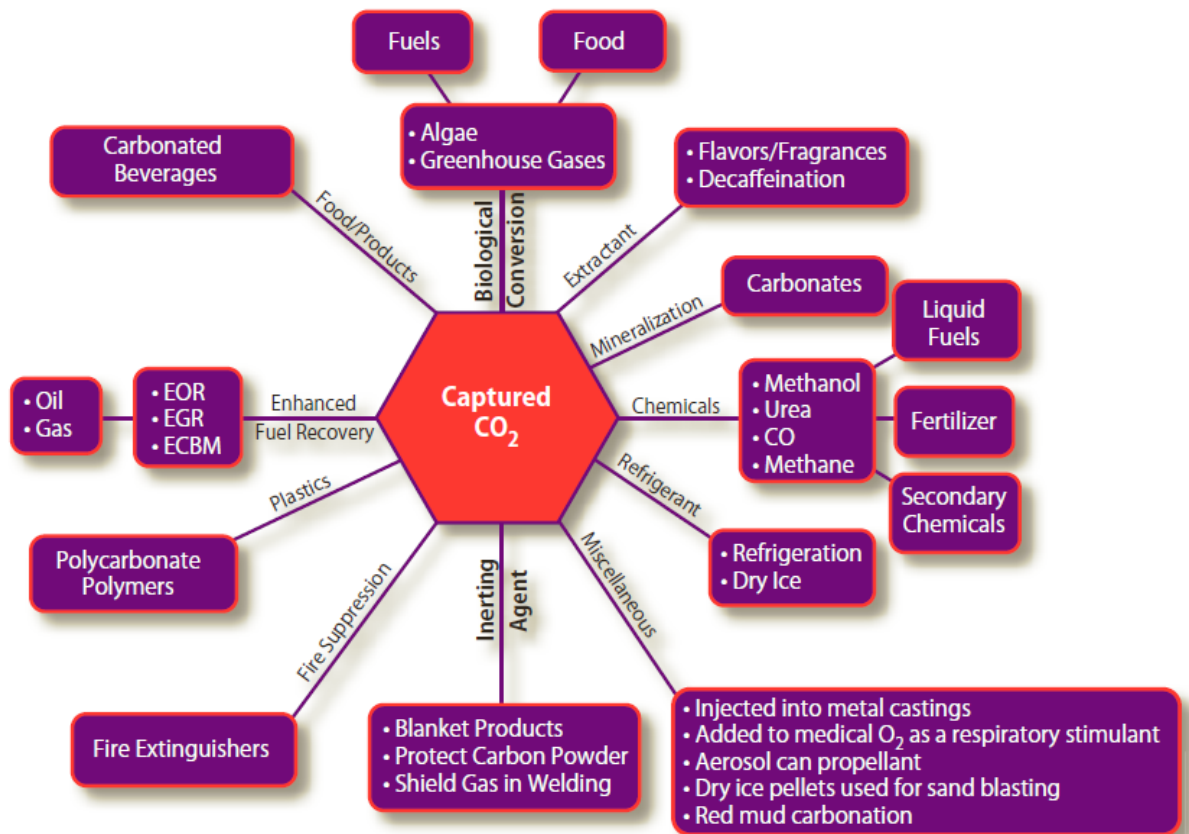


**Figure 1.11: potential reuse routes for captured CO<sub>2</sub> (NETL, 2013)**

It is not the scope of this introduction to detail each one of these potential pathways for CO<sub>2</sub> utilization. Basically, we can sort these applications into three main categories (ADEME, 2010):

- Use of CO<sub>2</sub> without reprocessing: some techniques are already commercially available. It is the case for enhanced oil and gas recovery and for the reuse of CO<sub>2</sub> in the food and beverage industry. CO<sub>2</sub> for enhanced oil and gas recovery is particularly appreciated since it increases the total recovery from an average hydrocarbon field by up to 50% (IEA, 2008). Supercritical CO<sub>2</sub> is also advantageously used as a solvent in many industrial applications.
- Chemical processing of CO<sub>2</sub>: in this case, CO<sub>2</sub> is chemically upgraded into valuable chemicals. Urea and polycarbonate production plants are already consuming large amounts of CO<sub>2</sub>. CO<sub>2</sub> can also be integrated in the production process of cements and other building materials. Moreover, it can be used as feedstock for the synthesis of common chemicals like methanol, formic acid, carbon monoxide, syngas... However,



this upgrading of CO<sub>2</sub> always requires energy, so that these processes are economically viable only in a few cases so far (ADEME, 2010).

- Biological processing of CO<sub>2</sub>: as an alternative to chemical processes for upgrading CO<sub>2</sub>, biological processes use sunlight as a cheap and sustainable source of energy. Microalgae have a promising potential in capturing CO<sub>2</sub> and can be processed into various products, including food, fuel and chemicals. The main challenge of this reuse route is the high energy input for the biomass transformation into chemicals. CO<sub>2</sub> is also sometimes used for growth enhancement in greenhouse cultures (Yara, 2013).

The large number and the diversity of the reuse routes for captured CO<sub>2</sub> seem very promising. This would convert CCS to CCUS, i.e. carbon capture, utilization and storage (CSLF, 2011). Indeed, a recent study has estimated that the various ways of CO<sub>2</sub> utilization have the potential of reducing the global CO<sub>2</sub> emissions by 3.7 Gt per year, equivalent to about 10% of the current annual emissions (Sridhar and Hill, 2011). Finally, reusing CO<sub>2</sub> could contribute not only to the reduction of the greenhouse gas emissions, but also to a sustainable society through the development of new economic activities.

### *CO<sub>2</sub> storage*

In the case of large scale implementation of CCS, gigantic amounts of CO<sub>2</sub> would be captured, so that the major part of the captured CO<sub>2</sub> could not be reused but would be injected underground. In geological structures, the CO<sub>2</sub> dissolves and progressively mineralizes to carbonate over several thousands of years. Different geological formations are studied for CO<sub>2</sub> storage (IPCC 2005):

- (Depleted) Oil and gas fields: this is related to the enhanced hydrocarbon recovery technology which is already a mature technology.
- Unmineable coal beds: CO<sub>2</sub> storage in coal seams has a limited capacity potential, so that it can be considered as a local solution only. However, it can gain interest if recovering methane from coal layers is achievable by CO<sub>2</sub> injection.
- Deep saline aquifers: saline formations have the largest storage capacities but they have been less studied than hydrocarbon fields. The Sleipner project in the North Sea is the most famous example of CO<sub>2</sub> storage in saline formations. Since 1996, about 1 Mt CO<sub>2</sub> has been injected each year at Sleipner.

A geological structure for CO<sub>2</sub> storage must satisfy three main characteristics (Cooper, 2009). Firstly, its capacity must be sufficient, which is related to its size but first of all to the porosity of its rock. Secondly, the rock permeability must allow the injection of CO<sub>2</sub>. And thirdly, a gas tight cap rock formation must preserve the containment of the injected fluid. The storage site should also be located at a minimal depth of 800m to ensure supercritical conditions for efficient CO<sub>2</sub> storage. To minimize transport costs, it should also be as close as possible to CO<sub>2</sub> emission sources.

Monitoring the storage safety over a long time-scale is a complex challenge. Figure 1.12 shows some of the many monitoring, evaluation, reporting and verification techniques developed for CO<sub>2</sub> storage.

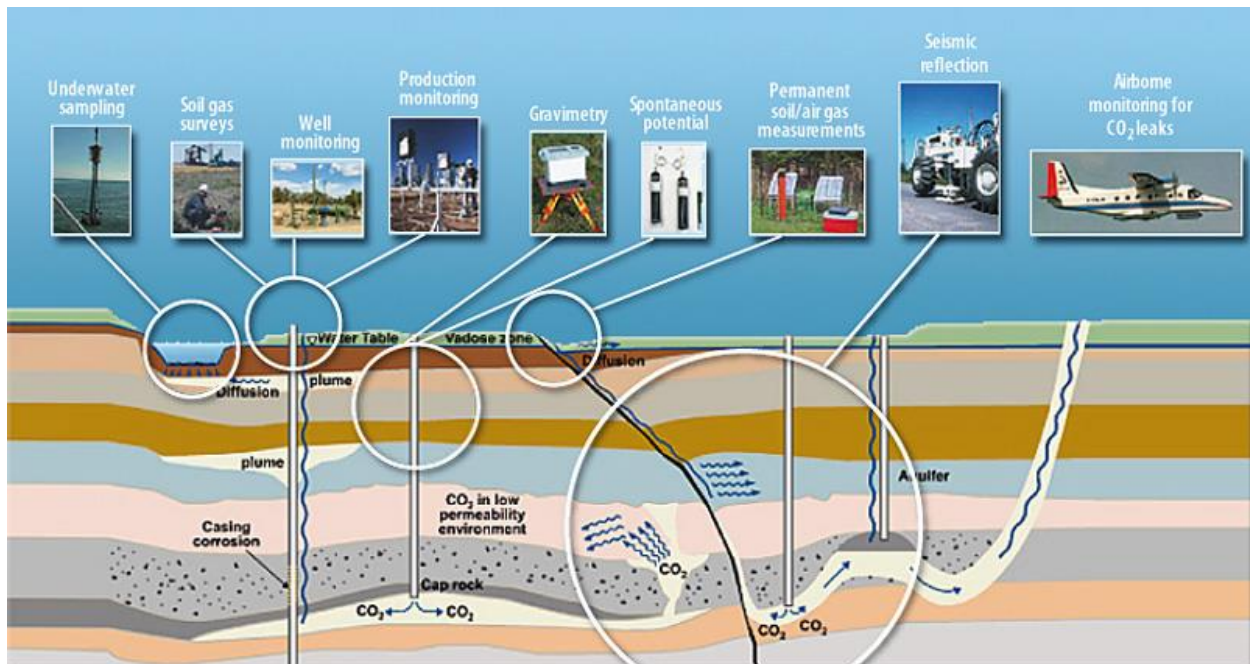


**Figure 1.12: monitoring techniques for CO<sub>2</sub> storage (CO<sub>2</sub> capture project, 2013)**

Although the time scale is very different, geological storage of CO<sub>2</sub> presents many similarities with natural gas storage which is already a commercial technology. Natural gas storage acts as a seasonal buffer for the distribution network: natural gas is stored in summer when the demand is low and is recovered in winter when the demand increases (Fluxys, 2013). Storage sites should also cope with any interruption of the natural gas delivery due to geopolitical issues or to technical incidents. Consequently, experience from natural gas storage may be useful for CO<sub>2</sub> storage.

In conclusion, the different CO<sub>2</sub> capture methods are part of a much larger process that includes transport, reuse of CO<sub>2</sub>, storage, monitoring... To give a complete overview on CCS (or rather CCUS), many non-technical considerations should also be mentioned, including economic challenges, geopolitical considerations, public perception... These subjects will not be described in the framework of this work, but more information about them can be found in the scientific literature.

### 3. Post-combustion capture with amine solvents

In the previous section, the main principles of carbon capture, utilization and storage have been presented. In this section, the focus is set on the post-combustion CO<sub>2</sub> capture by reactive absorption in amine solvents, which is the object of the present work. First, the process is described. Then, a list of existing pilots and commercial installations is presented. Finally, advantages and drawbacks of this technology are discussed.

#### 3.1 Process description

The benchmark solvent for the CO<sub>2</sub> reactive absorption is an aqueous solution of 30 wt% monoethanolamine (MEA, HO-CH<sub>2</sub>-CH<sub>2</sub>-NH<sub>2</sub>). The principle of this process is represented in figure 1.13.

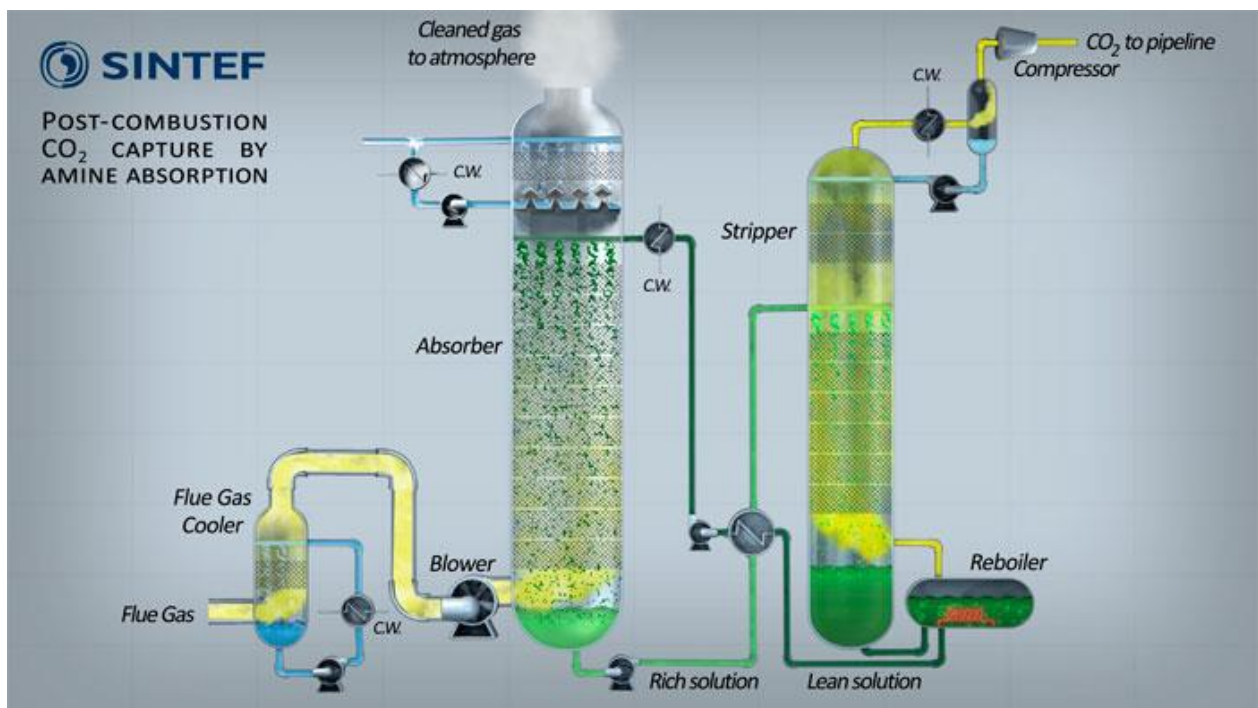


**Figure 1.13: flowsheet of the chemical absorption process (Sintef, 2013)**

In the case of a coal power plant, the flue gas contains<sup>3</sup> 14% CO<sub>2</sub>, 6% O<sub>2</sub>, 12% H<sub>2</sub>O and 68% N<sub>2</sub> (Laborelec, 2009). Different gas cleaning steps (not represented in figure 1.13) are usually present in European power plants to remove impurities from the flue gas. Among others, sulfur oxides can be almost completely removed by flue gas desulfurization (FGD) and nitrous oxides by selective catalytic reduction (SCR). In the case of post-combustion CO<sub>2</sub> capture, an additional wet pre-scrubbing treatment removes any remaining SO<sub>2</sub> and brings the flue gas to the desired temperature before CO<sub>2</sub> capture.

Then, after a compression step, the flue gas enters the absorption column or absorber. Carbon dioxide reacts with the amine solvent at temperatures varying between 40 and 60°C (~55°C in

<sup>3</sup> Volume percentages. To give an idea, flue gas from power plants contains 7-10% CO<sub>2</sub>, and flue gas from combined cycle gas turbine contains 3-4% CO<sub>2</sub> (volume fraction on a dry basis) (IPCC, 2005).

the case of MEA). This chemical absorption is an exothermic reaction. The absorption mechanism in the solvent can be summarized in two main steps: formation of a zwitterion (1.1) and instantaneous removal of a proton by a base B to form a carbamate (1.2). In aqueous solutions, the base B can be either water, an amine molecule or an OH<sup>-</sup> ion. Reaction 1.1 is rate-determining (Danckwerts, 1979; Versteeg and Van Swaaij, 1988).



After the absorption, the treated flue gas usually flows through a water-wash section to reduce the emissions of volatile solvent and degradation products. The washing section also regulates the temperature of the flue gas in order to control the amount of water exiting the process. A demister is also installed to prevent the emission of liquid droplets. The CO<sub>2</sub>-loaded solvent (also referred to as “rich solvent”) is pumped to a regeneration column (also named “stripper”) via a heat exchanger in which the rich solvent is pre-heated.

In the stripper, the solvent is regenerated at temperatures varying between 100 and 140°C (~120°C in the case of MEA). The purpose of the reboiler at the stripper bottom is to supply thermal energy for the solvent regeneration<sup>4</sup>. At this temperature, the absorption reaction is reversed, so that CO<sub>2</sub> is released from the solvent. The regenerated solvent (“lean solvent”) is fed back to the absorber via the rich-lean heat exchanger in which it pre-heats the rich solvent. A further heat exchanger cools the regenerated solvent down to the desired absorber entrance temperature.

The gaseous CO<sub>2</sub> stream after desorption contains some water that is recycled to the process by condensation, so that the final product may reach a CO<sub>2</sub>-purity of 99% by volume. Finally, the objective that is generally pursued in post-combustion processes is the removal of 90% of the CO<sub>2</sub> present in the power plant flue gas stream (Laborelec, 2009).

### 3.2 Main post-combustion capture projects

Table 1.2 lists the main post-combustion CO<sub>2</sub> capture installations using amine solvents. The first commercial capture plants (marked in bold) were designed more than 30 years ago for commercial CO<sub>2</sub> production. Besides commercial CO<sub>2</sub> production plants, the intensive research on post-combustion CO<sub>2</sub> capture for environmental purpose has started in the 2000ies. Different pilot installations have been developed around the world, with varying scale and capture solvents.

---

<sup>4</sup> This heat is supplied under the form of low-pressure steam from the power plant. The steam is preferentially extracted at the cross-over pipe between the intermediate and low pressure steam turbines (Jockenhövel et al., 2009b).

**Table 1.2: chronologic listing of the main CO<sub>2</sub> capture installations**

| Project  | Location                          | Operation start | Maximal CO <sub>2</sub> capacity (t/d) | Solvent                                    | Reference                          |
|--|-----------------------------------|-----------------|--|--|------------------------------------|
| <b>Dow chemical - Fluor Econamine</b>            | USA, Canada, Japan, Brazil...     | 1982            | 1000                                   | MEA  | Chapel et al., 1999                |
| <b>Kerr McGee - ABB Lummus</b>                   | Malaysia                          | 1978            | 800                                    | MEA  | Barchas et Davis, 1992             |
| <b>Kansai Mitsubishi CO<sub>2</sub> Recovery</b> | Asia and Middle-East              | 1999            | 450                                    | KS-1 amine                                 | Endo et al., 2011                  |
| International Test Center ITC                    | Saskatchewan, Canada              | 1999            | 4                                      | MEA, amine blends                          | Idem et al., 2006                  |
| SRP pilot plant                                  | UT Austin, Texas, USA             | 2002            | 5.28                                   | MEA, PZ, novel solvents                    | Seibert et al., 2011               |
| European projects FP6 CASTOR, FP7 CESAR          | Esbjerg, Denmark                  | 2006            | 24                                     | MEA, novel solvents                        | Knudsen et al., 2009; Cesar, 2012  |
| LTD pilot plant                                  | Stuttgart/Kaiserslautern, Germany | 2006            | 0.26                                   | MEA, novel solvents                        | Notz et al., 2007                  |
| Cato-2 Catcher Pilot                             | Maasvlakte, The Netherlands       | 2008            | 6                                      | MEA, novel solvents                        | Cato, 2012                         |
| Loy Yang CSIRO                                   | Loy Yang, Australia               | 2008            | 2.74                                   | Amine solvents                             | Cook, 2009                         |
| Niederaussem pilot plant                         | Niederaussem, Germany             | 2009            | 7.2                                    | MEA, novel solvents                        | Moser et al., 2011a                |
| CO2CRC H3 capture project                        | Hazelwood, Australia              | 2009            | 25                                     | Amines, NH <sub>3</sub> , membranes        | ZERO, 2013b                        |
| Sintef pilot plant (Tiller R&D Plant)            | Trondheim, Norway                 | 2010            | 0.5                                    | MEA, novel solvents                        | Mejdell et al., 2011               |
| CSIRO Tarong                                     | Kingaroy, Australia               | 2010            | 2.74                                   | MEA  | Stanwell, 2012                     |
| ENEL capture pilot                               | Brindisi, Italy                   | 2011            | 22                                     | MEA  | ZERO, 2013b                        |
| Plant Barry                                      | Mobile, Alabama, USA              | 2011            | 500                                    | KS-1 Amine                                 | MHI, 2012                          |
| Test Centre Mongstad (two pilots)                | Mongstad, Norway                  | 2012            | 203                                    | MEA, novel amines; chilled NH <sub>3</sub> | de Koeijer et al., 2011; TCM, 2012 |
| ROAD   | Maasvlakte, The Netherlands       | 2015            | 4 061                                  | MEA  | Huizeling and Weijde, 2011         |

It appears from table 1.2 that the largest post-combustion capture installations have been designed for commercial CO<sub>2</sub> production more than ten years ago. The largest modern facility for CO<sub>2</sub> capture in Plant Barry is based on a commercial technology developed by Kansai Mitsubishi which uses a proprietary amine solvent, KS-1. For comparison purpose, the ROAD project has also been mentioned even if not operational yet. This is one of many large-scale demonstration projects that have been planned recently but its realization is still uncertain. In the last years, many demonstration projects have been delayed or cancelled due to cost considerations (Rubin et al., 2012). However, there remains a critical need for demonstration projects to prove the technical and economic feasibility of large-scale CO<sub>2</sub> capture.

### *3.3 Advantages and drawbacks of post-combustion capture with amine solvents*

The main advantage of CO<sub>2</sub> post-combustion capture is its availability for retrofitting existing power plants (Figueroa et al., 2008). Among the different post-combustion techniques and at the current state of technology, reactive absorption in amine solvents is often considered as the most efficient method for CO<sub>2</sub> capture, or at least the most feasible route to large-scale implementation (Rubin et al., 2012; Svendsen et al., 2011). The main reason for that is the large experience gained in various applications like natural gas sweetening or commercial CO<sub>2</sub> capture from flue gas. Moreover, the development of CO<sub>2</sub> capture with amine solvents was based on MEA, an amine that rapidly reacts with CO<sub>2</sub> and that possesses a high CO<sub>2</sub> capacity on a mass basis (Brüder and Svendsen, 2012). However, two main drawbacks still affect the CO<sub>2</sub> chemical absorption in amine solvents, and especially in MEA: the high cost of the process and its environmental safety (Svendsen et al., 2011).

The cost of the post-combustion CO<sub>2</sub> capture is related to the capital cost for the capture plant and most notably to the operational cost of the process as represented in figure 1.14 (Abu-Zahra, 2009). Indeed, this latest contribution represents 76% of the cost of avoided CO<sub>2</sub>.

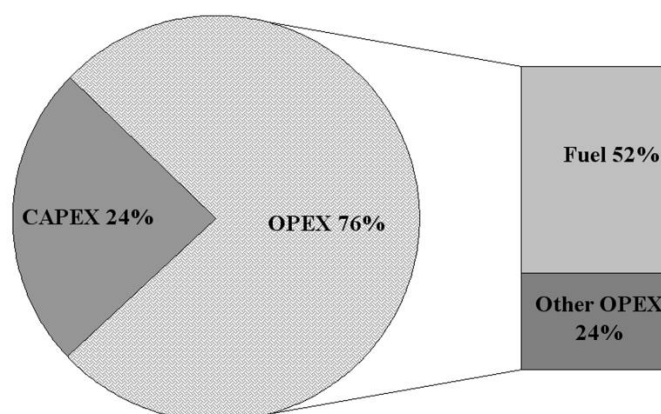


**Figure 1.14: Major contributions to the cost of avoided CO<sub>2</sub> (Abu-Zahra, 2009)**

This operational cost is mainly due to the additional fuel consumption in the power plant for providing regeneration energy and electricity to the CO<sub>2</sub> capture plant. As previously mentioned in table 1.1, an additional energy input of 29% per net kWh output is necessary to capture CO<sub>2</sub> in the case of a new supercritical pulverized coal power plant with post-combustion capture (Rubin et al., 2012). This energy penalty corresponds to an overall plant

efficiency drop from 40% to 31%. According to Abu-Zahra (2009), this leads to a cost of 37 € per ton of avoided CO<sub>2</sub> in the case of a 600 MWe coal-fired power plant (CO<sub>2</sub> capture with 30 wt% MEA). As a consequence, the cost of electricity would rise from 31.4 €/MWh up to 56 €/MWh. It is thus easy to understand that many studies on CO<sub>2</sub> capture have mainly focused on the reduction of this energy penalty. This has been partially achieved by using newly developed solvents and/or alternative process configurations (among others Mimura et al., 1995; Chakma 1997; Rochelle et al., 2011; Knudsen et al., 2011). Research in this field is still on-going.

Besides cost issues, the environmental safety of post-combustion capture with amine solvents also represents a critical issue. Creating a new environmental problem when solving an initial one must be strictly avoided (Svendsen et al., 2011). Two types of environmentally harmful chemicals may be emitted by the CO<sub>2</sub> capture process: the amine solvent and its degradation products.

The vapor pressure of the amine solvent above its aqueous solution can be significant, so that some amine may exit the process with the cleaned flue gas. In the case of MEA, solvent emissions can be kept very low by an optimal operation of the washing section (Mertens et al., 2012; Moser et al., 2011b). In comparison, significant emissions of AMP solvent were recorded during a pilot plant test with AMP/PZ (Mertens et al., 2012). This is in accordance with the higher volatility of AMP compared to MEA and PZ (Nguyen et al., 2010). Thus, volatility is a further essential parameter when selecting a new solvent. Based on own unpublished data, Svendsen et al. (2011) claim that optimal washing sections could bring amine emissions down to 0.01-0.05 ppm in the cleaned flue gas.

Amine degradation products may also be emitted by the capture process. Indeed, during the absorption, the amine solvent is in contact with oxygen from the flue gas, inducing oxidative degradation of the amine. The solvent is also heated in presence of CO<sub>2</sub> during the regeneration, inducing thermal degradation with CO<sub>2</sub>. If SO<sub>x</sub> and NO<sub>x</sub> impurities have not been correctly removed from the flue gas before the absorber, they may also cause amine solvent degradation. The amine solvent can degrade into gaseous as well as liquid degradation products that are classified as environmentally harmful emissions. Some recent studies at lab and pilot scale have evidenced that the operating conditions of the capture process have a direct impact on the formation and emission of degradation products (among others Mertens et al., 2012; Voice and Rochelle, 2013). However, there still remains a knowledge gap about the environmental impact of post-combustion CO<sub>2</sub> capture with amines (Shao and Stangeland, 2009).

## 4. Objectives

The main objective of this thesis is to gain a better understanding of the complex interactions between amine solvent degradation and CO<sub>2</sub> capture. This objective proceeds through two complementary approaches and their combination represents the main originality of this work.

The first approach is the experimental study of amine solvent degradation. The objective is to test the influence on degradation of operating parameters like temperature, agitation rate and flue gas composition. The influence of dissolved metals and degradation inhibitors in the solvent solution may also be studied since they may affect the degradation rate. However, amine degradation is a slow phenomenon and it is necessary to accelerate it for collecting data in a reasonable time framework. The main objectives of this task are the following:

- Design and construction of a test rig for accelerating solvent degradation.
- Development of analytical methods to characterize degraded solvents.
- Evaluation of the relevance of accelerated degradation conditions.
- Evaluation of the influence of operating parameters on degradation pathways.
- Quantification of the influence of operating parameters on the degradation rate.
- Quantification of the influence of dissolved metals and degradation inhibitors on the degradation rate.

The second approach is the simulation and optimization of the post-combustion CO<sub>2</sub> capture process with amine solvents. The Aspen Plus<sup>®</sup> software (Advanced System for Process Engineering) has been selected as a powerful simulation tool to model CO<sub>2</sub> capture. The main objectives of this task are the following:

- Development of a model for the simulation of the post-combustion capture process in static and dynamic operation modes.
- Evaluation of the relevance of this model to simulate industrial processes.
- Identification of process parameters having a large influence on the energy requirement of the CO<sub>2</sub> capture.
- Evaluation of alternative process configurations.
- Propositions for an optimal design of the CO<sub>2</sub> capture process.

Finally, the objective of this thesis is to combine both experimental and modeling approaches in order to develop a model of CO<sub>2</sub> capture taking solvent degradation into account. This is the main originality of this work. Indeed, available models focused so far on the reduction of the process energy penalty but only few of them did consider the impact of operating conditions on the process environmental penalty.



In the present work, the developed methodology is based on the current benchmark solvent for CO<sub>2</sub> capture, i.e. aqueous 30 wt% MEA. Developing a model for CO<sub>2</sub> capture that includes experimental degradation results should help us to understand the mutual influences of amine solvent degradation and process operating conditions. Finally, the objective is to propose optimal operating conditions that achieve a trade-off between energy and environmental penalties for the post-combustion CO<sub>2</sub> capture process.

This thesis has been performed in industrial partnership with the company Laborelec, member of the GDF SUEZ group. Laborelec is a Belgian technical competence center in energy processes and energy uses. It has been created in 1962 to offer technical expertise to Electrabel, the main electricity supplier in Belgium (Laborelec, 2009). Its interest for CO<sub>2</sub> capture is motivated by the objective of providing technical support to power plant operators in future CO<sub>2</sub> capture installations.

## Chapter II

# Experimental study of amine solvent degradation

*“I think that in the description of natural problems we ought to begin not with the Scriptures,  
but with experiments, and demonstrations.”*  
Galileo Galilei

## 1. Introduction

Amine solvent degradation can be defined as “an irreversible chemical transformation of alkanolamine into undesirable compounds resulting in its diminished ability to absorb CO<sub>2</sub>.” (Sexton, 2008). Until now, the impact of solvent degradation on the capture process has been evaluated by quantifying the specific solvent consumption per ton of captured CO<sub>2</sub>. In the case of a commercial CO<sub>2</sub> capture plant, the amine solvent consumption was estimated to 1.6 kg/ton CO<sub>2</sub> in the absence of SO<sub>x</sub> (Chapel et al., 1999). During a test campaign performed with MEA on the Esbjerg pilot in Denmark, the solvent consumption was of 1.4 kg/ton CO<sub>2</sub> (Knudsen et al., 2009). In Germany, Moser et al. (2011b) reported a MEA consumption of 0.3 kg/ton CO<sub>2</sub> at the Niederaussem pilot without using any additives<sup>5</sup>.

However, the impact of degradation is not limited to solvent consumption. Degradation also has a direct influence on the emissions of the post-combustion capture process. Harmful degradation products may be released to the environment with the cleaned flue gas or under the form of liquid waste and thus worsen the process environmental penalty.

Furthermore, the decrease of the initial amine concentration and the apparition of degradation products also modify the solvent properties. This induces negative consequences on the operational as well as the capital expenditures of the process, increasing the capture cost. However, there still remains a large knowledge gap in characterizing the effects of degradation on solvent properties. Based on the experience of CO<sub>2</sub> removal from hydrocarbon streams, various negative effects have been reported by Bedell (2009):

- Decrease of the solvent absorption capacity due to the lower amine concentration. Moreover, acidic degradation products react with amine to form heat stable salts (HSS) that cannot be regenerated at usual stripper temperatures. This further reduces the free amine concentration.
- Change in the vapor-liquid equilibrium and in the solution alkalinity, leading to higher regeneration energy. This effect has been evidenced by Dubois (2013) in the case of degraded MEA.
- Increase of the solvent viscosity, inducing a higher pumping work and a less effective mass transfer in the absorption and regeneration columns.
- Apparition of environmentally harmful degradation products, both in the liquid and gaseous phases. This induces additional costs for the recovery of degradation products and for a proper waste management.
- Apparition of foaming (Thitakamol and Veawab, 2008) and fouling in the columns due to the modifications of the solution properties.

---

<sup>5</sup> MEA consumption may be due to degradation or to solvent emission to the atmosphere. In the case of Knudsen et al. (2009) and Moser et al. (2011b), negligible MEA emissions were recorded in the gas phase, so that the MEA loss was mainly attributed to degradation. This is in agreement with the degradation products balance presented by Moser et al. (2011b).

- Increase of the solution corrosivity due to the presence of acids and chelating agents among the degradation products. This last point has an impact on the choice of the pipe and column materials, and consequently on the capital costs.

The present chapter describes the experimental results obtained regarding the degradation of 30 wt% MEA in water. First, the state of the art about solvent degradation is presented, with a description of the main degradation mechanisms and of the influence of dissolved metals on degradation. Indeed, metals have been reported to strongly influence the degradation rate of amine solvents. Possible answers that have been proposed to reduce the negative influence of solvent degradation on the process are also presented. Then, the methods used for the semi-batch experiments on the degradation test rig, for the thermal degradation experiments (batch reactors) and the analytical procedures are described. Finally, the experimental results of semi-batch and thermal experiments are presented and discussed. These results will be used in the next chapter dedicated to the modeling of post-combustion capture with assessment of solvent degradation.

## 2. State of the art

In this section, the different degradation mechanisms of amine solvents are described. Then, a summary of the main research studies performed in the field of MEA degradation is presented. The influence of dissolved metals on solvent degradation is also discussed. Finally, current solutions to reduce the negative effects of degradation are presented.

### 2.1 Degradation mechanisms

Depending on the operating conditions that the amine solvent faces, different degradation mechanisms can take place. These degradation mechanisms may occur simultaneously, leading to the formation of various degradation products. Four main degradation types have been identified in the case of aqueous MEA (Epp et al., 2011):

- **Thermal decomposition.** With the only effect of temperature, MEA degrades and decomposes above 200°C (Dow, 2003). This type of degradation is usually not observed in CO<sub>2</sub> capture conditions and will not be described in details.
- **Thermal degradation with CO<sub>2</sub>.** This type of degradation implies irreversible reactions between MEA and CO<sub>2</sub>. Such reactions are accelerated at high temperature, which is typically the case when the solvent is heated up in the stripper reboiler for regeneration (~120°C)<sup>6</sup>.
- **Oxidative degradation.** Oxidative degradation takes place due to the presence of oxygen in the flue gas. The contact between oxygen and the amine solvent is maximal in the absorber, but dissolved oxygen is also present in the solvent flowing to the stripper. Oxidative degradation is supposed to be a chain reaction catalyzed by the presence of dissolved metals (Bedell, 2011).
- **Reaction of MEA with flue gas contaminants SO<sub>x</sub> and NO<sub>x</sub>.** When not previously removed from the flue gas, SO<sub>x</sub> and NO<sub>x</sub> are hydrolyzed into inorganic acids in the absorber. These acids react with the amine via a reversible acid-base reaction to form salts.

Amine degradation leads to a large number and variety of degradation products. In the case of MEA, the main degradation products are summarized in figure 2.1 (based on Lepaumier et al., 2010). In most cases, the formation of these products can be explained based on the mechanisms of oxidative and thermal degradation with CO<sub>2</sub>. The main reaction pathways are described in the present section.

---

<sup>6</sup> Thermal degradation with CO<sub>2</sub> may also happen during the amine reclaiming process when the amine recovery is performed at high temperature (~150°C) as presented in section 2.4.

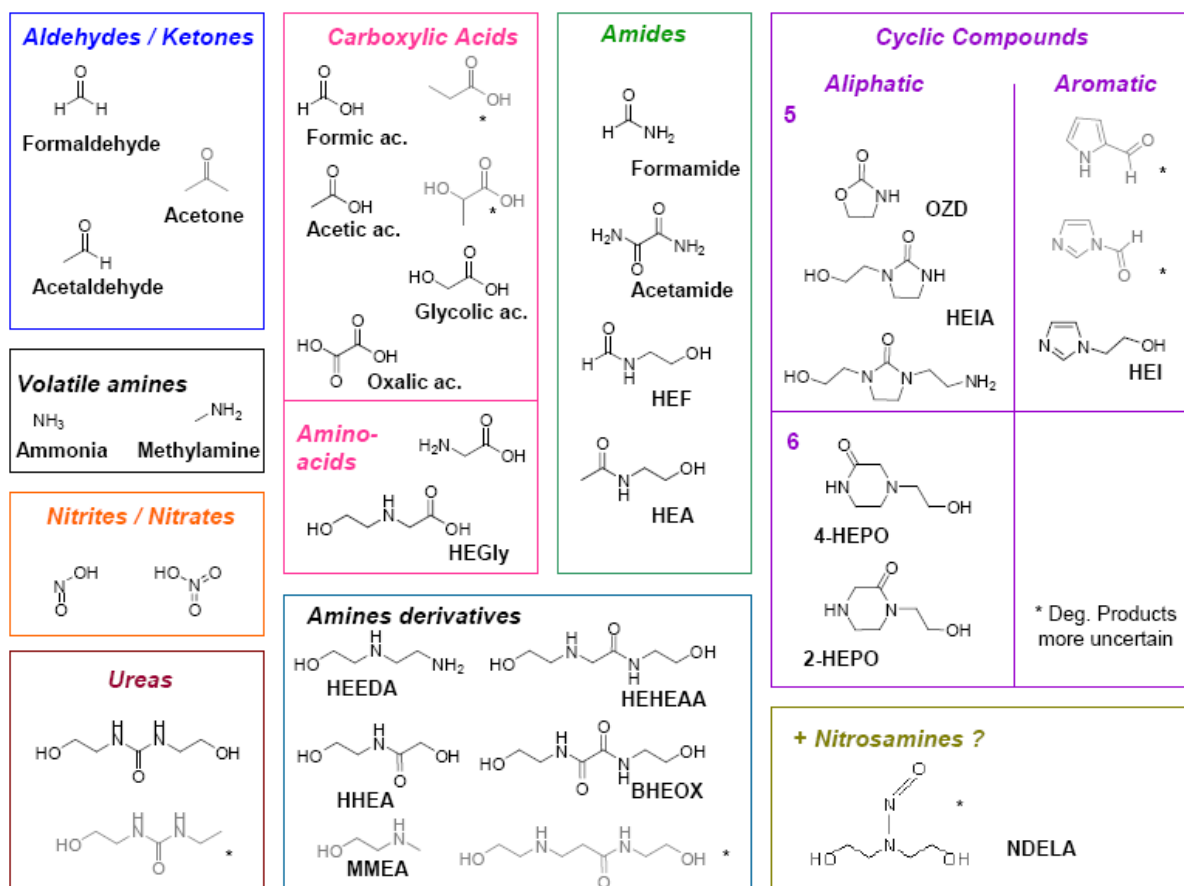


**Figure 2.1: degradation products of MEA**

### Thermal degradation with CO<sub>2</sub>

Thermal degradation with CO<sub>2</sub> implies irreversible reactions of amine with CO<sub>2</sub>. Interactions between gaseous CO<sub>2</sub> and the solvent are intentionally enhanced in the mass transfer columns so that MEA carbamates (HO-CH<sub>2</sub>-CH<sub>2</sub>-NH-COO<sup>-</sup>) are formed during the absorption. Those reactions are expected but carbamate species may further react at stripper temperatures, irreversibly forming degradation products.

In the presence of CO<sub>2</sub>, the main degradation products of MEA are HEIA (*N*-(2-hydroxyethyl)imidazolidone), HEEDA (2-(2-aminoethylamino)ethanol) and OZD (2-oxazolidinone) (Lepaumier, 2008). The oxazolidinone is an intermediate product formed by cyclisation of the amine carbamate as described in figure 2.2.

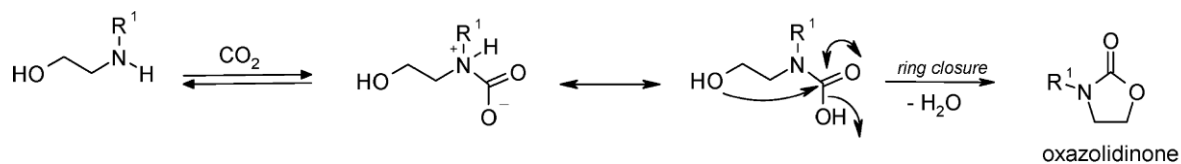


**Figure 2.2: oxazolidinone formation mechanism from MEA carbamate (R<sup>1</sup>=H)**

However, the oxazolidinone is not very stable and reacts with MEA to form an addition product called HEEDA. HEEDA can further react with CO<sub>2</sub> to form a carbamate that undergoes cyclisation (figure 2.3). This leads to HEIA, an imidazolidinone that is the main product of MEA thermal degradation with CO<sub>2</sub>.

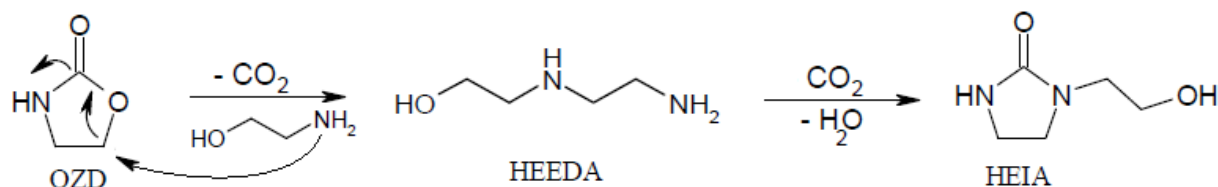
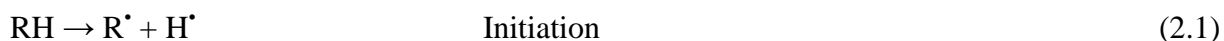


**Figure 2.3: imidazolidinone formation from oxazolidinone**

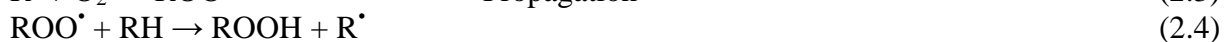
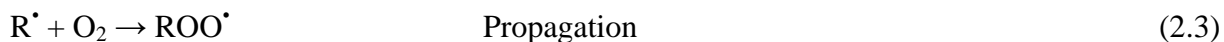
HEIA contributes to 65.5% of the identified degradation products of MEA thermal degradation under  $\text{CO}_2$ . HEEDA and OZD contribute respectively to 14.2% and 1.6% (Lepaumier, 2008). Remaining identified degradation products are a second MEA addition product and its corresponding imidazolidinone.

### *Oxidative degradation*

Most authors agree on the fact that oxidative degradation is a free radical chain reaction (Lepaumier, 2008; Bedell, 2011; Voice and Rochelle, 2011a). Free-radical chain reactions can be described by initiation, propagation and termination steps. During the initiation step, a free radical is formed by the cleavage of a homolytic covalent bond. This initiation may be due to temperature, light, or metal catalyst (Delfort et al., 2011).



The generated radicals may then react with oxygen to form peroxy radicals, which further react with a C-H bond via a hydrogen abstraction reaction, generating hydroperoxides. The chain reaction can further progress via the cleavage of hydroperoxides into two radicals (Delfort et al., 2011).



The termination step is the recombination of two radicals to form a stable molecule: the degradation product. In the case of MEA, the main degradation products are ammonia and carboxylic acids like formic, acetic, glycolic and oxalic acids (Voice and Rochelle, 2011a). Figure 2.4 summarizes this free radical chain reaction in the case of MEA (Delfort et al., 2011).

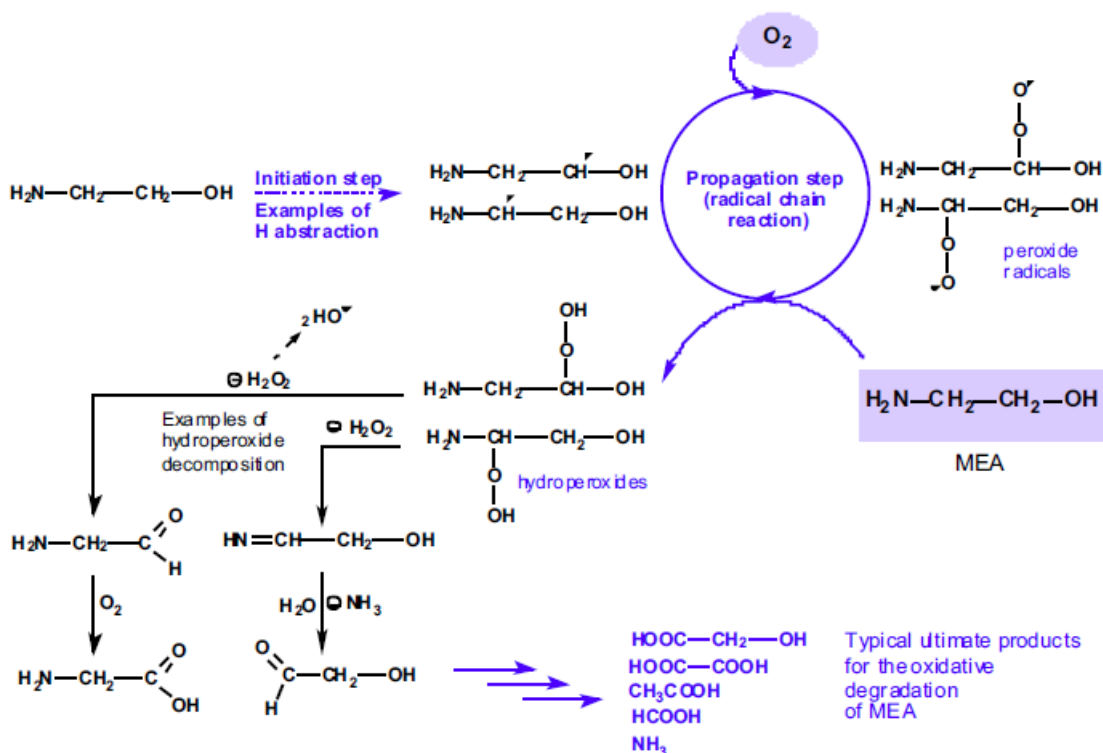


Figure 2.4: free radical chain reaction for MEA (Delfort et al., 2011)

Organic acids form heat stable salts (HSS) with MEA. They can also further react by dehydration with MEA and lead to other degradation products that have been identified in degraded MEA solutions (HEF, HEA, HEHEEA and BHEOX, see abbreviation list). The formation pathways are inspired by those presented by Lepaumier et al. (2011).

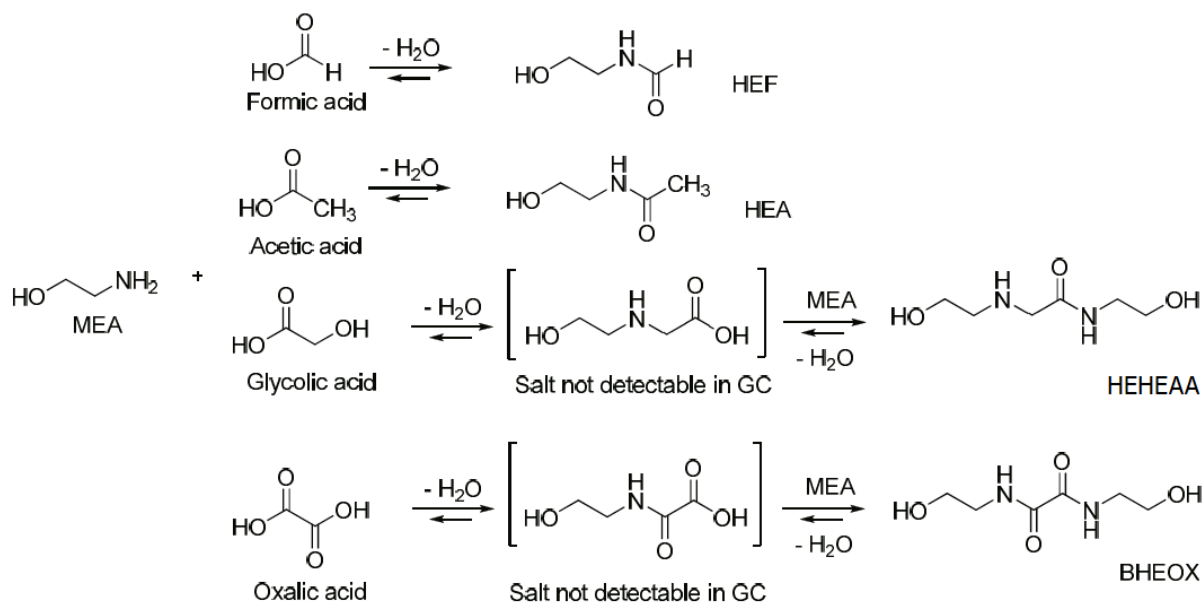
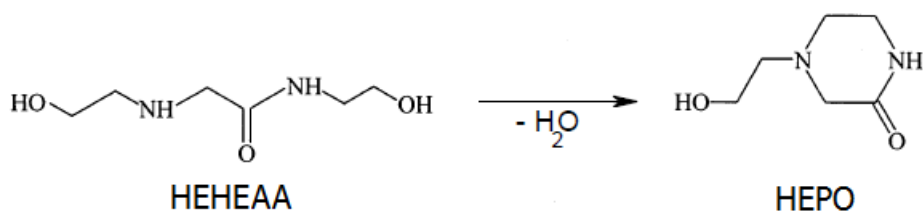


Figure 2.5: MEA degradation reactions with organic acids

Then, HEPO (4-(2-hydroxyethyl)piperazin-2-one) has been identified as a further important degradation product of MEA oxidative degradation. It may be formed by the cyclisation of HEHEEA (*N*-(2-hydroxyethyl)-2-(2-hydroxyethylamino)acetamide) (Strazisar et al., 2003).





**Figure 2.6: formation of HEPO**

Finally, HEI (*N*-(2-hydroxyethyl)imidazole) is a major degradation product of MEA and its formation pathway is still uncertain (Lepaumier et al., 2011). Voice et al. (2012) have proposed a condensation mechanism between two oxidative degradation products, a MEA/glyoxal imine and methanimine. This mechanism is represented in figure 2.7.

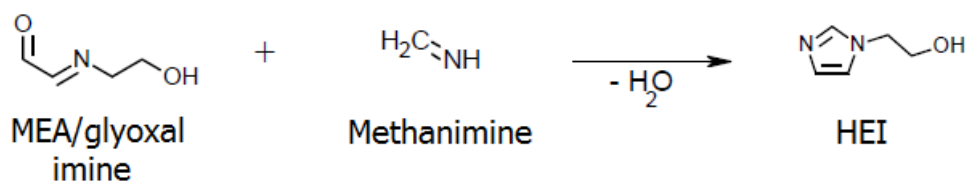


**Figure 2.7: formation of HEI (Voice et al., 2012)**

#### *Reaction of MEA with flue gas contaminants*

Similarly to MEA reacting with CO<sub>2</sub> to form carbamate salts, MEA can also react with SO<sub>2</sub>, NO and NO<sub>2</sub> contaminants present in the flue gas. During the absorption, these contaminants form inorganic acids in the solvent solution and react with MEA to form salts. Contrarily to heat stable salts resulting from MEA oxidative degradation, MEA salts formed with SO<sub>x</sub> and NO<sub>x</sub> can be recovered by reversing the reaction at high temperature (Epp et al., 2011).

Then, the formation of nitrosamines has raised concern in the last decade since those compounds are known carcinogens. Primary amines usually do not lead to the formation of stable nitrosamines (Challis and Challis, 1982). However, DEA is a secondary amine that may be present as an impurity in fresh MEA solutions or appear as a degradation product of MEA. In the presence of NO<sub>x</sub> (especially NO and NO<sub>2</sub>), DEA is susceptible to be nitrosated to a stable nitrosamine. Three nitrosamines (NDELA, NDMA and NMOR) have been detected in the case of MEA degradation with NO<sub>x</sub>. NDELA was the main nitrosamine formed (Fostås et al., 2011). Degradation pathways are detailed by Fostås et al. (2011).

However, SO<sub>x</sub> and NO<sub>x</sub> degradation will not be further detailed in this work, since gas cleaning steps taking place before CO<sub>2</sub> capture are able to remove flue gas contaminants to a large extent. Indeed, Moser et al. (2011a) report SO<sub>x</sub> and NO<sub>x</sub> concentrations of respectively 93 and 190 mg/m<sup>3</sup> after flue gas cleaning.

#### *MEA degradation in industrial CO<sub>2</sub> capture conditions*

Lepaumier et al. (2011) compared degraded MEA from pilot plant with thermal/oxidative degraded MEA from lab experiments. They did not study degradation with flue gas contaminants since the pilot plant was equipped with SCR and FGD units to clean the flue gas. The GC spectra presented in figure 2.8 compare pilot plant degraded MEA with lab samples. Detected degradation products are listed in table 2.1. Their respective number corresponds to the peak number in the GC spectra.

All oxidative degradation products detected in the lab experiments were detected in the pilot plant sample as well. On the contrary, thermal degradation products were less present in industrial degraded samples. Based on these observations, it seems that oxidative degradation is the dominant degradation mechanism in CO<sub>2</sub> capture at pilot scale.

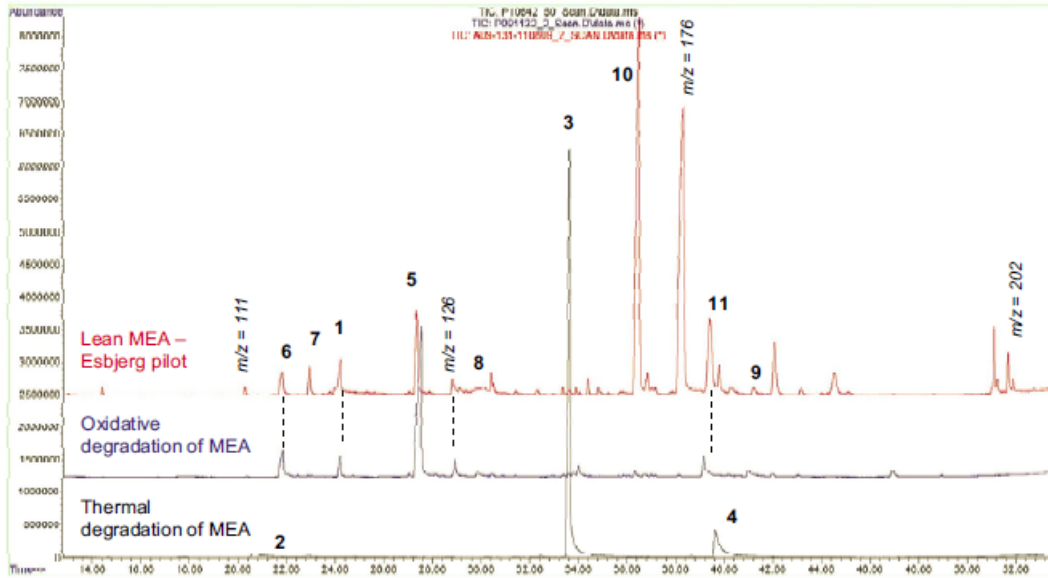


Figure 2.8: comparison of GC-MS spectra: lab and pilot degraded MEA samples (Lepaumier et al., 2011)

Table 2.1: degradation products detected by GC (Lepaumier et al., 2011)

| 1   | 2     | 3    | 4      | 5   | 6   | 7   | 8    | 9     | 10   | 11     |
|-----|-------|------|--------|-----|-----|-----|------|-------|------|--------|
| OZD | HEEDA | HEIA | AEHEIA | HEI | HEF | HEA | HHEA | BHEOX | HEPO | HEHEAA |

## 2.2 Main studies published about MEA degradation

Although the first studies of amine degradation were performed in the sixties, most of the works in this field were published during the last decade. Two research groups have been particularly active in this field for more than ten years: the University of Regina in Saskatchewan, Canada (URegina) and the University of Texas at Austin in the USA (UT Austin). Their main research interests are listed in tables 2.2 and 2.3. Other studies are presented in table 2.4, mainly reported by European research groups like the Norwegian University of Science and Technology (NTNU) and the French research institute IFP Energies Nouvelles (IFPEN). The main operating conditions for the study of MEA degradation are:

- the gas feed mode that can be discontinuous (batch mode) or continuous (semi-batch),
- the agitation rate in case of stirred reactors,
- the solvent volume (or flow rate in case of solvent loop),
- the temperature range,
- the gas feed pressure and composition,
- the experiment duration,
- the main analytical methods used to characterize the amine solvent and/or its degradation products.

Experimental study of amine solvent degradation

**Table 2.2: research interests and operating parameters at the University of Regina, Canada (n.a.: not applicable; n.s.: not specified)**

| Reference                                    | Research interest   | Gas feed   | Agitation (rpm) | Solvent volume | T (°C)  | P (bar)<br>Gas composition  | Run time (days) | Analysis          |
|--|---|--|-----------------|----------------|---------|---|-----------------|-------------------|
| Supap et al., 2001                           | Influence of solvent concentration, O <sub>2</sub> , temperature and agitation on MEA degradation kinetics  |  | 300             | 230 mL         | 120-150 | 2.41-3.45<br>O <sub>2</sub>   | 2-12            | GC-MS             |
| Bello and Idem, 2005                         | Influence of O <sub>2</sub> , CO <sub>2</sub> , temperature, MEA concentration on degradation; pathways of degradation reactions  |  | 300             | 230 mL         | 55-120  | 2.5-3.5<br>O <sub>2</sub> /CO <sub>2</sub>                              | 6-30            | GC-MS             |
| Lawal and Idem, 2005&2006; Lawal et al. 2005 | Influence of O <sub>2</sub> , CO <sub>2</sub> , presence of MDEA, temperature, MEA concentration on degradation; pathways of degradation reactions; ecotoxicity   |  | 500             | 450 mL         | 55-120  | 2.5<br>O <sub>2</sub> /CO <sub>2</sub>                                  | 6-30            | GC-MS, HPLC       |
| Bello and Idem, 2006                         | Influence of the corrosion inhibitor NaVO <sub>3</sub> on degradation kinetics  |  | 300             | 230 mL         | 55-120  | 3.5-4.5<br>O <sub>2</sub> /CO <sub>2</sub>                              | 6-30            | HPLC              |
| Supap et al., 2006                           | Analytical techniques: comparison and methods   | Discontinuous gas feed to compensate for pressure decrease | 500             | 450 mL         | 55-120  | 2.5-4.5<br>O <sub>2</sub> /CO <sub>2</sub>                              | 18-24           | GC-MS, HPLC, CE   |
| Uyanga and Idem, 2007                        | Influence of the corrosion inhibitor NaVO <sub>3</sub> and of SO <sub>2</sub> on degradation kinetics   | Discontinuous gas feed to compensate for pressure decrease | 505             | 450 mL         | 55-140  | 2.5<br>O <sub>2</sub> /N <sub>2</sub> /CO <sub>2</sub> /SO <sub>2</sub> | 5-10            | HPLC              |
| Supap et al., 2009                           | Kinetics of O <sub>2</sub> and SO <sub>2</sub> -induced degradation   |  | 500             | 450 mL         | 55-120  | 2.5<br>O <sub>2</sub> /N <sub>2</sub> /CO <sub>2</sub> /SO <sub>2</sub> | 6-13            | HPLC              |
| Supap et al., 2011a                          | Study of degradation inhibitors in the presence of O <sub>2</sub> , CO <sub>2</sub> and SO <sub>2</sub>   |  | 500             | 450 mL         | 120     | 2.5<br>O <sub>2</sub> /N <sub>2</sub> /SO <sub>2</sub>                  | n.s.            | HPLC              |
| Supap et al., 2011b                          | Influence of organic acids on further MEA degradation   |  | 500             | 450 mL         | 120     | 1-3<br>O <sub>2</sub> /N <sub>2</sub>                                   | 7               | GC-MS, CE         |
| Chanchev et al., 2011; Saiwan et al., 2013   | Influence of operating parameters (including O <sub>2</sub> , H <sub>2</sub> SO <sub>4</sub> , HNO <sub>3</sub> , MEA concentration, CO <sub>2</sub> , temperature) on the kinetics of NH <sub>3</sub> formation and on VOC formation |  | 500             | 450 mL         | 55-120  | 2.5<br>O <sub>2</sub> /CO <sub>2</sub>                                  | 7               | GC-TCD, GC-MS, CE |

Experimental study of amine solvent degradation

**Table 2.3: research interests and operating parameters at the University of Texas at Austin (n.a.: not applicable; n.s.: not specified)**

| Reference                                      | Research interest  | Gas feed                             | Agitation (rpm) | Solvent volume | T (°C)      | P (bar)<br>Gas composition   | Run time                         | Analysis                        |
|--|--|--------------------------------------|-----------------|----------------|-------------|--|----------------------------------|---------------------------------|
| Chi and Rochelle, 2001 & 2002                  | Influence of CO <sub>2</sub> -loading and inhibitors on NH <sub>3</sub> production rate  | Continuous<br>5 L/min                | 0               | 500 mL         | 55          | Atmospheric<br>Air/N <sub>2</sub> /CO <sub>2</sub>   | up to 8 hours                    | FTIR                            |
| Goff and Rochelle 2004; Goff, 2005             | Importance of O <sub>2</sub> -mass transfer and agitation rate; influence of Fe-Cu and of the presence of degradation products on degradation kinetics | Continuous<br>8 L/min                | 0-1450          | 550 g          | 55          | Atmospheric<br>Air/CO <sub>2</sub>   | 8-17 hours                       | FTIR                            |
| Goff and Rochelle, 2006                        | Test of oxidative degradation inhibitors for Fe-Cu catalyzed degradation   | Continuous<br>8 L/min                | 1400            | 550 g          | 55          | Atmospheric<br>Air/CO <sub>2</sub>   | n.a.                             | FTIR, TIC                       |
| Sexton, 2008; Sexton and Rochelle, 2009 & 2011 | Influence of gas flow rate; influence of dissolved metals and inhibitors on degradation; test of MEA-PZ blends; amine screening                        | Continuous<br>0.1 to<br>7.5 L/min;   | 1400            | 350-<br>400 mL | 55          | Atmospheric<br>Low flow:CO <sub>2</sub> /O <sub>2</sub><br>High flow:<br>Air/N <sub>2</sub> /CO <sub>2</sub> | 12-15 days                       | FTIR, IC (AC&CC), HPLC          |
| Davis and Rochelle, 2009; Davis, 2009          | Thermal degradation of different amines; influence of temperature, pressure and amine concentration on thermal degradation; degradation kinetics       | Batch                                | 0               | 10 mL          | 100-<br>150 | 1-8 bar<br>Vapor<br>pressure+CO <sub>2</sub>   | Few days<br>to several<br>months | IC (CC), HPLC, MS               |
| Voice and Rochelle, 2011a, 2011b & 2011c       | Oxidative degradation of various amines; influence of temperature, dissolved metals and inhibitors on degradation                                      | Continuous<br>5 L/min                | 1440            | 350 mL         | 40-70       | Atmospheric<br>Air/CO <sub>2</sub>   | 2-7 days                         | FTIR, IC (AC&CC)                |
| Voice and Rochelle, 2013                       | Influence of process variables on MEA degradation; influence of dissolved metals; degradation kinetics; degradation products                           | Continuous<br>0.1 to<br>7.65 mL/min; | 1440            | 350-<br>400 mL | 40-70       | Atmospheric<br>Low flow:CO <sub>2</sub> /O <sub>2</sub><br>High flow: Air/CO <sub>2</sub>                    | 2-14 days                        | FTIR, IC (AC&CC), HPLC, TOC, TN |

Experimental study of amine solvent degradation

**Table 2.4: research interests and operating parameters of other research groups (n.a.: not applicable; n.s.: not specified)**

| Reference(s)/<br>Main affiliation or<br>project name                                 | Research interest   | Gas feed                               | Agitation<br>(rpm)          | Solvent<br>volume       | T (°C)                | P (bar) <sup>7</sup><br>Gas<br>composition                 | Run<br>time       | Analysis                       |
|--|---|--|-----------------------------|-------------------------|-----------------------|--|-------------------|--------------------------------|
| Blachly and Ravner,<br>1965a, 1965b/ US Navy   | Influence of dissolved metals and inhibitors on MEA degradation; experience gained from submarine applications of CO <sub>2</sub> capture | Batch/continuous<br>300 mL/min         | 0                           | 300 mL<br>50 mL         | 55-98;<br>138-<br>149 | n.s.<br>Air/O <sub>2</sub> /CO <sub>2</sub>                | up to 6<br>weeks  | Kjeldahl TN;<br>titration      |
| Strazisar, 2003/<br>NETL, US DOE   | Analysis of reclaimer waste solutions from a commercial CO <sub>2</sub> capture plant; proposition of degradation pathways                | n.a.                                   | n.a.                        | n.a.                    | n.a.                  | n.a.   | n.a.              | GC-MS, GC-<br>FTIR, IC, ICP    |
| Notz et al., 2007; Notz,<br>2009/ University of<br>Stuttgart                         | Degradation screening of amines in the framework of the Cesar program   | Continuous<br>10-20 NmL/min            | 560-600                     | 350 g                   | 40-120                | 1-4<br>N <sub>2</sub> /O <sub>2</sub> /CO <sub>2</sub>     | 14 days           | GC-FID,<br>NMR                 |
| Knudsen et al., 2007 and<br>2009; Mertens et al.,<br>2013/ Dong Energy,<br>Laborelec | Emission results from test campaigns on the Esbjerg pilot (CASTOR and CESAR programs)   | Continuous<br>5,000 Nm <sup>3</sup> /h | mass<br>transfer<br>columns | 20<br>m <sup>3</sup> /h | 40-125                | Up to 2 bar<br>Coal power<br>plant flue gas                | several<br>months | GC,<br>Titration,<br>ICP, FTIR |
| Lepaumier, 2008;<br>Lepaumier et al.,<br>2009a, b, c/ IFPEN                          | Degradation pathways and products for different amines  | Batch                                  | 250                         | 40 mL                   | 140                   | 20<br>O <sub>2</sub> /CO <sub>2</sub> /N <sub>2</sub> /Air | 15 days           | GC-MS,<br>NMR                  |
| Eide-Haugmo et al.,<br>2011; Lepaumier et al.,<br>2011/ NTNU                         | Thermal stability of different amines   | Batch                                  | 0                           | 7 mL                    | 135                   | n.s.<br>vapor pressure<br>+CO <sub>2</sub>                 | 5<br>weeks        | LC-MS                          |

<sup>7</sup> In case of both batch and semi-batch experiments, the gas pressure and composition are related to the continuous gas feed mode

Experimental study of amine solvent degradation

**Table 2.4: continued (n.a.: not applicable; n.s.: not specified)**

| Reference(s)/<br>Main affiliation or<br>project name                      | Research interest   | Gas feed                               | Agitation<br>(rpm)          | Solvent<br>volume          | T (°C) | P (bar)<br>Gas<br>composition  | Run<br>time           | Analysis                        |
|---|---|--|-----------------------------|----------------------------|--------|--|-----------------------|---------------------------------|
| Bedell 2009 and 2011/<br>Dow Chemical;<br>Vevelstad et al., 2011/<br>NTNU | Theoretical studies about MEA degradation;<br>degradation pathways; degradation products  | n.a.                                   | n.a.                        | n.a.                       | n.a.   | n.a.   | n.a.                  | n.a.                            |
| Lepaumier et al., 2011/<br>NTNU   | Comparison between pilot and lab degraded MEA;<br>products and pathways for thermal and oxidative<br>degradation                              | Batch/continuous<br>357.5 mL/min       | n.s.                        | n.s.                       | 55-135 | atmospheric<br>Air/CO <sub>2</sub>                                       | 5<br>weeks;<br>9 days | LC-MS, GC-<br>MS                |
| Epp et al., 2011/<br>TU Dortmund  | Influence of flue gas contaminants on amine<br>degradation  | Batch/continuous<br>1 L/min            | n.s.                        | 60 g                       | n.s.   | n.s.<br>N <sub>2</sub> /O <sub>2</sub> /SO <sub>2</sub> /NO              | 100 h                 | Colorimetry                     |
| Fostås et al., 2011/<br>Statoil   | Influence of NO <sub>x</sub> on solvent degradation,<br>absorption-regeneration unit; study of reaction<br>pathways for nitrosamine formation | Continuous<br>30 Nm <sup>3</sup> /h    | mass<br>transfer<br>columns | 0.04<br>m <sup>3</sup> /h  | 44-120 | n.s.<br>N <sub>2</sub> /O <sub>2</sub> /CO <sub>2</sub> /NO <sub>x</sub> | 124 h                 | FTIR, LC-MS,<br>GC-MS           |
| Moser et al., 2011b/<br>RWE   | Emission results from test campaigns at the<br>Niederaussem pilot   | Continuous<br>1,550 Nm <sup>3</sup> /h | mass<br>transfer<br>columns | 3.5-6<br>m <sup>3</sup> /h | 40-120 | Atmospheric<br>Power plant flue<br>gas                                   | 5000 h                | GC-MS,<br>HPLC,<br>titration... |
| Delfort et al., 2011/<br>IFPEN  | Evaluation of inhibitors for MEA oxidative<br>degradation   | Continuous<br>116 NmL/min              | 1000-<br>1300               | 100 mL                     | 80     | Atmospheric<br>Air/CO <sub>2</sub>                                       | 7 days                | FTIR, IC                        |

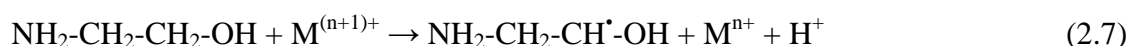
### 2.3 Influence of dissolved metals

Several works have reported that the presence of dissolved metals like iron (Fe), copper (Cu), chromium (Cr), nickel (Ni), manganese (Mn) and vanadium (V) catalyzes solvent degradation. Fe, Cr, Ni and Mn may leach from columns and pipes walls, and Cu and V are sometimes deliberately added to amine solutions as corrosion inhibitors. Table 2.5 lists the main studies about the effects of dissolved metals on amine degradation. Most of them have been performed at the UT Austin. The detailed results of this literature review can be found in appendix 1. In the present section, the main results are summarized.

First, the influence of metals on MEA degradation has only been studied for oxidative degradation and thermal degradation with CO<sub>2</sub>. No published results could be found about the influence of metals on thermal decomposition or on MEA reactions with flue gas contaminants. In the case of MEA thermal degradation with CO<sub>2</sub>, different studies have evidenced that the presence of metal has no influence on the degradation.

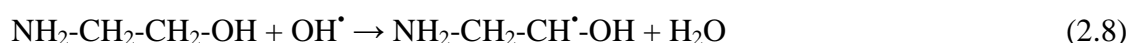
On the contrary, dissolved metals play a major role in oxidative degradation. Indeed, the presence of metals catalyzes the formation of free radicals, and thus the initiation of chain reactions. Bedell (2009, 2011) proposes three main pathways:

- Direct one-electron oxidation by a metal ion:



This reaction proceeds via the formation of a complex between MEA and the metal or between MEA, O<sub>2</sub> and the metal. The generation of MEA radicals initiates the chain reaction. Formation of metals complexes was observed by Kumar (1982) in the case of Ag<sup>2+</sup> with MEA. Bedell (2011) also reported complexes of Fe<sup>2+</sup> and Cu<sup>+</sup> with various amines.

- Hydrogen abstraction by a hydroxyl radical:



In this case, metals facilitate the propagation steps by catalyzing the generation of radicals from hydroperoxide as presented in figure 2.9 (Voice and Rochelle, 2011b).

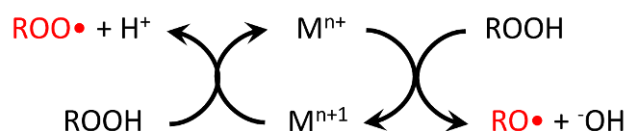


**Figure 2.9: decomposition of hydroperoxides by catalytic action of metals**

Moreover, the presence of hydroperoxides is also due to the catalytic action of metals. For instance, Bedell (2011) proposes following reactions with iron:



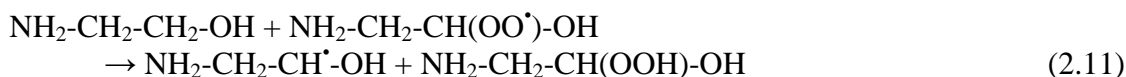
**Table 2.5: studies about metal effects on MEA degradation**

| Reference/<br>Affiliation                   | Research interest  | Metal   | Degradation<br>tracer                                    |
|---|--|---|--|
| Blachly and Ravner,<br>1965a/US Navy        | Stability of MEA solutions containing degradation inhibitors   | Fe <sup>0</sup> , Fe <sup>2+</sup> , Fe <sup>3+</sup> , Cr <sup>0</sup> ,<br>Cr <sup>6+</sup> , Ni <sup>0</sup> , Ni <sup>2+</sup> , Cu <sup>2+</sup> | NH <sub>3</sub> , Kjeldahl<br>TN, peroxides              |
| Blachly and Ravner,<br>1965b/US Navy        | Case study of a CO <sub>2</sub> capture process in submarines  | Undesired presence<br>of Fe and Cu <sup>a</sup>   | Kjeldahl TN,<br>MEA                                      |
| Kumar, 1982/<br>University of Notre<br>Dame | Effect of silver on complexation and oxidation of ethanolamines and diols                                      | Ag <sup>2+</sup>  | n.s.   |
| Chi and Rochelle,<br>2002/ UT Austin        | Effect of iron and of several degradation inhibitors on MEA oxidation  | Fe <sup>2+</sup> , Fe <sup>3+</sup> , Mn <sup>7+</sup>  | NH <sub>3</sub>  |
| Goff and Rochelle,<br>2003/ UT Austin       | Oxidative degradation of MEA at absorber conditions  | Fe <sup>2+</sup> , Cu <sup>2+</sup>   | NH <sub>3</sub>  |
| Goff and Rochelle,<br>2004/ UT Austin       | O <sub>2</sub> mass transfer effects   | Fe <sup>2+</sup> , Cu <sup>2+</sup>   | NH <sub>3</sub>  |
| Goff and Rochelle,<br>2006/ UT Austin       | Oxidation inhibitors for copper and iron catalyzed degradation   | Fe <sup>2+</sup> , Cu <sup>2+</sup> , Mn <sup>2+</sup> ,<br>Mn <sup>7+</sup>  | NH <sub>3</sub>  |
| Bello and Idem,<br>2006/ URegina            | Effect of corrosion inhibitor NaVO <sub>3</sub> on MEA oxidative degradation                                   | V <sup>5+</sup>   | MEA  |
| Sexton and Rochelle,<br>2006/ UT Austin     | Oxidation products of amines in CO <sub>2</sub> capture  | Cu <sup>2+</sup> , Fe <sup>3+</sup> , V <sup>5+</sup>   | organic acids,<br>EDA, NO <sub>2</sub> , NO <sub>3</sub> |
| Uyanga and Idem,<br>2007/ URegina           | Effect of corrosion inhibitor NaVO <sub>3</sub> on MEA O <sub>2</sub> and SO <sub>2</sub> -induced degradation | V <sup>5+</sup>   | MEA  |
| Sexton and Rochelle,<br>2009/ UT Austin     | Catalysts and inhibitors for MEA oxidation   | Cu <sup>2+</sup> , Cr <sup>3+</sup> , Ni <sup>2+</sup> , Fe <sup>2+</sup> ,<br>V <sup>5+</sup>  | NH <sub>3</sub> , carboxylic<br>acids, ...               |
| Davis, 2009/ UT<br>Austin                   | Effect of metals on MEA thermal degradation  | Cu, Cr, Ni, Fe, V   | MEA, HEEDA   |
| Captech, 2007                               | Effect of iron on MEA degradation  | Fe <sup>a</sup>   | n.s.   |
| Voice and Rochelle,<br>2011a/ UT Austin     | Oxidation of different amines at absorber conditions   | Fe <sup>2+</sup> , Cr <sup>3+</sup> , Ni <sup>2+</sup> ,  | NH <sub>3</sub> , MEA                                    |
| Voice and Rochelle,<br>2011b/ UT Austin     | Inhibitors screening with hot gas FTIR   | Fe <sup>2+</sup> , Cu <sup>2+</sup> , Mn <sup>2+</sup> , V,<br>Cr, Ni, Ti, Mo, Co, Sn,<br>Se, Ce, Zn <sup>a</sup>                                     | NH <sub>3</sub>  |
| Voice and Rochelle,<br>2011c/ UT Austin     | Catalysts and inhibitors screening for MEA oxidation   | Mn <sup>2+</sup> , Mn <sup>x+</sup> , Fe <sup>2+</sup> ,<br>Cr <sup>3+</sup> , Cu <sup>2+</sup> , V <sup>7+</sup>                                     | NH <sub>3</sub>  |

<sup>a</sup> Oxidation state not reported

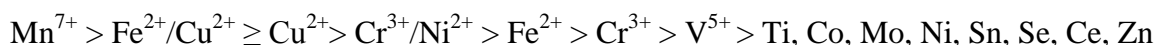


- Hydrogen abstraction by an organoperoxy radical:



where  $\text{NH}_2\text{-CH}_2\text{-CH}(\text{OO}\cdot)\text{-OH}$  is the reaction product of  $\text{NH}_2\text{-CH}_2\text{-CH}\cdot\text{-OH}$  and  $\text{O}_2$ . The MEA peroxide  $\text{NH}_2\text{-CH}_2\text{-CH}(\text{OOH})\text{-OH}$  further reacts to form stable degradation products.

Dissolved metals show varying potentials as catalysts for the oxidative degradation of MEA. Moreover, combinations of metals may increase the respective catalytic effects of the different metals, like in the presence of both iron and copper. Metals can be classified in decreasing order of oxidative potential as following:



$\text{Ag}^{2+}$  also shows an oxidative potential, but it has not been compared to other metals. On the contrary, it has been reported that  $\text{Mn}^{2+}$  has an inhibiting effect on degradation. This highlights the need for further studies to better understand metal catalyzed degradation pathways. Moreover, degradation products are observed in different proportions according to the metal catalyst used.

Finally, there is still a knowledge gap in the interactions between corrosion and degradation, inducing an important challenge for post-combustion  $\text{CO}_2$  capture. Indeed, there is a vicious circle between both phenomena. Degradation causes the apparition of corrosive products that corrode the pipe walls, thus releasing more metal ions into the solution. Considering that oxidative degradation is catalyzed by those metal ions, degradation is then worsened by the corrosion and vice-versa.

## 2.4 Possible answers to amine degradation

Various solutions have been proposed to limit the influence of degradation on the operation of a  $\text{CO}_2$  capture plant. Usual solutions in commercial plants are referred to as reclaiming processes. They aim at purifying the amine solvent that contains degradation products. However, it is also possible to act preventively in order to avoid solvent degradation, which is the objective of degradation inhibitors.

### ***Reclaiming methods***

The most commonly used reclaiming methods are described below based on the work of Cummings et al. (2007).

- Solvent purge and make-up: as mentioned by Cummings et al. (2007), “this method might not be opposed by your amine supplier”. It is a simple and widely used solution in commercial  $\text{CO}_2$  capture processes but it implies a large consumption of fresh amine. Moreover, the purged solvent must be properly disposed of, inducing additional waste treatment costs and a low environmental efficiency.

- Thermal distillation<sup>8</sup>: the amine solvent is vaporized in a distillation column, and the non-volatile degradation products are recovered in the sump of the column. This is an interesting technique if the concentration of degradation products is high. There is less waste generated in comparison to the first method but the energy requirement of distillation is an important drawback in this method, especially for less degraded solutions. Thermal reclaiming may also induce additional thermal degradation with CO<sub>2</sub> since the temperature in the bottom of the reclaiming may reach 150°C.
- Neutralization: a strong base, usually NaOH is added to the solution. The undesired acid contaminant that has formed a salt with MEA associates with the strong base and releases the amine. This method limits the effect of degradation products, but does not remove them, so that solvent properties may remain affected. An interesting alternative to NaOH has been proposed by Xu and Rochelle (2009). KOH is used as the strong base, leading to the precipitation of K<sub>2</sub>SO<sub>4</sub> crystals easily removable from the solvent. However, this method mainly addresses heat stable salts so that non-ionic degradation products are unaffected.
- Ion exchange: the same principle as for neutralization is used. The undesired acid contaminant that has formed a salt with MEA is exchanged with a friendly anion brought into the system by a resin. This is an interesting method from the economic point of view, but it only addresses ionic degradation products.
- Electrodialysis: ionic degradation products migrate through ion-selective membranes placed in an electric field. The energy requirement of this technique is advantageous but it produces more waste than ion exchange.

Independently of their efficiency, these methods are only used with already degraded amine solvents, so that they do not prevent degradation. As a consequence, many negative effects induced by degradation are not addressed by such techniques.

### ***Degradation inhibitors***

The use of degradation inhibitors may be an interesting alternative to reclaiming techniques. Indeed, some chemicals show the ability of inhibiting amine degradation, especially oxidative degradation. This attractive approach prevents the formation of degradation products, so that the fresh amine consumption is reduced, as well as the waste volume. However, degradation inhibitors may modify the solvent properties, and more research is needed to assess this effect. Indeed, the biodegradability of amine solvents should be preserved in order to limit the environmental penalty of solvent emissions (either due to solvent volatility or to accidental release) so that a trade-off is necessary between solvent stability and environmental safety. In the present work, the addition of degradation inhibitors is the only solution tested to limit the degradation of MEA solutions, so that a special insight on this topic is given in this section.

The role of a degradation inhibitor is to prevent or minimize the solvent degradation during the CO<sub>2</sub> capture process. However, no degradation inhibitor has been proposed so far to prevent MEA thermal decomposition, thermal degradation with CO<sub>2</sub> or NO<sub>x</sub> degradation, and only few studies have considered SO<sub>2</sub> degradation. The reasons are the following:

---

<sup>8</sup> Thermal distillation may be performed under vacuum for low volatile amine. It is not the case for MEA.

- Thermal decomposition of MEA occurs at temperatures higher than 200°C (Epp et al., 2011), so that there is no need to consider it in usual CO<sub>2</sub> capture processes.
- Degradation due to CO<sub>2</sub> results from the CO<sub>2</sub> absorption in MEA, a mechanism that is desired, so that inhibiting this mechanism does not make much sense.
- Degradation with NO<sub>x</sub> and SO<sub>x</sub> has rarely been studied because of the low SO<sub>2</sub> and NO<sub>x</sub> content achievable in power plant flue gas.

As a consequence, most studies about degradation inhibitors address oxidative degradation. Oxidative degradation inhibitors may be separated into three main categories based on the oxidative degradation mechanisms described in section 2.1 (Bedell, 2009).

- Chelating agents: they form a complex with dissolved metals, inhibiting their catalytic activity and limiting the initiation/propagation steps of the chain reaction.
- Radical and O<sub>2</sub> scavengers: as presented in section 2.1, dissolved O<sub>2</sub> forms peroxides in water. Radical scavengers react with the peroxides to form stable products and stop the chain reaction. They are also called O<sub>2</sub> scavengers since they stoichiometrically react with dissolved O<sub>2</sub>. Disadvantage of many radical scavengers is that they are consumed during the reaction and must be renewed.
- Stable salts like KCl, KBr or KCOOH increase the ionic strength of water, so that the solubility of gases in the solvent decreases (Goff and Rochelle, 2006). However, these salts appeared to be poor inhibitors, decreasing the NH<sub>3</sub> production by only 15% in the best case. They will not be further considered.

A detailed bibliographic study has been performed to identify the most efficient inhibitors for MEA degradation. Table 2.6 lists the main works that have been conducted in this subject. Most of them have been conducted at the UT Austin, the University of Regina, and at the IFP Energies Nouvelles (IFPEN). However, many inhibitors presented in table 2.6 are ineffective, or even enhance MEA degradation. These unsuccessful inhibitors will not be further discussed. The detailed results of this bibliographic study are presented in appendix 2. The main conclusions can be summarized as following:

- Chelating agents and radical/O<sub>2</sub> scavengers are the two main types of degradation inhibitors. Depending on the operating conditions, both seem to be very promising inhibitors.
- Combination of different inhibitors may also lead to excellent inhibition effect. Chelating agent HEDP (Hydroxyethylidene diphosphonic acid) may advantageously be combined with radical scavengers Inhibitor A or DTPA (diethylenetriamine pentaacetic acid) to decrease the MEA oxidative degradation.
- Good results were also reported for DMTD (dimercaptotriadiazole) and DTPMP (diethylenetriamine pentamethylene phosphoric acid), which is less stable but that can also be used as a corrosion inhibitor.

**Table 2.6: studies about degradation inhibitors (effective inhibitors are in bold letters)**

| Reference/ Affiliation                 | Objectives of the study                                     | Degradation inhibitor   | Degradation tracer                    |
|--|---|---|---------------------------------------|
| Johnson and McElwain, 1964/ US Navy    | Stability of MEA solutions                                  | <b>Bicine, HEDTA, EDTA, NH<sub>4</sub>VO<sub>3</sub></b>  | NH <sub>3</sub> , solution alkalinity |
| Blachly and Ravner, 1965a/ US Navy     | Stability of MEA solutions                                  | <b>Bicine, EDTA</b> , sodium mercaptobenzo thiazole, disalicylal propylenediamine, p-acetylaminophenol, o-aminophenol, quinalizarin, bis-acetylacetene ethylenediimine, propyl gallate, sorbitol, n-dimethylglycine, phthaloylglycine, diethylcyclohexylamine | NH <sub>3</sub> , total N, peroxides  |
| Blachly and Ravner, 1965b/ US Navy     | Case study of CO <sub>2</sub> capture process in submarines | <b>Bicine, EDTA</b>   | Total N, MEA normality                |
| Singh, 1970a/ Union Carbide            | Patent on degradation inhibitor                             | <b>Triethanolamine</b>  | MEA                                   |
| Singh, 1970b/ Union Carbide            | Patent on degradation inhibitor                             | <b>Gluconate</b>  | MEA                                   |
| Faucher, 1989/ Honeywell UOP           | Patent on degradation inhibitor                             | <b>MDEA</b>   | HSS, solution alkalinity              |
| McCullough et al., 1990/ Honeywell UOP | Patent on degradation inhibitor                             | <b>MDEA-Sb</b>  | HSS, solution alkalinity              |
| Chi and Rochelle, 2002/ UT Austin      | Effect of iron and degradation inhibitors                   | <b>Bicine, EDTA</b> , glycine, formaldehyde, DMMEA  | NH <sub>3</sub>                       |
| Goff and Rochelle, 2003/ UT Austin     | Oxidative degradation of MEA at absorber conditions         | <b>EDTA</b> , bicine, MDEA, phosphate   | NH <sub>3</sub>                       |
| Goff and Rochelle, 2004/ UT Austin     | O <sub>2</sub> mass transfer effects                        | Formaldehyde  | NH <sub>3</sub>                       |
| Lawal and Idem, 2005/ URegina          | Oxidative degradation of MEA-MDEA blends                    | <b>MDEA</b>   | MEA, MDEA                             |

**Table 2.6: continued (effective inhibitors are in bold letters)**

| Reference/ Affiliation               | Objectives of the study  | Degradation inhibitor   | Degradation tracer                      |
|--------------------------------------|--|---|---|
| Lawal et al., 2005/ URegina          | Inhibitor effect of MDEA                                       | <b>MDEA</b>   | MEA, MDEA                               |
| Lawal and Idem, 2006/ URegina        | Oxidative degradation kinetics of MEA-MDEA                     | <b>MDEA</b>   | MEA, MDEA                               |
| Goff and Rochelle, 2006/ UT Austin   | Oxidation inhibitors for copper and iron catalyzed degradation | Hydroquinone, ascorbic acid, Mn salts, <b>inh. A</b> , <b>Na<sub>2</sub>SO<sub>3</sub></b> , <b>formaldehyde</b> , EDTA, Na <sub>3</sub> PO <sub>4</sub> , Na <sub>2</sub> S <sub>4</sub> , potassium salts | NH <sub>3</sub>                         |
| Sexton and Rochelle, 2006/ UT Austin | Oxidation products of amines in CO <sub>2</sub> capture        | <b>Inhibitor A</b>  | Carboxylic acids, EDA, nitrite, nitrate |
| Sexton and Rochelle, 2009/ UT Austin | Catalysts and inhibitors for MEA oxidation                     | <b>Inh. A</b> , <b>inh. B</b> , EDTA, formaldehyde, Na <sub>2</sub> SO <sub>3</sub> , formate   | NH <sub>3</sub> , carboxylic acids, ... |
| Carrette and Delfort, 2009a/ IFPEN   | Patent on degradation inhibitor                                | Hydroquinone, <b>cystamine</b> , <b>2-mercaptoethylether</b> , <b>1-thioglycerol</b> , <b>2-2'-thiodiethanol</b> , <b>2-2'-dithiodiethanol</b>  | HSS                                     |
| Carrette and Delfort, 2009b/ IFPEN   | Patent on degradation inhibitor                                | Hydroquinone, <b>2-2' thiodiacetic acid</b> , <b>2-2' dithiodiacetic acid</b> , <b>3-3'-thiodipropionic acid</b> , <b>3-3'-dithiodipropionic acid</b> , <b>thioglycolic acid</b>                            | HSS                                     |
| Carrette and Delfort, 2009c/ IFPEN   | Patent on degradation inhibitor                                | Hydroquinone, <b>5-5'-dithiobis(1,3,4-thiadiazole-2(3H)-thione)</b> , <b>DMTD</b>   | HSS                                     |
| Delfort and Carrette, 2009a/ IFPEN   | Patent on degradation inhibitor                                | Hydroquinone, <b>Zn-diethyldithiocarbamate</b> , <b>Na-diethyldithiocarbamate</b> , <b>Bis(dimethylthiocarbamyl)disulfide</b> , <b>O-O'-Diisopropyldithiobis(thioformate)</b>                               | HSS                                     |

**Table 2.6: continued (effective inhibitors are in bold letters)**

| Reference/ Affiliation               | Objectives of the study                                  | Degradation inhibitor  | Degradation tracer         |
|--------------------------------------|--|--|----------------------------|
| Delfort and Carrette, 2009b/ IFPEN   | Patent on degradation inhibitor                          | Hydroquinone, <b>potassium-O,O'-diethyldithiophosphate, ammonium-O,O'-diethyldithiophosphate</b>   | HSS                        |
| Carrette and Delfort, 2010/ IFPEN    | Patent on degradation inhibitor                          | Hydroquinone, <b>Na-L-cystine, Na-L-cystéine</b>   | HSS                        |
| Carrette and Delfort, 2011/ IFPEN    | Patent on degradation inhibitor                          | <b>Na<sub>2</sub>SO<sub>3</sub>, Na-1H-1,2,4-triazole-3-thiol, Na-4-methyl-4H-1,2,4-triazole-3-thiol, 5-methyl-4H-1,2,4-triazole-3-thiol, 4-isopropyl-4H-1,2,4-triazole-3-thiol, 4-phenyl-4H-1,2,4-triazole-3-thiol, 1-methyl-1H-tetrazole-5-thiol, 1-[2-(dimethyl amino)ethyl]-1H-tetrazole-5-thiol</b> | MEA, NH <sub>3</sub>       |
| Supap et al., 2011a/ URegina         | Inhibitors for oxidative and SO <sub>2</sub> degradation | <b>Na<sub>2</sub>SO<sub>3</sub>, K-Na-tartrate, EDTA, NH<sub>2</sub>OH</b>   | MEA                        |
| Lemaire et al., 2011/ IFPEN          | Optimized CO <sub>2</sub> capture process HiCapt+        | <b>U2, V1, V2, Y1</b>  | MEA, NH <sub>3</sub> , HSS |
| Delfort et al., 2011/ IFPEN          | Inhibitors for MEA oxidation                             | Hydroquinone, ascorbic acid, hindered phenols, p-benzoquinone, hindered amines, <b>V1-&gt;V8</b>   | MEA, NH <sub>3</sub> , HSS |
| Voice and Rochelle, 2011a/ UT Austin | Oxidation of amines at absorber conditions               | <b>Inhibitor A</b>   | NH <sub>3</sub> , MEA      |
| Voice and Rochelle 2011b/ UT Austin  | Inhibitors screening with hot gas FTIR                   | <b>MDEA, HEDP, Na<sub>2</sub>SO<sub>3</sub>, DTPA, DMTD, DTPMP, inh. A, citric acid, nitrilotriacetic acid, ...</b>  | NH <sub>3</sub>            |
| Voice and Rochelle 2011c/ UT Austin  | Catalysts and inhibitors screening for MEA oxidation     | Inh. <b>O, V, X, Y, Z</b>  | NH <sub>3</sub>            |

Finally, attention must also be paid at distinguishing degradation inhibitors from corrosion inhibitors. Corrosion inhibitors like Cu and  $\text{NaVO}_3$  reduce the corrosive effect of the MEA solution. However, they usually catalyze the oxidative degradation of MEA. On the contrary, degradation inhibitors may contribute to a better solvent stability, but more research is needed to assess their impact in pilot plant conditions and their influence on the solvent chemistry.

### 3. Experimental methods

The experimental study of solvent degradation for CO<sub>2</sub> capture is a new research field at the University of Liège that has started in the framework of the present work. This implied the development of an experimental test rig and procedures that are presented in this section. First, the semi-batch degradation test rig where most experiments were conducted is described. Then, the batch reactors used for the study of thermal degradation under CO<sub>2</sub> are also presented. Furthermore, it has been necessary to develop in-house analytical methods to characterize degraded solvents. Additional analyses on degraded samples were also performed by other laboratories. These analytical methods are also briefly described in this section.

#### 3.1 *Semi-batch degradation test rig*

It has been evidenced that degradation takes place in industrial CO<sub>2</sub> capture units. However, degradation reactions show a slow kinetics. For instance, pilot scale tests during the CASTOR project showed a decrease of the amine concentration by 4% in 45 days (Lepaumier, 2008). For practical reasons, it is necessary to accelerate degradation in order to get experimental data within a reasonable timeframe. However, experimental conditions should also remain as representative as possible of the real CO<sub>2</sub> capture conditions, so that degradation mechanisms are similar.

The degradation test rig (DTR) developed at the University of Liège is represented in figure 2.10. During the design process, a special attention has been paid to enable flexible operating conditions. The test rig is composed of five main parts:

1. Degradation reactor.
2. Gas supply.
3. Water balance control: gas saturator (3a) and condenser (3b).
4. Gas outlet and FTIR analysis (Fourier transform infra-red spectroscopy).
5. Data acquisition and control panel.



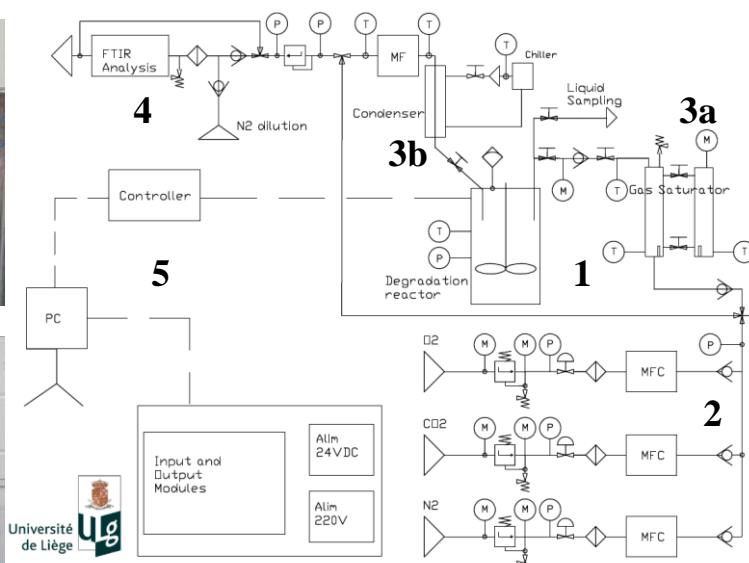
## Degradation reactor



## Gas saturator



## Gas supply



## Condenser



## FTIR



## Control Panel

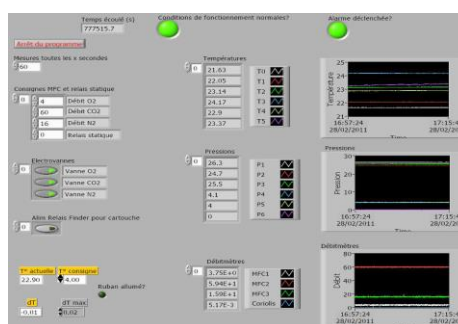


Figure 2.10: flowsheet of the degradation test rig

### Degradation reactor

The central part of the DTR is the degradation reactor. It is a stirred reactor model 4560 supplied by Parr Instrument Company. The reaction vessel is made of 316L stainless steel and has a capacity of 600 ml. Heating is performed by a heat mantle and pressure is regulated by a back-pressure regulator. The DTR has been proved and tested for operating at pressures up to 25 bar and temperatures up to 140°C. The agitation rate can reach up to 1400 rpm. A gas entrainment impeller combined with a hollow shaft agitator enhances the gas-liquid contact by recirculating gas from the reactor head into the liquid.

### ***Gas supply***

The DTR can be operated in batch or semi-batch mode depending on the gas feed mode (continuous gas flow or not)<sup>9</sup>. The gas feed is composed by mixing up to three different gases, usually O<sub>2</sub>, CO<sub>2</sub> and N<sub>2</sub>. The proportion of each gas can vary between 0 and 100%. The total gas flow rate can reach up to 1590 ml/min in normal conditions (0°C and 1 bar).

### ***Water balance control***

Because degradation experiments last for several days with continuous gas flow, it is important to pay attention at the water balance. Before entering the degradation reactor, the gas is saturated with water. Then, the gas exiting the reactor flows through a condenser where it is cooled down while the condensed water is recycled to the reactor. Without this equipment, the dry inlet gas would get loaded with water in the reactor and would quickly remove water from the system.

### ***Gas outlet and analysis***

The exhaust gas can be analyzed in an on-line FTIR analyzer before being released to the atmosphere. To prevent gas condensation in the pipes, the line between the back-pressure regulator and the FTIR analyzer is heated at 150°C. Moreover, the gas is diluted with hot nitrogen to facilitate the FTIR analysis.

### ***Data acquisition and control panel***

Two control systems are combined to operate the DTR. First, a controller provided with the reactor controls the temperature and the agitation rate of the reactor. Values are recorded on a computer. Then, other experimental parameters (other temperatures, pressures, mass flows) are acquired and controlled using a Labview<sup>®</sup> application.

### ***Experimental protocol***

First, 300 g of 30 wt% MEA solution is weighted into the reaction vessel. Then, CO<sub>2</sub> is blown into the closed reactor until the pressure starts to increase, which means that the CO<sub>2</sub> is not absorbed anymore<sup>10</sup>. The CO<sub>2</sub> loading of the solution lasts for approximately one hour at 390 Nml/min CO<sub>2</sub> and 400 rpm. The solution is then weighted and a 1.5 ml sample is taken. Then, the desired gas stream is sparged through the semi-batch reactor whose pressure is controlled by the back-pressure regulator. The degradation experiment starts when the heating it switched on.

In order to maintain the water balance during the experiment, the water temperature in the gas saturator is kept constant at 35°C. The temperature of cooling water for the condenser is regulated at 16.5°C<sup>11</sup>. The analysis of the outlet gas occurs on-line in the FTIR analyzer. Liquid phase is not analyzed on-line but a sampling port in the reactor head allows for liquid sampling during the experiment. Liquid samples are immediately cooled down and kept refrigerated to avoid further degradation. The experiments last for one or two weeks. At the end of the experiment, a liquid sample is collected. Then, the solution is cooled down to ambient temperature and degassed. It is weighted and stored at low temperature (~-4°C).

---

<sup>9</sup> On the liquid side, the DTR is always operated in batch mode.

<sup>10</sup> In case of experiments with no CO<sub>2</sub> in the flue gas, there is no previous CO<sub>2</sub> loading.

<sup>11</sup> The temperature difference between the saturator and the condenser is due to the pressure drop in the reactor that leads to a lower specific humidity of the saturated gas in the condenser.

A risk analysis about operating the DTR has been performed before the operation start. The results of this analysis are reported in appendix 3.

### *3.2 Batch degradation cylinders*

In order to test the thermal stability of amine solvents in the presence of CO<sub>2</sub>, experiments have also been conducted in batch conditions in smaller reactors. These batch reactors are 150 ml-cylinders made of stainless steel 316L. Figure 2.11 represents one of these cylinders.



**Figure 2.11: cylinder for thermal degradation with CO<sub>2</sub>**

For a typical experiment, the cylinders are filled up with 100 g of the solvent to be tested. Usually, this is MEA 30 wt% that has been loaded with CO<sub>2</sub> following the same procedure as for semi-batch experiments. Depending on the experiment, metals or degradation inhibitors can be added to the solution. Then, these cylinders are closed with caps and PTFE tape to prevent any leakage and they are set into a laboratory oven (type Memmert HCP108) at 120 or 140°C for three weeks. Every week, the cylinders are cooled down to room temperature and weighted to check for leakage. A sample is collected and the cylinder is returned back to the oven. After three weeks, the cylinders are cooled down, weighted, and a final sample is collected.

### *3.3 Analytical methods*

Disposing of reliable analytical techniques is an essential prerequisite for characterizing solvent degradation. Solvent degradation products appear in liquid and gas phase, but also in solid phase under the form of crystals that form in the DTR condenser. Different analytical methods have been developed as a part of this work within the Department of Applied Chemistry of the University of Liège. Furthermore, some analyses have also been performed by other laboratories. The main analytical methods are summarized in table 2.7 and described in the present section.

**Table 2.7: analytical methods for characterizing amine solutions**

|       | Method                                    | Objective   | Location                         |
|-------|---|---|----------------------------------|
| FTIR  | Fourier Transform Infra-red Spectroscopy  | Gas phase analysis (mainly NH <sub>3</sub> )  | Dept of Applied Chemistry - ULg  |
| HPLC  | High Pressure Liquid Chromatography       | MEA quantification  | Dept of Applied Chemistry - ULg  |
| GC    | Gas Chromatography                        | Identification and quantification of organic degradation products   | Dept of Applied Chemistry - ULg  |
| DD    | Density Determination                     | Measurement of the density of amine solutions   | Dept of Applied Chemistry - ULg  |
| IC    | Ionic Chromatography                      | Quantification of anionic degradation products (acetate, glycolate, oxalate...)   | Laborelec                        |
| TC-TN | Elemental analysis of Carbon and Nitrogen | Quantification of the total C and N content   | ETP-W research institute         |
| AAS   | Atomic Absorption Spectroscopy            | Quantification of dissolved metals (Fe, Cr, Ni, Mn...)  | Laboratory of Hydrogeology – ULg |
| CE    | Capillary Electrophoresis                 | Quantification of small ions (NH <sub>4</sub> <sup>+</sup> , Cl <sup>-</sup> , NO <sub>2</sub> <sup>-</sup> , NO <sub>3</sub> <sup>-</sup> ...) | Laboratory of Hydrogeology – ULg |
| KF    | Karl-Fischer analysis                     | Determination of water content  | Dept of Chemistry – ULg          |
| XRD   | X-Ray Diffraction                         | Solid analysis  | Dept of Chemistry – ULg          |

### ***Fourier Transform Infra-Red spectroscopy (FTIR)***

The objective of the FTIR spectrometer is to perform an on-line analysis of the gas phase emitted during the degradation experiment. Indeed, some degradation products are gaseous so that gas phase analysis must be considered for a rigorous study of amine degradation. FTIR analysis measures the absorbance of the gas sample at varying wavelengths in the infrared range. The absorbed wavelengths depend on the chemical bonds of the sample molecules, allowing for the identification of sample components. Moreover, according to the Beer-Lambert law, the absorbance is proportional to the concentration of the absorbing component so that quantification is also possible.

The FTIR analyzer is able to detect many components in the exhaust gas like NH<sub>3</sub>, water, CO<sub>2</sub> and MEA. According to previous studies (Chi et al., 2001; Knudsen et al, 2009) ammonia is one of the major oxidative degradation products of MEA. Thus the production of ammonia has been followed using the FTIR analyzer. Water and CO<sub>2</sub> have been identified but not quantified since it would not have brought useful information regarding MEA degradation. No MEA could be detected in the gas phase and no other compounds have been identified in the exhaust gas.

The FTIR device is represented in figure 2.12. It is a 6700 Nicolet FTIR supplied by Thermo Scientific. It has a 200 ml gas cell with a light pathway of 2 meters. The gas cell window is made of KBr. The resolution of the analyzer reaches up to  $0.125\text{ cm}^{-1}$  (expressed in wavenumber). The software Omnic 8 operates the spectrometer and acquires data. The main operating parameters for the FTIR analysis are in table 2.8.



**Figure 2.12: FTIR analyzer**

**Table 2.8: method parameters for FTIR analysis**

| Parameter                                   | Value                            |
|---|----------------------------------|
| Gas cell temperature                        | 150°C                            |
| Heated line temperature                     | 150°C                            |
| Set-point temperature for dilution nitrogen | 170°C                            |
| Dilution nitrogen flow rate                 | 560 ml/min                       |
| Measurement frequency                       | every 10 min                     |
| Resolution                                  | $4\text{ cm}^{-1}$               |
| Number of scans                             | 32/measurement                   |
| Spectral range                              | $4000 - 650\text{ cm}^{-1}$      |
| Integration domain for $\text{NH}_3$        | $979.68 - 900.61\text{ cm}^{-1}$ |
| Baseline for $\text{NH}_3$ integration      | $981.61 - 896.75\text{ cm}^{-1}$ |

The gas cell is heated to prevent any water condensation. Moreover, the analyzer is continuously purged with dry air and the detector is cooled with liquid nitrogen for a better sensitivity. Thus, continuous measurements during one week imply to refill the liquid nitrogen tank every 16 hours. Calibration regarding  $\text{NH}_3$  has been performed by the dilution of a  $\text{N}_2$  flow containing 9750 ppm  $\text{NH}_3$  supplied by Air Liquide. Relative measurement error is equal to 0.2% (see appendix 4 for the detailed error calculation).

Although the measurement error is very low, important perturbations may happen during the on-line FTIR monitoring, inducing some additional uncertainty on the  $\text{NH}_3$  production profile. This problem is mainly due to the formation of crystals inside the condenser<sup>12</sup>, which creates a solid plug and thus prevents the exhaust gas from exiting the condenser. This leads to a pressure increase in the degradation reactor, triggering safety alarms that shut down the gas supply. This may result in non-homogenous FTIR measurements.

The precipitation of crystals during amine degradation experiments was also reported by several research groups (Tönnies, 2011; Lepaumier, 2011). However, this crystalline deposit was not identified so far. Thermo-gravimetric differential scanning calorimetry (TG-DSC) combined with mass spectrometry showed that the crystals start to decompose above 60°C (figure 2.13), resulting in  $\text{NH}_3$ ,  $\text{CO}_2$  and water emission.

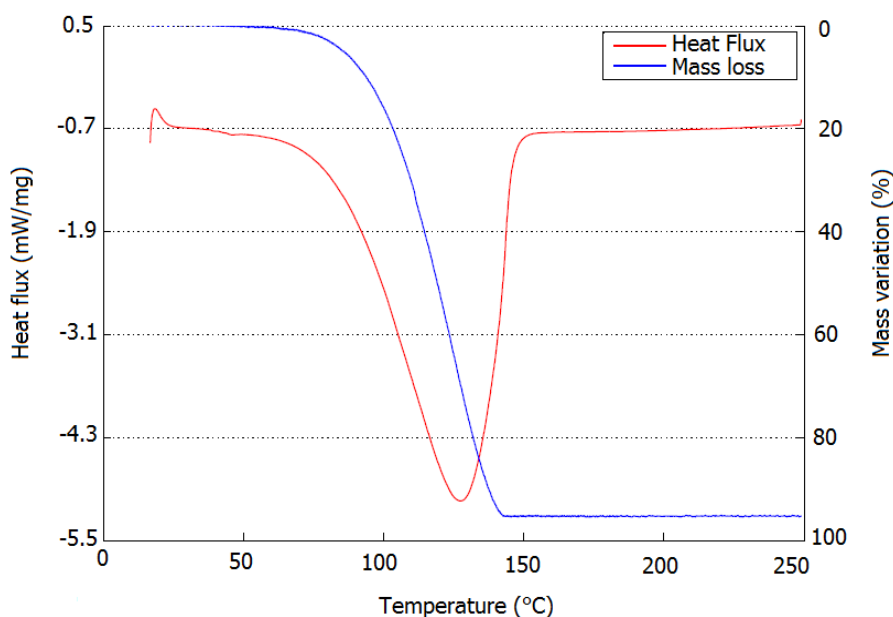


**Figure 2.13: TG-DSC spectrum of a crystal sample**

According to Meng (2004), the best identification method for ammonium salts is the X-Ray Diffraction (XRD). Thus, the crystal has been analyzed by XRD at the Department of Chemistry of the University of Liège. The observed spectrum corresponds perfectly with the spectrum of ammonium carbonate ( $\text{NH}_4\text{HCO}_3$ ) as shown in figure 2.14. Crystals of the same type have been produced in almost all experiments with a gas feed containing  $\text{O}_2$  and  $\text{CO}_2$ .

Finally, the precipitation of  $\text{NH}_4\text{HCO}_3$  captures one mole of  $\text{NH}_3$  per mole of crystal, inducing an error in the FTIR measurement of the  $\text{NH}_3$  production rate. As a consequence, the production of  $\text{NH}_3$  (in mol) during degradation experiments was estimated as following:

$$n_{\text{NH}_3, \text{produced}} = n_{\text{NH}_3, \text{measured at the FTIR}} + \frac{M_{\text{crystal}}}{MM_{\text{crystal}}} \quad (2.12)$$

<sup>12</sup> A further problem was also recorded, probably due to foaming. Indeed, a large and sudden peak in the  $\text{NH}_3$  emission was sometimes detected by the FTIR. This was combined with a relative humidity of 100% at the gas exhaust although the relative humidity of a saturated gas condensed at 4 barg and 20°C should be equal to 19.98% at 1 barg and 20 °C. Foaming was suspected but could not be evidenced.

- $n_{NH_3}$  is the mole number of ammonia (mol)
- $m_{crystal}$  is the mass of crystal (g) recovered when cleaning the condenser
- $MM_{crystal}$  is the molar mass of  $NH_4HCO_3$ , i.e. 79 g/mol

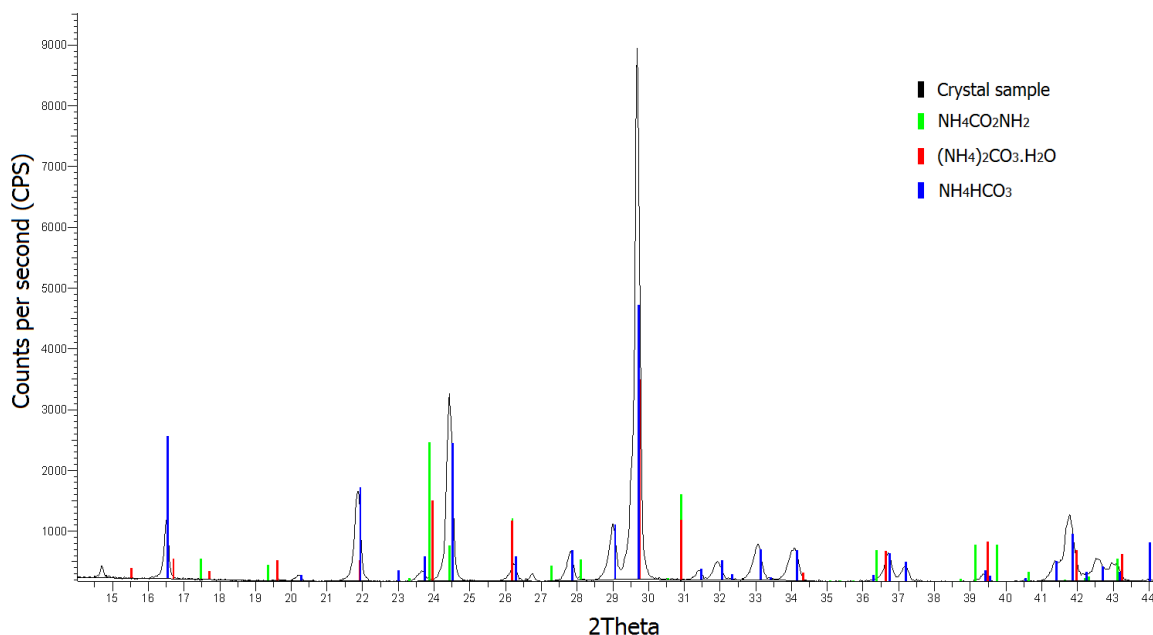


**Figure 2.14: XRD spectrum compared with different ammonium salts**

### *High-Pressure Liquid Chromatography (HPLC)*

The objective of this method is to quantify MEA in fresh as well as in degraded solvent samples. First, the liquid sample is injected into the HPLC column. The different constituents of the sample are eluted with different retention times, depending on their affinity with the column stationary phase and with the mobile phase (eluent). Then, the component is detected and quantified. The main elements of the HPLC analytical unit are listed in table 2.9 and the HPLC unit is represented in figure 2.15.

**Table 2.9: elements of the HPLC unit**

| Device                          | Specification(s)   | Type                              |
|---------------------------------|--|-----------------------------------|
| HPLC pump                       | Flow rate: 1.0 ml/min                                    | Waters 515                        |
| Automatic injector              | Injection volume: 5 $\mu$ l<br>Injection time: 20 min    | Waters 717+                       |
| Column thermostat               | Temperature: 30°C  | Merck T-6300                      |
| Refractive index detector (RID) | Sensitivity: 16<br>Scale Factor: 11<br>Temperature: 30°C | Waters 410                        |
| UV-visible detector             | Detection wavelength: 210 nm                             | Merck Hitachi L-4200              |
| Data acquisition unit           | n.a.   | PowerChrom 280,<br>version 2.5.13 |



**Figure 2.15: HPLC unit**

In the present work, three reverse-phase columns have been used. Their characteristics are given in table 2.10. In usual reverse phase columns, polar compounds elute first and non-polar compounds are retained in the column. Because MEA is a very polar compound, it elutes rapidly and it is usually poorly separated from its degradation products, so that the quantification is not accurate. Thus the use of more polar stationary phases may improve the retention of MEA. The third column listed in table 2.10 uses hydrophilic interaction chromatography (HILIC). This technology has evolved rapidly in the last few years with the resurgence of so-called “reverse-reverse phases” (McCalley, 2007). This type of column gives the longest retention time for MEA and performs the best separation.

**Table 2.10: characteristics of tested HPLC columns**

| Column name          | C18 Pyramid   | Nucleosil SA <sup>13</sup>  | Kinetex HILIC  |
|----------------------|---|---|--|
| Supplier             | Macherey-Nagel  | Macherey-Nagel  | Phenomenex   |
| Stationary phase     | Octadecyl carbon chains<br>-(CH <sub>2</sub> ) <sub>17</sub> -CH <sub>3</sub> | Benzenesulfonic acid<br>-(CH <sub>2</sub> ) <sub>3</sub> -C <sub>6</sub> H <sub>4</sub> -SO <sub>3</sub> Na | Unbounded silica<br>Si-OH  |
| Phase polarity       | Low   | Medium  | High   |
| Separation mechanism | Polar selectivity   | Strong cation exchange<br>interactions  | Hydrophilic interactions   |
| Carbon content       | 14%   | 6,5%  | 0%   |
| Column length        | 125 mm  | 250 mm  | 150 mm   |
| Internal diameter    | 4,6 mm  | 4 mm  | 4,6 mm   |
| Particule size       | 5 µm  | 5 µm  | 2,6 µm   |
| Eluant               | KH <sub>2</sub> PO <sub>4</sub> 8 mM in water,<br>pH=2.6                      | KH <sub>2</sub> PO <sub>4</sub> 5 mM in water,<br>pH=2.6  | NH <sub>4</sub> HCO <sub>2</sub> 5 mM in 90:10<br>acetonitrile:water, pH=3.2 |
| MEA retention time   | 1.5 min   | 5.5 min   | 16 min   |

<sup>13</sup> Method development based on the works of Kaminski et al. (2002) and Supap et al. (2006).



Two different detectors can be used, based respectively on the variation of the refractive index of the solution (Refractive Index Detector, RID) and on the absorbance of MEA in the UV-visible range. Figure 2.16 shows the absorbance spectrum of MEA<sup>14</sup>. However, in agreement with previous literature studies (Supap et al., 2006), it has been decided to quantify MEA using the RID detector. The UV-visible detector appears to be more adapted for the detection of degradation products, but this latest application has not been further developed.

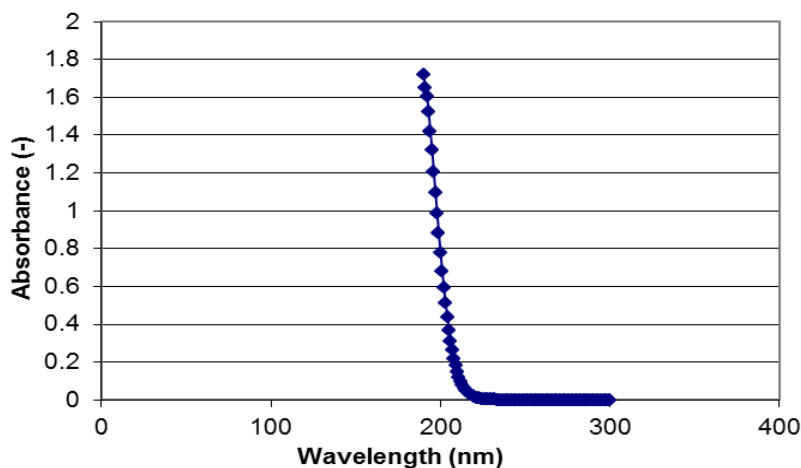


**Figure 2.16: absorbance range of MEA (pure MEA diluted 1:10,000 in water)**

The method development has been the objective of a 10-week internship performed at the University of Liège by a French student in chemical and process engineering (Bascougnano, 2012). The main results are listed below:

- The eluent for HILIC chromatography contains 10 vol% water and 90 vol% acetonitrile in order to ensure a low polarity of the mobile phase.
- The eluent is buffered at pH=3.2 with ammonium formate ( $\text{NH}_4\text{HCO}_2$ ) and formic acid ( $\text{HCOOH}$ ) so that MEA appears under its acidic form in the column, increasing its retention.
- Samples are diluted 1:10 with a solution of acetonitrile-water 50:50.
- Before each measurement campaign, a calibration is made with diluted solutions of MEA.

To determine the precision of this method, several measurements of the same sample were performed. The relative error of this analytical method was calculated to 0.76%. More details about the error evaluation are given in appendix 4.

### **Gas Chromatography (GC)**

The goal of this method is to identify and quantify organic degradation products of MEA. This identification is not performed in HPLC due to the overlapping of degradation products. In GC, a liquid sample is vaporized and injected into a capillary column. The column is set

<sup>14</sup> Spectrophotometer Specord 200 (Analytik Jena), analysis performed at the Center for Protein Engineering, Department of Chemistry, ULg.

inside an oven and its temperature is increased during the analysis. Degradation products are separated based on their affinity with the column stationary phase. The GC device used for the analysis is a GC 8000 Series (Fisons Instruments) coupled with a Flame Ionization Detector (FID) of type EL980 (Fisons Instruments). It is represented in figure 2.17. Signal acquisition and peak integration is achieved using the ChromCard software, version 1.18.



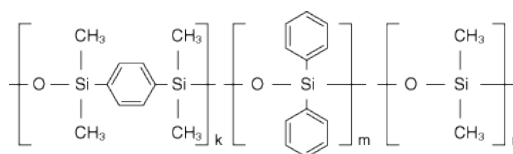
**Figure 2.17: gas chromatograph**

Based on the work of Supap et al. (2006), a GC column with an intermediate polarity has been chosen. Its characteristics are presented in table 2.11.

**Table 2.11: characteristics of the OPTIMA-35 MS GC column**

| Column name          | OPTIMA-35 MS                                |
|----------------------|---|
| Supplier             | Macherey-Nagel                              |
| Phase                | Cross-linked silarylene phase <sup>15</sup> |
| Separation mechanism | Polar selectivity                           |
| Polarity index       | 35% Phenyl / 65% Methyl-Polysiloxane        |
| Length               | 30 m  |
| Internal diameter    | 0.25 mm                                     |
| Film thickness       | 0.25 μm                                     |
| Carrier gas          | Helium                                      |

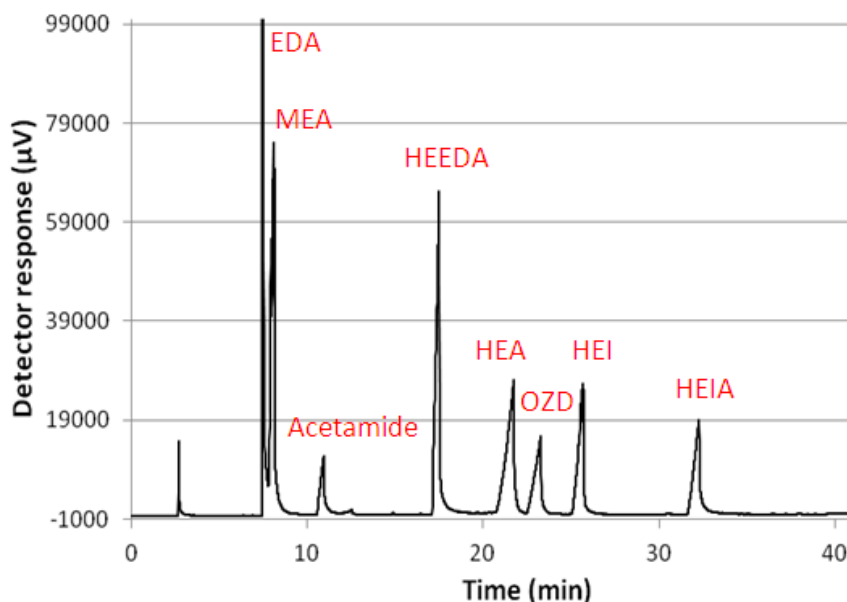
<sup>15</sup>Chemical structure of the stationary phase:



The main characteristics of the analytical method are:

- Samples are diluted 1:2 with deionized water containing 1 wt% of an internal standard. Diethylene glycol (DEG) has been selected as internal standard.
- Injection volume is 1  $\mu\text{l}$ . The syringe is engaged into the injector at 280°C during 10 s before starting the injection.
- Helium is used as a carrier gas. Its pressure is kept constant at 0.6 barg.
- The oven temperature program lasts for 45 minutes:
  1. The program starts at 35°C during 2 minutes.
  2. Then the temperature increases by 7°C/min for 15 minutes.
  3. From 140°C the temperature increases by 5°C/min for 20 minutes.
  4. At 240°C, the temperature is maintained during 8 minutes.
- The Flame Ionization Detector (FID) is fed with a mixture of hydrogen and air. The pressure of the air flow is regulated at 1.1 barg, the pressure of H<sub>2</sub> at 0.7 barg. The flame temperature is controlled at 300°C.

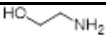
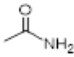
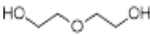
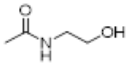
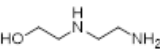
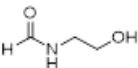
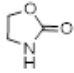
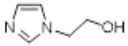
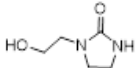
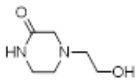
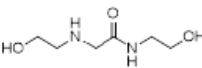
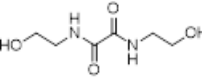
MEA degradation products were compared to standard solutions of previously reported degradation products (see figure 2.1). The GC spectrum represented in figure 2.18 contains some of the main products identified.



**Figure 2.18: GC spectrum of MEA and some degradation products**

Six of the main degradation products of MEA could be quantified by GC analysis. They are listed in table 2.12. Four further degradation products were identified, but additional tests are required to confirm the identification and to perform quantification.

**Table 2.12: main peaks identified in GC spectra of degraded MEA samples**

|        | Compound  | Structure   | Retention time (min) | Type              |
|--------|---|---|----------------------|-------------------|
| MEA    | monoethanolamine  |    | 7.6                  | Start amine       |
| AA     | acetamide   |    | 10.6                 | Identified        |
| DEG    | diethylene glycol   |    | 15.0                 | Internal standard |
| HEA    | <i>N</i> -(2-hydroxyethyl)acetamide                         |    | 16.9                 | Identified        |
| HEEDA  | <i>N</i> -(2-hydroxyethyl)ethylenediamine                   |    | 17.0                 | Quantified        |
| HEF    | <i>N</i> -(2-hydroxyethyl)formamide                         |    | 21.1                 | Identified        |
| OZD    | 2-oxazolidinone   |    | 22.5                 | Quantified        |
| HEI    | <i>N</i> -(2-hydroxyethyl)imidazole                         |   | 24.9                 | Quantified        |
| HEIA   | <i>N</i> -(2-hydroxyethyl)imidazolidinone                   |  | 31.5                 | Quantified        |
| HEPO   | 4-(2-hydroxyethyl)piperazine-2-one                          |  | 34.3                 | Quantified        |
| HEHEAA | <i>N</i> -(2-hydroxyethyl)-2-(2-hydroxyethylamino)acetamide |  | 36.8                 | Identified        |
| BHEOX  | <i>N,N'</i> -Bis(2-hydroxyethyl)oxamide                     |  | 38.7                 | Quantified        |

The quantification of degradation products is based on the use of an internal standard, in this case diethylene glycol (DEG). The concentration of a degradation product is calculated from the ratio of its peak area to the internal standard peak area. The objective is to limit the error related to the injection. Calibration curves have been determined for every quantified degradation product with a fit parameter  $R^2$  equal or higher than 0.99. Figure 2.19 shows the calibration curve for HEPO as an example.

Several injections of the same sample give a relative error lower than 2.5% in all cases apart for degradation product BHEOX. In this case, the relative error is about 12%, which can be due to the low concentration of BHEOX in the test sample. Details about error calculation are given in appendix 4.

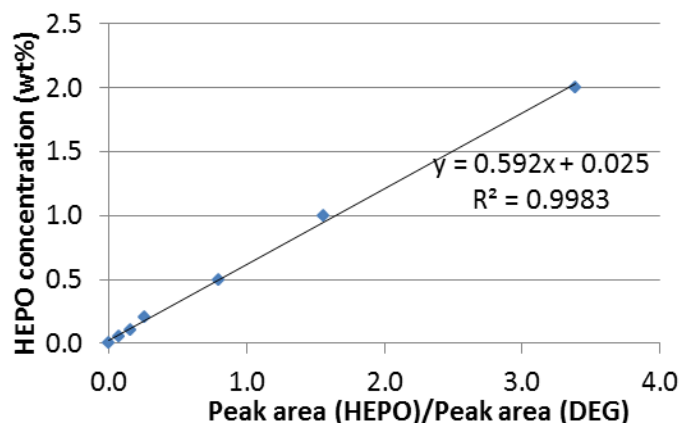


**Figure 2.19: GC calibration curve for component HEPO**

### ***Density Determination (DD)***

The density of amine solvents is necessary to convert experimentally measured weight concentrations (mol/kg) into volume concentrations for the calculation of kinetic parameters (mol/L). The density of 30 wt% aqueous amine solutions is close to that of water, but it varies when the amines are loaded with CO<sub>2</sub> or degraded.

The density measurement is performed by weighting 5 ml of the amine solution with an analytical balance (Ohaus AS200). The measurements are performed at constant temperature (20°C). The calculated relative error of this method is 0.15%.

### ***Ionic Chromatography (IC)***

This method was used to quantify small carboxylic salts like formate, oxalate, acetate and glycolate. The analysis has been performed at Laborelec using a Dionex Ionpac AS15 column and KOH as eluent. The device is an ICS2000 system supplied by Dionex. It is equipped with an automatic sampler AS DV and a DS6 heated conductivity cell. Calibrations are performed before and after each measurement campaign using 1000ppm standards that are diluted between 0.5 and 50 ppm.

However, the method has not been optimized for carboxylic acids so that the results should be rather considered as semi-quantitative. It was not possible so far to analyze all samples, so that only partial results are available for carboxylic acids.

### ***Elemental analysis of Carbon and Nitrogen (TC and TN)***

This method quantifies the total amount of carbon and nitrogen in degraded amine samples, which is useful to evaluate the mass balance of degradation experiments. It is based on the Dumas method which unfortunately does not distinguish organic and inorganic compounds. Amine samples undergo combustion with pure oxygen, producing CO<sub>2</sub>, water, SO<sub>2</sub> and N<sub>2</sub> (NO<sub>x</sub> are reduced to nitrogen in a reducing copper reactor). These elements are then quantified by GC with a thermal conductivity detector that compares the thermal conductivity of the samples with that of helium.

The device used for this analysis is an ECS 4010 elemental analyzer supplied by Costech Instruments. The calibration is performed by comparison with an acetanilide standard (71.09% C, 10.36% N) at different dilutions. The analyses were performed at the

EcoTechnoPole Wallonie (ETP-W), a research institute located in Liège. A relative error of 2.5% was claimed.

### ***Atomic absorption spectroscopy (AAS)***

The concentration of dissolved metal was quantified by the Laboratory of Hydrogeology at the University of Liège. The first objective of this method is to assess the qualitative evolution of the corrosion in the degradation reactor. Indeed, the amount of dissolved metals is expected to increase with more corrosive solutions and inversely, the presence of dissolved metals catalyzes the oxidative degradation of amine solutions.

The degradation reactor is made of stainless steel 316L, so that the main metals that can leach from the reactor vessel are Fe, Cr, Ni and Mn<sup>16</sup>. Identification of metals in atomic absorption spectroscopy is based on the absorption of specific wavelengths by metals. The Beer-Lambert law is used to quantify the concentration of metals in the sample. Analyses were performed using the flame spectrometer novAA<sup>®</sup>300 supplied by Analytik Jena. Calibration tests were performed with three solutions at 1.25, 2.5 and 6.5 mg/L for Fe, Cr, Ni and Mn. Prior to the analysis, the amine sample was diluted with water and acidified with HCl or HNO<sub>3</sub>. According to the operator, the relative standard deviations are usually below 10% for each metal but they may reach up to 45% in case of low metal concentrations.

### ***Capillary electrophoresis (CE)***

This method was used to quantify some anionic and cationic degradation products like NH<sub>4</sub><sup>+</sup>, NO<sub>2</sub><sup>-</sup>, NO<sub>3</sub><sup>-</sup>. Further anions like Cl<sup>-</sup> and F<sup>-</sup> were also analyzed due to their potential influence on corrosion in the DTR. This analysis was performed at the Laboratory of Hydrogeology at the University of Liège with a capillary ion analyzer 4000E supplied by Waters.

In capillary electrophoresis, the solution components are eluted along a capillary filled with an electrolyte solution. The elution takes place under the influence of an electric field, so that ions can be separated based on their size to charge ratio. Ions are detected by UV spectrometry at 185 nm for cations and 254 nm for anions. Amine samples are diluted with water, the dilution ratio depending on the sample conductivity. The quantification is performed according an internal standard method. For cationic products, the internal standard is Li<sup>+</sup>. For anionic products, it is ClO<sub>3</sub><sup>-</sup>. In the case of NH<sub>4</sub><sup>+</sup>, high uncertainties were reported due to matrix perturbation. Indeed, carbonates are present in large amounts in loaded amine samples and their peak may hide some other ions. Moreover, the measure of NH<sub>4</sub><sup>+</sup> may not be relevant due to the high volatility of ammonia. As a consequence, values for NH<sub>4</sub><sup>+</sup> may rather be considered as semi-quantitative.

### ***Karl-Fischer titration of water (KF)***

The Karl-Fischer analysis was performed by the Laboratory of Coordination and Radiochemistry, part of the Department of Chemistry at the University of Liège. The objective of this analysis is to determine the water content of amine solutions. This gives some information about the water mass balance in the degradation reactor. The principle of this method is a chemical titration based on the reaction of sulfur dioxide and iodine in the presence of water:

---

<sup>16</sup> Silicon was also analyzed in some experiments because solution contamination due to a thread lubricant was suspected. In this case, the concentrations of the calibration solutions were 50, 100 and 200mg/L.



As long as water is available in the sample, it reacts with  $\text{SO}_2$  and iodine which is progressively added to the sample. The titration end point is detected by potentiometry as soon as  $\text{I}_2$  is in excess in the sample. Amine samples were diluted 1:20 with Ethanol. 100  $\mu\text{l}$  of the diluted solution have been titrated using an 831 KF Coulometer Metrohm apparatus. The calibration was performed with aqueous solutions of MEA at concentrations of 12, 18, 24, 30 and 36 wt% MEA. The relative error of this method is lower than 1% (see appendix 4).

## 4. Semi-batch experiments

Since the beginning of the first test campaign in March 2011, 13 two-week experiments and 23 one-week experiments have been conducted using the degradation test rig. In this section, the main results of these 36 experiments are presented graphically and discussed. First, it was necessary to identify a base case for the study of accelerated solvent degradation. Moreover, the repeatability of the results is evaluated, and the error related to semi-batch degradation experiments is estimated for the base case experiment. Then, the influence of different process parameters is studied: O<sub>2</sub> and CO<sub>2</sub> content in the gas feed, agitation rate, experiment length and temperature. Finally, the influence of dissolved metals and degradation inhibitors is also studied. The detailed figures can be found in appendix 5.

### 4.1 Base case definition

The role of the base case experiment is to act as a reference point for studying the influence of operating parameters. In this section, a base case is defined and its relevance is evaluated by comparing the results with degraded MEA samples from two different CO<sub>2</sub> capture pilots.

The base case must present three main characteristics:

- Degradation must be observable.
- Degradation pathways must be similar to those occurring in CO<sub>2</sub> capture plants.
- Parameter values must be in an intermediate range so that they can be easily varied.

Different experiments have been performed to identify a suitable base case. Finally, the conditions presented in table 2.13 have been selected.

**Table 2.13: base case conditions for semi-batch degradation experiments**

| Parameter            | Value   |
|----------------------|---|
| Solvent              | 300 g of 30 wt% MEA loaded with CO <sub>2</sub><br>(1.47 mol MEA) |
| Temperature          | 120°C   |
| Pressure             | 4 barg  |
| Agitation rate       | 600 rpm   |
| Gas feed flow rate   | 160 Nml/min   |
| Gas feed composition | 5% O <sub>2</sub> / 15% CO <sub>2</sub> / 80% N <sub>2</sub>      |
| Experiment duration  | 1 week  |

Under these conditions, the total mole number of MEA decreased from 1.5 down to 1.14 moles over one week, which corresponds to a 24%-reduction. The parameter values are at intermediate ranges, and the degradation pathways are similar to those of degradation in CO<sub>2</sub>



capture pilots. Indeed, figure 2.20 compares the GC spectra of degraded MEA samples from two different CO<sub>2</sub> capture pilots with the GC spectrum of the base case experiment<sup>17</sup>. Although some products could not be identified, most degradation products obtained in the degradation test rig are similar to those obtained in industrial capture pilots. This indicates that the accelerated degradation under base case conditions follows the same pathways as degradation reactions taking place in pilot plants. Thus the relevance of accelerated degradation experiments in the DTR is confirmed.

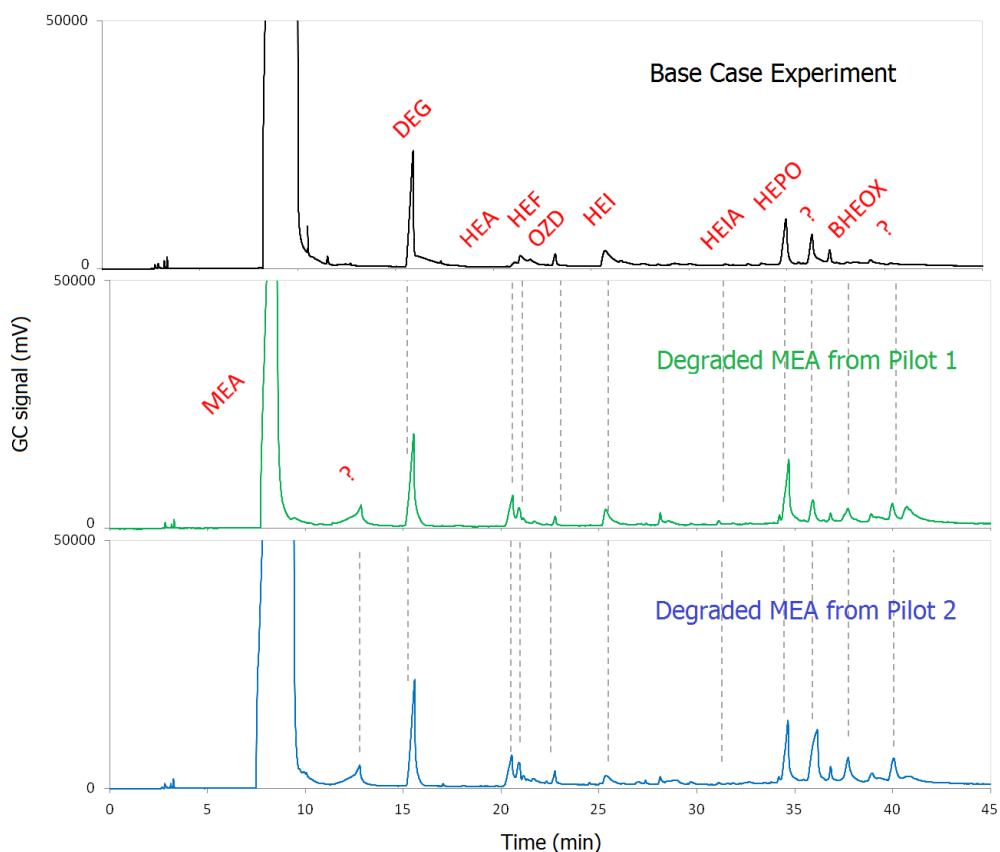


**Figure 2.20: GC comparison of the base case degradation (300 g, 30 wt% CO<sub>2</sub> loaded MEA, 120°C, 4 barg, 600 rpm, 160 Nml/min gas feed, 5% O<sub>2</sub>/15% CO<sub>2</sub>/80% N<sub>2</sub>, 1 week) with pilot plant degradation**

*In conclusion, base case conditions have been identified for the study of accelerated MEA degradation. Moreover, the resulting degradation products are similar to those observed in CO<sub>2</sub> capture pilots, suggesting similar degradation pathways.*

## 4.2 Evaluation of the experimental error

A detailed error calculation for the main analytical methods is presented in appendix 4. However, the objective of this section is to give an insight into the overall experimental error. Indeed, experimental studies imply numerous parameters and it would be very tedious to evaluate with precision the uncertainty of each variable. On the contrary, mass balances and redundant experiments may easily give a global overview of the experimental uncertainties.

<sup>17</sup> According to a non-divulcation agreement with the industrial partner Laborelec, the name of the pilot plants will not be communicated.

### Nitrogen balance

With the analytical means developed in this study (HPLC for the amine solvent, GC for the liquid degradation products, FTIR for the gaseous degradation products), it is possible to evaluate the total mole number of nitrogen in the fresh and degraded solvents<sup>18</sup>. Figure 2.21 shows the nitrogen balance for the base case experiment. At the beginning of the experiment, 300g of 30 wt% MEA contain 1.47 mol of nitrogen. At the end of the experiment, residual MEA and identified degradation products contain 1.32 mol of nitrogen (1.16 mol MEA, 0.03 mol nitrogen in liquid degradation products and 0.14 mol NH<sub>3</sub>). The remaining 0.15 mol can be attributed to unidentified degradation products. As a consequence, the nitrogen balance of MEA degradation experiments can be closed within the 10% range.

Furthermore, the result of the total nitrogen analysis for the liquid phase is also represented in figure 2.21. Using this method for the determination of the total nitrogen content in the degraded solvent, it appears that the liquid phase contains 1.24 mol of nitrogen at the end of the experiment. This is in relatively good agreement with the 1.19 mol of nitrogen in the degraded solvent measured under the form of MEA (1.16 mol) and liquid degradation products (0.03 mol).

Figure 2.21 evidences that ammonia is by far the most important degradation product of MEA in the test conditions. Since the MEA loss equals  $1.47 - 1.16 = 0.31$  mol, ammonia accounts for 45% of the MEA loss (0.14 mol). Moreover, it seems that significant amounts of unidentified nitrogen-containing products are present in the liquid phase ( $1.24$  mol  $- 1.19$  mol = 0.05 mol), although this value is lower than in the gas phase ( $1.47$  mol  $- 1.24$  mol  $- 0.14$  mol = 0.09 mol).

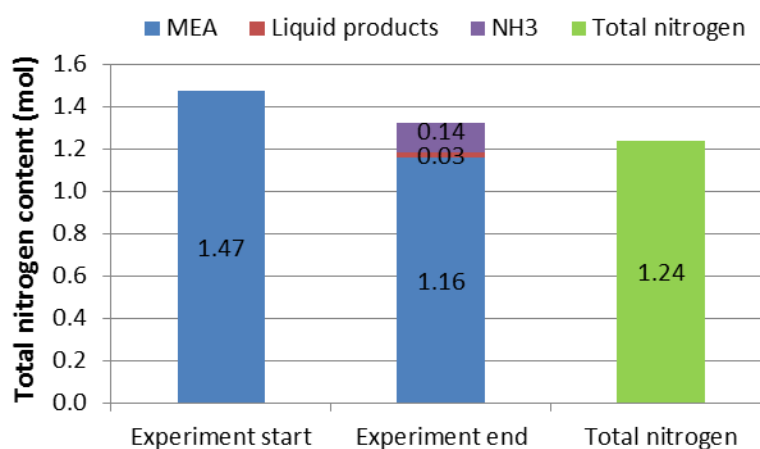


**Figure 2.21: nitrogen balance of the base case experiment (300 g, 30 wt% CO<sub>2</sub> loaded MEA, no additives, 120°C, 4 barg, 600 rpm, 160 Nml/min gas feed, 5% O<sub>2</sub>/15% CO<sub>2</sub>/80% N<sub>2</sub>, 1 week)**

The distribution of nitrogen-containing degradation products in the liquid phase is represented in figure 2.22 for the base case experiment. It appears that HEI and HEPO are the main products since they account for 71% of the identified nitrogen-containing liquid degradation products.

<sup>18</sup> Unfortunately, it was not possible to evaluate the carbon balance, since the CO<sub>2</sub> loading of degraded amine solutions could not be precisely measured. The development of an analytical method for this purpose should be considered as a perspective for further research.

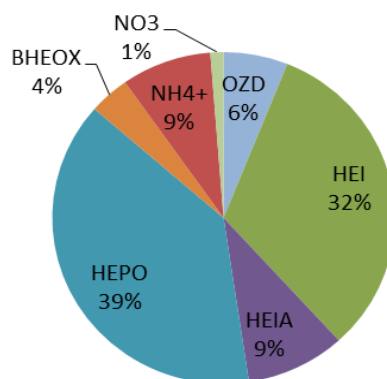


**Figure 2.22: distribution of identified nitrogen-containing degradation products in the base case experiment (300 g, 30 wt% CO<sub>2</sub> loaded MEA, no additives, 120°C, 4 barg, 600 rpm, 160 Nml/min gas feed, 5% O<sub>2</sub>/15% CO<sub>2</sub>/80% N<sub>2</sub>, 1 week)**

### Repetition experiment

A further tool to evaluate the uncertainty of experiments conducted on the degradation test rig is to perform a repetition experiment. In figure 2.23, the nitrogen balances of two experiments are presented: the base case experiment and a repetition of this base case conducted under similar conditions. At the end of each experiment, the nitrogen content calculated from the HPLC, GC and FTIR analyses is compared to the result of the total nitrogen analysis. The dashed line represents the initial mole amount of nitrogen in the amine solution. When comparing the results of the total nitrogen analysis with the amount of identified nitrogen in the liquid phase (residual MEA + liquid degradation products), it appears that the nitrogen mass balance in the liquid phase can be closed within 5% for both experiments. Moreover, the repetition of the base case experiment gives similar results, with a relative difference on the total nitrogen content lower than 4%.

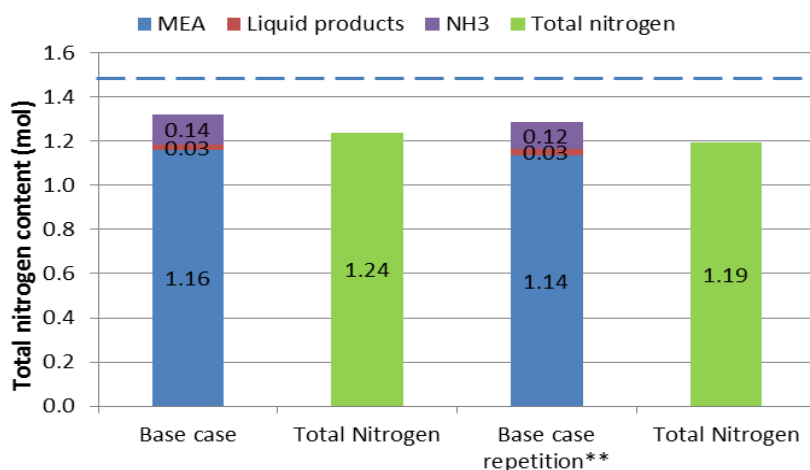


**Figure 2.23: nitrogen balance of the base case experiments<sup>19</sup> (300 g, 30 wt% CO<sub>2</sub> loaded MEA, no additives, 600 rpm, 120°C, 4 barg, 160 Nml/min gas feed, 5% O<sub>2</sub>/15% CO<sub>2</sub>/80% N<sub>2</sub>, 1 week)**

*In conclusion, the error on the total nitrogen balance during the base case experiment is lower than 10%. Moreover, the base case experiment could be repeated with a relative difference on the results lower than 5%.*

<sup>19</sup> \*\* Results of NH<sub>4</sub><sup>+</sup>, nitrites and nitrates are not available for the base case repetition experiment.

### 4.3 Influence of the gas feed

In the degradation test rig, all experiments were conducted in semi-batch conditions with continuous gas supply, except one batch experiment described in section 5. In this section, the influence of the gas feed composition is first studied in experiments with only N<sub>2</sub>, CO<sub>2</sub> or O<sub>2</sub>. Then, the influence of the O<sub>2</sub> and CO<sub>2</sub> concentrations in the gas supply is studied.

#### Gas composition

The stability of MEA in semi-batch conditions with only N<sub>2</sub> in the gas feed was studied before the determination of a base case. This experiment was conducted under following conditions: 120°C, 20 barg, 400 rpm, 200 Nml/min N<sub>2</sub> gas feed. Afterwards, starting from the base case experiment, the respective influences of CO<sub>2</sub> and O<sub>2</sub> have been successively studied. During these experiments, the gas flow rate is kept constant at 160 Nml/min. When the fraction of a component is reduced in the gas feed, it is compensated for with N<sub>2</sub>. For instance, during the CO<sub>2</sub> experiment with no O<sub>2</sub>, the gas feed composition is 15% CO<sub>2</sub>/85% N<sub>2</sub> instead of 5% O<sub>2</sub>/15% CO<sub>2</sub>/80% N<sub>2</sub> for the base case. In the O<sub>2</sub> experiment with no CO<sub>2</sub>, the gas feed composition is 5% O<sub>2</sub>/95% N<sub>2</sub>.

#### MEA loss and NH<sub>3</sub> emission

As represented in figure 2.24, almost no MEA loss is observed in the absence of oxygen in the gas feed. Moreover, the color of the solution remains unchanged, which is not the case in the presence of oxygen. This suggests that thermal degradation (with or without CO<sub>2</sub>) does not significantly take place at 120°C. On the contrary, degradation occurs in the presence of oxygen and NH<sub>3</sub> is detected. Since NH<sub>3</sub> is a typical product of MEA oxidative degradation, its production confirms the oxidative degradation mechanism. As expected, no ammonia is emitted when the gas feed is composed of CO<sub>2</sub> only.

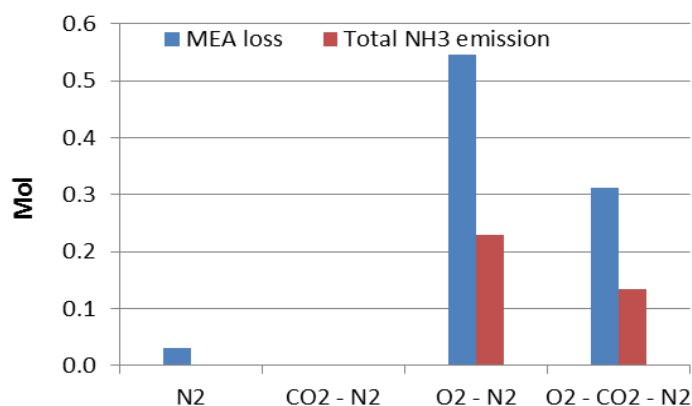


**Figure 2.24: influence of the gas feed composition on MEA degradation and NH<sub>3</sub> emission (300 g, 30 wt% CO<sub>2</sub> loaded MEA<sup>20</sup>, 120°C, 4 barg, 600 rpm, 160 Nml/min gas feed, 1 week)**

Moreover, figure 2.24 shows that CO<sub>2</sub> has an inhibiting effect on oxidative degradation. Indeed, the MEA loss is reduced from 0.55 mol in the O<sub>2</sub>-N<sub>2</sub> system down to 0.31 mol in the O<sub>2</sub>-CO<sub>2</sub>-N<sub>2</sub> system (initial MEA content: 1.47 mol). Similarly, the emission of ammonia is reduced in the presence of CO<sub>2</sub>, decreasing from 0.23 mol down to 0.14 mol.

<sup>20</sup> There is no previous CO<sub>2</sub> loading in experiments with no CO<sub>2</sub> in the gas feed. Moreover, the experiment with N<sub>2</sub> only was conducted at 20 barg, 400 rpm, 200 Nml/min N<sub>2</sub> and NH<sub>3</sub> emissions were not recorded in this case.

### Organic degradation products

Figure 2.25 shows that small amounts of HEPO are detected in the experiment with N<sub>2</sub> only, maybe due to an oxygen contamination during the experiment. In the experiment with CO<sub>2</sub> only, 0.002 mol of OZD are formed. OZD is a typical product of MEA thermal degradation with CO<sub>2</sub>, but since no further degradation product is detected, thermal degradation with CO<sub>2</sub> does not significantly take place at 120°C. On the contrary, HEI is a typical oxidative degradation product observed in the O<sub>2</sub>-N<sub>2</sub> and the O<sub>2</sub>-CO<sub>2</sub>-N<sub>2</sub> systems. Like NH<sub>3</sub>, its formation is reduced in the presence of CO<sub>2</sub>, confirming the inhibiting effect of CO<sub>2</sub> on the oxidative degradation of MEA. In the presence of both O<sub>2</sub> and CO<sub>2</sub>, there is more HEPO and further degradation products like BHEOX and HEIA appear.

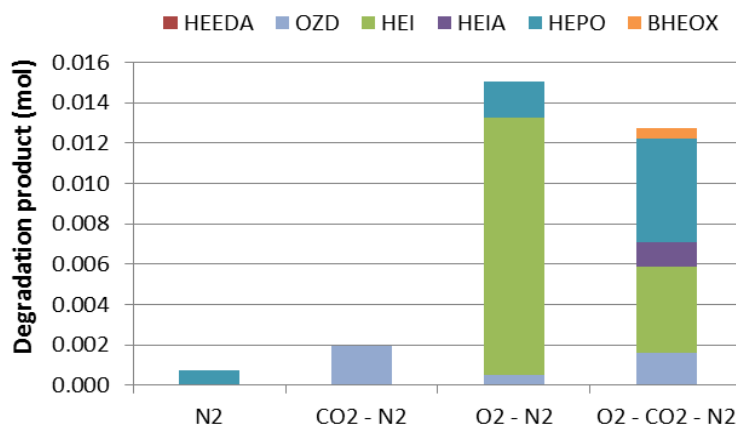


**Figure 2.25: influence of the gas feed composition on organic degradation products (300 g, 30 wt% CO<sub>2</sub> loaded MEA<sup>21</sup>, 120°C, 4 barg, 600 rpm, 160 Nml/min gas feed, 1 week)**

### Organic acids and dissolved metals

As presented in figure 2.26, glycolate is the main carboxylic acid detected in the O<sub>2</sub>-N<sub>2</sub> system, but its formation is inhibited in the O<sub>2</sub>-CO<sub>2</sub>-N<sub>2</sub> system. Formate, nitrate and NH<sub>4</sub><sup>+</sup> are also detected in both cases.

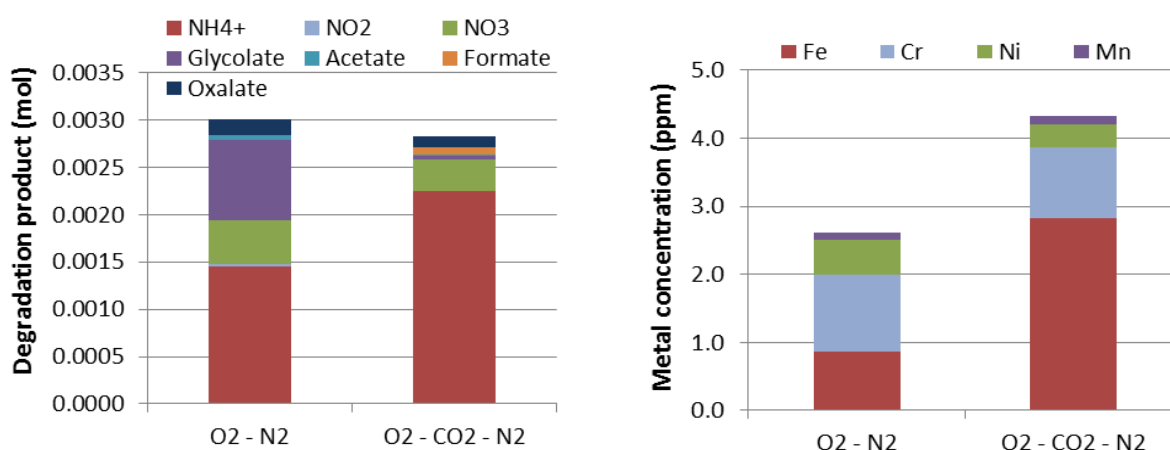


**Figure 2.26: influence of the gas feed composition on organic acids, nitrites and nitrates (left) and dissolved metal concentrations (right) (300 g, 30 wt% CO<sub>2</sub> loaded MEA<sup>21</sup>, 120°C, 4 barg, 600 rpm, 160 Nml/min gas feed, 5% O<sub>2</sub>, 1 week)**

<sup>21</sup> There is no previous CO<sub>2</sub> loading in experiments with no CO<sub>2</sub> in the gas feed.

Finally, figure 2.26 shows that the concentration of dissolved metals is higher in the case with both O<sub>2</sub> and CO<sub>2</sub> although the degradation extent is lower. However, the measured concentrations are very low, leading to a high uncertainty.

### *CO<sub>2</sub> concentration*

An inhibiting effect of the presence of CO<sub>2</sub> has been mentioned in the previous section. According to Goff and Rochelle (2004), the ionic strength of the amine solution increases at higher CO<sub>2</sub> loadings, leading to lower solubility and diffusion coefficient of O<sub>2</sub>. Increasing the CO<sub>2</sub> loading may thus inhibit the O<sub>2</sub> mass transfer. Another possible explanation is that the MEA carbamate formed in CO<sub>2</sub>-loaded solutions is less sensitive to oxidative degradation than the free amine. In this section, experiments are performed with 0%, 7.5%, 15% and 30% CO<sub>2</sub> in the gas feed to study the influence of the CO<sub>2</sub> concentration on solvent degradation.

### *MEA loss and NH<sub>3</sub> emission*

It appears from figure 2.27 that the MEA loss is increased by about 0.2 mol in the absence of CO<sub>2</sub> in the gas feed to reach 0.55 mol (initial MEA content: 1.47mol). However, when there is no CO<sub>2</sub> in the gas feed, the amine was not loaded with CO<sub>2</sub> prior to the degradation experiment. Moreover, the amine loss does not significantly vary when the CO<sub>2</sub> concentration increases in the gas feed. As a consequence, the inhibiting effect may be attributed to the CO<sub>2</sub> loading rather than to the CO<sub>2</sub> concentration in the gas feed.

The emission of NH<sub>3</sub> is plotted in the same graph. Similarly, the CO<sub>2</sub> concentration has no influence on NH<sub>3</sub> emissions, apart from the influence of the initial loading. It also appears that the MEA degradation is related to the emission of NH<sub>3</sub>, which is an oxidative degradation product. Combined with the independence of both MEA loss and NH<sub>3</sub> formation on the CO<sub>2</sub> concentration, this suggests that the oxidative degradation is the dominant reaction pathway.

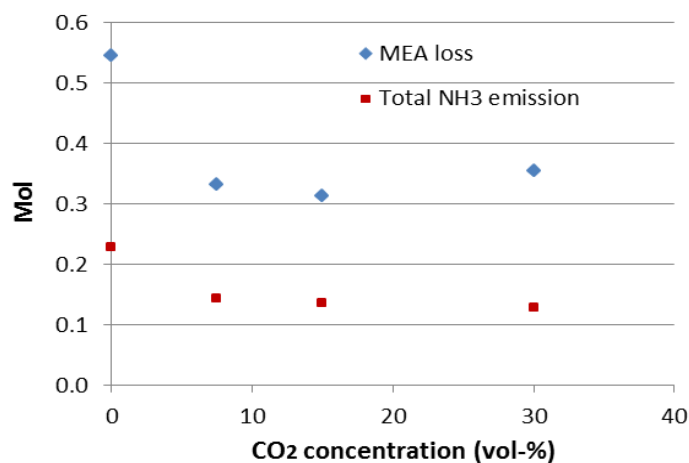


**Figure 2.27: influence of the CO<sub>2</sub> concentration in the gas feed on MEA degradation and NH<sub>3</sub> emission (300 g, 30 wt% CO<sub>2</sub> loaded MEA<sup>22</sup>, 120°C, 4 barg, 600 rpm, 160 Nml/min gas feed, 5% O<sub>2</sub>, 1 week)**

### *Organic degradation products*

Figure 2.28 shows that the presence of CO<sub>2</sub> implies the apparition of other products like HEIA and BEOX that are not present in the O<sub>2</sub>-N<sub>2</sub> system. However, no clear influence of the

<sup>22</sup> There is no previous CO<sub>2</sub> loading in experiments with no CO<sub>2</sub> in the gas feed.

CO<sub>2</sub> concentration can be observed on the distribution of degradation products, apart from the influence of the initial CO<sub>2</sub> loading.

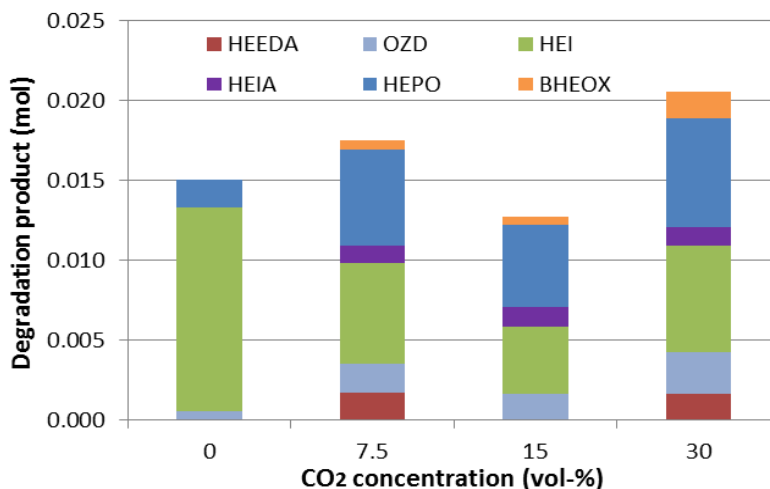


**Figure 2.28: influence of the CO<sub>2</sub> concentration in the gas feed on organic degradation products (300 g, 30 wt% CO<sub>2</sub> loaded MEA<sup>23</sup>, 120°C, 4 barg, 600 rpm, 160 Nml/min gas feed, 5% O<sub>2</sub>, 1 week)**

### Oxygen concentration

In this section, different experiments are performed with 0%, 5%, 7.5% and 10% O<sub>2</sub> in the gas feed to study the influence of the oxygen concentration on the degradation of MEA.

### MEA loss and NH<sub>3</sub> emission

It appears in figure 2.29 that the increase of the oxygen concentration in the gas feed seems to have a linear influence on the MEA degradation rate and the NH<sub>3</sub> emission. This dependency on O<sub>2</sub> confirms the presence of oxidative degradation in our test conditions. At 10% O<sub>2</sub> in the gas feed, the MEA loss reaches 55% (0.81 mol on an initial MEA content of 1.47 mol).

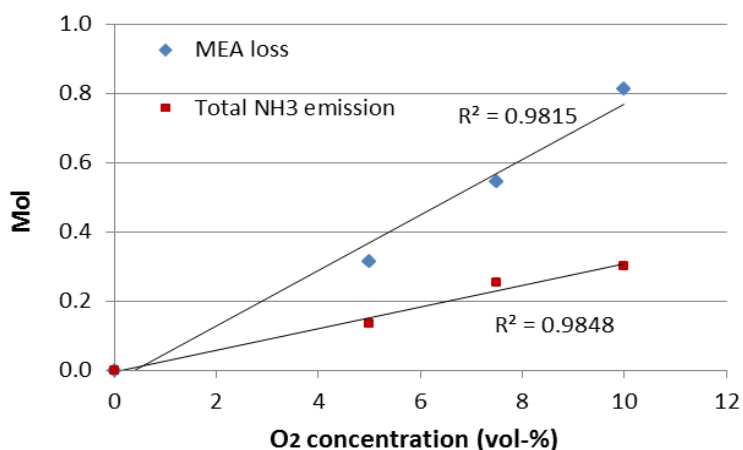


**Figure 2.29: influence of the O<sub>2</sub> concentration in the gas feed on MEA degradation and NH<sub>3</sub> emission (300 g, 30 wt% CO<sub>2</sub> loaded MEA, 120°C, 4 barg, 600 rpm, 160 Nml/min gas feed, 15% CO<sub>2</sub>, 1 week)**

<sup>23</sup> There is no previous CO<sub>2</sub> loading in experiments with no CO<sub>2</sub> in the gas feed.

Moreover, the relationship between the MEA loss and the O<sub>2</sub> concentration suggests that the apparent kinetics of the MEA oxidative degradation is close to a first-order rate regarding oxygen (a rigorous determination of the oxygen order will be performed in Chapter III when building the degradation model). Finally, the O<sub>2</sub>-dependency of MEA oxidative degradation can be related either to the oxygen availability in the liquid phase (mass transfer limitation) or to the kinetics of the chemical reaction. The influence of the agitation rate discussed in section 4.4 will give a further insight on this dependency.

#### Organic degradation products

The O<sub>2</sub> concentration in the gas feed has also an influence on the distribution of degradation products. It results from figure 2.30 that more HEI is formed when the O<sub>2</sub> concentration in the gas feed is increased. This is coherent with HEI as a major oxidative degradation product. On the contrary, the formation of HEPO and BHEOX does not depend on the O<sub>2</sub> concentration, although they are formed only when O<sub>2</sub> is present in the system.

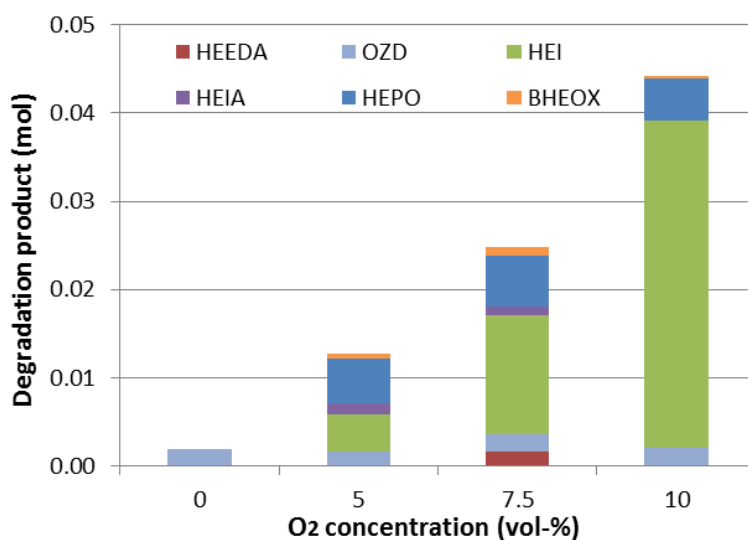


**Figure 2.30: influence of the O<sub>2</sub> concentration in the gas feed on organic degradation products (300 g, 30 wt% CO<sub>2</sub> loaded MEA, 120°C, 4 barg, 600 rpm, 160 Nml/min gas feed, 15% CO<sub>2</sub>, 1 week)**

*In conclusion, varying the gas feed composition leads to following observations:*

- Almost no degradation is observed in the absence of O<sub>2</sub> at 120°C, suggesting oxidative degradation as the main degradation pathway of MEA in the CO<sub>2</sub> capture process.
- The oxidative degradation of MEA seems to increase linearly with the O<sub>2</sub> concentration in the gas feed.
- The presence of CO<sub>2</sub> inhibits the oxidative degradation of MEA. However, the concentration of CO<sub>2</sub> in the gas feed has no influence.
- Ammonia, HEI and HEPO are the main oxidative degradation products observed.

#### 4.4 Influence of the agitation rate

Goff and Rochelle (2004) suggested that MEA oxidative degradation is limited by the gas to liquid oxygen transfer. This transfer is limiting in most studies due to low agitation rates. The objective of the present section is to determine if this is also the case for the experiments performed in the degradation test rig with enhanced gas circulation. Thus, different agitation rates (400, 600, 1000 and 1380 rpm) are tested for the O<sub>2</sub>-N<sub>2</sub> and the O<sub>2</sub>-CO<sub>2</sub>-N<sub>2</sub> systems.



*MEA loss and NH<sub>3</sub> emission*

As presented in figure 2.31, it appears that there is a linear relationship between the agitation rate and the degradation extent. When increasing the agitation speed, the specific power given to the system is increased, as well as the overall mass transfer coefficient. As a consequence, more oxygen is transferred to the liquid phase and the oxidative degradation is strongly enhanced. For instance, the MEA loss increases from 0.11 up to 1.25 mol in the O<sub>2</sub>-CO<sub>2</sub>-N<sub>2</sub> system. Figure 2.31 also confirms the inhibiting effect of CO<sub>2</sub> on MEA degradation since the MEA loss is lower for CO<sub>2</sub> loaded solutions at equivalent agitation rates<sup>24</sup>.

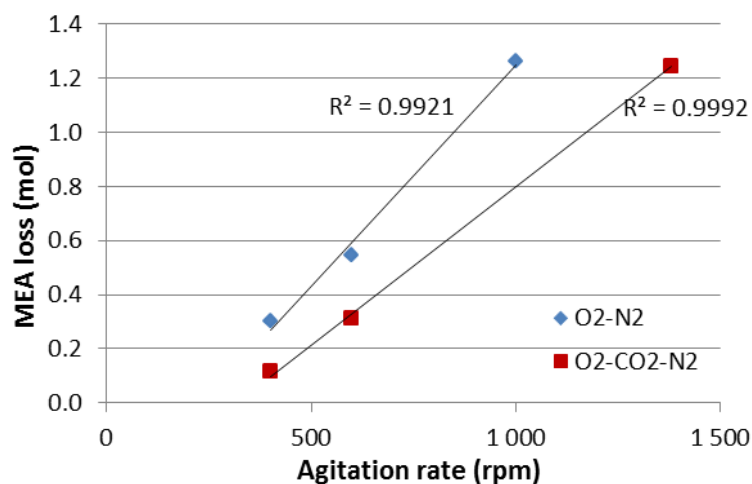


**Figure 2.31: influence of the agitation rate on MEA degradation (300 g, 30 wt% CO<sub>2</sub> loaded MEA<sup>25</sup>, 120°C, 4 barg, 5% O<sub>2</sub>, 160Nml/min gas feed, 1 week)**

As already mentioned, ammonia is the main product of MEA oxidative degradation. Its emission increases with the agitation speed as represented in figure 2.32 in the case of O<sub>2</sub>-N<sub>2</sub> gas feed with no previous CO<sub>2</sub> loading. The total amount of ammonia emitted over one week equals respectively 0.19, 0.23 and 0.67 mol for agitation rates of 400, 600 and 1000 rpm.

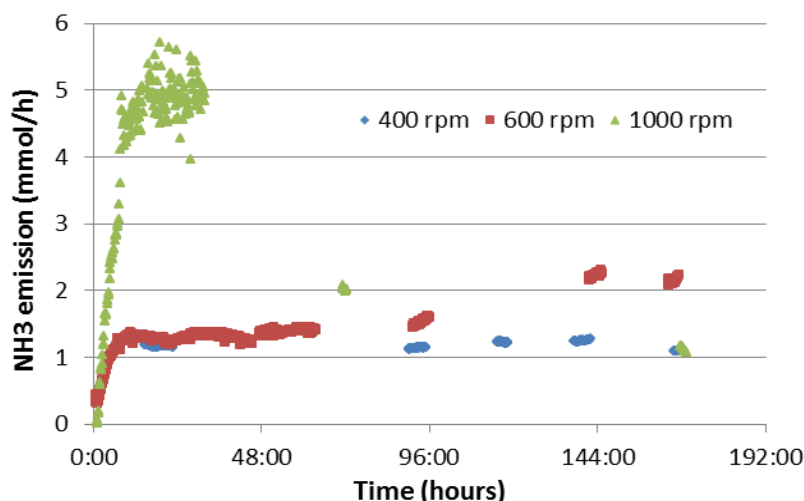


**Figure 2.32: influence of the agitation rate on NH<sub>3</sub> emission (300 g, 30 wt% unloaded MEA, 120°C, 4 barg, 160Nml/min gas feed, 5% O<sub>2</sub>/95% N<sub>2</sub>, 1 week)**

<sup>24</sup> The influence of agitation on MEA thermal degradation with a pure CO<sub>2</sub> gas feed has not been studied.

<sup>25</sup> There is no previous CO<sub>2</sub> loading in experiments with no CO<sub>2</sub> in the gas feed.

*Organic degradation products*

After 1-week degradation, HEI is the main degradation product in the liquid phase independently of the presence of CO<sub>2</sub> as presented in figure 2.33. The large amounts of HEI formed at high agitation rates confirm that oxidative degradation is the main reaction pathway and that it is limited by the oxygen transfer rate. At higher agitation rates, up to 0.11 mol HEI is formed. HEPO is also formed, but its formation seems less enhanced by the agitation rate.

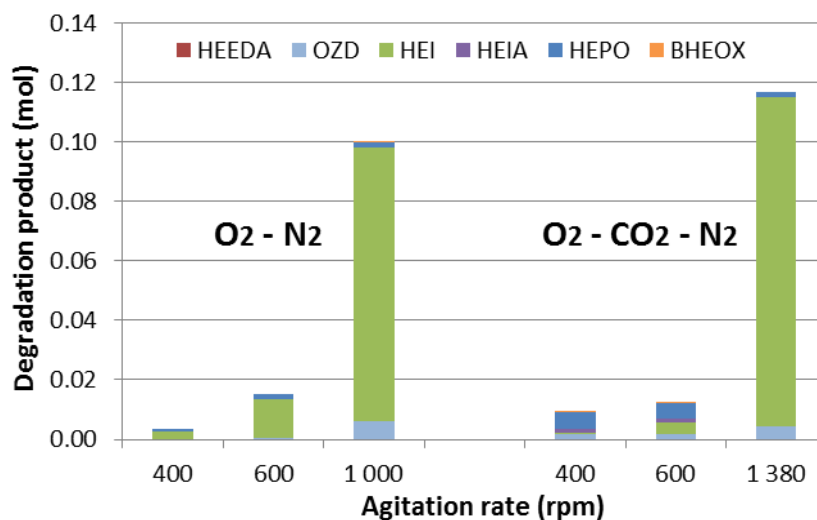


**Figure 2.33: influence of the agitation rate on organic degradation products (300 g, 30 wt% CO<sub>2</sub> loaded MEA<sup>26</sup>, 120°C, 4 barg, 160Nml/min gas feed, 5% O<sub>2</sub>, 1 week)**

At higher agitation rates, other products appear as shown in the GC spectrum of the sample degraded at 1380 rpm (figure 2.34). In addition to HEI, acetamide and HEF are the major oxidative degradation products observed in the GC spectrum at 1380 rpm but they were not quantified. Thus, high agitation rates clearly accelerate the oxidative degradation, but also lead to the formation of large amounts of alternative degradation products not representative of industrial CO<sub>2</sub> capture units (Pilot 2 in figure 2.34).

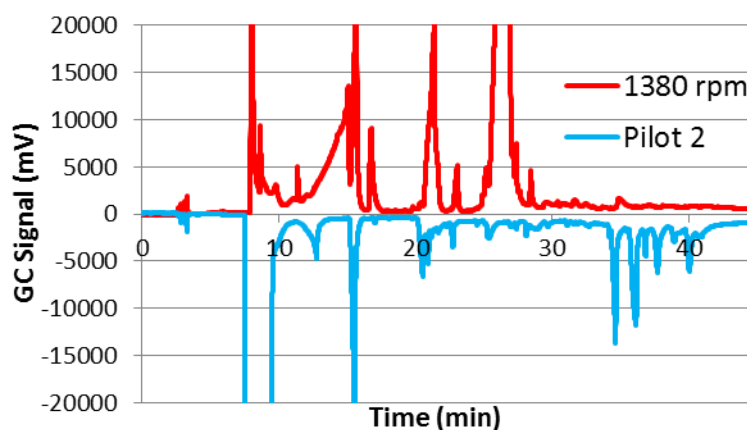


**Figure 2.34: GC comparison of the degradation at high agitation rate (300 g, 30 wt% CO<sub>2</sub> loaded MEA, 120°C, 4 barg, 1380 rpm, 160 Nml/min gas feed, 5% O<sub>2</sub>/15% CO<sub>2</sub>/80% N<sub>2</sub>, 1 week) with pilot plant degradation**

<sup>26</sup> There is no previous CO<sub>2</sub> loading in experiments with no CO<sub>2</sub> in the gas feed.

### Organic acids and dissolved metals

The concentration of organic acids increases at higher agitation rates, even if their total amount remains lower than 0.02 mol as presented in figure 2.35. Formate, oxalate and acetate are the most produced carboxylic acids. Their formation increases with the agitation rate which confirms that carboxylic acids are related to MEA oxidative degradation. More formate is produced at 400 rpm, but this may be due to the fact that organic acids were only analyzed after 2-week degradation for some experiments (experiments at 400 and 1000 rpm, resp. 1380 rpm, marked with a star \* in the figures).

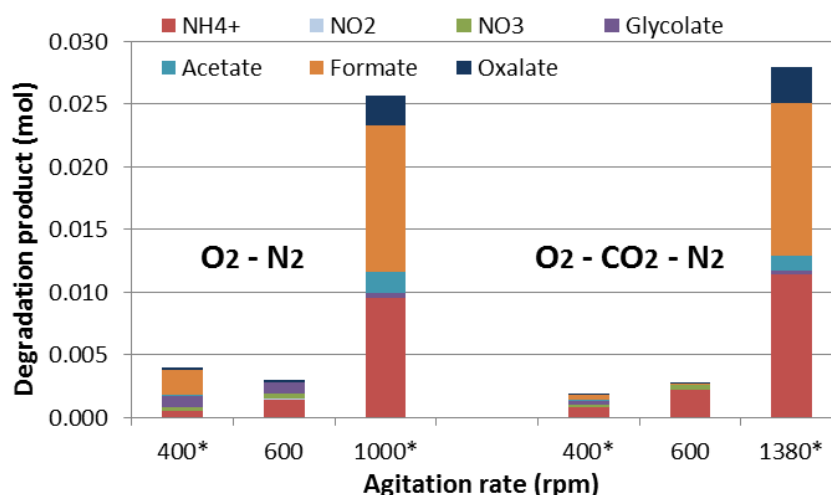


**Figure 2.35: influence of the agitation rate on the organic acids, nitrites and nitrates (300 g, 30 wt% CO<sub>2</sub> loaded MEA<sup>27</sup>, 120°C, 4 barg, 160Nml/min gas feed, 1 week)**

Finally, higher agitation rates increase the dissolved metal concentrations in the amine solution as shown in figure 2.36. Two combined effects may play a role: more metal ions leach from the vessel wall due to the higher mechanical constraints, and these dissolved metals lead to higher amounts of corrosive degradation products due to their catalytic effect on MEA oxidative degradation.

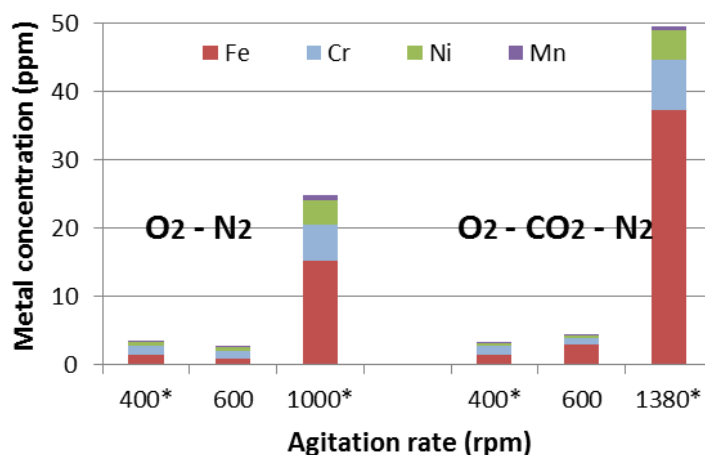


**Figure 2.36: influence of the agitation rate on dissolved metal concentrations (300 g, 30 wt% CO<sub>2</sub> loaded MEA<sup>27</sup>, 120°C, 4 barg, 160 Nml/min gas feed, 5% O<sub>2</sub>/15% CO<sub>2</sub>/80% N<sub>2</sub>, 1 week)**

<sup>27</sup> There is no previous CO<sub>2</sub> loading in experiments with no CO<sub>2</sub> in the gas feed.

In conclusion, varying the agitation rate leads to following observations:

- The oxidative degradation of MEA is limited by the oxygen mass transfer.
- Increasing the agitation rate leads to the formation of more  $\text{NH}_3$ ,  $\text{HEI}$  and formate.
- More dissolved metals are measured at higher agitation rates.

#### 4.5 Influence of the temperature

During the  $\text{CO}_2$  capture process, the amine solvent is continuously heated ( $120^\circ\text{C}$  in the stripper) and cooled down ( $40\text{-}60^\circ\text{C}$  in the absorber). In this section, different experiments are performed at  $55$ ,  $100$ ,  $120$  and  $140^\circ\text{C}$  to study the influence of temperature on degradation reactions.

##### MEA loss and $\text{NH}_3$ emission

Figure 2.37 shows that MEA degradation and  $\text{NH}_3$  emission seem to increase exponentially with temperature. At  $55^\circ\text{C}$ , almost no degradation is observed while the MEA loss reaches  $0.5$  mol at  $140^\circ\text{C}$  (initial MEA content:  $1.47$  mol). This evidences that temperature is a further limiting factor of MEA degradation. One could think that oxidative degradation is only limited by the oxygen mass transfer while thermal degradation with  $\text{CO}_2$  is limited by the temperature. However, the emission of  $\text{NH}_3$  also increases with temperature as presented in figure 2.37. Thus, the temperature dependency of the MEA degradation is not only due to the thermal degradation with  $\text{CO}_2$ , but also to the oxidative degradation.

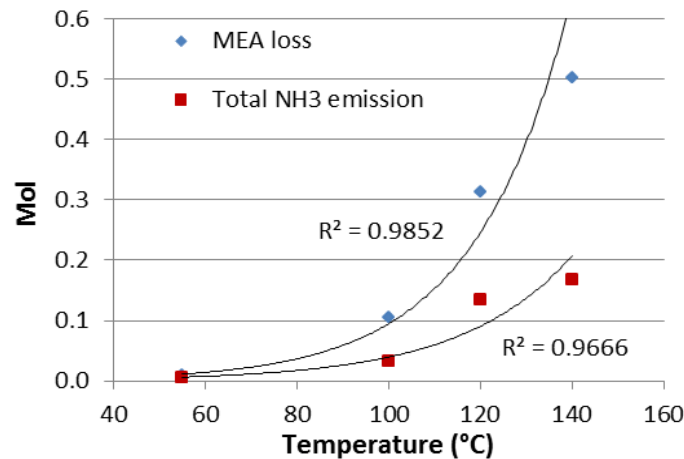


**Figure 2.37: influence of the temperature on MEA degradation and  $\text{NH}_3$  emission (300 g, 30 wt%  $\text{CO}_2$  loaded MEA, 600 rpm, 4 barg, 160 Nml/min gas feed, 5%  $\text{O}_2$ /15%  $\text{CO}_2$ /80%  $\text{N}_2$ , 1 week)**

As discussed in section 4.4, the oxygen mass transfer is the limiting step for MEA oxidative degradation. Figure 2.37 thus suggests that the oxygen transfer is enhanced at higher temperatures. Different phenomena may play a role on MEA oxidative degradation when the temperature is increased. In the case of combined absorption and chemical reaction (reactive absorption), the oxygen mass transfer can be approached by following equation<sup>28</sup>:

$$N_{\text{O}_2} = k_L \cdot a \cdot (C_{\text{O}_2}^{\text{interface}} - C_{\text{O}_2}^{\text{bulk}}) \cdot E \quad (2.14)$$

<sup>28</sup> The detailed description of reactive absorption is given in Chapter III, section 2.2.

- $N_{O_2}$  is the mass transfer of oxygen from the gas into the liquid (kmol/s)
- $k_L$  is the overall mass transfer coefficient (m/s)
- $a$  is the interface area (m<sup>2</sup>)
- $C_{O_2}$  is the concentration of oxygen, respectively at the interface and in the bulk (kmol/m<sup>3</sup>)
- $E$  is the enhancement factor (-)

The influence of temperature on equation 2.14 could be explained by different effects:

- Higher temperatures lead to a modification of the solvent physical properties like viscosity, surface tension, diffusivity coefficient... so that the interfacial area and the overall transfer coefficient may increase. For instance, the viscosity of aqueous 30 wt% MEA exponentially decreases with the temperature (Weiland et al., 1998), leading to an increase of the  $k_{L,a}$  value (Lemoine et al., 2003). This effect enhances the oxygen transfer.
- The concentration gradient in equation 2.14 may also be affected by the temperature since the solubility of oxygen decreases in the liquid solution at higher temperatures. Indeed, the solubility of a gas in a solvent can be estimated by Henry's law:

$$x_i = \frac{P_i}{K_H} \quad (2.15)$$

- $x_i$  is the gas molar fraction in the solvent (-)
- $P_i$  is the gas partial pressure (bar)
- $K_H$  is the Henry's constant (bar)

And the temperature dependency of Henry's constant can be derived from Van't Hoff equation:

$$K_H(T) = K_H(T^0) \cdot \exp \left[ -\frac{\Delta_s H}{R} \cdot \left( \frac{1}{T} - \frac{1}{T_0} \right) \right] \quad (2.16)$$

- $\Delta_s H$  is the enthalpy of solution (J/mol)
- $R$  is the universal gas constant (8.314 J/mol.K)
- $T$  is the temperature (K)
- $T_0$  is the reference temperature (298.15 °K)

At higher temperatures, the value of Henry's constant increases, leading to a lower gas solubility in the solvent solution. The value of the oxygen concentration at the interface decreases, so that the driving force for O<sub>2</sub> absorption is reduced and the mass transfer is lower.

However, the decreasing gas solubility at higher temperatures also plays a role for CO<sub>2</sub>. The CO<sub>2</sub> solubility in the amine solution is strongly dependent on the temperature since the ratio  $-\Delta_s H/R$  in equation 2.16 equals 2400 °K in the case of CO<sub>2</sub> and only 1700 °K for O<sub>2</sub> (Sander, 1999)<sup>29</sup>. As a consequence, the CO<sub>2</sub> is desorbed

<sup>29</sup> These values are valid for gas solubility in water. In an aqueous solution of 30 wt% MEA, values may differ.

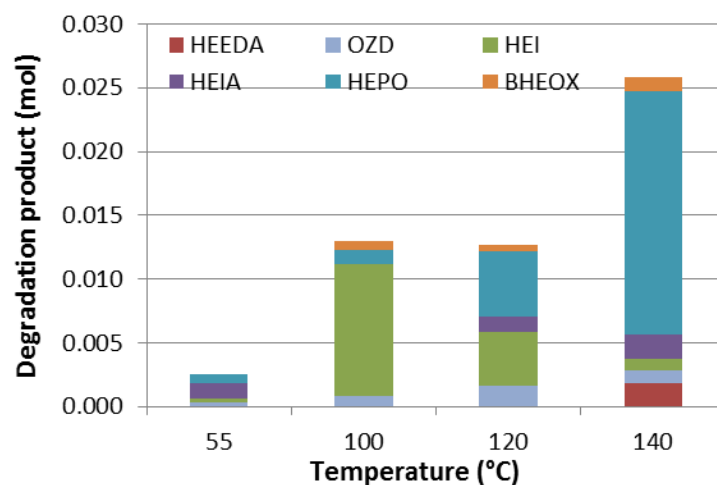
more rapidly than O<sub>2</sub> at higher temperatures and the inhibiting effect of CO<sub>2</sub> described in section 4.3 is reduced. Finally, the reduction of the oxygen solubility in the solvent may be compensated for by the lower CO<sub>2</sub> inhibiting effect at higher temperatures.

- The enhancement factor  $E$  in equation 2.14 describes the mass transfer acceleration due to the chemical reaction of O<sub>2</sub> with the amine solvent. When the temperature increases, the kinetics of the chemical reaction increases exponentially according to Arrhenius' law. Since the kinetic constant of the reaction may appear in the expression of the enhancement factor (see Chapter III, section 2.2), the enhancement factor may also vary exponentially with the temperature, inducing an exponential dependence of the oxygen mass transfer on the temperature.

Finally, these different effects are probably combined under the test conditions, leading to the dependency of the oxidative degradation rate on temperature observed in figure 2.37. Based on these experimental data, the apparent activation energy for oxidative amine degradation will be calculated in Chapter III.

#### *Organic degradation products*

When observing the degradation products in figure 2.38, it appears that more HEIA and HEEDA are formed at higher temperature. As already mentioned, HEIA and HEEDA have been identified as typical products of MEA thermal degradation with CO<sub>2</sub>. Since their production was not enhanced at higher CO<sub>2</sub> concentrations in the gas feed or at higher agitation rates, it confirms that the limiting factor for degradation with CO<sub>2</sub> is the temperature.



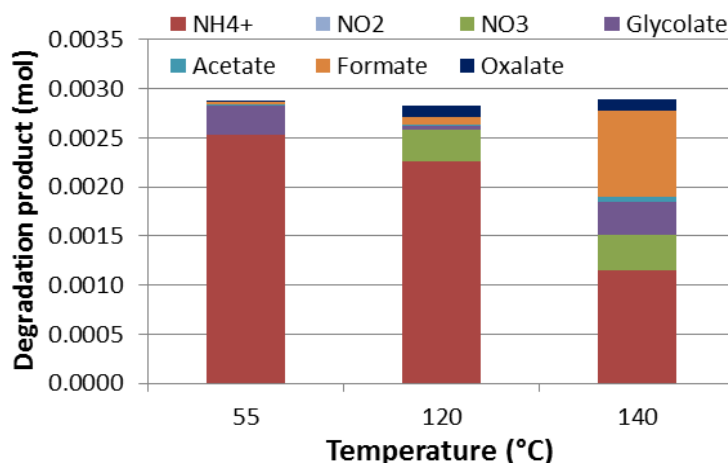
**Figure 2.38: influence of the temperature on organic degradation products (300 g, 30 wt% CO<sub>2</sub> loaded MEA, 600 rpm, 4 barg, 160 Nml/min gas feed, 5% O<sub>2</sub>/15% CO<sub>2</sub>/80% N<sub>2</sub>, 1 week)**

Figure 2.38 also shows that the formation of HEI, the major oxidative degradation product, is maximal at 100°C. It decreases at higher temperatures, although the oxidative degradation is increased as evidenced by the higher NH<sub>3</sub> emission. This is probably related to the lower thermal stability of HEI (Voice et al., 2012). Indeed, increasing the temperature also accelerates the further reactions of degradation products. Contrarily to HEI, the formation of HEPO is increased at high temperature. This confirms the condensation mechanism proposed by Strazisar et al. (2003) for the formation of HEPO. Indeed, condensation reactions release

water molecules, so that they are favored at higher temperatures due to water evaporation from the solution.

*Organic acids and dissolved metals*

More organic acids are formed with increasing temperature, especially formate and nitrate as shown in figure 2.39. On the contrary, the concentration of  $\text{NH}_4^+$  decreases. This is probably due to the high volatility of ammonia so that its liquid concentration decreases at higher temperature. However, the liquid concentration of  $\text{NH}_4^+$  is an order of magnitude lower than the  $\text{NH}_3$  emission.



**Figure 2.39: influence of the temperature on organic acids, nitrite and nitrate (300 g, 30 wt%  $\text{CO}_2$  loaded MEA, 600 rpm, 4 barg, 160 Nml/min gas feed, 5%  $\text{O}_2$ /15%  $\text{CO}_2$ /80%  $\text{N}_2$ , 1 week)**

As presented in figure 2.40, it seems that the concentration of dissolved metals leaching from the reactor vessel slightly increases with the temperature, maybe due to the higher amounts of corrosive degradation products in the solution. However, more tests would be necessary to understand the interactions between temperature, degradation and corrosion.

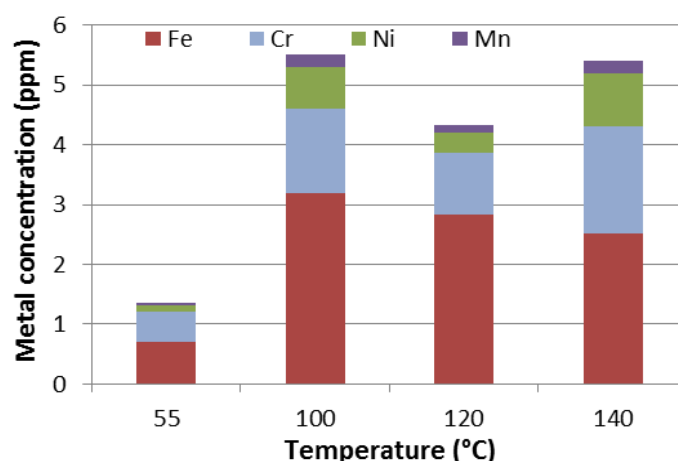


**Figure 2.40: influence of the temperature on dissolved metal concentrations (300 g, 30 wt%  $\text{CO}_2$  loaded MEA, 600 rpm, 4 barg, 160 Nml/min gas feed, 5%  $\text{O}_2$ /15%  $\text{CO}_2$ /80%  $\text{N}_2$ , 1 week)**

In conclusion, varying the temperature leads to following observations:

- The oxidative degradation of MEA seems to increase exponentially with the temperature. This can be explained by the dependency of the oxygen mass transfer on temperature.
- The formation of  $\text{NH}_3$ , HEPO and formate increases with the temperature, while the formation of HEI decreases.

#### 4.6 Influence of the test duration

The objective of this section is to study the evolution of degradation with time. Intermediate samples are compared on a mass concentration basis since mol amounts could not be determined at intermediate times (the total solution weight was not measured during the run).

##### MEA loss

As presented in figure 2.41 for two experiments with varying gas feed composition (5%  $\text{O}_2$ /15%  $\text{CO}_2$ /80%  $\text{N}_2$  and 5%  $\text{O}_2$ /30%  $\text{CO}_2$ /65%  $\text{N}_2$ ), the mid-term sample after 3 days shows an intermediate degradation level. The time evolution of MEA degradation seems to be linear but it is difficult to conclude since many degradation reactions take place and some degradation products further react with MEA.

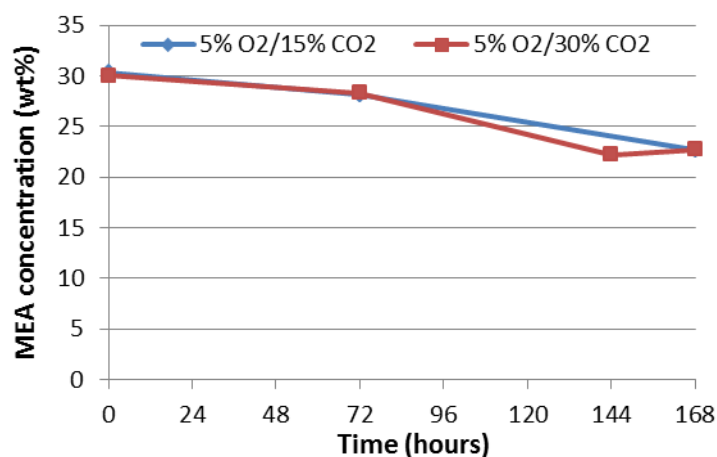


**Figure 2.41: evolution of the MEA concentration with time (300 g, 30 wt%  $\text{CO}_2$  loaded MEA, 120°C, 4 barg, 160 Nml/min gas feed, 5%  $\text{O}_2$ /30%  $\text{CO}_2$ /65%  $\text{N}_2$ , 1 week)**

##### Organic degradation products

Figure 2.42 represents the time evolution of organic degradation products for the experiment with 30%  $\text{CO}_2$  in the gas feed. HEEDA and HEIA, typical products of MEA thermal degradation with  $\text{CO}_2$ , are formed very slowly and could not be detected in the intermediate samples. Regarding HEPO and HEI, the formation rate seems to vary linearly with time. This is also the case for BHEOX. Finally, it seems that the amount of OZD reaches a maximum after 6 days, which tends to confirm that OZD is an intermediate degradation product that further reacts to form HEEDA and HEIA.



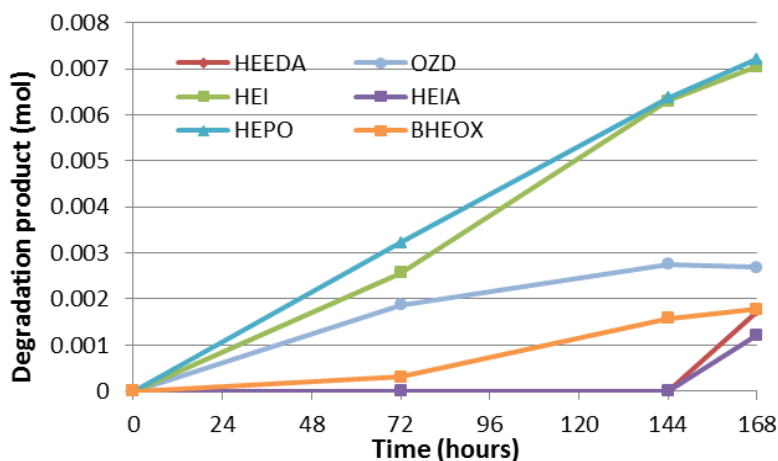


**Figure 2.42: evolution of the organic degradation products with time (300 g, 30 wt% CO<sub>2</sub> loaded MEA, 120°C, 4 barg, 160 Nml/min gas feed, 5% O<sub>2</sub>/30% CO<sub>2</sub>/65% N<sub>2</sub>, 1 week)**

*In conclusion, it seems that degradation evolves linearly with time. However, further reactions of MEA with degradation products may lead to nonlinear time evolution.*

#### 4.7 Influence of additives

The objective of this section is to test the influence of dissolved metals on the MEA degradation rate and to study the potential of inhibitors for reducing the degradation extent.

##### *Dissolved metals*

The effect of single metals on MEA degradation has already been described in the literature as mentioned in section 2.3. Dissolved metals enhance the oxidative degradation of MEA due to their catalytic effect in the formation of free radicals. Under base case conditions, metal does not leach from the reactor vessel since the dissolved metal concentration at the end of the experiment is lower than 3 ppm for iron and lower or equal to 1 ppm for chromium, nickel and manganese. In this section, a mix of stainless steel metals is added to the solution in order to study their influence on MEA degradation. Based on the concentrations of Fe, Cr, Ni and Mn measured during a MEA test campaign on a real CO<sub>2</sub> capture plant, corresponding amounts of metal salts have been added in our experiments. The concentration of dissolved metals in the initial base case experiment with metal mix has been analyzed by atomic absorption spectroscopy as presented in table 2.14.

**Table 2.14: metal concentrations in amine solution**

| Metal            | Measured metal concentrations in Pilot 2 (ppm) | Initial metal concentration in the base case experiment with metals (ppm) | Corresponding metal salt                            |
|------------------|--|---|---|
| Fe <sup>2+</sup> | 52   | 52.8  | FeSO <sub>4</sub> ·7H <sub>2</sub> O                |
| Cr <sup>3+</sup> | 5  | 1.4   | CrK <sub>8</sub> S <sub>2</sub> ·12H <sub>2</sub> O |
| Ni <sup>2+</sup> | 6  | 5.3   | NiSO <sub>4</sub> ·6H <sub>2</sub> O                |
| Mn <sup>2+</sup> | 2  | 1.4   | MnSO <sub>4</sub> ·1H <sub>2</sub> O                |

*MEA loss and NH<sub>3</sub> emission*

As expected, the presence of dissolved metals enhances MEA degradation as shown in figure 2.43. The MEA loss rises by 58% from 0.31 mol in the base case up to 0.49 mol with dissolved metals in the solution. Similarly, the total emission of ammonia increases, which indicates that metal ions catalyze the oxidative degradation of MEA as mentioned by Bedell (2011).

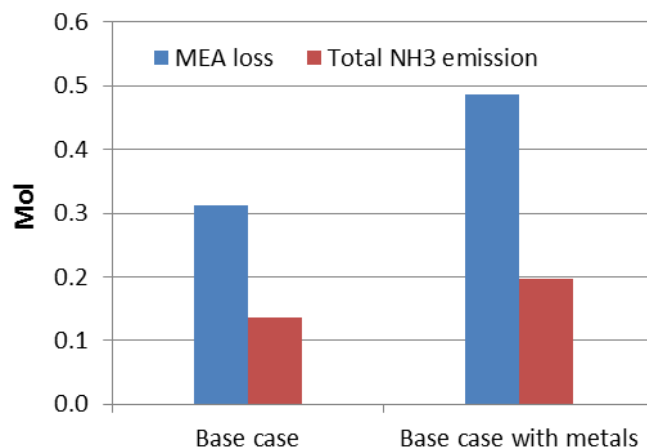


**Figure 2.43: influence of dissolved metals on MEA degradation and NH<sub>3</sub> emission (300 g, 30 wt% CO<sub>2</sub> loaded MEA, 600 rpm, 120°C, 4 barg, 160 Nml/min gas feed, 5% O<sub>2</sub>/15% CO<sub>2</sub>/80% N<sub>2</sub>, 1 week)**

*Organic degradation products*

The influence of metals is confirmed by figure 2.44 which represents the distribution of organic degradation products for the base case experiment with and without metals. The formation of the oxidative degradation product HEI is significantly increased by the addition of metals. On the contrary, metals do not seem to show any catalytic effect on MEA thermal degradation with CO<sub>2</sub> since no significant effect is observed on the concentrations of typical thermal degradation products like OZD, HEEDA and HEIA.

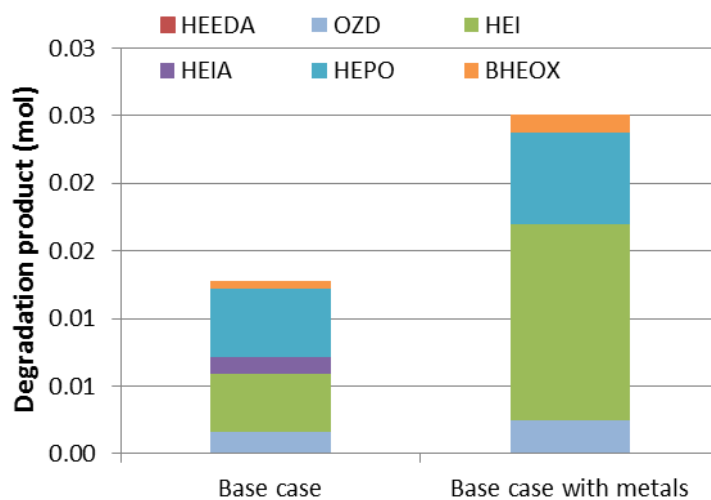


**Figure 2.44: influence of dissolved metals on organic degradation products (300 g, 30 wt% CO<sub>2</sub> loaded MEA, 600 rpm, 120°C, 4 barg, 160 Nml/min gas feed, 5% O<sub>2</sub>/15% CO<sub>2</sub>/80% N<sub>2</sub>, 1 week)**

### Organic acids

In the presence of dissolved metals, the concentration of organic acids increases as represented in figure 2.45. This is especially the case for formate and glycolate. The concentration of nitrate is also higher. Oxalate and  $\text{NH}_4^+$  are also present in larger concentrations in the experiment with metals.

Carboxylic acids concentrations in degraded samples from pilot plants are also reported in figure 2.45. Under industrial  $\text{CO}_2$  capture conditions, the main carboxylic acids formed are formate and glycolate. These acids are less present in the base case without metals. However, in the presence of dissolved metals, formate and acetate also clearly appear in the sample degraded in the DTR. This suggests that dissolved metals play an important role in MEA degradation under industrial  $\text{CO}_2$  capture conditions.

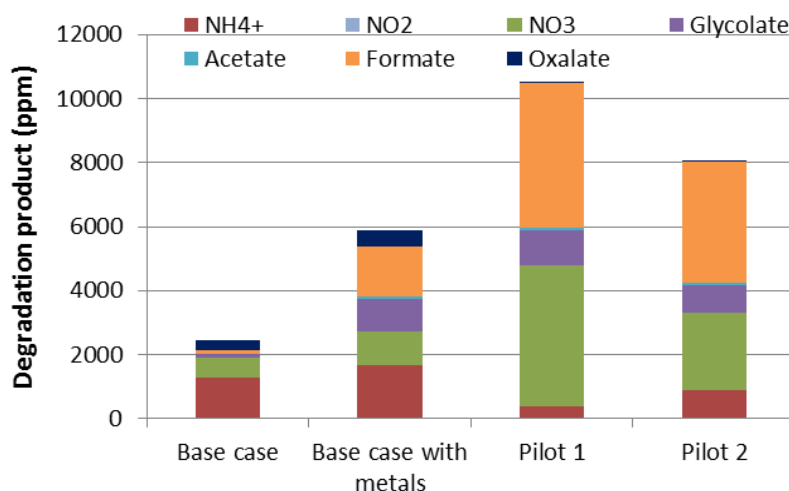


**Figure 2.45: influence of dissolved metals on organic acids, nitrite and nitrate (300 g, 30 wt%  $\text{CO}_2$  loaded MEA, 600 rpm,  $120^\circ\text{C}$ , 4 barg, 160 Nml/min gas feed, 5%  $\text{O}_2$ /15%  $\text{CO}_2$ /80%  $\text{N}_2$ , 1 week)**

### Degradation inhibitors

Based on the literature review summarized in section 2.4, several degradation inhibitors have been selected and tested in the degradation test rig. So far, these inhibitors have only been tested in oxidative degradation conditions, i.e. at moderate temperature ( $\sim 55^\circ\text{C}$ - $80^\circ\text{C}$ ) in the presence of oxygen. The objective of the present study is to evaluate their influence on MEA degradation in accelerated degradation conditions. The following inhibitors have been tested in the degradation test rig:

- The first one has been developed at the University of Texas at Austin. Its composition has not been divulged, so that it is called “inhibitor A”. One liter of MEA 30 wt% containing 100 mMol/kg inhibitor A (between 0.5 and 5 wt%) has been received from Alexander Voice, PhD student at the University of Texas at Austin. Inhibitor A is a radical scavenger, which means that it reacts with free radicals and stops the propagation of chain reactions.
- The second inhibitor is one of many inhibitors patented by the French research institute IFPEN. It is called DMTD (dimercaptotriazazole,  $\text{C}_2\text{H}_2\text{N}_2\text{S}_3$ ) and it also works by reacting with free radicals. 1 wt% of the inhibitor was added to the solution.

- The third inhibitor is HEDP (hydroxyethylidene diphosphonic acid,  $C_2H_8O_7P_2 \cdot H_2O$ ). In this case, the inhibition mechanism is different. Indeed, HEDP is a chelating molecule that forms complexes with metals, so that the catalytic effect of dissolved metals is reduced. 1 wt% of the degradation inhibitor was added to the amine solution.
- A combination of 100 mMol/kg inhibitor A with 1 wt% HEDP has also been studied to observe the combined effect of chelating inhibitors and radical scavengers.

Finally, the thermal stability of different inhibitors including those already mentioned has been studied in batch reactors (see section 5.3).

In order to get as close as possible to real  $CO_2$  capture operations, the metal mix described in the previous section ( $Fe^{2+}$ ,  $Cr^{3+}$ ,  $Ni^{2+}$ ,  $Mn^{2+}$ ) is added to the amine solution with the inhibitor to be tested. As a consequence, experiments with degradation inhibitors are compared to the base case with metals described in the previous section. Other operating parameters remain similar to the initial base case.

#### *MEA loss and $NH_3$ emission*

Figure 2.46 presents the MEA loss and the total ammonia emission for each experiment. It appears that Inhibitor A and DMTD are very efficient. Indeed, the degradation rate is reduced and very little ammonia is emitted. The decrease of the ammonia emission indicates that Inhibitor A and DMTD inhibit the oxidative degradation of MEA. On the contrary, HEDP is not successful at limiting MEA degradation or  $NH_3$  emission in the test conditions. Moreover, the combination of Inhibitor A with HEDP is less efficient than Inhibitor A only.

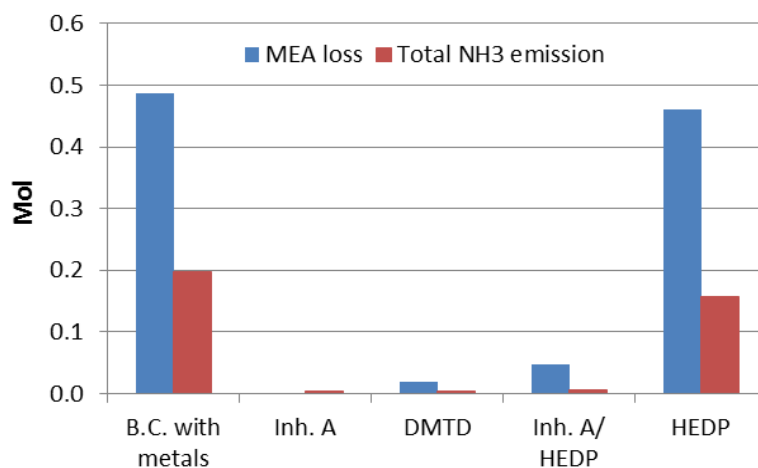


**Figure 2.46: influence of inhibitors on MEA degradation and  $NH_3$  emission (300 g, 30 wt%  $CO_2$  loaded MEA, 600 rpm,  $120^\circ C$ , 4 barg, 160 Nml/min gas feed, 5%  $O_2$ /15%  $CO_2$ /80%  $N_2$ , 1 week)**

#### *Organic degradation products*

The inhibition of the oxidative degradation by Inhibitor A and DMTD is confirmed by the absence of HEI in these experiments as evidenced in figure 2.47. However, more OZD is produced in the DMTD experiment, but no explanation could be advanced. Finally, similar amounts and types of degradation products are formed with HEDP compared to the base case with metals. This confirms the inefficiency of HEDP at inhibiting MEA degradation.

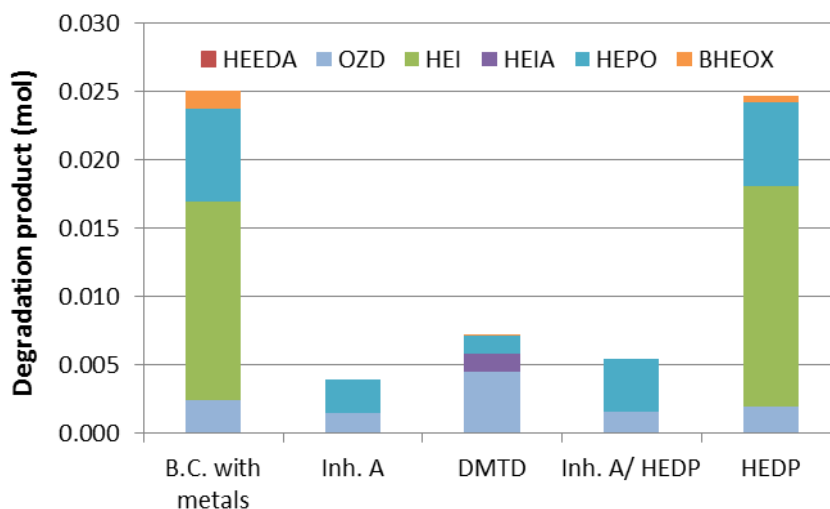


**Figure 2.47: influence of inhibitors on organic degradation products (300 g, 30 wt% CO<sub>2</sub> loaded MEA, 600 rpm, 120°C, 4 barg, 160 Nml/min gas feed, 5% O<sub>2</sub>/15% CO<sub>2</sub>/80% N<sub>2</sub>, 1 week)**

#### *Organic acids and dissolved metals*

Similar results are obtained regarding the production of nitrates and carboxylic acids (figure 2.48). DMTD and Inhibitor A both prevent the production of formate, but more glycolate is formed with Inhibitor A. In the case of DMTD, ammonium is also produced.

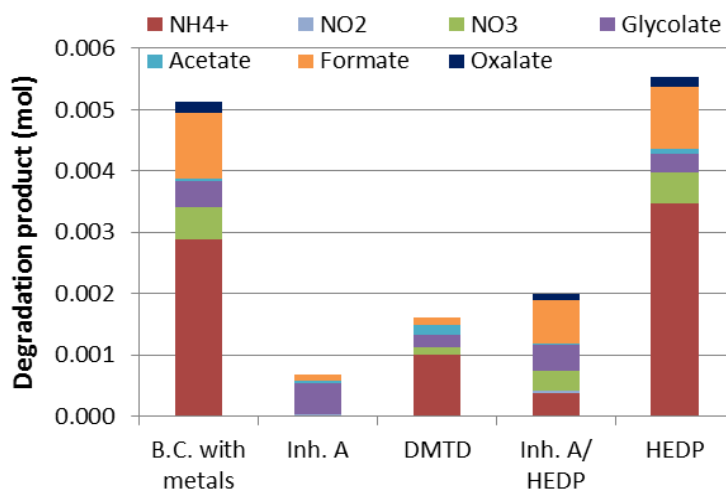


**Figure 2.48: influence of inhibitors on organic acids, nitrite and nitrate (300 g, 30 wt% CO<sub>2</sub> loaded MEA, 600 rpm, 120°C, 4 barg, 160 Nml/min gas feed, 5% O<sub>2</sub>/15% CO<sub>2</sub>/80% N<sub>2</sub>, 1 week)**

*In conclusion, the addition of metals and degradation inhibitors leads to following observations:*

- *Dissolved metals catalyze the oxidative degradation of MEA but have no effect on the thermal degradation with CO<sub>2</sub>.*
- *NH<sub>3</sub>, HEI, formate and glycolate are the main products enhanced by the addition of dissolved metals.*
- *Inhibitor A and DMTD successfully inhibit the oxidative degradation of MEA.*
- *HEDP is not successful at inhibiting the oxidative degradation of MEA.*

## 5. Batch Experiments

Totally, 20 experiments were performed under batch conditions: 19 experiments in batch degradation cylinders and one experiment using the DTR in batch mode. The objective of batch experiments is to study the MEA thermal degradation with CO<sub>2</sub>. Contrarily to the study of oxidative degradation, there is no need for a continuous gas supply. Moreover, figure 2.49 shows that similar degradation products are obtained in the batch experiment performed in the DTR and in the degradation cylinders: HEEDA, HEIA, and a product that has not been identified, Product 20. These products are typical products of the MEA thermal degradation with CO<sub>2</sub>. Thus, since similar results can be obtained in degradation cylinders compared with the DTR, degradation in the cylinders is preferred due to the possibility of running up to seven experiments in parallel.

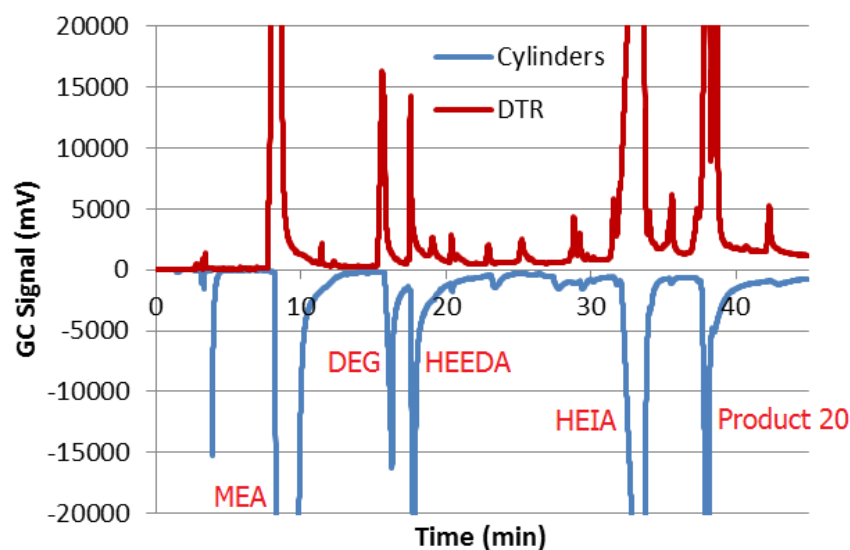


**Figure 2.49:** comparison of MEA batch degradation in cylinders (100 g, 30 wt% CO<sub>2</sub> loaded MEA, no gas feed, 140°C, 3 weeks) and in the DTR (300 g, 30 wt% CO<sub>2</sub> loaded MEA, 400 rpm, 120°C, 20 barg, no gas feed, 2 weeks)

In this section, the influence of the CO<sub>2</sub> loading is first presented and then the effect of temperature on MEA thermal degradation with CO<sub>2</sub>. Simultaneously, the influence of metals is also studied by adding the same metal mix as described in section 4.7. Finally, seven experiments have been performed with promising inhibitors proposed to prevent MEA oxidative degradation. The stability of the inhibited MEA solutions under thermal degradation with CO<sub>2</sub> is evaluated. Results are presented graphically, but the detailed figures can be found in appendix 5.

### 5.1 Influence of CO<sub>2</sub>

As mentioned in the description of the different degradation mechanisms, the thermal degradation of MEA is not expected to happen in the absence of CO<sub>2</sub> at temperatures below 200°C. On the contrary, thermal degradation with CO<sub>2</sub> is expected at 140°C (Lepaumier, 2008).

### MEA loss

The influence of CO<sub>2</sub> on the thermal degradation of MEA is confirmed by figure 2.50. When the solution is not loaded with CO<sub>2</sub>, there is almost no MEA loss over 3 weeks while the MEA loss reaches 37.4% in the presence of CO<sub>2</sub><sup>30</sup>. Furthermore, figure 2.50 clearly shows that dissolved metals do not influence MEA thermal degradation with CO<sub>2</sub>.

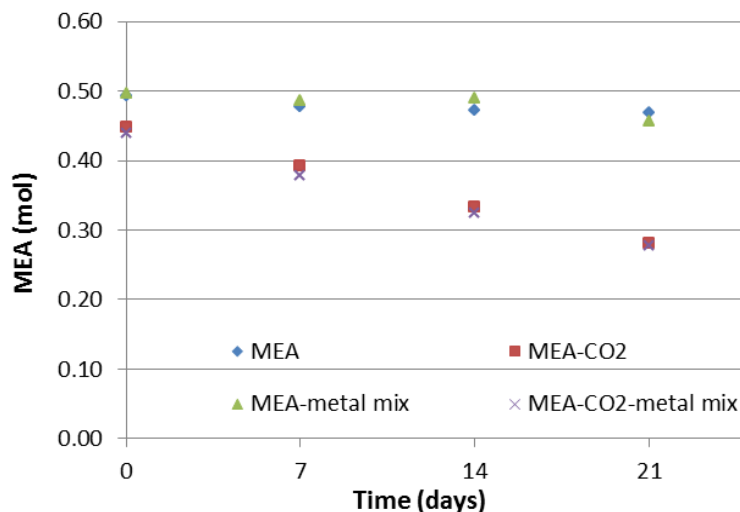


**Figure 2.50: influence of CO<sub>2</sub> and dissolved metals on MEA thermal degradation with CO<sub>2</sub> (100 g, 30 wt% MEA, no gas feed, 140°C, 3 weeks)**

### Organic degradation products

Figure 2.51 shows that the main identified products of MEA thermal degradation with CO<sub>2</sub> are HEEDA and HEIA, and in a less extent, OZD. This is in agreement with the degradation mechanisms presented in section 2.1. The small amounts of degradation products formed in non-loaded solutions may be due to CO<sub>2</sub> contamination since the solutions were not degassed before testing.

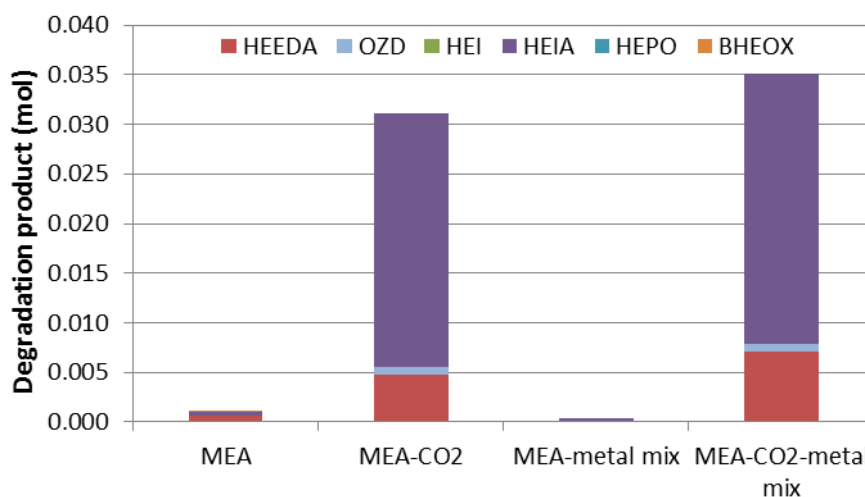


**Figure 2.51: influence of CO<sub>2</sub> on thermal degradation products (100 g, 30 wt% MEA, no gas feed, 140°C, 3 weeks)**

<sup>30</sup> In each case, 100 g of solution is set in the degradation reactors. In the case of loaded solutions, the initial mole number of MEA is lower due to the dilution effect of the CO<sub>2</sub> loading.

The time evolution of the formation of thermal degradation products is represented in figure 2.52. Indeed, the concentration of OZD and HEEDA goes through a maximum while the concentration of HEIA increases linearly. This confirms the degradation mechanism described in section 2.1 that considers OZD and HEEDA as intermediate products that further react to form HEIA. Again, no significant difference is observed in the presence of dissolved metals in the solution.

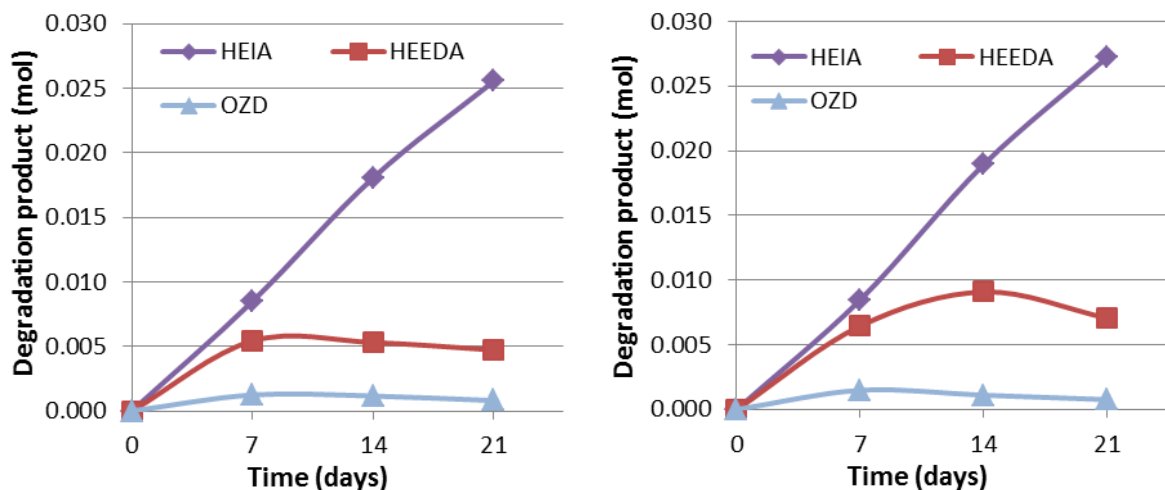


**Figure 2.52:** formation of degradation product over time in the case of loaded MEA (left) and loaded MEA with metal mix (right) (100 g, 30 wt% CO<sub>2</sub> loaded MEA, no gas feed, 140°C, 3 weeks)

In conclusion, the influence of CO<sub>2</sub> on MEA thermal degradation can be summarized as:

- MEA thermal degradation at 140°C does not occur in the absence of CO<sub>2</sub>.
- In the presence of CO<sub>2</sub>, the main degradation products are HEIA and HEEDA.
- Dissolved metals have no influence on the thermal degradation of MEA.

## 5.2 Influence of temperature

The results in semi-batch mode have shown that MEA thermal degradation with CO<sub>2</sub> strongly depends on the temperature since CO<sub>2</sub> degradation products are much more present at 140°C than at 120°C. This section studies the influence of temperature in batch experiments.

### MEA loss

Figure 2.53 confirms that MEA loss due to thermal degradation with CO<sub>2</sub> is very low at 120°C. On the contrary, loaded MEA clearly degrades at 140°C. Similar results have been obtained when testing the thermal stability of MEA solutions that have previously undergone oxidative degradation<sup>31</sup>. It seems that the thermal degradation rate is lower in the case of the solution that initially contains oxidative degradation products. However, the CO<sub>2</sub> loading of the oxidative degraded solution is expected to be lower than the loading of fresh MEA solutions, but this could not be measured. This lower CO<sub>2</sub> loading may explain the lower thermal degradation rate with CO<sub>2</sub>.

<sup>31</sup> Degraded solutions were prepared by mixing 50 g of fresh CO<sub>2</sub> loaded MEA with 50 g of degraded MEA from Pilot 2.



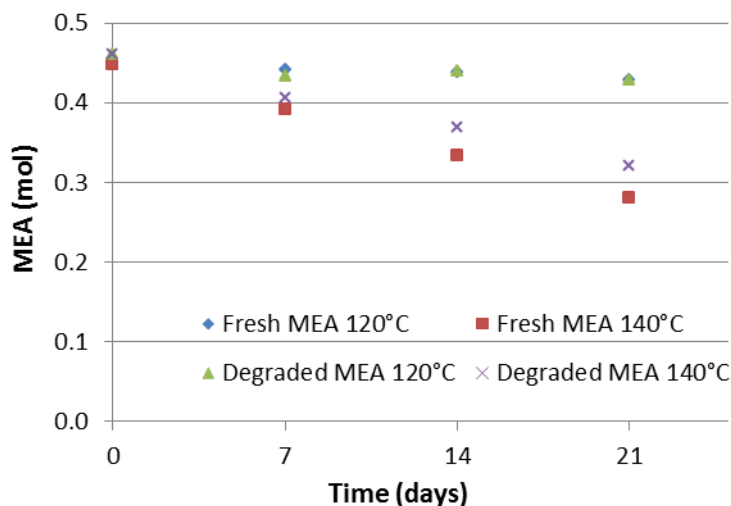


**Figure 2.53: influence of the temperature on MEA thermal degradation with CO<sub>2</sub> (100 g, 30 wt% CO<sub>2</sub> loaded MEA, no gas feed, 3 weeks)**

#### Organic degradation products

Figure 2.54 indicates that the limiting step in thermal degradation with CO<sub>2</sub> may be the formation of HEIA since the formation of HEEDA already takes place at 120°C, although at a lower extent. Thus, increasing the temperature up to 140°C especially increases the formation rate of HEIA. Oxidative degradation products like HEI, HEPO and BHEOX do not form in the test conditions but were present in the initial degraded solution. The lower concentration of HEIA in the presence of oxidative degraded solution could be explained by the lower CO<sub>2</sub> loading of the initial solution.

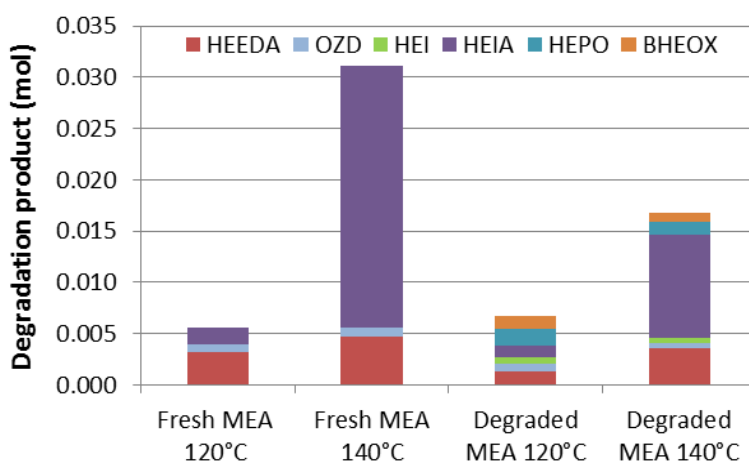


**Figure 2.54: influence of temperature on thermal degradation products (100 g, 30 wt% CO<sub>2</sub> loaded MEA, no gas feed, 3 weeks)**

*In conclusion, the influence of the temperature on MEA degradation with CO<sub>2</sub> can be summarized as:*

- *Almost no thermal degradation with CO<sub>2</sub> is observed at 120°C, but thermal degradation is confirmed at 140°C.*
- *The presence of oxidative degradation products in the initial solution seems to slightly inhibit the thermal degradation with CO<sub>2</sub> at 140°C. However, this may be due to a lower CO<sub>2</sub> loading of the oxidative degraded solution.*

### 5.3 Influence of degradation inhibitors

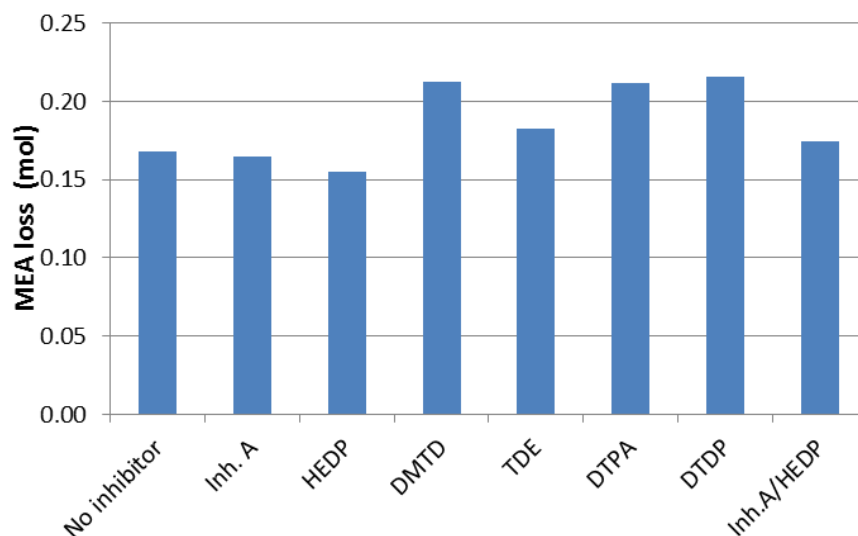
As mentioned in section 2.4, no degradation inhibitor has been developed to prevent MEA thermal degradation with CO<sub>2</sub> because the dominant degradation pathway is the oxidative degradation. However, oxidative degradation inhibitors may be degraded at stripping temperatures or even worse, have a negative influence on the thermal stability of loaded MEA solutions. Table 2.15 lists the six inhibitors tested at 140°C at an inhibitor concentration of 1 wt%. All these inhibitors are radical scavengers, apart from of HEDP which is a chelating agent. Moreover, a combination of Inhibitor A and HEDP has also been tested. In this case, the total inhibitor concentration is then 2 wt%.

**Table 2.15: oxidative degradation inhibitors tested in batch reactors**

|        | Compound                              | Composition  | CAS number |
|--------|---------------------------------------|--|------------|
| Inh. A | Inhibitor A                           | Not divulgated   | n.a.       |
| HEDP   | 1-hydroxyethylidene diphosphonic acid | C <sub>2</sub> H <sub>8</sub> O <sub>7</sub> P <sub>2</sub> · H <sub>2</sub> O                             | 25211-86-3 |
| DMTD   | 2,5-dimercapto-1,3,4-thiadiazole      | C <sub>2</sub> H <sub>2</sub> N <sub>2</sub> S <sub>3</sub>  | 1072-71-5  |
| TDE    | 2-2'-thiodiethanol                    | C <sub>4</sub> H <sub>10</sub> O <sub>2</sub> S  | 111-48-8   |
| DTPA   | diethylenetriaminepentaacetic acid    | [(HOOCCH <sub>2</sub> ) <sub>2</sub> NCH <sub>2</sub> CH <sub>2</sub> ] <sub>2</sub> NCH <sub>2</sub> COOH | 67-43-6    |
| DTDP   | 3,3'-Dithiodipropionic acid           | C <sub>6</sub> H <sub>10</sub> O <sub>4</sub> S <sub>2</sub>   | 1119-62-6  |

#### MEA loss

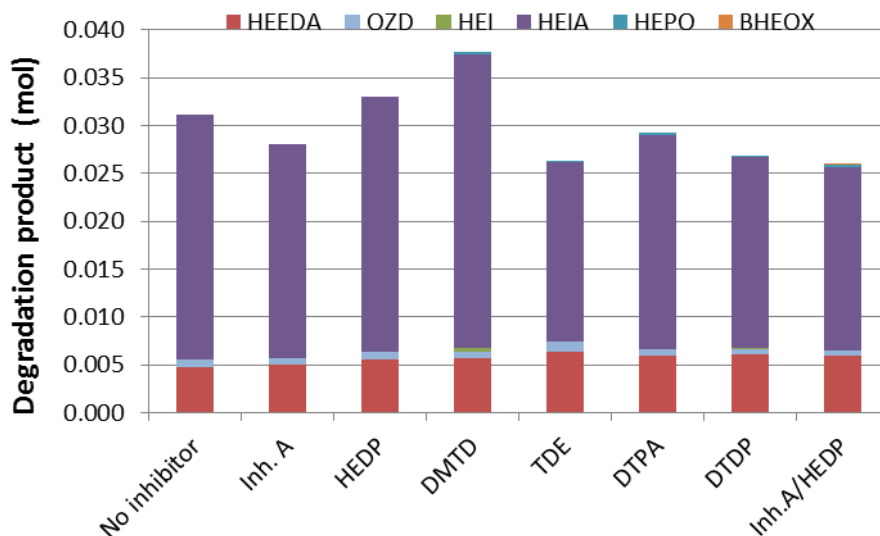
Figure 2.55 shows that three oxidative degradation inhibitors clearly enhance MEA thermal degradation with CO<sub>2</sub> after 3 weeks: DMTD, DTPA and DTDP. TDE also slightly increases the MEA loss. Finally, Inhibitor A and HEDP have no significant effect on the thermal stability of the solution.



**Figure 2.55: thermal stability of loaded MEA solutions with degradation inhibitors (100 g, 30 wt% CO<sub>2</sub> loaded MEA, no gas feed, 140°C, 3 weeks)**

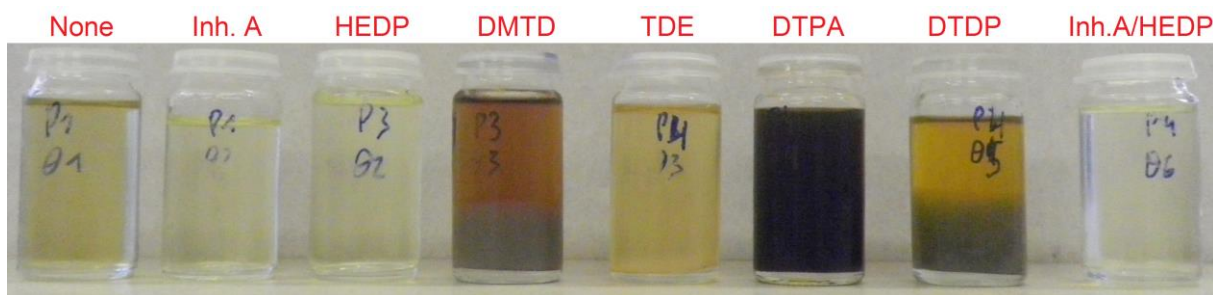
*Organic degradation products*

Figure 2.56 confirms that HEEDA and HEIA are the major degradation products. Product 20 is also present in all GC spectra but was not identified. No other major product was observed in GC apart from a large peak detected at 22 minutes in the experiment with TDE. However, other degradation products may be present in the solutions, though not recorded in GC.



**Figure 2.56: influence of inhibitors on thermal degradation products (100 g, 30 wt% CO<sub>2</sub> loaded MEA, no gas feed, 140°C, 3 weeks)**

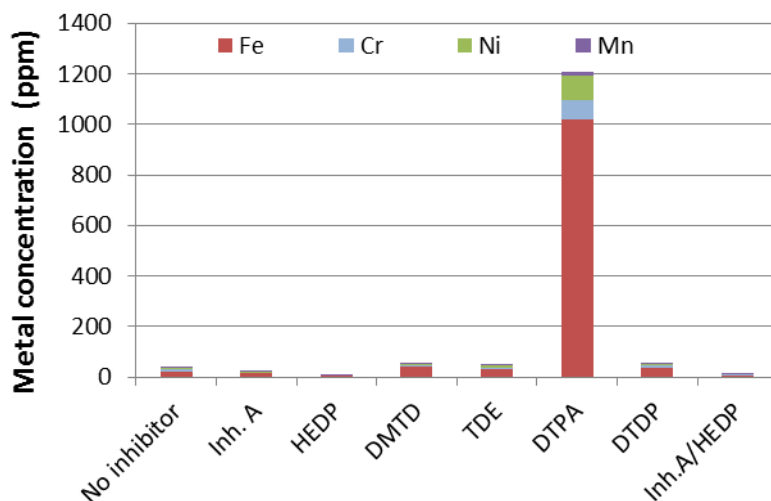
Figure 2.57 shows the colors of degraded samples after 3-week experiments. In the case of DMTD and DTDP, a liquid-liquid phase separation appears. In the case of DTPA, the degraded solution is completely black, as it is usually the case in oxidative degradation experiments. On the contrary, the solution remains transparent in the presence of Inhibitor A or HEDP. This indicates that HEEDA, HEIA or Product 20 are not responsible for the coloration. As a consequence, the coloration in the inhibited solutions (DMTD, TDE, DTPA and DTDP) may result from additional degradation products that are not usually present in thermal degraded MEA solutions.



**Figure 2.57: batch degraded samples with degradation inhibitors**

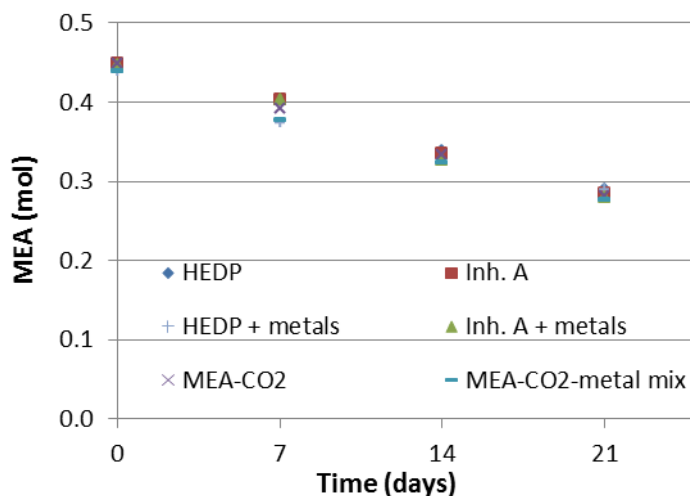
*Dissolved metals*

Figure 2.58 shows that the metal concentrations measured in the solution inhibited with DTPA are much larger than in the other experiments (no addition of dissolved metals in the initial solution). This could also result from the formation of additional degradation products that are very corrosive. More research should be necessary to identify those additional degradation products.



**Figure 2.58: influence of inhibitors on GC thermal degradation products (100 g, 30 wt% CO<sub>2</sub> loaded MEA, no gas feed, 140°C, 3 weeks)**

Finally, the metal mix previously described has been added in the initial MEA solutions inhibited with Inhibitor A or HEDP to see the combined influence of dissolved metals and inhibitors on the thermal degradation with CO<sub>2</sub>. In figure 2.59, the resulting MEA degradation confirms that dissolved metals have no significant influence on MEA thermal degradation with CO<sub>2</sub> whether HEDP or Inhibitor A are present or not.



**Figure 2.59: influence of metals and inhibitors on MEA thermal degradation (100 g, 30 wt% CO<sub>2</sub> loaded MEA, no gas feed, 140°C, 3 weeks)**

*In conclusion, following observations result from the test of oxidative degradation inhibitors:*

- Inhibitor A and HEDP have no effect on MEA thermal degradation with CO<sub>2</sub>.
- TDE slightly increases the thermal degradation of MEA with CO<sub>2</sub>.
- DMTD, DTPA and DTDP significantly increase the thermal degradation of MEA with CO<sub>2</sub>.
- In the case of DTPA, thermal degradation products strongly enhance the corrosivity of the solution.

## 6. Conclusions

In this chapter, the importance of amine solvent degradation has been highlighted. Degradation experiments have been performed in the degradation test rig, which consists in a heated and agitated pressure reactor with continuous gas feed. A base case experiment has been performed during one week with 30 wt% CO<sub>2</sub> loaded MEA with following operating conditions:

- 120°C
- 4 barg
- 600 rpm
- 160 ml/min gas feed
- 5% O<sub>2</sub> / 15% CO<sub>2</sub> / 80% N<sub>2</sub> gas feed composition

In base case conditions, similar degradation pathways and extents are observed in comparison with degraded samples from CO<sub>2</sub> capture pilots. Moreover, the nitrogen balance of MEA degradation experiments can be closed within the 10% range and the results of the base case experiment could be repeated with a relative difference lower than 4%.

The influence of different operating parameters on MEA degradation has been studied: gas feed composition, agitation rate, and temperature. Following results have been observed:

- Oxidative degradation is the main degradation pathway taking place in industrial CO<sub>2</sub> capture conditions. Almost no degradation could be observed in the absence of oxygen at 120°C.
- Oxidative degradation is increased at higher O<sub>2</sub> concentrations in the gas feed. Moreover, the influence of the agitation rate evidences that oxidative degradation is limited by the oxygen mass transfer between the gas and the liquid phases. It appears that this mass transfer is increased at higher agitation rates and higher temperatures.
- The main product resulting from the oxidative degradation of MEA is ammonia, which accounts for 45% of the MEA loss in the base case experiment. Further important oxidative degradation products are HEI and HEPO.
- The initial CO<sub>2</sub> loading of the solvent inhibits the oxidative degradation but the CO<sub>2</sub> concentration in the gas feed has no influence on the degradation.
- Dissolved metals (Fe, Cr, Ni, Mn) catalyze the oxidative degradation and enhance the formation of NH<sub>3</sub>, HEI, formate and glycolate.
- Among the different oxidative degradation inhibitors tested, inhibitor A (provided by the University of Texas at Austin) and DMTD (patented by the IFPEN) successfully inhibit the oxidative degradation of MEA. HEDP shows no inhibiting effect on MEA oxidative degradation.

Besides semi-batch experiments in the degradation test rig, thermal degradation experiments with CO<sub>2</sub> have been performed in batch degradation reactors during three weeks. The influence of temperature and CO<sub>2</sub> has been quantified, as well as the influence of promising

oxidative degradation inhibitors on MEA thermal degradation with CO<sub>2</sub>. Following results have been reported:

- Almost no degradation could be observed in the absence of CO<sub>2</sub>.
- In the presence of CO<sub>2</sub>, little degradation of MEA could be observed at 120°C. On the contrary, significant MEA degradation is observed at 140°C.
- HEIA is the main thermal degradation product of MEA. HEEDA and OZD have also been identified, but they further react to form HEIA, which appears as an end-degradation product.
- Dissolved metals (Fe, Cr, Ni, Mn) do not influence the thermal degradation of MEA with CO<sub>2</sub>, independently of the presence of CO<sub>2</sub>.
- Inhibitor A and HEDP show no influence on the MEA thermal degradation with CO<sub>2</sub>, while other inhibitors like DMTD, TDE, DTPA and DTDP increase the thermal degradation of loaded MEA solutions.
- DTPA leads to a strong increase of the solution corrosivity in thermally degraded solutions.

Finally, these experimental results will be considered in the next chapter for the development of a global CO<sub>2</sub> capture model that takes MEA degradation into account.

## Chapter III

# Simulation of the CO<sub>2</sub> capture process

*“Computers are useless. They can only give you answers.”*  
*Pablo Picasso*

# 1. Introduction

As discussed in Chapter I, one of the main drawbacks of the CO<sub>2</sub> capture process is its large penalty on the power plant efficiency. Indeed, the energy requirements of CO<sub>2</sub> capture units are much larger than the energy requirement for other environmental control systems installed in current power plants like desulfurization or denitrification systems. Recently designed supercritical power plants with high efficiency are less affected by the CO<sub>2</sub> capture energy penalty than old low-efficient plants (Rubin et al., 2012). However, the overall plant efficiency still drops from 40% to 31% in the case of a new supercritical pulverized coal power plant.

The energy that is withdrawn from the power plant is supplied to the CO<sub>2</sub> capture process under the form of steam and electricity. It is composed of three main shares (ibid.):

- ~ 60% for thermal solvent regeneration,
- ~ 30% for CO<sub>2</sub> compression,
- ~ 10% for auxiliary equipment (fans, pumps...).

In this framework, the simulation of the capture process is an important part of the technology development that may avoid running some long and costly experiments. Simulations have the potential to give a better understanding of the process, leading to the optimization of the operating conditions and to the reduction of the process energy penalty. There are two main types of simulations:

- Steady-state simulations consider the stationary process, which is by definition time-independent. They may contribute to identify key operating parameters and propose optimal values for these parameters to increase the process energy efficiency. They also have the potential of virtually testing alternative flowsheet configurations for which experimental testing would induce large equipment transformation costs.
- Dynamic simulations consider the evolution of process variables with time. Transient operations may be frequent in CO<sub>2</sub> capture plants and often result from varying steam availability in the power plant, which can be related to the varying electricity demand. Dynamic models may be used to test and develop control strategies for regulating the process variables during these transient modes. The control of the process is also useful to stabilize it in case of unexpected perturbations.

The present chapter begins with the description of the state-of-the-art CO<sub>2</sub> capture modeling. Usual thermodynamic and reactive absorption models are discussed and the main simulation works regarding CO<sub>2</sub> capture with MEA are also presented. Then, four different models are described. The first two models are developed in steady-state mode to compare different assumptions for the CO<sub>2</sub> reactive absorption: the equilibrium assumption (neglecting mass transfer limitations) and the rate-based assumption (considering mass transfer limitations). The next model is a dynamic model based on an equilibrium assumption, with the objective of studying the transient behavior of the capture process. Last but not least, the degradation model has been developed in steady-state mode using a rate-based assumption.



This latest model is one of the main innovations of the present work. Based on the experimental degradation results described in Chapter II, the MEA degradation kinetics is included into a global model of the CO<sub>2</sub> capture process. Both thermal and oxidative degradation pathways are taken into account in the degradation model, which is also compared to some previously published attempts for modeling solvent degradation.

Finally, the simulation results are presented and discussed for each model. The impact of operating conditions on the energy penalty is first studied in order to compare the equilibrium and rate-based approaches. Then, the dynamic simulation and the performances of the proposed control strategy are presented. In the end, the results of the degradation model are exposed and compared to the degradation extents reported in existing pilot plants. The influence of key process variables on the formation of degradation products is also studied, as well as the influence of some process modifications improving the global process efficiency. Optimal operating conditions are proposed as a trade-off between environmental and energy penalties of the CO<sub>2</sub> capture process. This last point evidences the potential of such models to contribute to the large-scale design of post-combustion CO<sub>2</sub> capture plants.

## 2. State of the art

In this section, the most critical points for modeling the CO<sub>2</sub> capture process are reported and the solutions proposed in the literature are described. First, the main thermodynamic methods modeling the properties of amine solutions in the presence of CO<sub>2</sub> are presented. Indeed, electrolyte solutions like amine solvents require a special attention since they show large deviations from ideality. Then, the phenomena taking place in the absorber and stripper are considered, since they form the basis of the CO<sub>2</sub> capture process. The main modeling approaches for the hydrodynamics, mass transfer, and chemical reactions related to the reactive absorption are discussed. Finally, significant steady-state simulation studies of the CO<sub>2</sub> capture process are also presented. Pilot plant models, optimization studies and simulations of alternative flowsheet configurations are mentioned, as well as some dynamic studies of the process. The few attempts reported in the literature for including degradation phenomena in the process model are also presented.

### 2.1 Thermodynamic model

A good thermodynamic model is an essential prerequisite for modeling the CO<sub>2</sub> capture process. Indeed, the macroscopic properties of solvent solutions are determined by variables like temperature, pressure and component activities in the solution. These variables are themselves depending on molecular interactions taking place in multi-component solutions. A suitable description of the molecular interactions is thus essential for estimating the solution properties, and consequently, for any reliable process modeling.

In the case of solvents for the CO<sub>2</sub> capture process, the amine solution contains large quantities of ionic species called electrolytes. Due to strong inter-molecular interactions, electrolyte solutions show large deviations from ideality. These non-idealities can be estimated in two main ways (Austgen, 1989):

- Empirical models are using experimentally fitted parameters to correlate equilibrium relations in electrolyte solutions. They are of practical and simple use since they require less complex calculations than theoretical models. However, they do not rigorously calculate the composition of the liquid phase. Furthermore, they usually show a low predictive potential outside the range of the experimental data used for parameter fitting. The most used empirical model for amine solutions is the Kent-Eisenberg model (Kent and Eisenberg, 1976). This model predicts phase equilibrium data for CO<sub>2</sub> and H<sub>2</sub>S in MEA and DEA solvents by setting all activity coefficients to unity and determining the value of two equilibrium constants to force a fit with experimental data. The Kent-Eisenberg model is still used for CO<sub>2</sub> capture applications (e.g. Fouad et al., 2012) and alternative empirical models have been proposed as well. For instance, the model developed by Gabrielsen et al. (2005) evaluates vapor-liquid equilibria of three amine systems (MEA, MDEA and DEA) using four experimentally-regressed parameters. Another model computes apparent activity coefficients to fit with experimental data for the MEA-H<sub>2</sub>O-CO<sub>2</sub> and the MDEA-H<sub>2</sub>O-CO<sub>2</sub> systems (Hoff et al., 2004).
- Semi-empirical models also imply parameter adjustment based on experimental data but they rely on theoretical assumptions, which is not the case for pure empirical models. The main semi-empirical models are the equations of state and the activity

coefficient models. Due to their respective pros and cons, these methods are often combined to represent electrolyte solutions. Equations of state describe the gas phase properties while liquid phase properties are derived from activity coefficient models. These two types of thermodynamic models are detailed in the present section.

For comparison purposes, Tobiesen et al. (2008) have modeled and validated a stripping column for MEA regeneration with two different thermodynamic models: the empirical model proposed by Hoff et al. (2004) and the semi-empirical model of Deshmukh and Mather (1981). Each model has been fitted with two different experimental data sets, resulting into four thermodynamic models. They observed similar model prediction accuracy with, as long as the same experimental data set was used for adjusting thermodynamic model parameters. However, this was not the case when different data sets were used, highlighting the importance of reliable experimental data for fitting thermodynamic model parameters.

### *Activity coefficient models*

The composition and subsequently the properties of a mixture depend on two types of equilibria (Zemaitis et al., 1986)<sup>32</sup>:

- Phase equilibria are reached when the chemical potential of a component is the same in all present phases.
- Chemical equilibria are reached when the chemical potential of products equals the chemical potential of reactants.

The variation of the chemical potential of a component with respect to its reference state is represented by the following equation:

$$\mu_i = \mu_i^0 + RT \ln a_i \quad (3.1)$$

- $\mu_i$  is the chemical potential of component i (J/mol)
- $\mu_i^0$  is the chemical potential of component i at its reference state (J/mol)
- $a_i$  is the activity of component i (-)
- $R$  is the universal gas constant (8.314 J/mol.K)
- $T$  is the temperature (°K)

The reference state is an arbitrarily chosen standard state, usually the pure component at the system temperature and pressure. This reference state is described as the symmetric reference state. However, in the case of ions, it is impossible to isolate pure ions, so that the reference state for ions is the infinite dilution in water. Similarly, the reference state for non-condensable gases is the infinite dilution in the solvent. This so-called asymmetric reference state is used in most thermodynamic model of electrolyte solutions. However, a recent study has proposed the hypothetical state of pure fused salt as the reference state for ions, claiming for a better consistency in non-aqueous solvents and mixed electrolyte solvents (Song et Chen, 2009).

---

<sup>32</sup> Solubility equilibria can be considered as a third equilibrium type, but they will not be discussed since no salt precipitation is observed in the H<sub>2</sub>O-MEA-CO<sub>2</sub> system under usual CO<sub>2</sub> capture conditions.

The chemical activity of a component in a mixture can be described as its normalized active concentration, or in other terms, as its availability towards a chemical reaction or phase equilibrium. The relationship between a component's activity and its mole fraction is achieved using the activity coefficient  $\gamma_i$ :

$$a_i = \gamma_i \cdot x_i \quad (3.2)$$

- $\gamma_i$  is the activity coefficient of component i (-)
- $x_i$  is the mole fraction of component i (-)

Using equations 3.1 and 3.2, the chemical potential of a component in a mixture becomes:

$$\mu_i = \mu_i^0 + RT \ln x_i + RT \ln \gamma_i \quad (3.3)$$

The third term of equation 3.3 is defined as the excess chemical potential  $\mu_i^{ex}$ . It reflects the deviation of the actual chemical potential to ideality. In ideal mixtures, there is no interaction between the different components so that all activity coefficients tend to unity and the third term of equation 3.3 equals zero for each component. However, electrolyte solutions present important deviations from ideality regarding their properties and phase equilibrium characteristics. In this case, activity coefficients must be determined for each component.

Besides, the chemical potential of a component can also be defined as the partial Gibbs free energy at constant temperature, pressure and composition for any component  $j \neq i$ :

$$\mu_i = \left( \frac{\partial G}{\partial n_i} \right)_{T,P,n_{j \neq i}} \quad (3.4)$$

- $G$  is the Gibbs free energy (J)
- $n_i$  (resp.  $n_j$ ) is the mole number of component i (resp. component j) (mol)

Similarly to the excess chemical potential, the excess Gibbs free energy is defined as the difference between the actual Gibbs free energy of the mixture and the Gibbs free energy of an ideal mixture:

$$G^{ex} = G - G^{id} \quad (3.5)$$

From equations 3.3, 3.4 and 3.5, it results that activity coefficients can be derived from the excess Gibbs free energy:

$$\ln \gamma_i = \frac{1}{RT} \left( \frac{\partial G^{ex}}{\partial n_i} \right)_{T,P,n_{i \neq j}} \quad (3.6)$$

As listed by Renon (1996), many different methods have been proposed to estimate the excess Gibbs free energy or the activity coefficients of electrolyte systems. Most of them are based on the Debye-Hückel theory that considers electrostatic attraction forces between oppositely charged ions. The contribution of this ionic attraction must be considered when calculating

the Gibbs free energy of the system, combined with usual contributions of non-ionic species. Many different formulations for this electrostatic potential energy have been proposed (e.g. Guggenheim, 1935; Pitzer, 1973; Deshmukh and Mather, 1981).

Finally, the most used models are perhaps the local contribution models. They are based on a local contribution model for non-electrolyte solutions, which is then corrected by adding short-range interaction terms to Gibbs free energy to account for electrostatic interactions. The basic non-electrolyte local contribution model is the NRTL (nonrandom two-liquid) model developed by Renon and Prausnitz (1968), which assumes that the local composition around a molecule is influenced by the interactions of this molecule with its environment. The NRTL model possesses three main advantages that make it particularly well adapted as a basis for electrolyte models (Chen, 2006):

- It considers local interactions between nearest neighboring species, which is the central modeling point of view for electrolyte solutions.
- It is a model that can be formulated in a simple way from a calculation point of view.
- It is widely accepted and used in the industry.

As a consequence, the electrolyte version of this model has been developed and it is currently one of the most used models for CO<sub>2</sub> capture solvents. This electrolyte nonrandom two-liquid (eNRTL) model is based on two main assumptions (Chen et al., 1982; Chen and Evans, 1986):

- Like-ion repulsion: repulsion forces between similarly charged ions (cations or anions) are extremely large. As a consequence, there is no cation in the local environment of other cations, and respectively no anion in the local environment of other anions.
- Local electro-neutrality: the local ionic charge around a central particle equals zero.

The eNRTL model calculates the activity coefficients of a non-ideal mixture based on the excess Gibbs free enthalpy of the mixture according to equation 3.7, in which the excess Gibbs free energy is composed of three terms:

$$G^{ex} = G^{ex,PDH} + G^{ex,Born} + G^{ex,local} \quad (3.7)$$

The first term in equation 3.7 is the Pitzer-Debye-Hückel contribution that accounts for long range ion-ion electrostatic interactions. The reference state for this contribution is the ion infinite dilution in the mixed solvent. To make it compatible with the reference state of infinite dilution in water, the Born term is added. This term can be considered as a correction for the difference between the dielectric constant of water and the mixed solvent for long-range electrostatic interactions. The third term is the local (or short-range) interaction contribution and it is the main particularity of the eNRTL model. This term contains binary parameters that are adjusted on experimental data. More details about these different contributions to the excess Gibbs energy in the eNRTL model can be found in the literature.

Finally, the eNRTL model has been refined by Bollas et al. (2008). Some simplifying assumptions of the original model were removed to provide a more rigorous framework for

the simulation of multi-electrolyte solvents. This refined model has been applied to amine solvents for CO<sub>2</sub> capture by Hessen et al. (2010). However, the increased complexity of this model makes its implementation unsuitable in its refined form. In conclusion, the initial eNRTL model has been used in the present work.

### *Equations of state*

Equations of state are very useful to describe thermodynamic properties of both liquid and vapor phases over a wide range of temperatures and pressures. They require binary parameters for fitting experimental vapor-liquid equilibrium data. However, they are not adapted to describe highly non-ideal mixtures like electrolyte solutions, so that they are only used for the description of the vapor phase properties in electrolyte systems. Since equations of state are not particular to electrolyte systems, the theoretical basis of these models are not detailed in this work but can be easily found in the literature. The most used equations of state for CO<sub>2</sub> capture solvents are the following:

- The Redlich-Kwong equation of state (Redlich and Kwong, 1949) is widely used, especially for addressing hydrocarbon systems.
- The Peng-Robinson equation of state (Peng and Robinson, 1976) leads to similar results compared with the Redlich-Kwong equation in usual pressure and temperature ranges.
- A recent study (van Elk et al., 2009) uses the electrolyte equation of state proposed by Fürst and Renon (1993) in both liquid and vapor phase. This equation considers an expression of the Helmholtz free energy instead of the Gibbs free energy. However, this model is still in development and requires experimental validation.
- Finally, the PC-SAFT (Perturbed-Chain Statistical Associating Fluid Theory) equation of state has been developed by Gross and Sadowski (2001) to describe complex macromolecular systems. The PC-SAFT equation of state has been successfully applied to the MEA-H<sub>2</sub>O-CO<sub>2</sub> system by Zhang et al. (2011) to provide accurate vapor phase fugacity coefficients even at high pressures.

In this work, the Redlich-Kwong equation of state is used for modeling gas phase properties.

## *2.2 Reactive absorption*

CO<sub>2</sub> capture in amine solvents is based on the reversible transfer of CO<sub>2</sub> from the gas phase into the liquid phase where it reacts with the amine solvent. The mass transfer and the chemical reaction of CO<sub>2</sub> are taking place in the mass transfer columns which are the central part of the CO<sub>2</sub> capture process. Thus, the fluid hydrodynamics in the columns also plays an essential role. In other words, three main physical or chemical phenomena take place in the CO<sub>2</sub> capture process:

- Hydrodynamics: amine solvent and flue gas flow in counter current through the column packing. Their intimate contact is optimized by using an appropriate column packing. The objective is to maximize the specific interfacial area in order to enhance the CO<sub>2</sub> transfer between gas and liquid. However, attention must also be paid at keeping the column pressure drop as low as possible.

- Mass transfer: at the phase interface, CO<sub>2</sub> is transferred from the flue gas into the amine solvent. However, the mass transfer may be slowed down due to physical diffusivity limitations.
- Chemical reaction: CO<sub>2</sub> chemically reacts with the amine solvent, which enhances the CO<sub>2</sub> mass transfer. The chemical reaction is not instantaneous and its rate is characterized by kinetics parameters.

It is important to highlight that these three aspects are strongly inter-dependent, increasing the modeling complexity. For instance, if the stream hydrodynamics is modified by using a different column packing, the subsequent modification of the interfacial area will affect the mass transfer. Furthermore, if fluid properties like density or viscosity are modified during the chemical reaction with CO<sub>2</sub>, the mass transfer in the column will be impacted and the vapor and liquid flow rates as well.

In the present section, these three phenomena are first discussed separately and the different modeling approaches are presented in each case. Then, the combination of these models to simulate the reactive absorption (resp. desorption) in mass transfer columns is presented.

### *Fluid hydrodynamics*

The determination of vapor and liquid flow rates in the column is essential to calculate hydrodynamic parameters like the liquid holdup or the interfacial area. These parameters play an essential role in the calculation of mass transfer and chemical reactions. Different flow models are considered for this purpose and experimental correlations are examined.

### *Flow models*

Vapor and liquid flow rates are usually determined by discretizing the column in several stages and calculating mass and heat balances around the vapor and liquid phases for each column stage. Figure 3.1 represents a column stage as described in the RateSep model of the simulation software Aspen Plus (Zhang et al., 2009).

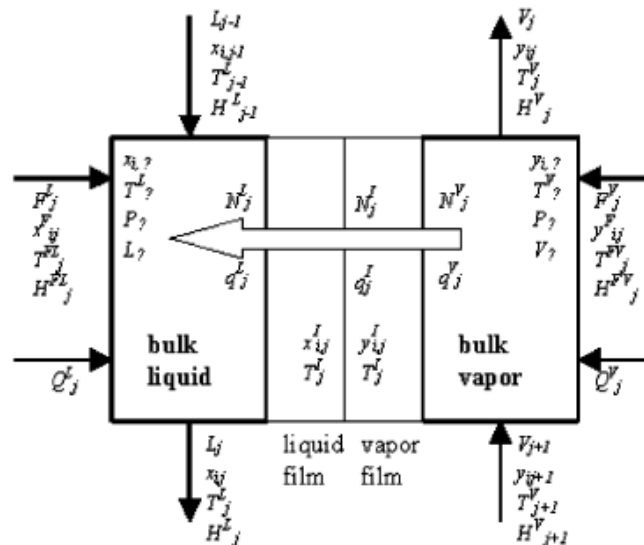


Figure 3.1: schematic view of a column stage, RateSep model (Zhang et al., 2009)

Different flow models are proposed to take bulk properties into account for the determination of liquid and vapor mass balances, basically considering either a plug flow with low back mixing or a perfect mixing on each stage:

- Mixed flow: the bulk properties for each phase are assumed to be the same as the outlet conditions of that phase leaving the stage. For instance, the bulk properties of the liquid on stage  $j$  are the same as the bulk properties of the liquid flowing down to stage  $j+1$ .
- Countercurrent flow: the bulk properties of each phase are an average between the inlet and outlet bulk properties.
- Vapor plug flow: the liquid bulk properties on a stage are the same as the outlet conditions for the liquid phase, while the vapor bulk properties are an average between the inlet and outlet bulk conditions. The outlet pressure is used.
- Vapor plug flow with average pressure: bulk properties are determined in the same way as by the vapor plug flow, only the average value between inlet and outlet pressures is used.

However, Zhang et al. (2009) show that the flow model has a minor impact on the prediction of the column performance. They observe no significant difference between the two vapor plug flow models but report that the mixed flow model describes the column temperature profile slightly better. As a consequence, the mixed flow model has been selected for the present study.

An alternative to the discretization of the mass transfer columns in several stages is the use of Computational Fluid Dynamics (CFD). This method has been recently applied for the detailed determination of fluid hydrodynamics in CO<sub>2</sub> capture columns (Raynal and Royon-Lebeau, 2007; Raynal et al., 2011). This alternative approach allows a rigorous calculation of velocity fields and a description of the liquid and vapor phase distribution in the column. Moreover, it can be advantageous to determine the influence of fluid properties on the stream hydrodynamics and on the mass transfer parameters. Scale-up of mass transfer columns can also benefit of that rigorous approach. However, CFD determination of column hydrodynamics is rather an alternative to measurements since it requires complex calculations that could hardly be included in a global process simulation.

#### *Experimental correlations*

Since mass transfer calculations require hydrodynamic parameters that are usually not calculated rigorously, experimental correlations must be used. These correlations are fitted using experimental data of three types:

- Hydrodynamic data (flow velocity, liquid residence time, ...)
- Fluid properties (viscosity, diffusion coefficient, density, ...)
- Packing data (characteristic lengths of packing corrugation, specific area, ...)

The main hydrodynamic and transfer parameters as well as some reference correlations used in this work are listed in table 3.1.



**Table 3.1: main correlations for hydrodynamic and transfer parameters**

| Parameter                                      | Correlation  |
|--|--|
| Mass transfer coefficient and interfacial area | Random Packing: Onda et al., 1968; Bravo and Fair, 1982<br>Structured packing: Bravo et al., 1985; Bravo et al., 1992; Billet and Schultes, 1993 |
| Heat transfer coefficient                      | Chilton-Colburn method (Taylor and Krishna, 1993)  |
| Liquid holdup                                  | Stichlmair et al., 1989; Bravo et al., 1992; Billet and Schultes, 1993   |
| Pressure drop and flooding limit               | Stichlmair et al., 1989; Olujić, 1999; Correlations supplied by the packing vendor   |

Correlations for heat transfer calculation use a different approach that does not require packing data. The Chilton-Colburn analogy between heat and mass transfer equations is used to determine the heat transfer coefficient  $h$ :

$$St_H \cdot Pr^{2/3} = St \cdot Sc^{2/3} \quad (3.8)$$

- $St_H$  is the Stanton number for heat transfer (-)
- $Pr$  is the Prandtl number (-)
- $St$  is the Stanton number (-)
- $Sc$  is the Schmidt number (-)

$$St_H = \frac{h}{\bar{\rho} \cdot c_p \cdot \bar{u}} \quad Pr = \frac{c_p \cdot \mu}{\lambda} \quad St = \frac{\bar{k}}{\bar{u}} \quad Sc = \frac{\mu}{\bar{\rho} \cdot \bar{D}} \quad (3.9)$$

- $h$  is the heat transfer coefficient (W/m<sup>2</sup>.K)
- $\bar{\rho}$  is the average density (kg/m<sup>3</sup>)
- $c_p$  is specific heat capacity (J/kg.K)
- $\bar{u}$  is the average flow velocity (m/s)
- $\bar{D}$  is the average diffusivity (m<sup>2</sup>/s)
- $\bar{k}$  is the average mass transfer coefficient (m/s)
- $\mu$  is the viscosity (kg/m.s)
- $\lambda$  is the thermal conductivity (W/m.K)

A recent review has shown that a large variety of correlations has been proposed to determine hydrodynamic, heat and mass transfer parameters in the case of structured packed columns for CO<sub>2</sub> capture (Razi et al., 2012). However, this study has also shown that significant differences may be observed between the different correlations. This is mainly due to invalid model assumptions, poor experimental data and uncertainties in the resolution of complex equation systems. For instance, Simon et al. (2011) have modeled a CO<sub>2</sub> absorption column

using two different approaches for the determination of mass transfer coefficients. Indeed, they compared the Billet and Schultes correlation (Billet and Schultes, 1999) with experimentally determined mass transfer coefficients using a wetted-wall bench. They observed that using laboratory determined mass transfer coefficients improves the model prediction. The influence of the mass transfer correlation was also confirmed by Tönnies et al. (2011) using rigorous rate-based calculations for the mass transfer model. Up to 26% deviation was observed in the CO<sub>2</sub> capture rate for the absorber, principally due to large deviations in the estimation of the interfacial area. Indeed, values ranging from 106 to 471 m<sup>2</sup>/m<sup>3</sup> were calculated, depending on the correlation.

To compensate for correlations uncertainties, simulation packages like Aspen Plus propose additional factors for adjusting calculated interfacial areas and heat transfer coefficients to experimental values, so that model validation can be facilitated by fitting these parameters. The value calculated from the correlation is thus multiplied by this fitting factor provided by the user to corroborate experimental results.

Finally, the correlations used in the present work are described in section 3.1 and no experimental fitting parameter has been added.

### *Mass transfer*

There are basically two ways to deal with the modeling of mass transfer phenomena in the case of reactive absorption:

- **Equilibrium assumption:** this modeling approach considers that mass transfer columns are composed of successive equilibrium stages. On each stage, a perfect equilibrium is achieved, so that the liquid phase flowing to the lower stage is in equilibrium with the gas rising to the upper stage. Mass and heat transfer limitations are neglected.
- **The rate-based approach:** this method implies the rigorous calculation of mass transfer rates in the column at non-equilibrium conditions. Heat and mass transfer limitations are taken into account.

Although the first approach is computationally less intensive, it tends to overestimate the efficiency of the absorption (respectively desorption) process since mass and heat transfer limitations are neglected. This approach can be corrected using Murphree stage efficiencies, assuming that only a fraction of the fluid reaches the equilibrium while the remaining fraction passes unchanged through the stage. This method implying Murphree efficiencies has been applied to CO<sub>2</sub> capture processes by Øi (2012). However, the concept of Murphree stage efficiency does not rely on any theoretical basis, so that it has only a poor prediction potential.

On the contrary, the rate-based approach is based on theoretical assumptions and the drawbacks due to more intensive computational calculations are usually compensated for by an increased model precision. The rate-based modeling is currently the standard state-of-the-art method for CO<sub>2</sub> capture modeling. It requires a good characterization of the fluid properties, as well as of the column hydrodynamics.

In this section, the main mass transfer models for rate-based calculations are presented. Different modeling approaches have been proposed to describe the interfacial contact between fluid phases, possibly in the presence of chemical reactions. The main models are briefly described here on the basis of the review made by Razi et al. (2012).

*Film model*

The film model (Withman, 1923) considers a steady state. At the interface between the gas and vapor phases, there is a stagnant film layer on both sides of the interface where the mass transfer resistance is located. Figure 3.2 represents the concentration profiles at the interface in the case of a component A transferred from the vapor phase into the liquid phase. It is assumed that there is no reaction in the gas film. Three cases are represented:

1. There is no reaction between component A and the liquid in the film.
2. There is a chemical reaction taking place in the liquid film.
3. This chemical reaction is fast and component A totally reacts in the liquid film.

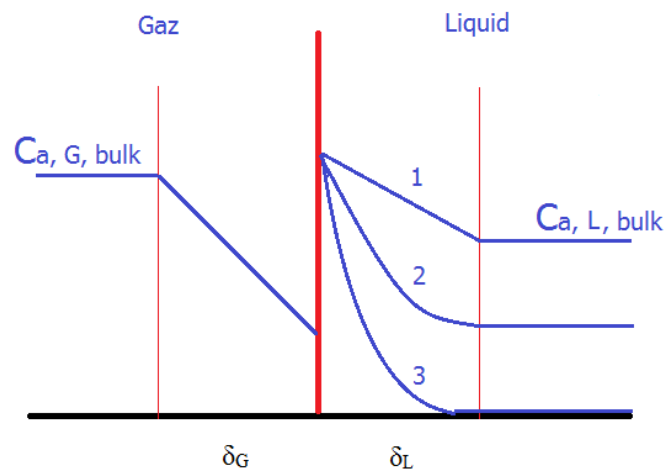


**Figure 3.2: interface concentration profiles in the film model**

In the film theory, the physical mass transfer coefficient is proportional to the diffusion coefficient and inversely proportional to the film thickness:

$$K_L^0 = \frac{D_{A,L}}{\delta_L} \quad (3.10)$$

- $K_L^0$  is the physical mass transfer coefficient (m/s)
- $D_{A,L}$  is the diffusion coefficient of component A in the liquid (m<sup>2</sup>/s)
- $\delta_L$  is the thickness of the liquid film (m)

*Penetration model*

The Higbie penetration theory (Higbie, 1935) considers that the mass transfer is not a stationary phenomenon. Fluid elements periodically migrate from the liquid bulk to the interface where they remain during a contact time  $\tau$ , allowing the mass transfer of component A from the gas into the liquid phase. This model is represented in Figure 3.3.

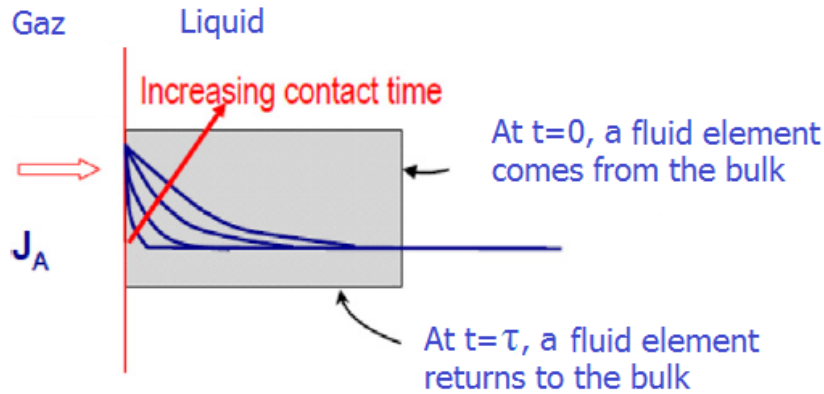


**Figure 3.3: interface concentration profiles of the Higbie penetration model**

In this model, the physical mass transfer coefficient is proportional to the square root of the diffusion coefficient and inversely proportional to the square root of the contact time:

$$K_L^0 = \sqrt{\frac{4 \cdot D_{A,L}}{\pi \cdot \tau}} \quad (3.11)$$

- $\tau$  is the residence time of the liquid at the interface (s)

#### *Surface renewal model*

The Danckwerts surface renewal model (Danckwerts, 1951) is based on the same assumption of unsteady state model as the Higbie penetration model. Furthermore, it considers that convective movements at the interface (Marangoni effects) lead to a not-constant contact time. The relationship between the physical mass transfer coefficient and the diffusion coefficient becomes:

$$K_L^0 = \sqrt{D_{A,L} \cdot s} \quad (3.12)$$

- $s$  is the rate of surface renewal (s<sup>-1</sup>)

Finally, it seems that the choice of the mass transfer model is not the most critical issue as long as the chemical reactions and mass-transfer phenomena are rigorously calculated at the interface (Tobiesen et al., 2007).

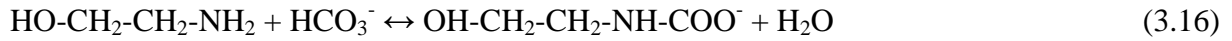
In the present work, the equilibrium and the rate-based approaches have been tested and compared using the simulation package Aspen Plus. The mass transfer model used for the rate-based approach is the film model on both liquid and gas sides. The film thickness is calculated in Aspen Plus as the ratio of the average diffusivity to the average mass transfer coefficient. Moreover, the gas film is a simple film while the liquid film is discretized into 5 points. Indeed, each film region is two times thicker than the next region closer to the interface in order to describe the region close to the interface as precisely as possible.

#### **Chemical reactions**

Chemical reactions can be modeled in two main ways. The first approach only considers chemical equilibria that are thermodynamically determined, while the second one takes chemical kinetics into account.

*Equilibrium reactions*

In the MEA-CO<sub>2</sub>-H<sub>2</sub>O system, the following reactions are taking place in the case of the CO<sub>2</sub> capture processes:



When considering only thermodynamically-determined equilibria, it is assumed that the reaction rate is so fast that kinetic limitations can be neglected. Thus, the distribution of reactants and products is calculated based on chemical equilibrium constants defined as:

$$K_{eq} = \prod_{i=1}^N (x_i \cdot \gamma_i)^{\alpha_i} \quad (3.18)$$

- $K_{eq}$  is the equilibrium constant (-)
- $\alpha_i$  is the stoichiometric coefficient of component i in the reaction equation (-)

According to Van't Hoff's law, equilibrium constants depend on the temperature according:

$$\frac{d \ln K_{eq}}{dT} = \frac{\Delta_r H}{RT^2} \quad (3.19)$$

- $\Delta_r H$  is the reaction enthalpy (J/mol)

The equilibrium constants can be calculated in two main ways. First, empirical models can be used to determine equilibrium constants based on experimental data. Alternatively, when the thermodynamic fluid properties are precisely calculated, equilibrium constants can be computed from the reference Gibbs free energies of the components, using the semi-empirical thermodynamic models described in section 2.1.

*Kinetic reactions*

Among the reactions listed above, the most critical ones are the reactions describing the reactive absorption of CO<sub>2</sub> (equations 3.14 and 3.16). In the kinetic approach, these reactions are not considered as instantaneous anymore so that kinetic limitations must be considered. The reaction rates are calculated according to:

$$r = k_0 \cdot e^{-\frac{E_a}{RT}} \cdot \prod_{i=1}^N C_i^{\alpha_i} \quad (3.20)$$

- $r$  is the reaction rate (kmol/m<sup>3</sup>.s)

- $k_0$  is the pre-exponential factor [(kmol/m<sup>3</sup>.s)/((kmol/m<sup>3</sup>)<sup>Σ<sub>i</sub>α<sub>i</sub>}]</sup>
- $E_a$  is the activation energy (J/mol)
- $R$  is the universal gas constant (8.314 J/mol.K)
- $T$  is the temperature (K)
- $C_i$  is the concentration of component i (kmol/m<sup>3</sup>)
- $N$  is the number of components (-)

If the stoichiometry of the reaction is known, the only kinetic parameters that must be experimentally determined are the pre-exponential factor and the activation energy. An alternative to this equation is to calculate reaction rates based on activities instead of concentrations. In this case, the pre-exponential constant is expressed in kmol/m<sup>3</sup>.s, which is the same unit as the reaction rate. Thus, this leads to:

$$r = k_0 \cdot e^{-\frac{E_a}{RT}} \cdot \prod_{i=1}^N (x_i \cdot \gamma_i) \quad (3.21)$$

Finally, using the phase composition determined either by equilibrium or kinetics reactions, the fluid properties are evaluated using activity coefficient methods, equations of state, or empirical models as discussed in the previous section. In the present work, both equilibrium and kinetics approaches have been evaluated for describing the reaction of CO<sub>2</sub> with the amine solvent.

### ***Reactive absorption models***

As already mentioned, fluid hydrodynamics, chemical reactions and mass transfer are strongly inter-dependent phenomena. In particular, the transfer coefficients determined from a mass-transfer model may be used to characterize the physical absorption of CO<sub>2</sub> in the amine solvent, but they do not consider the chemical reaction of CO<sub>2</sub> with the amine. However, chemical reactions taking place at the gas-liquid interface strongly enhance the reactive absorption. Considering mass transfer as independent of chemical equilibria would only lead to unreliable results. In this section, two main methods to include chemical reactions in the rate-based mass transfer model are described.

### ***Enhancement factor***

As already mentioned in Chapter II (section 4.5), an enhancement factor  $E$  can be introduced for considering the mass transfer acceleration due to the chemical reactions in the liquid film. It is defined as the ratio of the actual mass transfer coefficient to the pure physical mass transfer coefficient. The driving force for the mass transfer of component i is the concentration difference between the bulk and the interface. This mass transfer is increased by the enhancement factor as following:

$$N_i = k_L \cdot a \cdot (C_i^{interface} - C_i^{bulk}) \cdot E \quad (3.22)$$

- $N_i$  is the mass transfer of component i (kmol/s)
- $k_L$  is the overall mass transfer coefficient (m/s)
- $a$  is the interface area (m<sup>2</sup>)
- $C_i$  is the concentration of component i, respectively at the interface and in the bulk (kmol/m<sup>3</sup>)
- $E$  is the enhancement factor (-)

The enhancement factor depends on the reaction kinetics and on the diffusion coefficients of the components implied in the reaction. It can be expressed in function of the Hatta number, a dimensionless number that compares the chemical reaction kinetics with the pure physical mass transfer. If considering a first-order reaction between absorbed component A and solvent component B taking place in the liquid phase, the Hatta number can be defined as:

$$Ha = \frac{\sqrt{D_{A,L} \cdot k \cdot C_{B,L}}}{K_L^0} \quad (3.23)$$

- $D_{A,L}$  is the diffusion coefficient of component A in the liquid phase (m<sup>2</sup>/s)
- $k$  is the kinetic constant of the chemical reaction between absorbed component A and solvent component B (L/mol.s)
- $C_{B,L}$  is the concentration of component B in the liquid bulk (mol/L)
- $K_L^0$  is the physical mass transfer coefficient (m/s)

Based on the reaction kinetics and on the mass transfer model, different expressions for the enhancement factor have been proposed. According to Dubois (2013), the mass transfer model has no significant influence on the numerical value of the enhancement factor. Faramarzi et al (2010) have compared three expressions of the enhancement factor based on the film model for the reactive absorption of CO<sub>2</sub> in MEA. These expressions are listed in table 3.2.

**Table 3.2: different expressions of the enhancement factor**

| Enhancement factor  | Reaction type                      | Reference                        |
|---|------------------------------------|----------------------------------|
| $E = \frac{\sqrt{Ha^2 \cdot \frac{E_\infty - E}{E_\infty - 1}}}{\tanh \sqrt{Ha^2 \cdot \frac{E_\infty - E}{E_\infty - 1}}}$ | Second-order irreversible reaction | Van Krevelen and Hoftijzer, 1948 |
| $E = \sqrt{\frac{4E_\infty(E_\infty - 1)}{1 + Ha^2}} \cdot \frac{1 + Ha^2}{2(E_\infty - 1)}$                                | Second-order irreversible reaction | Astarita et al., 1983            |
| $E = Ha$  | Pseudo-first order reaction        | Kucka et al., 2003               |

Many expressions of the enhancement factor E use the parameter  $E_\infty$ , which is the enhancement factor for an infinitely fast reaction. In the film theory, it is defined as:

$$E_\infty = 1 + \frac{D_{MEA} \cdot C_{MEA}^{bulk}}{2 \cdot D_{CO_2,L} \cdot C_{CO_2}^{interface}} \quad (3.24)$$

- $D_{MEA}$  is the diffusion coefficient of MEA in water (m<sup>2</sup>/s)
- $D_{CO_2,L}$  is the diffusion coefficient of CO<sub>2</sub> in the liquid phase (m<sup>2</sup>/s)

Finally, the enhancement factor reduces to the Hatta number in the case of a pseudo-first order reaction<sup>33</sup>. Faramarzi et al (2010) did not observe any significant difference between the three expressions of E as evidenced in figure 3.4. However, when no enhancement factor was considered, the modeling results did not successfully predict experimental results. Thus, the use of an enhancement factor may be a useful solution for describing the reactive absorption.

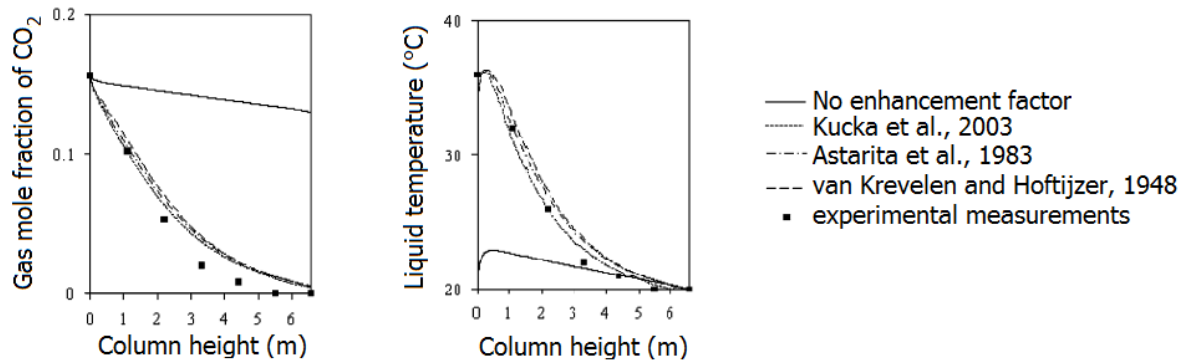


**Figure 3.4: influence of the enhancement factor expression on the absorption performance (Faramarzi et al., 2010)**

#### *Rigorous resolution*

The mass transfer acceleration taking place during reactive absorption can be more rigorously described than by the use of an enhancement factor. Basically and according to Fick's law, the diffusion of a component is proportional to its concentration gradient, which acts as the driving force for diffusional transfer (Rehfeldt and Stichlmair, 2006):

$$J_1 = -D_{12} \cdot \nabla C_1 \quad (3.25)$$

- $J_1$  is the diffusive flux of component 1 (mol/m<sup>2</sup>.s)
- $D_{12}$  is the diffusion coefficient of component 1 into component 2 (m<sup>2</sup>/s)
- $\nabla C_1$  is the concentration gradient of component 1 (mol/m<sup>3</sup>.m)

However, different phenomena have been observed that cannot be described by Fick's law:

- In the presence of a concentration gradient, they may not be any diffusion flux due to a diffusion barrier.
- A diffusive flux may be observed in the absence of concentration gradient due to osmotic diffusion for instance.
- The diffusion of a component may take place in the same direction as its concentration gradient.

Such phenomena mainly take place in non-ideal multi-component mixtures. In this case, the Maxwell-Stefan equations provide a better approach suitable for non-electrolyte systems

<sup>33</sup> The fundamental assumption for a pseudo-first order reaction is that the concentration of solvent B in the film is not affected by the reaction with absorbing component A. As a consequence, the absorption rate can be written as:  $r = k \cdot C_A \cdot C_B \approx k' \cdot C_A$



(Rehfeldt and Stichlmair, 2007). This approach assumes that the chemical potential gradient (first term of equation 3.26) is the driving force for diffusion of component *i* and that it is counter-balanced by molecular friction forces (second term of equation 3.26):

$$\frac{x_i}{RT} \cdot \nabla_{(T,P)} \mu_i = - \sum_{j=1}^n \frac{x_i x_j}{D_{ij}} (v_i - v_j) \quad (3.26)$$

- $x_i$  is the mole fraction of component *i* (-)
- $\nabla_{(T,P)} \mu_i$  is the chemical potential gradient of component *i* at constant temperature and pressure (J/mol)
- $R$  is the universal gas constant (8.314 J/mol.K)
- $T$  is the temperature (K)
- $n$  is the number of components in the mixture (-)
- $D_{ij}$  is the Maxwell-Stefan diffusivity coefficient (m<sup>2</sup>/s)
- $v_i - v_j$  is the velocity difference between components *i* and *j* (m/s)

In the case of ideal chemical systems, the Maxwell-Stefan equations reduce to the Fick's law. Moreover, an exact solution of Maxwell-Stefan equations has been proposed by Krishna and Standart (1976) in the case of a film model.

However, an additional term must be considered in electrolyte solutions, leading to the extended Maxwell-Stefan equations (3.27). This formulation considers that electric forces play the role of an additional diffusion driving force (Ahmadi, 2011).

$$\frac{x_i}{RT} \cdot \nabla_{(T,P)} \mu_i + x_i z_i \frac{F}{RT} \nabla \Phi_e = - \sum_{j=1}^n \frac{x_i x_j}{D_{ij}} (v_i - v_j) \quad (3.27)$$

- $z_i$  is the ionic charge of component *i* (-)
- $F$  is the Faraday constant (96 485 C/mol)
- $\Phi_e$  is the electric potential (V = J/C)

Thus the second method to combine mass transfer and chemical reactions is to perform rigorous calculations of the extended Maxwell-Stefan equations. Once again, different mass transfer models can be used like the film model or the penetration model. The mass transfer rate is not estimated using an enhancement factor anymore, but is computed from partial mass balances and chemical models calculations. This method is computationally more intensive but should yield more precise results.

In a recent paper, Meldon and Morales-Cabrera (2011) have compared the numerical resolution of the Maxwell-Stefan equations with the results of the enhancement factor method based on the film theory with a pseudo-first order reaction kinetics. They observed excellent agreement between both methods. Similarly, Tobiesen et al. (2007) have developed a rigorous absorber model based on the penetration theory. They calculated the resulting enhancement factor and compared it with three enhancement factor expressions based on the film theory. They observed that all expressions modeled the experimental results quite well, as long as the CO<sub>2</sub> loading of the MEA solvent was low. However, at higher loadings, the enhancement

factors based on the film theory were overestimated and the model prediction was unreliable. Only the rigorous resolution of the penetration mass transfer model gave acceptable results.

Finally, the extended Maxwell-Stefan equations are solved by the simulation tool Aspen Plus that has been used in the present work. This method describes the mass transfer acceleration more precisely than with an enhancement factor. Indeed, chemical reactions taking place in the liquid film can be modeled by Aspen Plus, so that there is no need to consider enhancement factors for modeling the mass transfer acceleration at the gas-liquid interface.

### *2.3 Main modeling studies about CO<sub>2</sub> capture with MEA*

Many simulation works about post-combustion CO<sub>2</sub> capture have been reported in the scientific literature, especially during the last decade. Most of the published models simulate stationary operating modes. Calculations are considerably simplified in such steady-state models since they do not consider the time dependency of process variables. Steady-state models may pursue three different objectives, which are presented in this section. First, they can be used to simulate and accompany the experimental campaigns of a pilot plant that has been erected. Second, they can study the influence of process variables and find optimal operating conditions. And third, they can simulate alternative process configurations that may be more difficult to test experimentally due to cost issues.

Besides steady-state models, some dynamic models of the CO<sub>2</sub> capture process are also presented. The time dependency of process variables into account and the process temporal evolution is studied. Dynamic models provide a useful help for transient regime description and may contribute to develop efficient process control strategies.

Finally, some studies are also presented that consider solvent degradation reactions in the steady-state process. Both oxidative and thermal degradation of MEA with CO<sub>2</sub> are discussed and the drawbacks of existing degradation models are evidenced.

#### *Process modeling tools*

Different simulation software packages have been used for modeling the CO<sub>2</sub> capture process. Following the discussion presented in section 2.1, the different modeling tools can propose a variety of thermodynamic models and properties data banks. They may also offer equilibrium vs. rigorous rate-based calculations of the transfer phenomena, and different approaches to include (or not) chemical reactions in the mass transfer model may be proposed. Figure 3.5 graphically summarizes the main modeling features in terms of mass transfer and reaction precision according to the review published by Kenig et al. (2001).

Some software packages propose graphical interfaces in which the user can build the process flowsheet by assembling equation blocks. In other software packages, the process equations must be entered by the user. Some modeling tools have been developed as in-house tools especially for CO<sub>2</sub> capture applications, while other packages are commercially available and can model a large range of processes. Table 3.3 lists some of the main simulation packages used for modeling the CO<sub>2</sub> capture process (Luo et al., 2009; Øi, 2012). In the present work, the simulation tool Aspen Plus has been used.

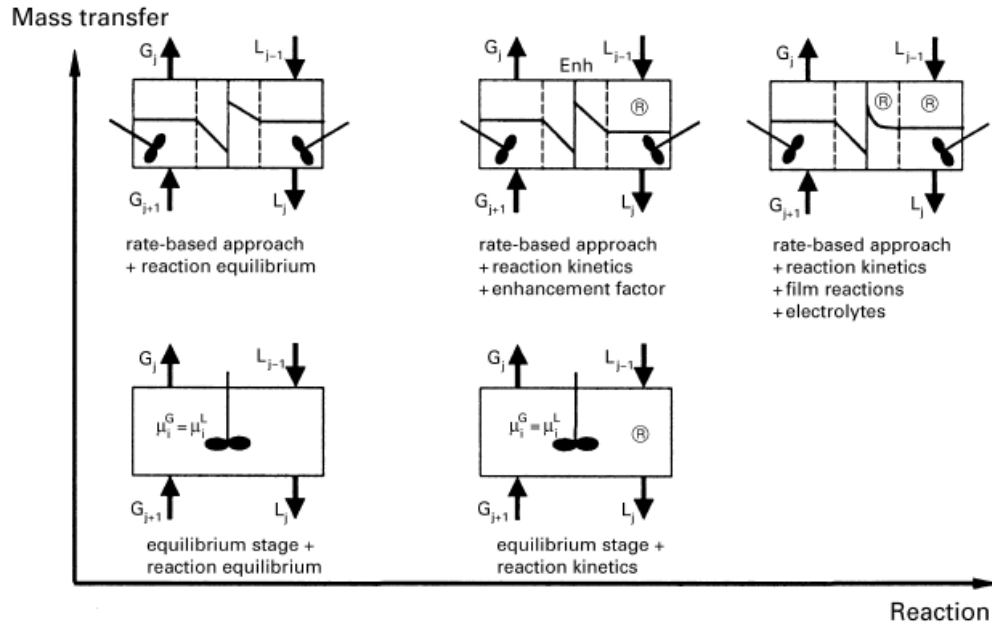


**Figure 3.5: model complexity for the simulation of reactive absorption (Kenig et al., 2001)**

**Table 3.3: main modeling software packages for the CO<sub>2</sub> capture process**

| Name                             | Description   | Thermodynamic package used for CO <sub>2</sub> capture | Mass transfer model                 |
|----------------------------------|---|--|-------------------------------------|
| Aspen Plus, Aspen Custom Modeler | Design, optimization and monitoring of industrial processes                       | eNRTL  | Rigorous mass transfer calculations |
| Aspen Hysys                      | Design, optimization and monitoring of petrochemical and air separation processes | Kent-Eisenberg   | Murphree stage efficiencies         |
| Protreat                         | Acid gas absorption   | Kent-Eisenberg or Li-Mather                            | Rigorous mass transfer calculations |
| Chemasim                         | BASF in-house simulation tool   | eNRTL  | Rigorous mass transfer calculations |
| Promax                           | Design and optimization of chemical processes and refineries                      | eNRTL  | Not specified                       |
| CO2SIM                           | SINTEF in-house simulation tool, restricted to CO <sub>2</sub> capture processes  | Deshmukh-Mather  | Rigorous mass transfer calculations |

Other environments for numerical computation include Matlab and gPROMS, in which thermodynamic and mass transfer model equations are entered by the user. These simulation tools are rather used for dynamic simulations.

***Pilot plant models***

Six main pilot units have been described in modeling studies. These units are all reported in section 3.2 of Chapter I. The modeling studies do not assess the largest pilot units, but rather small experimental capture units developed for research purposes and for which results are not confidential. These six pilot units are listed below. All operate with 30 wt% MEA except if specified otherwise.

- The SRP pilot plant at the University of Texas at Austin has been built in 2002 and modeled by Zhang et al. (2009) for 30 wt% MEA. The model has been developed in Aspen Plus using the eNRTL thermodynamic package and rate-based mass transfer calculations. The model was also developed using the equilibrium stage assumption for comparison purpose, and the superiority of the rigorous rate-based calculation has been evidenced. The influence of rate-based parameters has been studied and the predictive potential of the model has been highlighted. Plaza et al. (2009, 2010) have successfully extended this model to 35 wt% MEA and confirmed the excellent fitting of the model with experimental data.
- The Esbjerg pilot plant is the largest pilot unit for which modeling studies have been published. It started operating in 2006 and simulation results were successfully compared to experimental results by Dugas et al. (2009) using the rate-based model of Aspen Plus. Absorber temperature profiles appeared to be slightly over-predicted by the simulation, while CO<sub>2</sub> concentration profiles perfectly fitted experimental absorber data. In his PhD thesis, Abu-Zahra (2009) compared the experimental results to simulation results obtained with both rate-based and equilibrium stage models. The superiority of rate-based simulations was confirmed, especially for describing column temperature profiles. A rate-based simulation of the Esbjerg pilot plant was also developed by Lemaire et al. (2011). This model has been then adapted to model a large-scale CO<sub>2</sub> capture plant based on the HiCapt+ process developed at the IFPEN.
- From 2007, a new simulation package called CO2SIM has been developed at the Sintef research institute in Norway for modeling post-combustion CO<sub>2</sub> capture units. Tobiesen et al. (2007, 2008) have separately validated the absorber and stripper columns based on experimental results with an average absolute deviation lower than 10% in all cases. In 2011, a larger pilot plant for CO<sub>2</sub> capture, the Tiller pilot, started operating at the Sintef facility in Trondheim. This new pilot unit was successfully modeled and validated for flue gas from natural gas combustion by Mejdell et al. (2011). The Tiller validated model was also used to model and optimize a mobile test unit developed by Aker Clean Carbon, but no additional model validation has been performed on the mobile test unit (Tobiesen and Schumann-Olsen, 2011).
- The pilot plant at the Technical University of Kaiserslautern has first been modeled by Notz during his PhD thesis (Notz, 2009) with the simulation tool CHEMASIM. Using the eNRTL thermodynamic package and a rigorous mass-transfer model, the standard deviation between experimental and simulation results in the column profiles was kept under 10% except at high liquid flow rates. In this case, the higher deviation was explained by a limited validity range for the selected mass transfer correlation. Tönnies et al. (2011) and Kale et al. (2011) have also modeled this pilot unit using respectively the Aspen Plus and Aspen Custom Modeler simulation tools. In both cases, the eNRTL thermodynamic package was used and a rigorous mass transfer model was applied.

- The same simulation tool CHEMASIM, has also been used by Moser et al. (2011c) to describe the Niederaussem pilot plant. The simulated temperature profiles of the mass transfer columns have been found to be in excellent agreement with the experimentally determined temperature profiles. Similarly, the reboiler heat duty has been predicted by the model with less than 6% deviation compared to the experimental results.
- The last pilot plant that has been modeled is the Tarong pilot plant. Cousins et al. (2011) have modeled the pilot unit using the simulation tool Protreat with a Deshmukh-Mather thermodynamic model and rigorous mass transfer calculations. No validation data are presented, but the model is used to study various process alternative configurations.

Finally, it seems that almost no pilot plant model has been proposed before 2009, perhaps due to the complexity of precisely modeling mass transfer phenomena in a rigorous rate-based simulation. Significant computational improvements performed in the five last years, among others the development of the Aspen Plus RateSep model, may have enhanced the rigorous modeling of pilot plants. One notable exception is the model proposed by Freguia and Rochelle (2003) that has been validated with commercial capture plant data provided by Fluor Daniel. This model uses the eNRTL package and an approximate film model for mass-transfer calculations in Aspen Plus, but large standard deviations (up to 30%) between simulation results and experimental data have been reported. On the contrary, current models described previously fitted the experimental data with less than 10% standard deviation.

### ***Optimal operating conditions***

According to the study performed in Aspen Plus by Freguia and Rochelle (2003), non-optimized operating conditions may increase the process energy requirement by up to 50%, for example when the solvent flow is 30% smaller than the optimal value. As a consequence, it is essential to identify the most influent process variables and to optimize their operating values.

In their work, Freguia and Rochelle (2003) stated that the reboiler duty may be reduced by up to 10% for an optimized process in comparison with the base case process of commercial CO<sub>2</sub> capture plants. To achieve this result, they studied the influence of different process and design variables on the reboiler duty:

- Solvent flow rate: there is an optimum flow rate for CO<sub>2</sub> capture. Indeed, the thermal energy consumption at the reboiler is divided in three contributions that vary in opposite ways with the solvent flow rate:
  - The sensible heat for heating the solvent to the regeneration temperature, which increases at higher solvent flow rates.
  - The desorption heat for desorbing CO<sub>2</sub> in the stripper, which does not depend on the solvent flow rate as long as the CO<sub>2</sub> capture rate is kept constant.
  - The stripping heat for generating a vapor stream in the column, which increases at low solvent flow rates in order to achieve a better regeneration of the MEA solvent.

- Stripper pressure: increasing the pressure in the stripper affects the vapor-liquid equilibrium so that the temperature of the CO<sub>2</sub> desorption is increased. Due to its strong dependency on temperature according to Henry's law (Majer et al., 2008), the CO<sub>2</sub> partial pressure increases more than proportionally in the stripper and the MEA regeneration is improved.
- MEA concentration: a higher amine concentration increases the driving force for the CO<sub>2</sub> mass transfer in the absorber and improves the global process efficiency.
- Column packing heights: the interfacial area is proportional to the packing size, so that increasing the packing height may improve the mass transfer. This effect is observed in the absorber but not in the stripper due to lower mass transfer resistance at desorption temperature.

Using an equilibrium stage model in Aspen Plus, Abu-Zahra et al. (2007a) have confirmed the influence of these process variables with the exception of the column packing heights that have not been varied. The thermal energy requirement reaches a minimum value of 3.0 GJ/ton CO<sub>2</sub>, which represents a 23%-reduction compared to the base case process. This improvement was mainly due to a higher MEA concentration (40 wt%) and a higher stripper pressure (2.1 bar), although these conditions may lead to increased solvent degradation and corrosion as acknowledged by the authors. The influence of this parametric study on the process economics was evaluated in a second paper (Abu-Zahra et al., 2007b) for the case of a 600 MWe coal-fired power plant.

Finally, Øi (2007) has evaluated the influence of the solvent flow rate and temperature at the absorber inlet. The model is applied to a natural gas-fired power plant and uses Murphree stage efficiencies in Aspen Hysys. An optimum for the solvent flow rate was identified and it has been observed that a lower solvent temperature at the absorber inlet improves the CO<sub>2</sub> absorption as well as the global process efficiency. However, the effect of the stripper pressure could not be correctly modeled due to convergence problems.

In the present work, the main operating parameters that will be studied are the influence of the MEA concentration, the stripper pressure and the solvent flow rate.

### *Alternative process configurations*

Many propositions to modify the process flowsheet have been submitted for reducing the energy penalty of CO<sub>2</sub> capture. They may address both the absorption step as well as the desorption one. Although some of these process modifications have been tested experimentally (Knudsen et al., 2011), no model validation using alternative process configurations has been reported yet.

#### *Absorber intercooling*

One of the most studied alternative flowsheet configuration implies a heat exchanger to intercool the solvent flow between two absorption stages as represented in figure 3.6. Since the absorption is an exothermal process, this method reduces the average absorption temperature and improves the CO<sub>2</sub> mass transfer. This increases the process efficiency and reduces its energy requirement.

According to Freguia and Rochelle (2003), the intercooling reduces the reboiler duty by about 4%. On their side, Cousins et al. (2011) have determined that the best location for the intercooler location was at the bottom stages of the column. They have observed a 6% reduction of the reboiler duty. The optimal intercooler position has been confirmed by Léonard and Heyen (2011a) at one fourth of the column height from the sump, reducing the process energy requirement by about 4%. Moreover, Karimi et al. (2011a) have also observed that the intercooling effect was more advantageous at lower MEA concentrations.

The positive intercooling effect was confirmed by Plaza et al. (2010) that reported a reduction of the absorber packing height by 13% but the effect on the reboiler duty was not studied. Finally, Kvamsdal et al. (2011a) have studied the combined effect of absorber intercooling and flue gas pre-cooling at the absorber entrance. While the intercooling reduces the reboiler duty by 6%, the flue gas pre-cooling reduces it by 13%. If both modifications are combined, the reduction reaches 16%. Kvamsdal et al. (2011a) have also performed this study for 30 wt% piperazine, evidencing that the effect of intercooling and pre-cooling was even more pronounced in this case than with MEA.

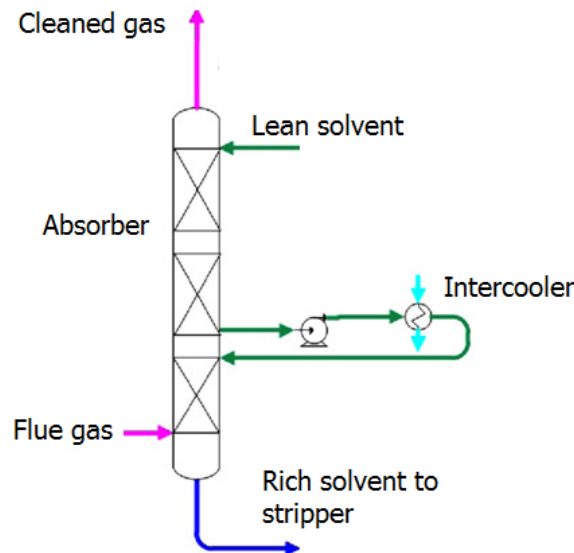


**Figure 3.6: flowsheet of the absorber intercooling (Cousins et al., 2011)**

#### *Lean vapor compression*

The lean vapor compression (LVC) has been patented by Benson and McCrea (1979) and is one of the best process improvement described in the literature. The goal of the modification is to reduce the reboiler duty contribution dedicated to the generation of stripping steam. As presented in figure 3.7, the hot regenerated solvent is flashed at the stripper outlet and the generated vapor (about 90% water and 10% CO<sub>2</sub>) is sent back to the stripper bottom after recompression. There, it acts as auxiliary stripping steam, thus allowing a reduction of the reboiler heat duty. Some cooling water is mixed to the compressed vapor to regulate its temperature and to bring it back to the saturated state (vapor desuperheating).

Karimi et al. (2011b) present the lean vapor compression as the optimal configuration for energy saving since it implies few additional equipment and significantly reduces the reboiler duty. Indeed, the reboiler duty is reduced by up 27%, but due to the increased compression work, the process energy savings are estimated to 9%. Cousins et al. (2011) confirm the significant reduction of the reboiler duty (19% in their case), but they did not calculate the energy saving considering an increased compression work. Léonard and Heyen (2011a) have

reported a 20%-reduction of the reboiler duty due the lean vapor compression, which corresponds to a reduction by 14% of the process energy requirement.

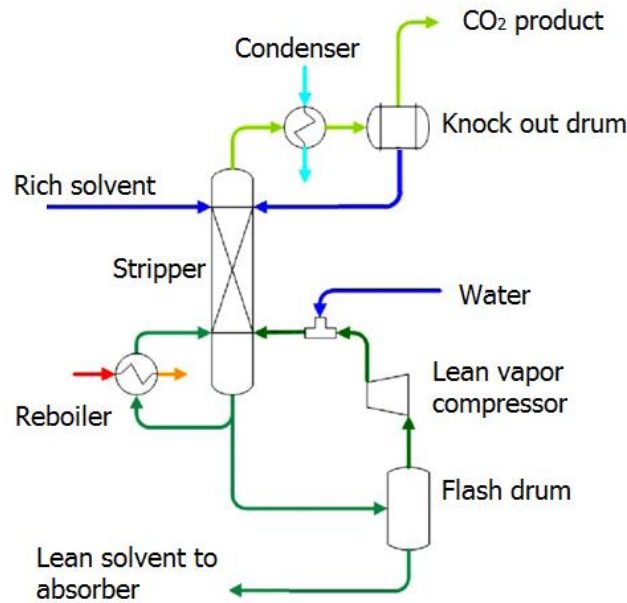


**Figure 3.7: flowsheet of the lean vapor compression (Cousins et al., 2011)**

#### *Split-flow configuration*

The first modeling work of a split-flow configuration for CO<sub>2</sub> capture has been performed by Aroonwilas (2005). The principle of this configuration is to divide a main solvent flow (rich or lean) into two partial flows that are injected at different locations of the mass-transfer column. Depending on the divided stream(s), different configurations are possible. One of them is represented in figure 3.8.

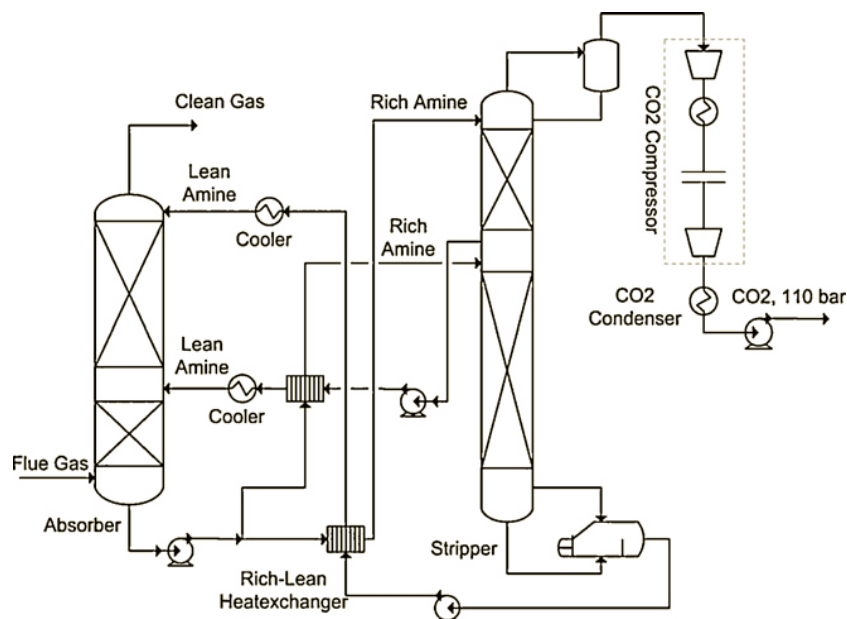


**Figure 3.8: flowsheet of the split-flow configuration (Karimi et al., 2011b)**

Cousins et al. (2011) have tested two different split-flow configurations (rich solvent split and slip stream from the stripper injected at a midpoint location in the absorber). In both cases, the



reboiler duty decreases by about 11%. Both options are combined in the configuration tested by Karimi et al. (2011b) and represented in figure 3.8. The resulting reboiler duty decreases by 16% although the global process energy saving was estimated to 11% due to additional pumping costs. In the case of a slip stream from the stripper injected in the absorber, Léonard and Heyen (2011b) have reported that the optimum return stage in the absorber is located at the column mid-height, resulting in a reboiler duty decrease of 4%.

### Stripper Interheating

Similarly to the absorber intercooling, the solvent flow can be interheated between two stripper stages. The heat is provided by the hot regenerated solvent as represented in figure 3.9. This configuration has been modeled by Van Wagener and Rochelle (2011) and the resulting process energy saving was estimated to 5%.

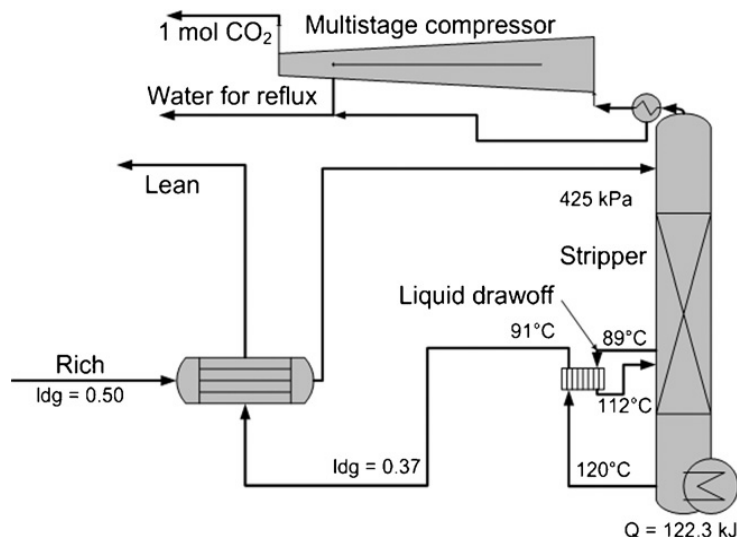


**Figure 3.9: flowsheet of the stripper interheating (Van Wagener and Rochelle, 2011)**

### Multi-pressure stripper

In the Lean Vapor Compression configuration, energy is recovered from the hot regenerated solvent. The idea of the multi-pressure stripper is to recover the energy from the CO<sub>2</sub> product. In the basic process, the CO<sub>2</sub> at the stripper outlet is compressed for further transportation. In the multi-pressure stripper configuration, the first CO<sub>2</sub> compression stages are located between stripper stages, so that the compression heat can be directly recovered in the stripper. Furthermore, the rich solvent flowing from a high-pressure stage down to a lower pressure stage is flashed, and the generated vapor reduces the reboiler duty contribution for stripping steam.

Jassim and Rochelle (2006) propose three pressure levels for the stripper, operating respectively at 2, 2.8 and 4 bar. The reboiler duty reduction reaches 23% with multi-pressure stripper compared to the base case stripper operated at 2 bar. However, due to the additional CO<sub>2</sub> compression steps, the process energy savings are estimated to 10%. The same configuration has been studied by Karimi et al. (2011b) leading to similar conclusions.

Alternatively, the stripper stages can be replaced by simple flash drums operated at different pressures (Plaza et al., 2010). However, according to Van Wagener and Rochelle (2011), this option increases the process energy requirement, especially at low CO<sub>2</sub> loadings.

Finally, a combination between the split-flow and the multi-pressure stripper has been proposed by Oyenekan and Rochelle (2007) and improved by Van Wagener and Rochelle (2011). This so-called matrix configuration is represented in figure 3.10. The reduction in the process energy requirement has been estimated to 3%.

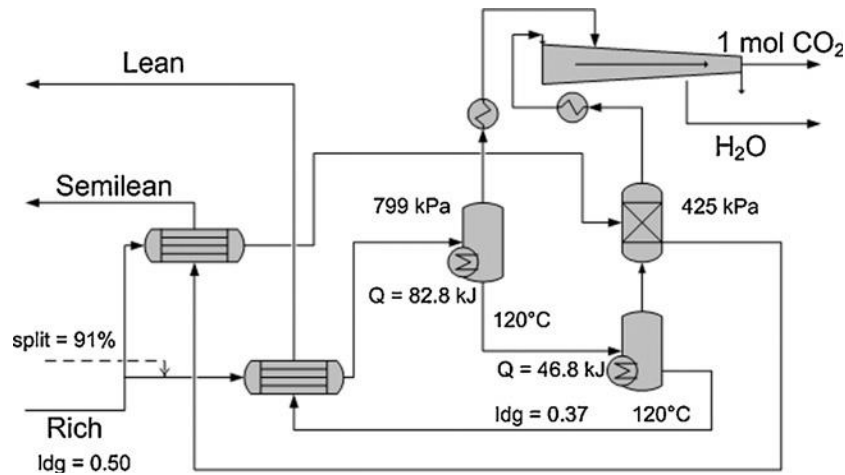


**Figure 3.10: flowsheet of the double matrix configuration (Van Wagener and Rochelle, 2011)**

In the present study, two alternative flowsheet configurations will be tested among those presented. The absorber intercooling and the lean vapor compression have been selected since they significantly improve the process efficiency with only small equipment modifications.

### *Dynamic models*

Compared to steady-state studies, the dynamic behavior of capture plants has only been investigated more recently. However, coal and gas-fired power plants rarely operate in constant load since the electricity demand continuously varies. As a consequence, the flue gas flow rate varies, as well as the amount of available steam for amine solvent regeneration.

The objectives of dynamic simulations are thus to study the time evolution of process variables in transient operations, for instance the start-up or the shut-down phases of a CO<sub>2</sub> capture unit, or its transition between different load regimes. Moreover, control strategies can be implemented into a dynamic model to evaluate their efficiency at regulating process variables like temperatures, liquid levels in column sumps or the CO<sub>2</sub> capture rate.

Table 3.4 lists some of the main dynamic modeling works. Some of those studies only model the mass transfer columns, while others consider the whole capture process. The objectives of the study and the simulation tool are reported in Table 3.4.

**Table 3.4: dynamic modeling studies of the CO<sub>2</sub> capture process**

| Reference                  | Objective  | Simulation tool      |
|----------------------------|--|----------------------|
| Kvamsdal et al., 2009      | Dynamic behavior of the absorber during start-up and load reduction transitions  | gPROMS               |
| Lawal et al., 2011         | Dynamic behavior of the CO <sub>2</sub> capture process in response to flue gas composition changes due to oxygen-enriched coal combustion | gPROMS               |
| Lin et al., 2011           | Control strategies at varying capture and solvent flow rates   | Aspen Plus Dynamics  |
| Panahi and Skogestad, 2011 | Identification of optimum control variables for the capture process  | Unisim               |
| Karimi et al., 2012        | Influence of the split-flow and the lean vapor compression configurations on the process dynamic behavior                                  | Unisim               |
| Harun et al., 2011         | Influence of load transition with 50% reduction of the flue gas flow rate  | gPROMS               |
| Ziaii et al., 2011         | Minimization of the process energy requirement at varying power plant loads  | Aspen Custom Modeler |
| Pröllß et al., 2011        | Control strategy (model predictive control) at different flue gas loads  | Modelica             |
| Gaspar and Cormos, 2012    | Study of the start-up process in the absorber for four amine solvents (MEA, DEA, MDEA, AMP)  | Matlab/Simulink      |
| Léonard et al., 2013       | Control strategy for maintaining the water balance and study of the transition between different flue gas loads                            | Aspen Plus Dynamics  |

### ***Degradation models***

Only five degradation models have been identified in the literature, maybe due to few experimental data available. The first study proposes a model for the rate of MEA degradation, but this kinetic model has not been implemented in a global process simulation. Then, two studies make a link between degradation and process modeling, but still without including degradation reactions. Finally, two studies include degradation reactions within the process model.

1. First, Supap et al. (2001) have proposed a kinetic model describing the apparent degradation rate of MEA in the presence of oxygen and CO<sub>2</sub>. This model has been improved by Uyanga and Idem (2007) to take sulfur-induced degradation into account. Finally, Supap et al. (2009) have refined the 2007 model to better describe the degradation at low CO<sub>2</sub> loadings. The authors propose a degradation rate for MEA that may be written as:

$$-r_{MEA} = \frac{k_0 \cdot e^{-\frac{E_a}{RT}} \cdot [MEA]^a \cdot ([O_2]^b + [SO_2]^c)}{1 + k[CO_2]^d} \quad (3.28)$$

The degradation rate is expressed in kmol/m<sup>3</sup>.h, and values for the kinetics parameters are proposed. These values are compared with experimental values of the present work in section 3.3. However, this model is based on several questionable assumptions:

- Experimental degradation results are obtained in a degradation reactor with discontinuous gas feed. Gas is supplied when the reactor pressure decreases below a minimum set-point value, and the gas supply is stopped once the maximum set-point value is reached. Thus, the formation of gaseous degradation products is hampered since there is no gas exhaust. Moreover, the relevance of such operating conditions to describe industrial CO<sub>2</sub> capture degradation is not discussed.
  - MEA degradation is estimated by measuring the rate of MEA disappearance. Thus it is not distinguished between CO<sub>2</sub>, O<sub>2</sub> and SO<sub>2</sub> degradation. For instance, the NH<sub>3</sub> emission rate has not been recorded in this study although NH<sub>3</sub> is one of the main degradation products of MEA.
  - Reported degradation rates are initial degradation rates, since the rate is given by the slope of the MEA concentration-time curve at the experiment start.
  - The dissolved oxygen concentration of MEA solutions is calculated using the correlation proposed by Rooney and Daniels (1998), which supposes that solutions are saturated with oxygen. This leads to a surprisingly high kinetics order for oxygen (~ 3).
2. The second degradation model has been proposed by Freguia and Rochelle (2003) and considers the effect of solvent degradation in the process model. Degradation reactions are not included into the model, but the influence of heat stable salts (HSS) on the process efficiency is evaluated. The presence of HSS is modeled by considering the presence of formate in the solvent solution, with an estimated HSS loading of 0.1 mol formate/mol MEA. However, no thermodynamic data was available for formate. The authors report that the presence of formate in the solution decreases the reboiler duty by 2%.
  3. Based on in-house experimental results for oxidative amine degradation, Sexton (2008) has used a large-scale Aspen Plus model to estimate the specific amount of degraded MEA. Three options are discussed. The most relevant one considers the oxygen mass transfer as the limiting step for MEA oxidative degradation. In this case, Sexton (2008) evaluates the oxygen consumption rate as following:

$$O_2 \text{ Consumption Rate} = N_s \cdot k_L \cdot a \cdot \frac{P_{O_2}}{H_{O_2}} \quad (3.29)$$

- $N_s$  is the number of stages in the absorber (-)
- $k_L$  is the liquid mass transfer coefficient (m/s)
- $a$  is the interfacial area in the packing (m<sup>2</sup>/m<sup>3</sup>)
- $P_{O_2}$  is the oxygen partial pressure (bar)
- $H_{O_2}$  is the Henry's law constant for oxygen (bar.m<sup>3</sup>/kmol)

Assuming an experimentally determined stoichiometry of 1.5 mol MEA/mol O<sub>2</sub>, Sexton (2008) has calculated a MEA degradation rate of 0.92 kg/ton CO<sub>2</sub>. This is in the same range as published results of commercial CO<sub>2</sub> capture plants that have reported a MEA consumption varying from 0.3 up to 1.6 kg/ton CO<sub>2</sub> (respectively Moser et al., 2011b and Chapel et al., 1999). However, degradation reactions were not introduced in the simulation model.

4. In his PhD thesis, Davis (2009) has experimentally studied the thermal degradation of MEA. Based on the results, he has developed a kinetic model of MEA thermal degradation. Figure 3.11 shows the four main degradation products considered for modeling the MEA thermal degradation.

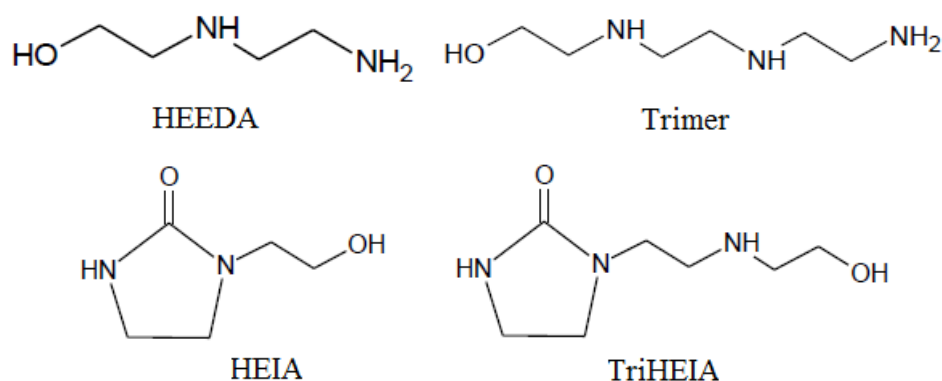


**Figure 3.11: main degradation products considered by Davis (2009) for modeling the MEA thermal degradation**

Reaction stoichiometry, activation energy and pre-exponential constants have been identified for every degradation product (HEEDA, Trimer, HEIA, TriHEIA and “Poly”, an additional degradation product accounting for unidentified polymeric degradation products). Oxazolidinone has also been identified but is not considered since it could not be quantified precisely. The thermal degradation of MEA with CO<sub>2</sub> is predicted at varying temperature and CO<sub>2</sub> loading. For instance, figure 3.12 shows the good agreement between the model prediction and the experimental points at 135°C and at a CO<sub>2</sub> loading equal to 0.4.

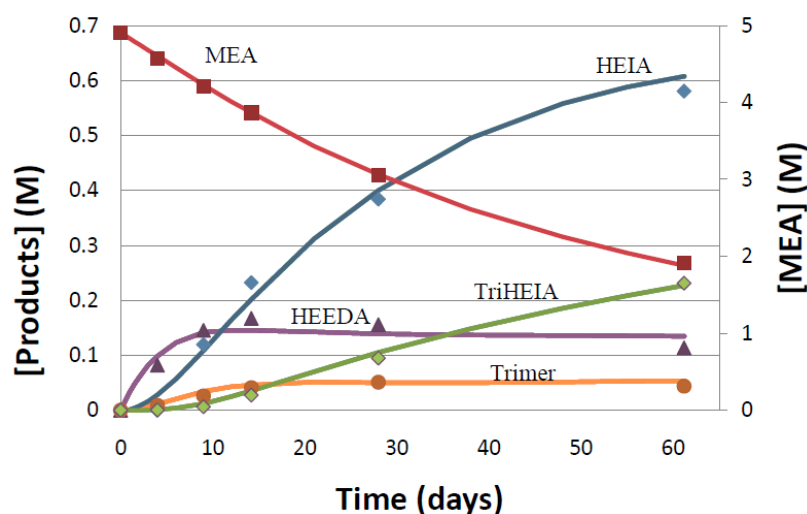


**Figure 3.12: model predictions (curves) and experimental results (points) for 35 wt% MEA, at 135°C and 0.4 mol CO<sub>2</sub>/mol MEA (Davis, 2009)**

Moreover, the degradation rate of MEA reported after 21 days (about 32%) is quite similar to the degradation rate observed for MEA thermal degradation with CO<sub>2</sub> in Chapter II, section 5.1 (37.4%). The small difference may be attributed to slightly varying operating conditions since Davis (2009) has studied the degradation of 35 wt% MEA at 135°C instead of 30 wt% MEA at 140°C.

Finally, Davis (2009) has implemented his kinetic model for MEA thermal degradation into an Aspen Plus simulation of the CO<sub>2</sub> capture process. Following the assumption that a higher stripper pressure leads to an increased degradation but simultaneously to a reduced reboiler duty, a trade-off was identified between the energy cost and the MEA cost as represented in figure 3.13.

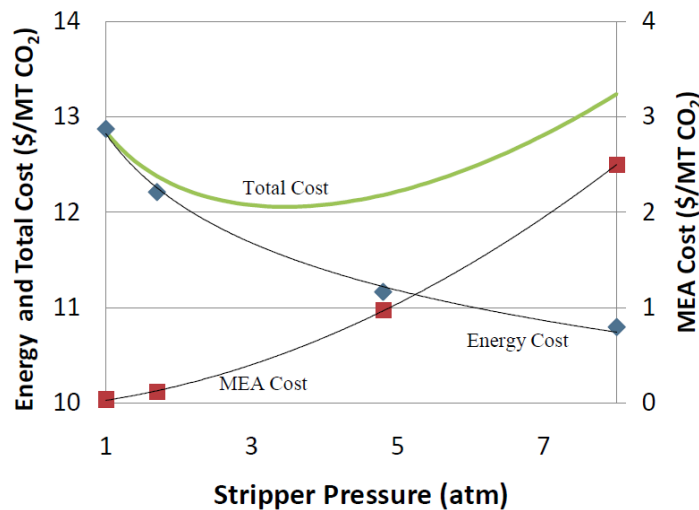


**Figure 3.13: influence of the stripper pressure on the process energy and MEA costs**

- The last study modeling degradation reactions has been performed by Thong et al. (2012). This model is based on literature data for solvent degradation. MEA thermal degradation has been modeled using the kinetic model described by Davis (2009, see above) while the kinetic model for MEA oxidative degradation has been provided by Uyanga and Idem (2007, see the first degradation model described above). SO<sub>x</sub> degradation has been considered based on Uyanga and Idem (2007) as well. Nitrosamine formation from NO<sub>x</sub> has been included in the model based on the data published by Strazisar (2003), although few experimental data were available.

In order to simulate MEA degradation, two stirred tank reactors have been separately modeled within the CO<sub>2</sub> capture flowsheet. The solvent stream leaving the absorber has been duplicated and fed to a stirred tank reactor simulating the oxidative degradation. Similarly, the solvent stream leaving the stripper has been duplicated and fed to a reactor simulating the thermal degradation. It has been assumed that the MEA degradation over time could be represented by the degradation taking place in stirred tank reactors with varying residence times ranging from time  $t = 0$  up to  $t = 6$  weeks. Degraded MEA solutions are then duplicated and fed back to the global process flowsheet, in which the presence of degradation products in the gaseous emissions has been studied.

The main limitations of this model are the following:

- No continuous gas feed is reported to enter the stirred tank reactors, so that the oxygen dissolved in the solvent is rapidly consumed in the oxidative degradation reactor and the reaction is limited by the oxygen availability. This is less a problem in the reactor simulating thermal degradation with CO<sub>2</sub>, since amine solutions exiting the stripper still contain substantial amounts of CO<sub>2</sub> even after regeneration. The main consequence of the absence of gas feed is thus a severe underestimation of the oxidative degradation, leading to inconsistent results. The rate of MEA degradation has not been reported, but the rate of NH<sub>3</sub> emission is estimated by the model to  $1.10^{-10}$  g/ton CO<sub>2</sub>, while Moser et al. (2011b) reports NH<sub>3</sub> emissions of about 100 g/ton CO<sub>2</sub>.
- The model does not consider any mass transfer limitations in the stirred tank reactors. However, mass transfer limitations play an essential role in MEA oxidative degradation.
- Data for oxidative reaction kinetics are based on the kinetic model of Uyanga and Idem (2007), which is similar to the model proposed by Supap et al. (2009), with the same limitations. Experimental data have been obtained in discontinuous gas feed mode whose relevance has not been evidenced compared to real CO<sub>2</sub> capture plant conditions.

To summarize, the pros and cons of the five published degradation models are listed in table 3.5. The main conclusion is that the MEA oxidative degradation is usually poorly modeled, although it appears from our experimental results that it is the main degradation phenomenon taking place in capture plants conditions.

**Table 3.5: objectives and drawbacks of published degradation models**

| Reference                                 | Objective  | Limitations  |
|---|--|--|
| Uyanga and Idem, 2007; Supap et al., 2009 | Kinetics models of MEA degradation including CO <sub>2</sub> , SO <sub>2</sub> and O <sub>2</sub> degradation  | Discontinuous gas supply for all degradation experiments, no mass transfer limitations, no process modeling  |
| Freguia and Rochelle, 2003                | Influence of heat stable salts on the CO <sub>2</sub> process efficiency                                       | Degradation reactions not included in the process model  |
| Sexton, 2008                              | Estimation of industrial oxidative degradation based on experimental results                                   | Degradation reactions not included in the process model  |
| Davis, 2009                               | Detailed reaction modeling of thermal degradation based on in-house experimental data                          | Oxidative degradation not considered   |
| Thong et al., 2012                        | Complete degradation overview (oxidative, thermal with CO <sub>2</sub> , SO <sub>x</sub> and NO <sub>x</sub> ) | Based on data from Uyanga and Idem (2007) for O <sub>2</sub> and SO <sub>2</sub> degradation (discontinuous gas supply), no mass transfer limitations in the modeled degradation reactors, few experimental data for NO <sub>x</sub> degradation |

### 3. Model construction

Different models have been developed to simulate the CO<sub>2</sub> capture process. In the first part of the modeling study, two steady-state models have been built to describe a Mobile Pilot Unit (MPU) treating a flue gas load of 2500 Nm<sup>3</sup>/h. Design data have been provided by the industrial partner Laborelec. These two first models, referred to as “MPU models” have been used to study the influence of the mass transfer model on the simulation results. The **equilibrium model** is a first approach to simulate the CO<sub>2</sub> capture process. It is based on the assumption of equilibrium stages for the mass transfer columns, so that heat and mass transfer limitations are neglected. Moreover, chemical reactions are assumed to be kinetics-independent and thus to instantaneously reach the equilibrium. On the contrary, the **rate-based model** rigorously calculates mass transfers in the columns and considers the chemical kinetics of the CO<sub>2</sub> absorption and desorption.

In the further parts of the modeling study, the initial models have been improved to get closer to an already existing capture unit, namely the Esbjerg Pilot Plant developed in the framework of the European projects FP6 CASTOR and FP7 CESAR. This pilot plant treats a flue gas load of 5000 Nm<sup>3</sup>/h. The advantage of the Esbjerg Pilot Plant is that design data and experimental results are easily available in the literature, which is not the case for the first models. Thus, a potential validation of the models based on the Esbjerg Pilot Plant may be performed in future works, contrarily to the two MPU models.

In the second part of the study, a **dynamic model** is used to study the dynamic behavior of the CO<sub>2</sub> capture process. Like the equilibrium model, it is based on the assumption of equilibrium stages for mass transfer columns and the chemical kinetics is not considered, assuming instantaneous equilibria. This equilibrium assumption is the only one option allowed in Aspen Plus Dynamics since it considerably facilitates the calculations in dynamic mode.

Finally, in the third part, the **degradation model** simulates the steady-state CO<sub>2</sub> capture process with consideration of degradation reactions. The rate-based modeling of degradation reactions is based on the experimental results for MEA oxidative and thermal degradation with CO<sub>2</sub> that are described in Chapter II. As previously mentioned, this model is one of the main innovations of the present work, combining global process modeling and assessment of solvent degradation.

All models developed in this work simulate a carbon capture process with flue gas from a coal-fired power plant. The solvent used for the reactive absorption is an aqueous solution of 30 wt% monoethanolamine (MEA) and the process is designed to capture 90% of the CO<sub>2</sub> feed. Steady-state models are developed using the software Aspen Plus (versions 7.0, 7.2 and 8.0), while Aspen Plus Dynamics (version 7.3) is used for dynamic simulations. All simulations are performed using the electrolyte NRTL activity coefficient model, with the Redlich-Kwong equation of state for vapor phase calculations.

In this section, the construction of the equilibrium and the rate-based models of the Mobile Pilot Unit is first described. Then, considering the Esbjerg Pilot Plant, the dynamic model is first presented and the control strategy that has been used is described. Finally, the major construction assumptions used for the degradation model are justified. They are discussed and compared to the few previous attempts to include solvent degradation in a global process simulation.



### 3.1 Mobile Pilot Unit models

The equilibrium and the rate-based models are both based on design data from the Mobile Pilot Unit, a pilot unit for which our industrial partner Laborelec has collaborated to the design process. They treat a flue gas slipstream of 2500 Nm<sup>3</sup>/h<sup>34</sup> which is composed of 14% CO<sub>2</sub>, 12% H<sub>2</sub>O, 6% O<sub>2</sub>, 68% N<sub>2</sub> (volume percentages). The flowsheet of the MPU modeled in Aspen Plus is represented in figure 3.14. The main design data are listed in table 3.6.

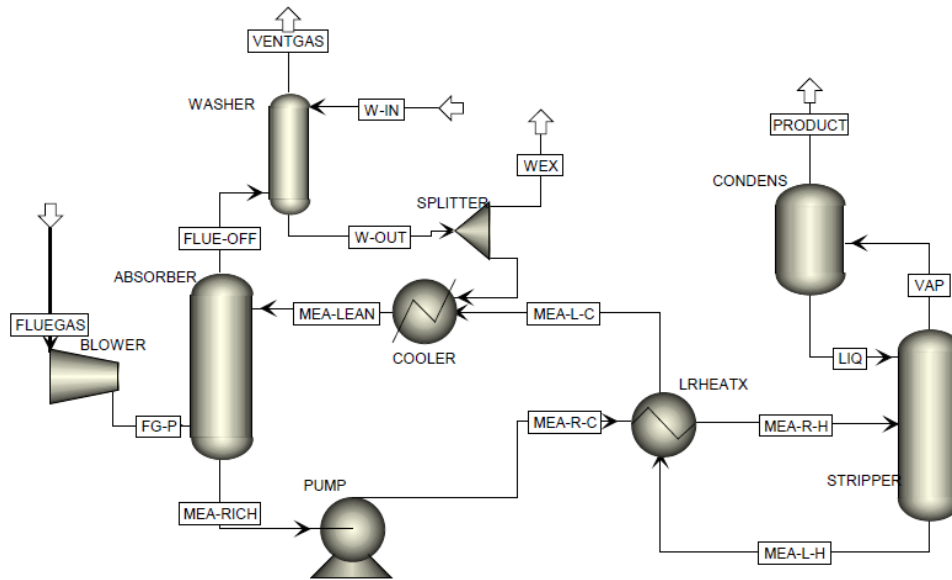


Figure 3.14: flowsheet of the Mobile Pilot Unit

Table 3.6: design characteristics of the MPU

| Block/Input streams      | Specifications  |
|--------------------------|---|
| Flue gas                 | F=2500 Nm <sup>3</sup> /h; T=49.6°C; P=1.013 bar          |
| Washing water (W-In)     | F=450 kg/h; T=30°C; P=1.013 bar                           |
| Flue gas blower          | Isentropic, ΔP=0.1 bar                                    |
| Absorber                 | P <sub>top</sub> =1.013 bar; ΔP=-0.1 bar                  |
| Solvent pump             | ΔP=2.3 bar  |
| Lean-rich heat exchanger | A=80 m <sup>2</sup> ; ΔP=0 bar; U=850 W/m <sup>2</sup> .K |
| Stripper                 | P <sub>top</sub> =2 bar; ΔP=-0.3 bar                      |
| Solvent cooler           | T=40°C, P=1.013 bar                                       |
| Stripper condenser       | T=40°C, P=2 bar   |
| Washer                   | P <sub>top</sub> = 1.013 bar; ΔP=0 bar                    |

<sup>34</sup> Normal state: 0°C; 1.013 bar

- $F$  is the flow rate (Nm<sup>3</sup>/h)
- $T$  is the temperature (°C)
- $P$  is the pressure (bar)
- $\Delta P$  is the pressure variation, a negative value indicates a pressure drop (bar)
- $A$  is the heat exchanger area (m<sup>2</sup>)
- $U$  is the heat transfer coefficient (W/m<sup>2</sup>.K)
- $P_{top}$  is the pressure at the top of the mass transfer column (bar)

Two different modeling approaches have been used for describing the reactive absorption. In the first approach, the mass transfer in columns is modeled by the succession of equilibrium stages. In the second one, rigorous rate-based calculations of the mass transfer are performed based on packing data. In this latest case, rigorous resolution of the extended Maxwell Stefan equations is performed by Aspen Plus in order to combine mass transfer and chemical reactions in the liquid film.

For both equilibrium and rate-based models, many simplifying assumptions have been made: the column pressure profiles have been roughly estimated and a washing column with an input water flow has also been added after the absorber. In real processes, the washing is performed inside the absorption column and only a small water make-up is required.

In order to assist the convergence of process loop calculations, initial values are given for three process streams, called tear streams. It has been decided to tear following streams:

- The solvent stream at the absorber inlet.
- The solvent stream at the stripper inlet.
- The reflux stream at the stripper condenser outlet.

Finally, it is necessary to ensure that the water mass balance in the process is closed. Indeed, water accumulation or water loss in the steady-state process would make the calculations diverge. A dedicated calculation block has been added for solving this design specification. The water balance in the solvent loop is thus ensured by varying the fraction of the washing water recycled to the process via the splitter block (see figure 3.14).

In the following sections, the main assumptions specific to the equilibrium model and the rate-based model are separately presented and discussed.

### ***Equilibrium model***

In this model, columns are simulated by the succession of equilibrium stages in which no mass or heat transfer limitation occurs. As a consequence, the equilibrium stages do not correspond to real column packing stages so that packing characteristics or column dimensions are not necessary. The number of stages for both columns was determined in a preliminary study as a trade-off between model precision and calculation complexity (Léonard, 2009). The absorber is modeled by four equilibrium stages and the washer by two stages. The stripper contains eight equilibrium stages (including the reboiler), with the two upper stages being used as a washing section, so that the amine solvent is fed at the top of the third stage.

The equilibrium reactions of this model are listed in table 3.7. Equilibrium constants are computed using experimental parameters supplied by Aspen Plus (Aspentech, 2008) and based on the works of Austgen et al. (1989) and Jou et al.(1982, 1993a, 1993b) according to:

$$\ln K_{eq} = A + \frac{B}{T} + C \cdot \ln T + D \cdot T \quad (3.30)$$

**Table 3.7: parameters used for the determination of equilibrium constants in the equilibrium model**

| Reaction  | A         | B         | C        | D         |
|---|-----------|-----------|----------|-----------|
| $\text{HO-CH}_2\text{-CH}_2\text{-NH}_2 + \text{H}_3\text{O}^+ \leftrightarrow \text{HO-CH}_2\text{-CH}_2\text{-NH}_3^+ + \text{H}_2\text{O}$ | -3,038325 | -7008,357 | 0        | -0,003135 |
| $\text{CO}_2 + 2 \text{H}_2\text{O} \leftrightarrow \text{H}_3\text{O}^+ + \text{HCO}_3^-$  | 231,465   | -12092,1  | -36,7816 | 0         |
| $\text{HCO}_3^- + \text{H}_2\text{O} \leftrightarrow \text{H}_3\text{O}^+ + \text{CO}_3^{2-}$   | 216,049   | -12431,7  | -35,4819 | 0         |
| $\text{HO-CH}_2\text{-CH}_2\text{-NH}_2 + \text{HCO}_3^- \leftrightarrow \text{OH-CH}_2\text{-CH}_2\text{-NH-COO}^- + \text{H}_2\text{O}$     | 1.86999   | -3340.79  | 0        | 0         |
| $2 \text{H}_2\text{O} \leftrightarrow \text{H}_3\text{O}^+ + \text{OH}^-$   | 132,899   | -13445,9  | -22,4773 | 0         |

Aspen Plus offers two calculation approaches for electrolyte systems. In both cases, the composition of the liquid phase is rigorously calculated. In the true component approach, the unit operation blocks are solved using mass balances for each component, including electrolytes. On the contrary, in the apparent component approach, mass balances only imply apparent components, so that electrolytic dissociation is not considered for solving block models. In the equilibrium model, the apparent component approach is used since it significantly reduces the number of equations that have to be solved.

### ***Rate-based model***

In this model, the mass and heat transfer limitations of the reactive absorption are considered. To perform rigorous mass transfer calculations and solve the extended Maxwell-Stefan equations, the column packing must be specified. Packing data are listed in table 3.8, as well as the number of packing stages for each column. In rate-based calculations, stages do not correspond to equilibrium stages but rather to discretization points over the column height for rate-based calculations. Further parameters for the rate-based description of the mass transfer are also listed. These parameters have been described in section 2.2. The numbers of stages as well as other parameter values have been selected based on the work of Zhang et al. (2009) and on correlations proposed by Aspen Plus (Aspentech, 2008) for random packing.

**Table 3.8: packing characteristics and parameters for rate-based calculations**

| Parameter  | Absorber   | Stripper   |
|--|--|--|
| Packing  | IMTP50, Norton, Metal  | IMTP50, Norton, Metal  |
| Packing height   | 17m  | 13m  |
| Section diameter   | 1.1m   | 1.1m   |
| Number of stages   | 17   | 23 (reboiler and washing included)   |
| Washing section  | Washing column with 2 equilibrium stages   | 3-stage washing section included in the 23 stages of the stripping column                                |
| Flow model   | Mixed  | Mixed  |
| Mass transfer coefficient and interfacial area correlation | Onda et al., 1968  | Onda et al., 1968  |
| Heat transfer coefficient correlation                      | Chilton-Colburn method   | Chilton-Colburn method   |
| Liquid hold-up correlation                                 | Stichlmair et al., 1989  | Stichlmair et al., 1989  |
| Pressure drop correlation                                  | Confidential vendor correlation (Sulzer Chemtech)  | Confidential vendor correlation (Sulzer Chemtech)  |
| Mass transfer model  | Rate-based film model, simple film in gas phase, liquid film discretized with 5-point film <sup>35</sup> | Rate-based film model, simple film in gas phase, liquid film discretized with 5-point film <sup>35</sup> |

The chemical reactions and equilibrium constants that have been defined for the equilibrium model have also been used in the rate-based model for all flowsheet blocks but the mass transfer columns. Indeed, reaction kinetics has been considered in the absorber and the stripper columns besides mass transfer calculations. Thus, in the absorber and the stripper, the two equilibrium reactions describing the absorption of CO<sub>2</sub> have been replaced by kinetically determined reactions. These reactions are presented in table 3.9 and the resulting reaction rates can be derived from equation 3.20 (section 2.2). A kinetic order of 1 has been assumed for each reactant except water which has not been considered in the reaction kinetics. The values for the kinetic parameters in molar concentration units are provided by Aspen Plus (Aspentech, 2008) based on the works of Hikita et al. (1977) and Pinsent et al. (1956).

Finally, the true component approach is used in the rate-based model. Since electrolytes play an essential role in rated-based mass transfer calculations, they must be precisely described inside the column blocks. As a consequence, the apparent component approach may not be satisfying and the true component approach has been selected instead.

<sup>35</sup> Moreover, a film discretization ratio of 2 is specified, which means that the thickness of each film region is twice as large as the thickness of the next region closer to the interface.

**Table 3.9: reactions and rate parameters in the MEA-CO<sub>2</sub>-H<sub>2</sub>O system**

| Kinetics reaction   | $k_0$<br>(kmol/m <sup>3</sup> .s)/(kmol/m <sup>3</sup> ) <sup><math>\sum \alpha_i</math></sup> | $E_a$<br>J/mol |
|---|--|----------------|
| $\text{CO}_2 + \text{OH}^- \rightarrow \text{HCO}_3^-$  | 4.32e+13   | 55 433.8       |
| $\text{HCO}_3^- \rightarrow \text{CO}_2 + \text{OH}^-$  | 2.38e+17   | 123 223        |
| $\text{OH-CH}_2\text{-CH}_2\text{-NH}_2 + \text{CO}_2 + \text{H}_2\text{O} \rightarrow \text{OH-CH}_2\text{-CH}_2\text{-NH-COO}^- + \text{H}_3\text{O}^+$ | 9.77e+10   | 41 236.7       |
| $\text{OH-CH}_2\text{-CH}_2\text{-NH-COO}^- + \text{H}_3\text{O}^+ \rightarrow \text{OH-CH}_2\text{-CH}_2\text{-NH}_2 + \text{CO}_2 + \text{H}_2\text{O}$ | 2.7963e+20   | 72 089.5       |

### 3.2 Dynamic model

Since no experimental results were available from the Mobile Pilot Unit, it has been decided to continue the modeling work based on the Esbjerg Pilot Plant, which was developed as part of European Framework Programmes 6 and 7 (CASTOR and CESAR, respectively). This decision has been made to leave open the possibility of a potential model validation based on experimental results from the Esbjerg Pilot Plant. Design data for modeling this pilot plant have been retrieved from different papers (Knudsen et al., 2009; Kvamsdal et al., 2011b; Knudsen et al., 2011). The treated flue gas flow rate at the Esbjerg Power Plant equals 5000 Nm<sup>3</sup>/h. The flue gas composition has been assumed to be that of a typical coal-fired power plant, i.e. 14% CO<sub>2</sub>, 12% H<sub>2</sub>O, 6% O<sub>2</sub>, 68% N<sub>2</sub>.

During the development of the dynamic model, a steady-state model is required to initialize dynamic simulations. Thus, the model improvements for considering the Esbjerg Pilot Plant are first described in steady-state mode. Then, the adaptation of this steady-state model to a dynamic model is presented and the developed control strategy is explained.

#### *Steady-state model of the Esbjerg Pilot Plant*

In comparison to the previously described MPU models (see section 3.1), different improvements have been added to consider the Esbjerg Pilot Plant. Some of them are represented in figure 3.15:

- A flue gas pre-cooler has been added before the absorber to reduce the flue gas temperature and thus improve the absorption efficiency. The flue gas is cooled down to 40°C.
- The washing water inlet has been replaced by a closed washing water loop in order to reduce the process water consumption. A heat exchanger has been added to control the temperature of the washing water.
- The IMTP random packing of the absorber has been upgraded to the Mellapak 2X structured packing according to Kvamsdal et al. (2011b). As a consequence, the correlations proposed by Bravo et al. (1985) replace the correlations proposed by Onda et al. (1968) for the determination of the mass transfer coefficients and the interfacial area. Similarly, the correlation proposed by Bravo et al. (1992) for the hold-up calculation replaces the correlation of Stichlmair et al. (1989).

- The values for the equilibrium constants used to describe the CO<sub>2</sub>-MEA-water system are not retrieved from the literature anymore but result from Gibbs free energy calculations. Indeed, according to AspenTech (2012), more data have been regressed to fit the Gibbs free energies so that all equilibrium constants can be computed from Gibbs free energies, making the model thermodynamically more consistent.

The same tear streams have been used as in the MPU models and initial values have been given for the liquid stream at the washer inlet to tear the washing water loop as well. The water balance is now regulated by varying the washing water temperature. Indeed, the water content of the clean flue gas exiting the process depends on the washing temperature. Thus, the washing water temperature may be used to regulate the process water balance. Compared to the use of a water make-up stream, this method significantly reduces the water consumption of the process. Finally, a convergence block has been added to achieve 90% CO<sub>2</sub> capture rate by varying the reboiler heat duty. It was previously adjusted by varying the reboiler duty by trial and error.

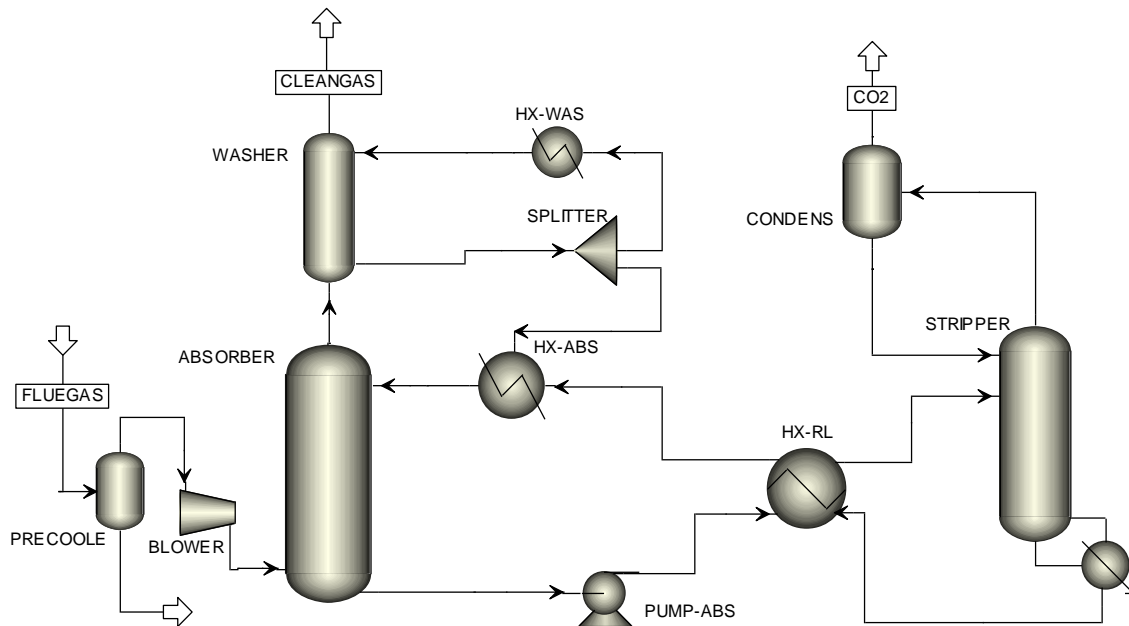


**Figure 3.15: steady-state model flowsheet of the Esbjerg Pilot Plant**

### *Dynamic model of the Esbjerg Pilot Plant*

The steady-state model of the Esbjerg Pilot Plant had to be adapted for dynamic simulations. First, since Aspen Plus Dynamics does not allow the use of rigorous mass transfer models in dynamic simulations, the columns have been studied with the assumption of equilibrium stages. The absorber has been modeled by three equilibrium stages and the washer by two stages. The stripper contains nine stages (including two stages for the washing section). These values have been determined thanks to the experience gained on the MPU models. Indeed, the number of equilibrium stages has been determined so that the resulting CO<sub>2</sub> absorption (respectively desorption) rate is similar to that observed in the MPU rate-based model.

Furthermore, pressure-driven dynamic modeling requires pressure drops to be precisely calculated for all blocks that may induce delays and dead times in the process. As a consequence, coherent pressure profiles have been calculated using design specifications in

steady-state mode. Different additional pumps have been added to better reflect real processes and pressure drops in mass transfer columns are calculated from vendor-supplied correlations. Moreover, several valves allow the control of flow rates and pressures and a solvent buffer tank is included in the solvent loop.

Finally, the vessel geometries and initial liquid hold-ups are detailed in table 3.10. Column sumps are designed so that their volume is twice the total column hold-up volume in steady-state mode. Other vessels are designed so that the steady-state flow rate of the inlet stream would fill them up within one minute if no outlet stream is considered. All vessels are vertical cylinders and the initial volume fraction filled with liquid is equal to 0.5 in all vessels.

**Table 3.10: Vessel geometries for dynamic simulations**

| Vessel              | Vessel height<br>m | Vessel diameter<br>m | Initial liquid volume<br>m <sup>3</sup> |
|---------------------|--------------------|----------------------|---|
| Flue gas pre-cooler | 0.2                | 0.3                  | 7.07e-3                                 |
| Absorber sump       | 2                  | 1.1                  | 9.50e-1                                 |
| Washer sump         | 0.5                | 1.1                  | 2.38e-1                                 |
| Stripper sump       | 1                  | 1.1                  | 4.75e-1                                 |
| Stripper condenser  | 0.3                | 0.2                  | 4.71e-3                                 |
| Solvent buffer tank | 0.8                | 0.8                  | 2.01e-1                                 |

Heat exchangers also possess a dead volume at both inlet and outlet sides. These volumes are presented in table 3.11. No initial liquid fraction is required for the dynamic simulation of heat exchangers.

**Table 3.11: Heat exchanger geometries for dynamic simulations**

|                                 | Washer cooler | Rich-lean solvent heat exchanger (cold side) | Rich-lean solvent heat exchanger (hot side) | Stripper outlet cooler | Absorber inlet cooler |
|---------------------------------|---------------|--|---|------------------------|-----------------------|
| Inlet volume<br>m <sup>3</sup>  | 0.0089        | 0.2588                                       | 0.2588                                      | 0.0057                 | 0.0136                |
| Outlet volume<br>m <sup>3</sup> | 0.0089        | 0.2588                                       | 0.2588                                      | 0.0057                 | 0.0136                |

The resulting steady state model has then been moved to the dynamic mode, leading to the dynamic model displayed in figure 3.16, with blue lines representing the control loops.

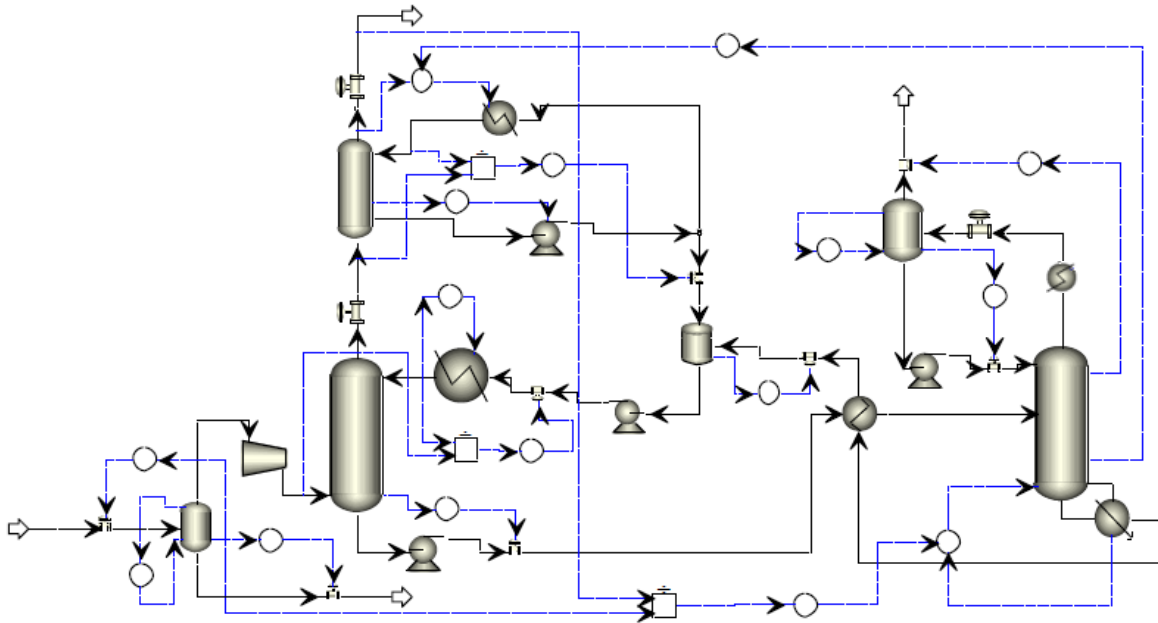


**Figure 3.16: dynamic model flowsheet of the Esbjerg Pilot Plant**

Thirteen degrees of freedom have been identified in the process flowsheet. They correspond to valves and heat duties. In the same time, thirteen constraints have been listed, so that no degree of freedom is left for optimization. The pairing between constraints and degrees of freedom is the following:

- The sump liquid levels of the absorber, the flue gas pre-cooler, the stripper condenser and the solvent buffer tank are controlled by valves which regulate the outlet liquid flow rates.
- The sump liquid level of the washer is controlled by a variable-speed pump at the outlet liquid flow rate. This increases the regulation flexibility compared to a valve.
- The temperatures of the flue gas pre-cooler, the stripper outlet flow and the solvent flow at the absorber inlet are fixed at 40°C by appropriate heat flows in the corresponding equipment, assuming perfect control.
- The stripper pressure is fixed at 1.7 bar by regulating the CO<sub>2</sub> outlet flow rate.
- Absorber and washer liquid to gas ratios are controlled by inlet liquid flow rates.
- The CO<sub>2</sub> capture rate is maintained at 90% by varying the reboiler heat duty.
- The stripper sump level is reflecting the water balance in the process. The regulation is achieved by varying the washing water temperature at the washer entrance.

This latest point is a main difference compared to most previous dynamic studies where the water balance is usually regulated by a water make-up stream. The regulation by the washing temperature minimizes the process water consumption, as already mentioned. Finally, controllers are tuned using the SIMC method described by Skogestad (2006). The results of the dynamic simulations are presented in section 4.2.



### 3.3 Degradation model

The degradation model is a steady-state model of the CO<sub>2</sub> capture process in which kinetics reactions for solvent degradation have been included. The purpose of this model is the study of the process energy requirement with assessment of solvent degradation. The present section first describes the kinetics model for MEA degradation that has been determined from the experimental study in Chapter II. Then, the integration of these degradation reactions in the global process model and the main modeling assumptions are presented.

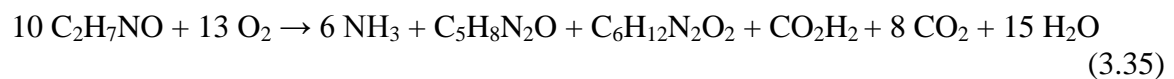
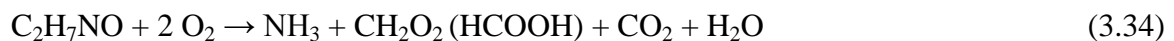
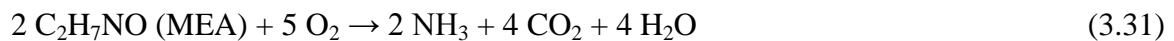
#### *Kinetics model of solvent degradation*

In this kinetics model, both oxidative degradation and thermal degradation of MEA with CO<sub>2</sub> are considered. In first approach, it has been decided to neglect the presence of dissolved metals and degradation inhibitors in the solvent solution. For each degradation mechanism, an apparent reaction is proposed and its stoichiometry and kinetics parameters are discussed. The resulting kinetics model is then compared to alternative models reported in the literature.

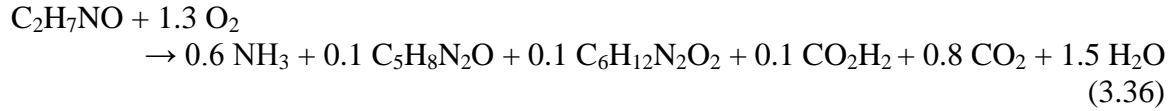
#### *Oxidative degradation*

Based on the experimental results presented in Chapter II, an apparent degradation reaction has been considered for the MEA oxidative degradation with following assumptions:

- The oxidative degradation of MEA is an irreversible reaction.
- The main degradation products are ammonia, HEI, HEPO and HCOOH. Formic acid, which is the acidic form of formate, has been considered in order to include the formation of heat stable salts in the model, although it was not identified as a main degradation product in our test conditions. However, it is the main carboxylic acid identified in degraded MEA samples from pilot plants and it has been reported in many experimental studies (among others by Sexton and Rochelle, 2009).
- Many different degradation reactions take place in the phenomenon called “oxidative degradation”. For each main degradation product, a formation reaction is proposed which is balanced with CO<sub>2</sub> and water. Ammonia appears as a degradation product in all reactions. Since the exact reaction mechanisms are still unknown, these reactions are thus apparent reactions that are weighted in accordance with the distribution of degradation products observed in Chapter II to lead to an overall reaction balance:



This overall reaction is equivalent to (reaction is weighted to describe the degradation of one mol MEA):



Reaction 3.36 has been considered as the apparent reaction of oxidative degradation. In order to determine its kinetics, three additional simplifying assumptions have been made:

- Since MEA is not the limiting reactant and is present in large excess in the bulk, its influence on the degradation kinetics is neglected in a first approach.
- It has been evidenced in Chapter II that the concentration of CO<sub>2</sub> has no influence on oxidative degradation, as long as CO<sub>2</sub> is present in the system. Since CO<sub>2</sub> is always present in the capture process, even in lean solvents (typical lean loading values are 0.2 mol CO<sub>2</sub>/mol MEA), the influence of CO<sub>2</sub> on oxidative degradation is neglected.
- The concentration of dissolved O<sub>2</sub> in the solvent has been approximated by Henry's law for oxygen in water. However, Henry's law describes the dissolved concentration of a gas at saturation, which is not the case in the mass-transfer limited system. Thus, the oxygen transfer may be overestimated and the kinetic constant of the reaction rate underestimated<sup>36</sup>.

Finally, the reaction rate of the MEA oxidative degradation can be expressed as:

$$r = k_0 \cdot e^{-\frac{E_a}{RT}} \cdot C_{\text{O}_2}^a \quad (3.37)$$

The values for the pre-exponential constant  $k_0$ , the activation energy  $E_a$  and the kinetic order of oxygen  $a$  are reported in table 3.12. They have been determined by minimizing the sum of squared differences between the model-predicted degradation rates and the observed degradation rates based on a set of eleven degradation experiments. The parameter regression has been performed with the solver tool embedded in the Microsoft Excel 2010 software.

**Table 3.12: kinetics parameters of the oxidative degradation of MEA**

| Parameter                |       | Unit                           | Value     |
|--------------------------|-------|--------------------------------|-----------|
| Pre-exponential constant | $k_0$ | (mol/L.s)/(mol/L) <sup>a</sup> | 535 209.3 |
| Activation energy        | $E_a$ | J/mol                          | 41 729.8  |
| Oxygen order             | $a$   | -                              | 1.46      |

<sup>36</sup> The only other relation that has been retrieved for describing the oxygen solubility is a correlation proposed by Rooney and Daniels (1998) which describes the dissolved oxygen concentration in a solvent saturated with O<sub>2</sub>. However, the use of this correlation leads to questionable results and physically inconsistent values for the kinetics parameters (reaction order of 5 regarding oxygen). Moreover, the results obtained in Aspen Plus based on the correlation proposed by Rooney and Daniels (1998) lead to a degradation rate (1.7e-5 kg MEA/ton CO<sub>2</sub>) that is about 2.10<sup>-4</sup> times lower than the degradation rate observed in pilot plants (0.284 kg/ton CO<sub>2</sub>; Moser et al., 2011). This evidences the importance of a correct estimation of the oxygen solubility in amine solvents for further model improvements.

The operating conditions of the eleven degradation experiments used for the regression are reported in table 3.13. Detailed results of these degradation experiments may be retrieved in appendix 5. Non specified conditions are similar to the base case experiment (see Chapter II: 1 week, 600 rpm, 4 barg, 160 Nml/min gas feed). Experiments performed at different agitation rates, in the presence of dissolved metals or in the presence of degradation inhibitors have not been included in the kinetics parameter regression. Indeed, different agitation rates are not representative of the pilot plant degraded samples presented in Chapter II and dissolved metals or degradation inhibitors are not considered in the kinetics model of MEA degradation in first approach.

The observed degradation rate for each experiment (in mol MEA/L.s) has been calculated by dividing the mol number of degraded MEA by a run time of one week (604 800 s) and a solvent volume of 0.3 liters. Although the initial quantity of solvent equals 0.3 kg (before CO<sub>2</sub> loading), the effect of density has been neglected since the density of fresh 30 wt% MEA has been measured to 1.004 kg/L.

**Table 3.13: experiments for determining the kinetics of MEA oxidative degradation**

| Temperature | O <sub>2</sub> concentration<br>in gas feed | CO <sub>2</sub> concentration<br>in gas feed | Model-predicted<br>degradation rate | Observed degradation<br>rate |
|-------------|---|--|-------------------------------------|------------------------------|
| C           | vol-%                                       | vol-%  | mol MEA/L.s                         | mol MEA/L.s                  |
| 55          | 5   | 15   | 1.30e-7                             | 1.00e-8 <sup>37</sup>        |
| 100         | 5   | 15   | 8.25e-7                             | 5.79e-7                      |
| 100         | 5   | 15   | 8.25e-7                             | 3.08e-7                      |
| 120         | 0   | 15   | 0                                   | 1.00e-8 <sup>37</sup>        |
| 120         | 5   | 7.5  | 1.64e-6                             | 1.83e-6                      |
| 120         | 5   | 15   | 1.64e-6                             | 1.72e-6                      |
| 120         | 5   | 15   | 1.64e-6                             | 1.86e-6                      |
| 120         | 5   | 30   | 1.64e-6                             | 1.96e-6                      |
| 120         | 7.5   | 15   | 2.95e-6                             | 3.00e-6                      |
| 120         | 10  | 15   | 4.50e-6                             | 4.48e-6                      |
| 140         | 5   | 15   | 3.03e-6                             | 2.77e-6                      |

Finally, figure 3.17 compares the observed degradation rates with the model-calculated degradation rates based on the results presented in table 3.13. The model predicts most experimental degradation rates with less than 15% deviation (represented by the dashed

<sup>37</sup> In these cases, no MEA degradation could be observed. However, in order to facilitate the parameter regression, the observed degradation rate has been arbitrarily set to 1.00e-8.

lines). However, the uncertainty is higher in case of low degradation rates, for which the precise determination of the degradation rate is uneasy due to experimental uncertainties.

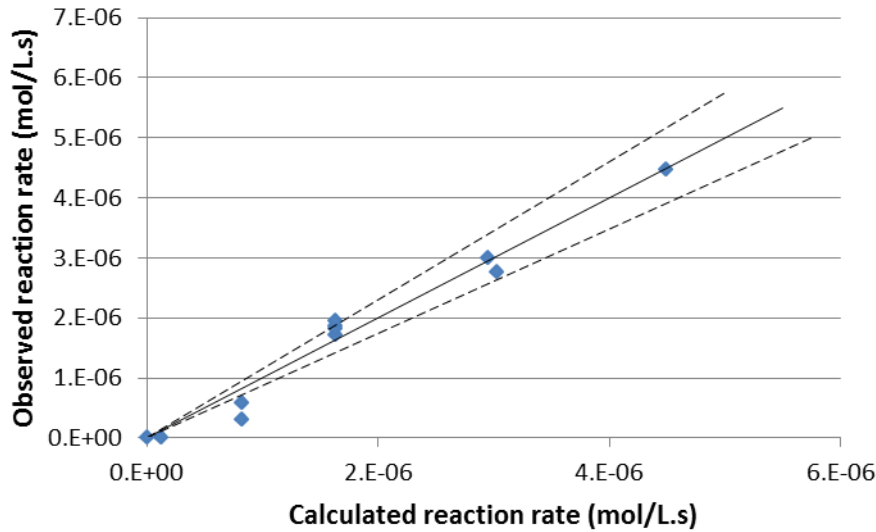
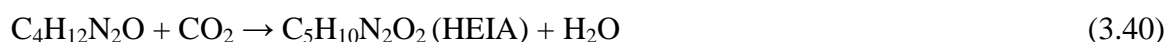
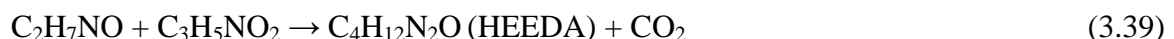
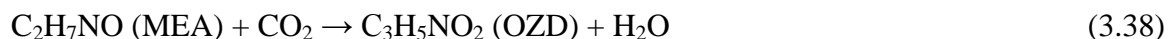


**Figure 3.17: model agreement with observed degradation rates for the oxidative degradation of MEA**

#### *Thermal degradation with CO<sub>2</sub>*

Since thermal degradation with CO<sub>2</sub> is not the main degradation pathway in industrial pilot plants, it has been less studied in the experimental part of this work, and only a few experimental points have been collected regarding the thermal degradation as a function of temperature or of CO<sub>2</sub> concentration. Indeed, most thermal degradation experiments have been performed to test the thermal stability of oxidative degradation inhibitors or the influence of dissolved metals, which are not considered in the present degradation model. However, it is still possible to propose an apparent reaction for MEA thermal degradation with CO<sub>2</sub> based on following assumptions:

- The thermal degradation of MEA with CO<sub>2</sub> is an irreversible reaction.
- HEIA is the main end-product of MEA thermal degradation with CO<sub>2</sub>. OZD and HEEDA have been identified as intermediate degradation products.
- Based on degradation mechanisms that have been detailed in Chapter II, the following degradation pathway for MEA thermal degradation with CO<sub>2</sub> has been assumed:



This reaction is equivalent to (reaction is weighted to describe the degradation of one mol MEA):



Reaction 3.42 has been considered as the apparent reaction of MEA thermal degradation with CO<sub>2</sub>. In order to determine the kinetics of this reaction, the influence of the MEA concentration on the degradation rate has been neglected, assuming that MEA is not the limiting reactive. Thus, the reaction kinetics can be described as following:

$$r = k_0 \cdot e^{-\frac{E_a}{RT}} \cdot C_{\text{CO}_2}^b \quad (3.43)$$

The values for the pre-exponential constant  $k_0$ , the activation energy  $E_a$  and the kinetic order of CO<sub>2</sub>  $b$  are reported in table 3.14. They have been determined following the same method than described for the MEA oxidative degradation, using the Excel 2010 solver. Since the MEA thermal degradation with CO<sub>2</sub> was not the prior interest of the present work, only three degradation experiments have been used for parameter regression.

**Table 3.14: kinetics parameters of the thermal degradation of MEA with CO<sub>2</sub>**

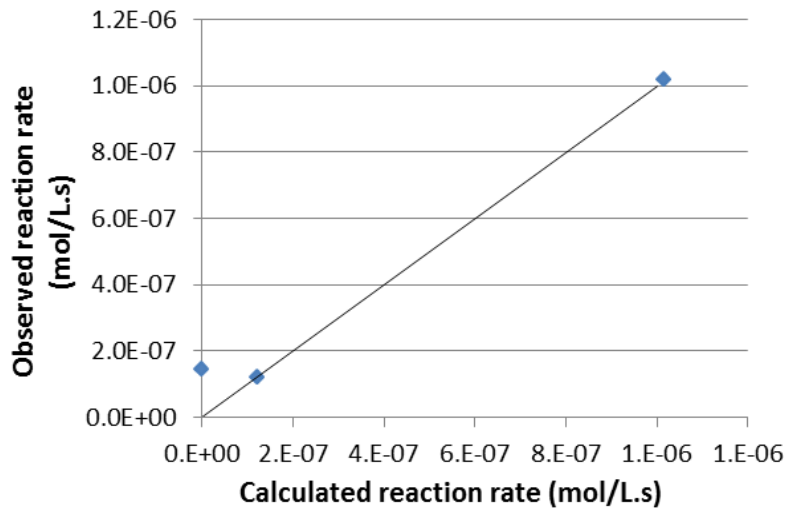
| Parameter                |       | Unit                            | Value   |
|--------------------------|-------|---------------------------------|---------|
| Pre-exponential constant | $k_0$ | (mol/L.s)/(mol/L) <sup>ab</sup> | 6.27e11 |
| Activation energy        | $E_a$ | J/mol                           | 143 106 |
| CO <sub>2</sub> order    | B     | -                               | 0.9     |

The operating conditions of these experiments are reported in table 3.15. They have been performed in batch cylinders with no gas supply and no dissolved metals or degradation inhibitors. Detailed results of these degradation experiments may be retrieved in appendix 5. The observed degradation rate for each experiment (in mol MEA/L.s) has been calculated by dividing the mol number of degraded MEA by a run time of three weeks (1 814 400 s) and a solvent volume of 0.0909 liters. This volume corresponds to a solution weight of 0.1 kg divided by a density of loaded solvent of 1.1 kg/L.

**Table 3.15: experiments for determining the kinetics of MEA thermal degradation with CO<sub>2</sub>**

| Temperature | Initial CO <sub>2</sub> loading | Model-predicted degradation rate | Observed degradation rate |
|-------------|---------------------------------|----------------------------------|---------------------------|
| C           | mol CO <sub>2</sub> /mol MEA    | mol MEA/L.s                      | mol MEA/L.s               |
| 120         | 0.44                            | 1.21e-7                          | 1.19e-7                   |
| 140         | 0.44                            | 1.02e-6                          | 1.02e-6                   |
| 140         | 1.00e-8 <sup>38</sup>           | 2.55e-13                         | 1.44e-7                   |

Finally, figure 3.18 compares the observed degradation rate with the model-calculated degradation rate. As mentioned, only a few experimental points are available for the rate determination, so that it was not possible to estimate the model precision.

**Figure 3.18: model agreement with observed degradation rates for the oxidative degradation of MEA**

#### *Comparison with literature models*

In this section, the proposed kinetics model for MEA degradation is compared to the model proposed by Supap et al. (2009) for MEA degradation (oxidative, thermal and SO<sub>2</sub>) and to the model of Davis (2009) for MEA thermal degradation with CO<sub>2</sub>.

First, the kinetics model developed by Supap et al. (2009) considers a global degradation rate including O<sub>2</sub>, CO<sub>2</sub> and SO<sub>2</sub>-induced degradation. The concentration of MEA is also considered. According to the authors, O<sub>2</sub>, CO<sub>2</sub> and SO<sub>2</sub> can be absent of the system without affecting the model usability. They express the reaction rate as:

<sup>38</sup> There was no CO<sub>2</sub> loading in this case. However, in order to facilitate the parameter regression, the CO<sub>2</sub> loading has been arbitrarily set to 1.00e-8.

$$-r_{MEA} = \frac{k_0 \cdot e^{-\frac{E_a}{RT}} \cdot [MEA]^a \cdot ([O_2]^b + [SO_2]^c)}{1 + k[CO_2]^d} \quad (3.44)$$

Table 3.16 compares the kinetic parameters proposed by Supap et al. (2009) with those determined in the present work.

**Table 3.16: comparison of kinetics parameters for oxidative degradation**

| Parameter                         |       | Unit   | Supap et al. (2009) | This work |
|-----------------------------------|-------|--|---------------------|-----------|
| Pre-exponential constant          | $k_0$ | $(\text{kmol/m}^3)^{1-a} / [(\text{kmol/m}^3)^{ab} + (\text{kmol/m}^3)^{ac}] \cdot \text{s}$ | 1.87e6              | 5.35e5    |
| CO <sub>2</sub> kinetics constant | $k$   | $(\text{kmol/m}^3)^{-d}$   | 1.18                | 0         |
| Activation energy                 | $E_a$ | J/mol  | 29 403              | 41 729.8  |
| MEA order                         | $a$   | -  | 0.015               | 0         |
| Oxygen order                      | $b$   | -  | 2.91                | 1.46      |
| SO <sub>2</sub> order             | $c$   | -  | 3.52                | -         |
| CO <sub>2</sub> order             | $d$   | -  | 0.18                | 0         |

Different observations can be made:

- The MEA concentration shows a very limited influence (MEA order = 0.015) on the rate of the MEA degradation<sup>39</sup>, which is in agreement with our assumption to neglect the MEA concentration in a first approach for the reaction rate expression.
- CO<sub>2</sub> shows an inhibiting influence on MEA degradation according to Supap et al. (2009), whatever the operating conditions. In the present work, we confirm the inhibiting influence of CO<sub>2</sub>, but only in the case of oxidative degradation. On the contrary, we observe that thermal degradation with CO<sub>2</sub> is enhanced at higher CO<sub>2</sub> concentrations. Thus, thermal degradation with CO<sub>2</sub> is not correctly considered by Supap et al. (2009). In the present study, the influence of the CO<sub>2</sub> concentration is not considered for MEA oxidative degradation (equation 3.37) as previously justified<sup>40</sup>. However, this influence is considered for the thermal degradation with CO<sub>2</sub> (equation 3.43) where it cannot be neglected.
- The reaction order proposed by Supap et al. (2009) for oxygen is unexpectedly high and does not seem to reflect physical reaction pathways. This is related to the use of the correlation proposed by Rooney and Daniel (1998) for estimating the solubility of oxygen in the amine solvent. Similar to Henry's law, this correlation also estimates the

<sup>39</sup> MEA concentration has been varied from 18 wt% to 43 wt% by Supap et al. (2009)

<sup>40</sup> See page 136: as long as CO<sub>2</sub> is present in the system, its concentration in the gas feed has no influence on the oxidative degradation. As a consequence, the proposed model is only valid in the presence of CO<sub>2</sub>.

concentration of dissolved oxygen in a solvent that is saturated with oxygen. However, it leads to inconsistent results as already mentioned.

- Significant differences are observed between the values proposed by Supap et al. (2009) and this work for the pre-exponential constant and the activation energy. Besides the determination of the oxygen concentration, this may also be related to the different gas feed mode used for degradation experiments, discontinuous for Supap et al. (2009) and continuous in the present work.

Similarly, it is possible to compare the kinetics model proposed for the thermal degradation of MEA with CO<sub>2</sub> with the model developed by Davis (2009). Davis proposes five thermal degradation reactions with CO<sub>2</sub>, leading to five different degradation products (HEEDA, MEA Trimer, Polymeric products, HEIA, TriHEIA).

In the present work, only the irreversible formation of HEIA is considered. Indeed, HEIA has been found to be the main end-degradation product, which is in agreement with the experimental results presented by Davis (2009). Table 3.17 compares the values of the kinetics parameters proposed by Davis (2009) based on his own results with the values proposed in this work.

**Table 3.17: comparison of kinetics parameters for the formation of HEIA**

| Parameter                | Unit                           | Davis (2009) | This work |
|--------------------------|--------------------------------|--------------|-----------|
| Pre-exponential constant | Depending on the rate equation | 4.14e11      | 6.27e11   |
| Activation energy        | J/mol                          | 138 072      | 143 106   |
| CO <sub>2</sub> order    | -                              | 1            | 0.9       |

The reaction order of CO<sub>2</sub> has not been experimentally determined by Davis (2009) but it is assumed based on degradation pathways. Finally, although the rate equation proposed by Davis (2009) for the formation of HEIA considers intermediate products, the kinetics parameters proposed in both models are in good agreement which suggests that both models would lead to similar results.

#### *Integration of degradation in the global process model*

In this section, three main assumptions regarding the modeling of degradation reactions are discussed:

- The simulation model is supposed to run in steady-state mode.
- Degradation reactions are supposed to mainly take place in the mass transfer columns.
- Solvent purge and make-up streams have been neglected.

These assumptions have led to the definition of a base case model of the CO<sub>2</sub> capture process with assessment of solvent degradation.



*Steady-state mode*

As already mentioned, degradation reactions show a slow kinetics so that it is difficult to observe the formation of degradation products over a short time range. Thus, one could think that the best way to include degradation in a process simulation is to run a dynamic simulation of the process with degradation reactions and to observe the accumulation of degradation products over large time ranges. However, dynamic simulations are not adapted to describe small modifications over long time scale (several months). Moreover, it is essential to consider mass transfer limitations when modeling degradation phenomena, and the developed dynamic model using Aspen Plus Dynamics only allows the use of equilibrium models. Finally, it has been decided to include the degradation in a steady-state model.

*Degradation in mass transfer columns*

Thong et al. (2012) have proposed to model degradation reactions taking place in the capture process in a separate reactor that would be fed with solvent and for which the solvent residence time can be arbitrarily varied from a few seconds to several months. This approach has not been selected for three main reasons:

- This approach implies to decouple the time scale of the degradation reactions from the CO<sub>2</sub> capture process, making it unsuited to study the influence of operating process parameters on degradation.
- It appears from the experimental study that it is necessary to consider mass transfer limitations while modeling solvent degradation, which is not the case in the reactor model proposed by Thong et al. (2012).
- No gas supply has been identified in the separate reactors proposed by Thong et al. (2012), so that the available (dissolved) oxygen is rapidly consumed and the degradation extent is severely underestimated, whatever the residence time in the degradation reactor.

Thus it has been assumed that the best way to model degradation reactions is to include them in the absorber and stripper columns, which better reflects the actual process operating conditions. Moreover, the rate-based assumption has been preferred to the equilibrium assumption for the calculation of mass transfers in columns. Finally, degradation in the other flowsheet blocks has been neglected in a first approach.

*Absence of solvent purge and make-up streams*

The degradation model has been initially designed with a purge and a MEA make-up stream as represented in figure 3.19. The optimal purge flow rate was determined so that the concentration of any degradation product accumulating in the solvent loop remains below 0.1 wt%. This resulted into a purge flow rate of 24 kg/h. In industrial CO<sub>2</sub> capture plants, the purge stream can be reclaimed to remove degradation products and sent back to the solvent loop. However, the reclaiming process has not been integrated in the Aspen Plus model.

Moreover, since the formation rate of degradation products is very low, accumulating degradation products do not prevent the simulation to converge even in the absence of purge and make-up streams. This implies that the calculation converges although the tear streams of the solvent loop are not rigorously in mass balance. As a consequence, it has been decided to neglect the purge and make-up streams in a first approach in order to facilitate the calculation

convergence. Finally, degradation rates are quantified by the formation of degradation products in the mass transfer columns since column reactions are precisely calculated by Aspen Plus at the contrary of solvent loop concentrations.

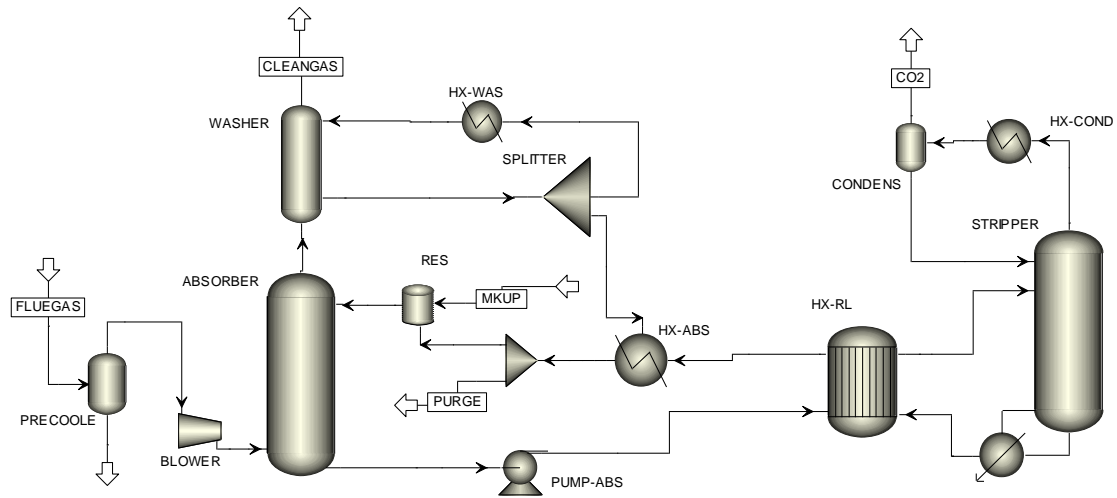


**Figure 3.19: flowsheet of the CO<sub>2</sub> capture model with solvent purge and make-up**

#### *Integrated degradation model*

Finally, summing up the previously described assumptions, the proposed kinetics model of MEA degradation has been included within the mass transfer columns of a global process model for CO<sub>2</sub> capture, working in steady-state mode with no solvent purge or make-up stream. The resulting global model works in the rate-based mode and considers the improvements described in section 3.2 for the steady-state model of the Esbjerg Pilot Plant (among others the washing water loop, flue gas pre-cooler and structured packing...).

Moreover, the kinetic parameters for the CO<sub>2</sub> absorption reactions have been updated according to AspenTech (2012) to describe reaction rates based on component activities instead of molarities. The updated values are listed in table 3.18, and they correspond to the rate equation 3.21 presented in the section 2.2:

$$r = k_0 \cdot e^{-\frac{E_a}{RT}} \cdot \prod_{i=1}^N (x_i \cdot \gamma_i) \quad (3.21)$$

A kinetic order of 1 has been assumed for each reactant except water which has not been considered in the reaction kinetics. It appears from table 3.18 that the reaction describing the MEA carbamate dissociation into MEA and CO<sub>2</sub> considers different kinetics parameters in the absorber and the stripper. Actually, the values are still based on the work of Hikita et al. (1977) but are adapted to describe the reaction rate more precisely at different temperature ranges (40-80°C in the absorber, 100-140°C in the stripper).

**Table 3.18: reactions and rate parameters in the MEA-CO<sub>2</sub>-H<sub>2</sub>O system**

| Reactions  | k <sub>0</sub><br>kmol/m <sup>3</sup> .s | E <sub>a</sub><br>J/mol |
|--|--|-------------------------|
| CO <sub>2</sub> + OH <sup>-</sup> --> HCO <sub>3</sub> <sup>-</sup>  | 1.33e+17                                 | 55 470.9                |
| HCO <sub>3</sub> <sup>-</sup> --> CO <sub>2</sub> + OH <sup>-</sup>  | 6.63e+16                                 | 107 416.5               |
| OH-CH <sub>2</sub> -CH <sub>2</sub> -NH <sub>2</sub> + CO <sub>2</sub> + H <sub>2</sub> O --> OH-CH <sub>2</sub> -CH <sub>2</sub> -NH-COO <sup>-</sup> + H <sub>3</sub> O <sup>+</sup>               | 3.02e+14                                 | 41 264.3                |
| OH-CH <sub>2</sub> -CH <sub>2</sub> -NH-COO <sup>-</sup> + H <sub>3</sub> O <sup>+</sup> --> OH-CH <sub>2</sub> -CH <sub>2</sub> -NH <sub>2</sub> + CO <sub>2</sub> + H <sub>2</sub> O<br>(absorber) | 5.52e+23                                 | 69 157.6                |
| OH-CH <sub>2</sub> -CH <sub>2</sub> -NH-COO <sup>-</sup> + H <sub>3</sub> O <sup>+</sup> --> OH-CH <sub>2</sub> -CH <sub>2</sub> -NH <sub>2</sub> + CO <sub>2</sub> + H <sub>2</sub> O<br>(stripper) | 6.5e+27                                  | 95 383.7                |

In addition to the reactions listed in table 3.18, one apparent reaction for MEA oxidation (equation 3.36) and one for MEA thermal degradation with CO<sub>2</sub> (equation 3.42) have been added to the model. The kinetics parameters of these reactions have been presented in tables 3.12 and 3.14 respectively. As a consequence, these two degradation reactions are now considered in the rate-based model of the CO<sub>2</sub> capture process.

Finally, the degradation products appearing in these degradation reactions have to be specified in Aspen Plus. Component data for NH<sub>3</sub> and HCOOH have been retrieved from Aspen Plus databases. However, no data were available for HEI, HEPO and HEIA, but they could be estimated by Aspen Plus based on their molecular structure. In a first approach, these components have been defined as non-volatile to facilitate the liquid-vapor equilibria calculations. Considering the high molecular weights of these components (respectively 112, 144 and 130 g/mol), this non-volatility assumption appears relevant.

In conclusion, a simulation model of the CO<sub>2</sub> capture process has been proposed that considers solvent degradation. Thanks to this degradation model, it is possible to study the influence of the process operating conditions on both the process energy requirement and on the degradation extent. The results of this model, as well as the results of the MPU models and of the dynamic model are presented in the next section.

## 4. Simulation results

Most CO<sub>2</sub> capture models have been developed to study the influence of operating variables on the process energy requirement. However, the process environmental penalty has only been considered in very few studies. For instance, oxidative degradation has been integrated in only one process modeling study (Thong et al., 2012), which relies on questionable assumptions regarding experimental data. Thus, the present section explores different modeling pathways and finally proposes a model that evaluates both the energy and the environmental penalties of the CO<sub>2</sub> capture process.

First, the models based on design data of the Mobile Pilot Unit are compared to evaluate the influence of the equilibrium and rate-based approaches for modeling the CO<sub>2</sub> reactive absorption. The influence of operating parameters on the process energy requirement is studied for both models, and the column temperature profiles are compared.

Then, the potential of dynamic simulations is evidenced by a practical application using the dynamic model. It is supposed that the energy available for the capture plant is reduced in order to increase the electricity availability during the daily peak hours. Two different strategies for temporarily reducing the CO<sub>2</sub> capture rate, and thus the energy requirement of the capture plant, are evaluated.

Finally, results gained with the degradation model are presented. The influence of the main operating variables on solvent degradation and on emission of degradation products is reported. Furthermore, alternative flowsheet configurations are evaluated from both energy and environmental points of view. Finally, optimal operating conditions are proposed that consider the process energy requirement as well as the emission of degradation products.

### 4.1 Equilibrium and rate-based model comparison

Two different models have been developed based on design data of a Mobile Pilot Unit as described in section 3.1. The equilibrium model makes the assumption that mass transfer columns can be modeled by the succession of equilibrium stages in which mass and heat transfer limitations are neglected. On the contrary, the rate-based model rigorously calculates the mass transfer in the columns. Moreover, the rate-based model also considers the chemical kinetics of the CO<sub>2</sub> reactive absorption. In this section, a sensitivity analysis of key operating variables is performed using both models. Then, the temperature profiles of the mass transfer columns are discussed for each model.

#### *Sensitivity study*

Three main process variables have been identified based on the works of Freguia and Rochelle (2003) and Abu-Zahra (2007a). These variables are the solvent flow rate, the pressure of the stripper and the concentration of the MEA solvent. A sensitivity analysis is performed by varying successively each variable while other operating parameters are kept constant. The flue gas flow rate equals 2500 Nm<sup>3</sup>/h (14% CO<sub>2</sub>, 12% H<sub>2</sub>O, 6% O<sub>2</sub>, 68% N<sub>2</sub>) and the CO<sub>2</sub> capture rate is kept constant at 90%. However, no experimental data are available for the simulated pilot plant. As a consequence, predicted behaviors are compared with values reported in the literature when available, but no precise validation has been performed.

*Solvent flow rate*

The presence of a minimum reboiler duty depending on the solvent flow rate has been experimentally observed by several pilot plant studies with minimum reboiler heat duties varying between 3.5 and 3.7 GJ/ton CO<sub>2</sub> depending on the process configuration (Knudsen et al., 2009; Knudsen et al., 2011; Moser et al., 2011c). As mentioned in section 2.3, the thermal energy supplied to the CO<sub>2</sub> capture process contributes to heat the solvent, to generate stripping steam, and to desorb CO<sub>2</sub>. Since these three contributions vary in opposite ways with the solvent flow rate, an optimum solvent flow rate can be identified.

Figure 3.20 confirms that both modeling approaches identify an optimal solvent flow rate at about 12.5 m<sup>3</sup>/h. Regarding the energy requirement, both model gives values similar to those reported in the literature (between 3.5 and 3.7 GJ/ton CO<sub>2</sub>). Moreover, since mass transfer limitations and chemical kinetics are neglected in the equilibrium model, the model is closer to ideality and the energy requirement is smaller than in the rate-based model.

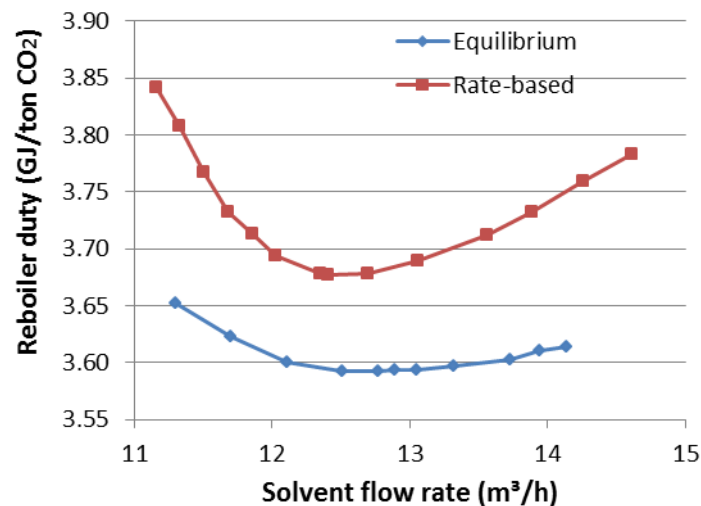


**Figure 3.20: influence of the solvent flow rate on the process thermal energy requirement**

*MEA concentration*

When the concentration of MEA increases in the solution, the driving force for the absorption of CO<sub>2</sub> is increased as it can be deduced from the expressions of the enhancement factor and the Hatta number in section 2.2. As a consequence, the process efficiency is increased, as shown in figure 3.21. Again, the rate-based model leads to higher values for the reboiler duty due to chemical kinetics and physical transfer limitations.

Due to corrosion and degradation issues, 40 wt% MEA solutions are usually not selected for industrial CO<sub>2</sub> capture experiments. However, an improved process using an aqueous solution of 40 wt% MEA with degradation inhibitors has been developed by the IFPEN (Lemaire et al., 2011). This optimized process has been tested at the ENEL pilot plant and first results indicate that regeneration energies may be reduced by 0.2-0.3 GJ/ton CO<sub>2</sub> in comparison to the 30 wt% MEA solvent (Bouillon et al., 2010), which is in good agreement with the improvement predicted by the model.

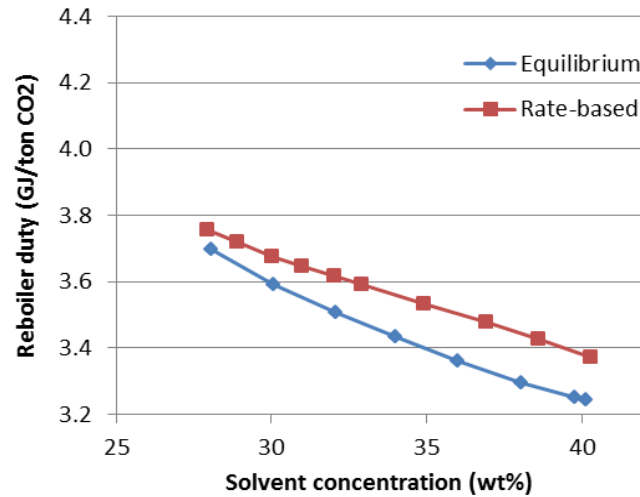


**Figure 3.21: influence of the MEA concentration on the process thermal energy requirement**

#### *Stripper pressure*

Increasing the pressure leads to higher temperatures in the stripper. This temperature variation modifies the solubility of gases in the liquid solvent, which can be estimated by Henry's law. In the case of CO<sub>2</sub>, the Henry's constant strongly depends on temperature as already mentioned (see Chapter II, section 4.5). As a consequence, the equilibrium partial pressure of CO<sub>2</sub> increases rapidly with temperature, and the driving force for the CO<sub>2</sub> desorption is enhanced. The process efficiency is improved and less thermal energy is required.

This is confirmed by figure 3.22 for both modeling approaches. Again, the rate-based model leads to higher values for the process energy requirement than the equilibrium model, since the equilibrium model is closer to the ideality.

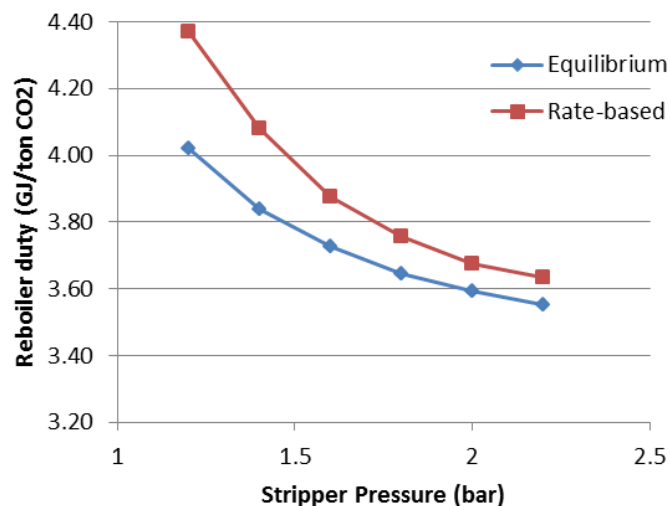


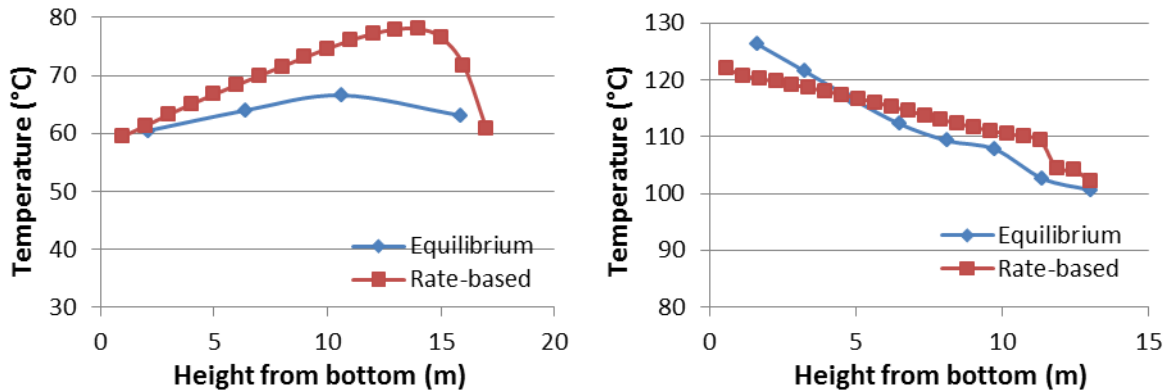
**Figure 3.22: influence of the stripper pressure on the process thermal energy requirement**

Moser et al. (2011c) have reported a decrease of the specific energy consumption of the Niederaussem pilot plant by about 0.1 GJ/ton when increasing the pressure from 1.5 bar up to 1.75 bar. However, a further increase of the pressure to 1.9 bar does not seem to bring an

additional advantage, maybe due to heat losses in the stripper and in the lean-rich heat exchanger which are neglected in the simulation.

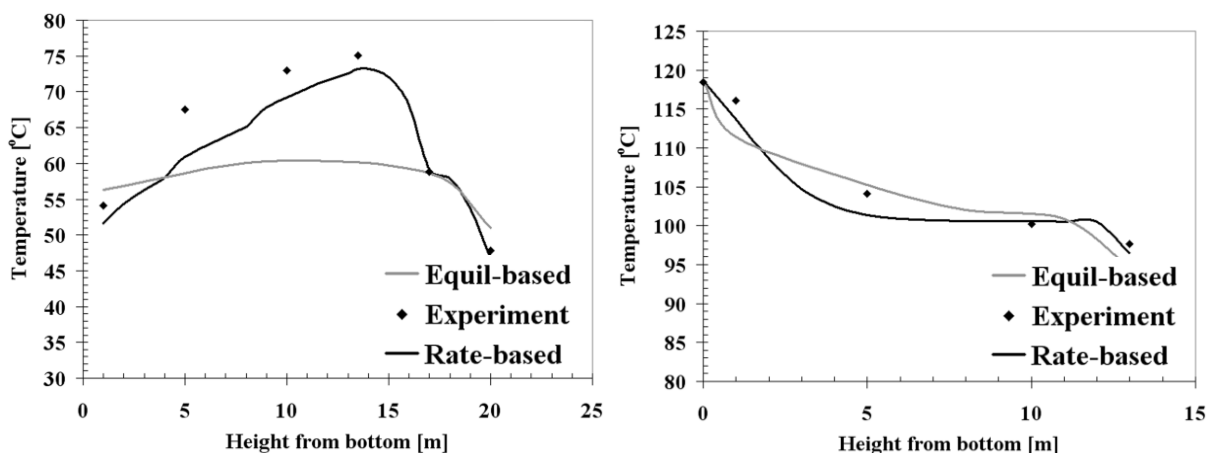
### Temperature profiles

Figure 3.23 represents the predicted temperature profiles of the solvent in the absorber and the stripper for both equilibrium and rate-based models. The absorber height equals 17 m, while the height of the stripper equals 13 m with a washing section at the top of the column. Since no design data is required for the equilibrium model, it has been assumed that the column height is equally divided between the four theoretical equilibrium stages.



**Figure 3.23: liquid temperature profiles of the absorber (left) and the stripper (right)**

No experimental plant data from the Mobile Pilot Unit were available for the simulated configuration. However, Abu-Zahra (2009) reports similar temperature profiles for the equilibrium and the rate-based models of the Esbjerg Pilot Plant as presented in figure 3.24. Moreover, he has compared simulated temperature profiles with experimental data and he has observed that the rate-based model better fits experimental data than the equilibrium model. This was expected since the assumption of equilibrium stages may provide globally acceptable data for the CO<sub>2</sub> capture process, but do not describe precisely the mass transfer phenomena taking place inside the columns.



**Figure 3.24: temperature profiles of the absorber (left) and the stripper (right) as reported by Abu-Zahra, 2009**

## 4.2 Dynamic modeling

Steady-state simulations are very useful to identify optimal operating conditions, or to simulate alternative process configurations. However, they give no insight on the dynamic behavior of CO<sub>2</sub> capture plants in case of process start-up or shut-down, process perturbations or transitions between different operating modes. The objective of this section is thus to present the potential of dynamic simulations for modeling unsteady-state behaviors in the CO<sub>2</sub> capture process. First, the strategy described in section 3.2 for controlling the water balance is evaluated by its ability to react to small process disturbances. Then, the flexibility of the capture process is studied when less energy is available at the power plant due to an increase of the electricity demand.

### *Water balance control*

Regulating the water balance of the solvent loop is a complex issue in CO<sub>2</sub> capture plants. So far, dynamic simulations usually consider a water make-up flow which is varied to regulate the process water balance. However, this leads to very high water consumption which is unsuitable for large-scale capture units. Thus, an alternative control strategy has been simulated, in agreement with the proposition of Kvamsdal et al. (2010). In this strategy, no water make-up is necessary and the water balance is controlled by regulating the amount of water exiting the process with the cleaned flue gas. This is achieved by controlling the temperature of the water entering the absorber washing section. The liquid level at the stripper bottom is set free so that it reflects the accumulation or loss of water in the process. In other words, if the liquid level in the stripper increases (respectively decreases), the temperature of the washing water is increased (resp. decreased) by the control system, so that the flue gas exiting the process contains more (resp. less) water. Consequently, more water exits the process and the liquid level in the stripper is brought back to its set-point value.

The efficiency of this control strategy has been evaluated by simulating small process disturbances. For that purpose, the set-points of several controlled variables have been slightly modified and the resulting behavior of the other controlled variables has been observed. For instance, the capture rate set-point has been set at 89% instead of 90%. Then, the effect of this modification on other controlled variables like the liquid levels in mass transfer columns has been observed. The main process variables that have been modified are listed in table 3.19, as well as the simulated variation of the set-point value.

**Table 3.19: simulated disturbances for the evaluation of the process strategy stability**

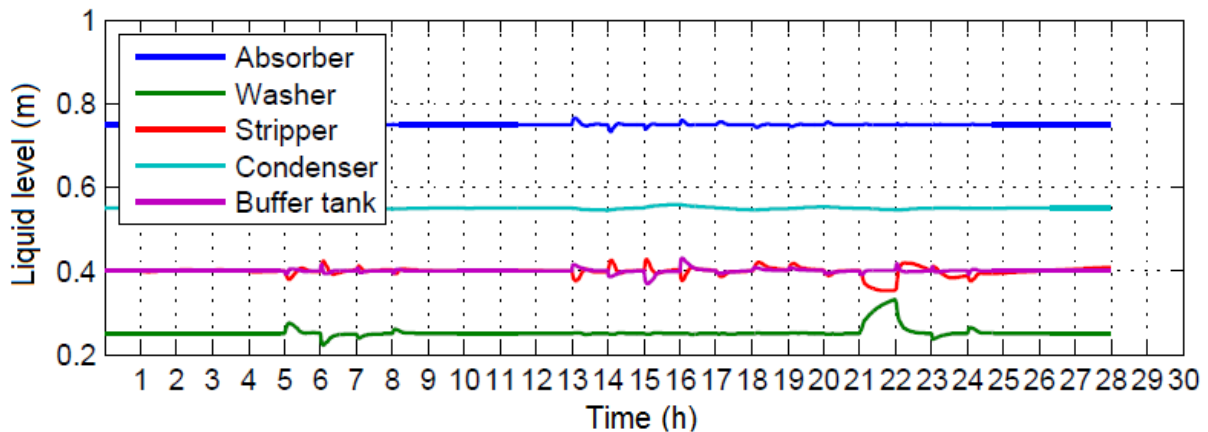
| Process variable                          | Set-point | Disturbance |
|---|-----------|-------------|
| Capture rate                              | 90%       | ± 1%        |
| Solvent temperature at the absorber inlet | 40°C      | ± 3°C       |
| Stripper condenser temperature            | 40°C      | ± 3°C       |
| Stripper pressure                         | 1.7 bar   | ± 0.1 bar   |
| L/G ratio in the absorber                 | 4.1 kg/kg | ± 0.2       |
| L/G ratio in the washer                   | 4.1 kg/kg | ± 0.2       |



Figure 3.25, 3.26 and 3.27 present the effect of simulated disturbances on the process stability. For each process variable listed in table 3.19, four set-point changes have been successively applied each hour: increase of the set-point, return to the base case, decrease of the set-point and return to the base case. For instance, the capture rate set-point is successively set at 91% (t=1h), 90% (t=2h), 89% (t=3h) and back to 90% (t=4h).

In all cases studied, the process answer is rapid and the simulated disturbances have no adverse effect on the process stability. Liquid level variations in the columns are kept within a few centimeters as shown in figure 3.25. One exception has been observed at t=21h due to the increase of the liquid to gas ratio in the washer. This problem was due to the washing pump, which could not cope with the increased liquid flow, leading to liquid accumulation in the washer and to a decrease of the liquid level in the stripper. The problem could be solved in further simulations by using a more powerful pump in the washing water loop.

Moreover, the resulting capture rate deviation is kept within 1% (except at t=22h, which is a consequence of the washing water pump problem) and the process thermal energy consumption stabilizes within a few minutes as represented in figure 3.26 and 3.27. In conclusion, the control strategy at nominal operating point can efficiently reject the simulated process disturbances and the good regulation of the liquid level in the stripper evidences that the water balance is successfully controlled.



**Figure 3.25: effect of simulated process disturbances on the liquid levels**

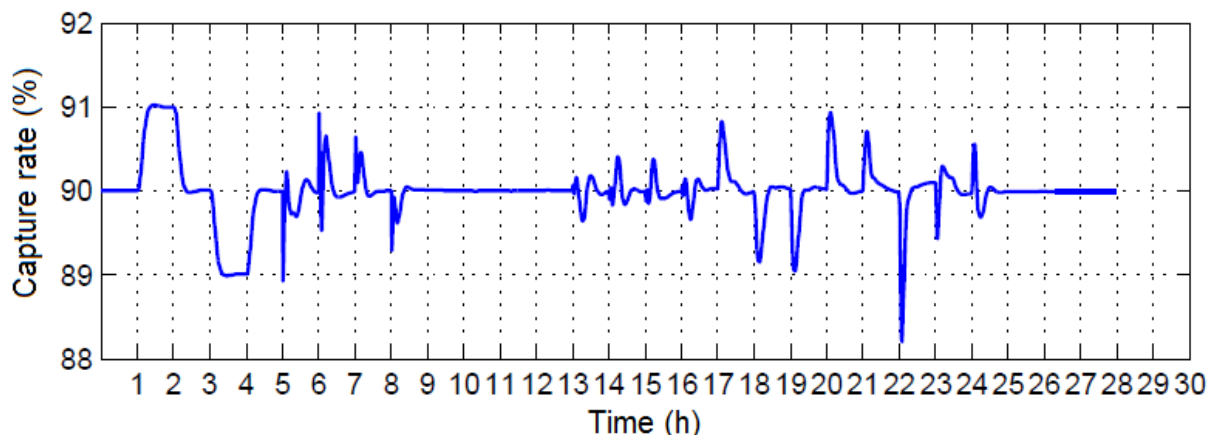


**Figure 3.26: effect of simulated process disturbances on the CO<sub>2</sub> capture rate**

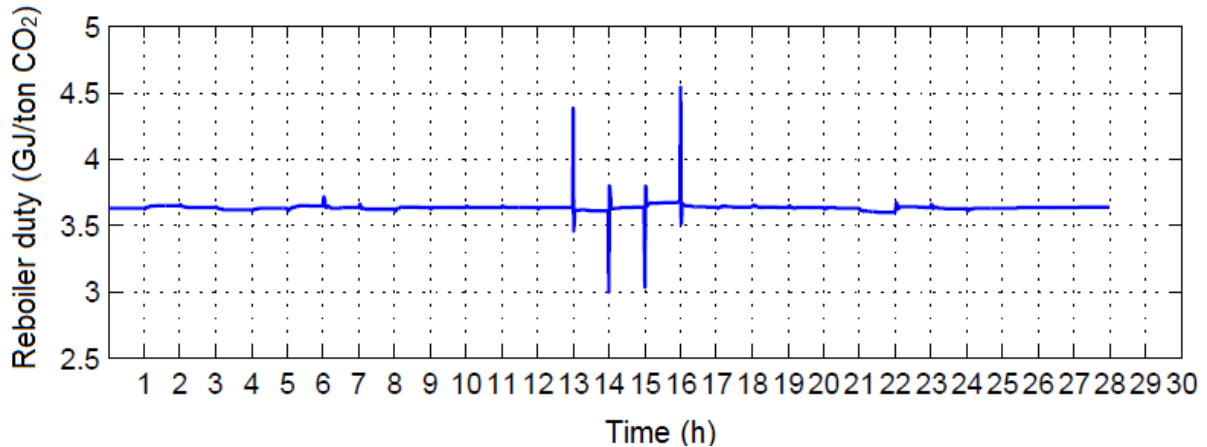


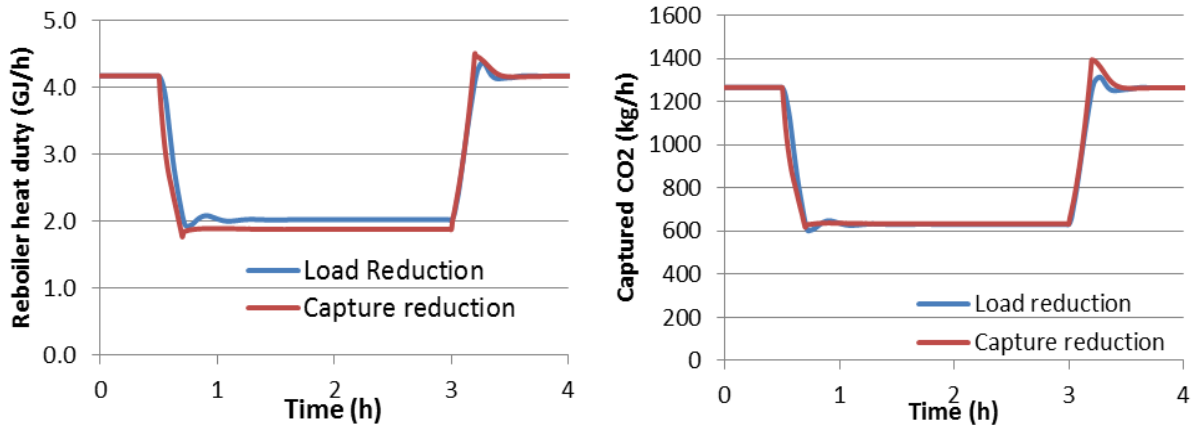
**Figure 3.27: effect of simulated process disturbances on the process thermal energy requirement**

### *Capture flexibility*

In order to ensure maximum flexibility for power plants equipped with CO<sub>2</sub> capture, it is essential to study the dynamic behavior of the capture process when the electricity demand increases, for instance in case of daily peak hours that may last for 2-3 hours. Electricity production can be temporarily increased by reducing the CO<sub>2</sub> capture rate, and thus the steam consumption of the solvent regeneration. Since the electricity demand peaks usually do not last very long, it is not recommended to totally shut down the capture installation, but rather to reduce its energy consumption. Two scenarios can be envisaged:

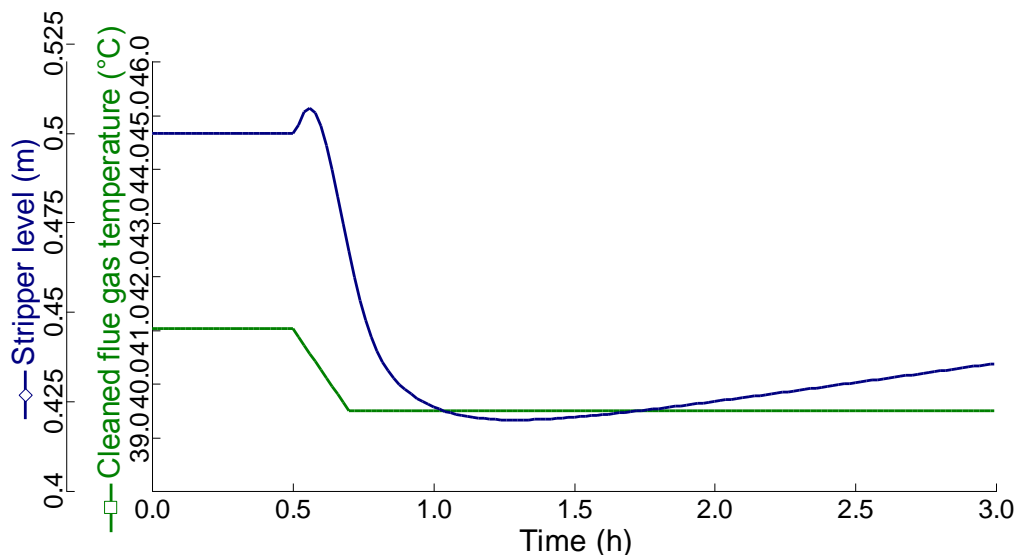
- Reduction of the capture rate: the capture rate set-point (usually set at 90%) is decreased while the flue gas load is kept constant as well as the solvent flow rate. As a consequence, the amine solvent needs to be less regenerated and less steam is required at the stripper reboiler. Thus, the extra steam is available to increase the electricity production of the power plant.
- Reduction of the flue gas load: the flue gas flow rate treated by the capture plant (usually 5000 Nm<sup>3</sup>/h in the present model) is reduced by venting a part of the flue gas to the atmosphere before the absorber. As a consequence, the solvent flow rate is decreased to keep a constant liquid over gas ratio in the mass transfer columns, and less steam is required to regenerate the smaller solvent flow.

Figure 3.28 compares the evolutions of the reboiler duty and of the flow rate of captured CO<sub>2</sub> for a 50% reduction of the flue gas load and a 50% reduction of the capture rate set-point. Both reductions take place over 12 minutes and the capture plant is returned to its nominal operating mode after stabilization. It appears that reducing the capture set-point leads to a slightly lower reboiler duty (1.89 GJ/h compared to 2.03 GJ/h for the load reduction scenario) at equivalent flow rate of captured CO<sub>2</sub>.



**Figure 3.28: two scenarios for reducing the process energy requirement over 12 minutes**

However, these strategies must be adapted in case of larger reductions and faster transitions. For instance, when the capture rate set-point is decreased down to 10% in 12 minutes, the stripper liquid level could not be stabilized as represented in figure 3.29. Indeed, at a capture rate of 10%, the amine solvent is barely regenerated and absorbs very little CO<sub>2</sub> in the absorber. Since the absorption is an exothermic reaction, the flue gas temperature in the absorber does not increase enough and the temperature of the cleaned flue gas released to the atmosphere decreases as shown in figure 3.29. This temperature decrease is observed even if the flue gas is not cooled anymore in the washing section. Consequently, less water exits the process with the cleaned flue gas and water accumulates in the stripper where the liquid level is set free. Since the stripper liquid level rises very slowly (about 1cm/h), it will only be problematic if the 10%-capture rate regime lasts for many hours.



**Figure 3.29: effect of a CO<sub>2</sub> capture rate decrease down to 10% capture on the stripper liquid level**

Similarly, when reducing the flue gas load down to 10% of its nominal value, the solvent mass flow is reduced to keep the L/G ratio constant. As a consequence, column hold-ups decrease and liquid levels increase in all flowsheet blocks so that level controllers are not able to stabilize the process anymore. The solution is to use an additional solvent buffer tank or to

adapt the set-point of the liquid level controllers during the load reduction ramp. In this case, it is possible to reduce the flue gas load down to 10% of its nominal value in only 6 minutes.

Finally, these examples show the potential of dynamic simulation at predicting the process behavior during unsteady-state operating modes. However, the model precision is limited due to the use of an equilibrium-stages assumption with the simulation tool Aspen Plus Dynamics.

### *4.3 Degradation modeling*

The experimental results presented in Chapter II have led to the formulation of reaction rates for the oxidative and thermal degradation of MEA with CO<sub>2</sub>. The resulting kinetics model has been included in a steady-state rate-based model as described in section 3.3. Thus the objective of the present section is to evaluate the information that can be gained if degradation is included in the process model.

First, the results obtained in the base case configuration including degradation are discussed. Then, the influence on degradation of some process operating variables will be quantified, and some flowsheet improvements will be evaluated from the energy and environmental points of view. Finally, optimal operating conditions will be proposed for the CO<sub>2</sub> capture process.

#### ***Base case degradation***

Table 3.20 lists the formation rates of degradation products as well as the MEA degradation rate in the absorber and the stripper. The emissions in the cleaned flue gas and the CO<sub>2</sub> product streams are also reported, before and after passing the column washing sections. Since HEI, HEPO and HEIA are not present in the component database of Aspen Plus, they have been assumed as nonvolatile components, so that there are not present in the gas streams. The liquid temperature and the vapor oxygen content at the top and bottom stages of the columns are also indicated.

All degradation and emission values have been normalized by the amount of captured CO<sub>2</sub> which equals 1.24 ton/h in the simulation (90% capture rate, 5000 Nm<sup>3</sup>/h flue gas). Due to the stoichiometry of the oxidative degradation (equation 3.36), HEPO, HEI and HCOOH show equivalent formation rates in kmol/ton CO<sub>2</sub>, but the values in kg/s differ according the components molar weights.

**Table 3.20: degradation and emission results of the base case model**

| Parameter                                 | Unit                   | Absorber | Stripper | Total  |
|---|------------------------|----------|----------|--------|
| MEA degradation                           | kg/ton CO <sub>2</sub> | 8.2e-2   | 1.4e-5   | 8.2e-2 |
| NH <sub>3</sub> formation                 | kg/ton CO <sub>2</sub> | 1.4e-2   | 8.4e-7   | 1.4e-2 |
| HCOOH formation                           | kg/ton CO <sub>2</sub> | 6.1e-3   | 3.8e-7   | 6.1e-3 |
| HEI formation                             | kg/ton CO <sub>2</sub> | 1.5e-2   | 9.2e-7   | 1.5e-2 |
| HEPO formation                            | kg/ton CO <sub>2</sub> | 1.9e-2   | 1.2e-6   | 1.9e-2 |
| HEIA formation                            | kg/ton CO <sub>2</sub> | 1.1e-5   | 1.1e-5   | 2.2e-5 |
| MEA emission before washing               | kg/ton CO <sub>2</sub> | 2.3      | 1.6e-1   | 2.4    |
| NH <sub>3</sub> emission before washing   | kg/ton CO <sub>2</sub> | 1.1e-2   | 6.3e-3   | 1.8e-2 |
| HCOOH emission before washing             | kg/ton CO <sub>2</sub> | 9.0e-4   | 2.6e-4   | 1.1e-3 |
| MEA emission after washing                | kg/ton CO <sub>2</sub> | 8.7e-4   | 9.4e-9   | 8.7e-4 |
| NH <sub>3</sub> emission after washing    | kg/ton CO <sub>2</sub> | 9.5e-3   | 3.0e-3   | 1.3e-2 |
| HCOOH emission after washing              | kg/ton CO <sub>2</sub> | 1.1e-4   | 1.4e-5   | 1.2e-4 |
| Top stage liquid temperature              | °C                     | 57.4     | 96.6     | -      |
| Bottom stage liquid temperature           | °C                     | 51.1     | 115.6    | -      |
| Top stage vapor O <sub>2</sub> content    | mol%                   | 6.3%     | 9.6e-3%  | -      |
| Bottom stage vapor O <sub>2</sub> content | mol%                   | 6.1%     | 7.0e-14% | -      |

It appears that the degradation model correctly describes the influence of process operating conditions on degradation. Indeed, it confirms major pilot plant observations:

- More oxidative degradation products (NH<sub>3</sub>, HEI, HEPO, HCOOH) are formed than thermal degradation products with CO<sub>2</sub> (HEIA) over the entire process. This confirms that oxidative degradation is the dominant degradation pathway in CO<sub>2</sub> capture plants as already evidenced by Lepaumier et al. (2011).
- Oxidative degradation mainly takes place in the absorber, suggesting that the low temperature in the absorber does not prevent oxidative degradation in the presence of high oxygen concentrations. This is confirmed by pilot plant observations that report higher NH<sub>3</sub> emissions in the cleaned flue gas than in the product stream (Moser et al., 2011b). Moreover, ammonia is confirmed as the main degradation product.
- Thanks to the washing section, MEA losses due to solvent emission are negligible in comparison with MEA degradation in the absorber. Moreover, NH<sub>3</sub> emissions after the washing section are much higher than MEA emissions in accordance with Moser et al. (2011b). Almost all the produced NH<sub>3</sub> is emitted.

As a consequence, the MEA loss due to the oxidative degradation in the absorber ( $8.2\text{e-}2$  kg/ton CO<sub>2</sub>) is about 100 times higher than the sum of other MEA losses due to degradation in the stripper and solvent emission ( $8.9\text{e-}4$  kg/ton CO<sub>2</sub>).

Furthermore, the amount of degraded MEA is in the same order of magnitude compared with CO<sub>2</sub> capture plant results, although the predicted values are lower. Indeed, the total MEA loss equals 0.082 kg MEA/ton CO<sub>2</sub> and recent pilot plant results (Moser et al., 2011b) report a degradation rate of 0.284 kg MEA/ton CO<sub>2</sub> in the absence of degradation inhibitors.

This deviation can be explained by three assumptions that have been made to model solvent degradation in a first approach, leading to underestimated MEA consumption rates:

- The presence of flue gas contaminants like SO<sub>x</sub> and NO<sub>x</sub> has not been considered in this model.
- In the framework of the experiments in the degradation test rig, the solubility of oxygen in amine solvents has been approached by Henry's law that provides the solubility of oxygen-saturated solutions. However, mass transfer limitations play a role in the degradation reactor as evidenced when varying the agitation rate. Thus, the oxygen solubility is overestimated and the resulting kinetic constant is underestimated.
- The presence of dissolved metals catalyzes the oxidative degradation of MEA and accelerates the degradation kinetics. This has been evidenced by the experiment performed with dissolved metals, in which the degradation rate has been increased by 58% compared to the base case without metals. However, the influence of dissolved metals has not been considered in the proposed simulation model in a first approach.

Finally, the degradation model provides useful information about the influence of operating conditions on MEA degradation and on the emission of degradation products. Moreover, the lower values for the predicted solvent consumption compared to pilot plant results can be explained by the modeling assumptions.

### *Sensitivity study*

In this section, the influence of four process variables on the environmental and energy penalties of the CO<sub>2</sub> capture process is discussed. The selected process variables are the variables identified in section 4.1 plus the oxygen concentration in the flue gas. The flue gas flow rate equals 5000 Nm<sup>3</sup>/h (14% CO<sub>2</sub>, 12% H<sub>2</sub>O, 6% O<sub>2</sub>, 68% N<sub>2</sub>) and the CO<sub>2</sub> capture rate is kept constant at 90%.

#### *Solvent flow rate*

The influence of the solvent flow rate on the process energy requirement has been discussed in section 4.1. The same influence can be observed in the degradation model treating a larger flue gas flow rate as represented in figure 3.30. Moreover, the rate of the MEA loss over the entire process (degradation and emission in the absorber and stripper) has also been reported in figure 3.30. It appears that the total MEA loss slightly increases with the solvent flow rate, by about  $1\text{e-}2$  kg/ton CO<sub>2</sub> for an increase by 4 m<sup>3</sup>/h of the solvent flow rate. This small increase of the MEA loss may be due to a higher liquid holdup in the mass transfer columns, leading to longer solvent residence times and enhanced degradation in the absorber and stripper.

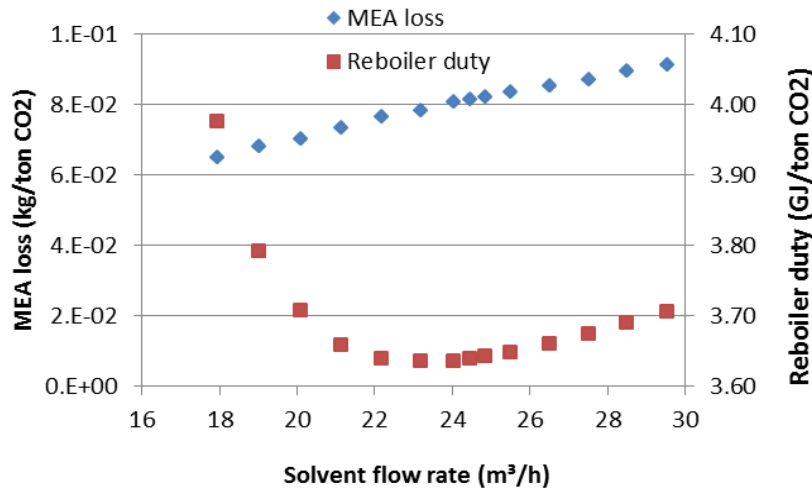


**Figure 3.30: influence of the solvent flow rate on the process energy and environmental penalties**

The increase of the MEA loss at higher solvent flow rates is mainly due to oxidative degradation as confirmed in figure 3.31 by the distribution of degradation products over the entire process. In order to facilitate the comparison between the different degradation products, the MEA loss, the MEA emission and the formation of degradation products over the entire process have been reported in kmol/ton CO<sub>2</sub>. As a consequence, the production rates of HEPO, HEI and HCOOH are equivalent due to the reaction stoichiometry. It appears clearly that the MEA thermal degradation, which is evidenced by HEIA, can be neglected compared to oxidative degradation. The same argumentation is also valid for the MEA loss due to emission.

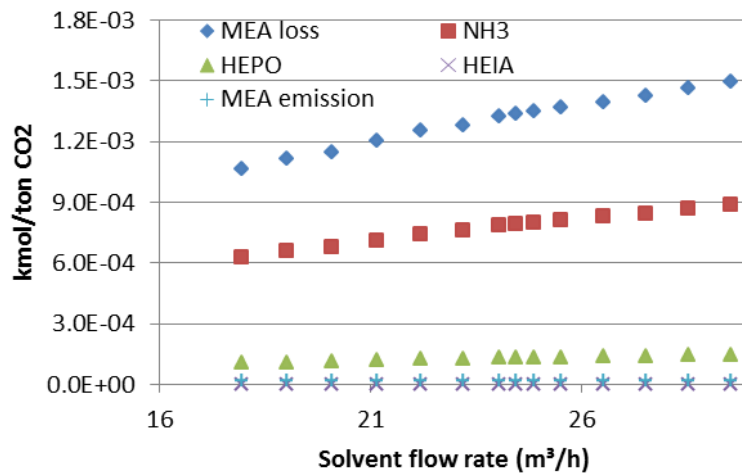


**Figure 3.31: influence of the solvent flow rate on the degradation products**

#### *Oxygen content*

Varying oxygen contents in the flue gas may result from different operating modes of the coal (or natural gas) combustion in the power plant. In the absence of oxygen, almost no degradation is observed in figure 3.32. Moreover, it appears that the MEA degradation increases more than proportionally with the oxygen content in the flue gas since doubling the oxygen concentration from 6% to 12% induces an increase of the MEA loss by 175% from 0.08 to 0.22 kg/ton CO<sub>2</sub>. Finally, no significant influence of the oxygen content in the flue gas has been observed on the thermal energy requirement of the process.

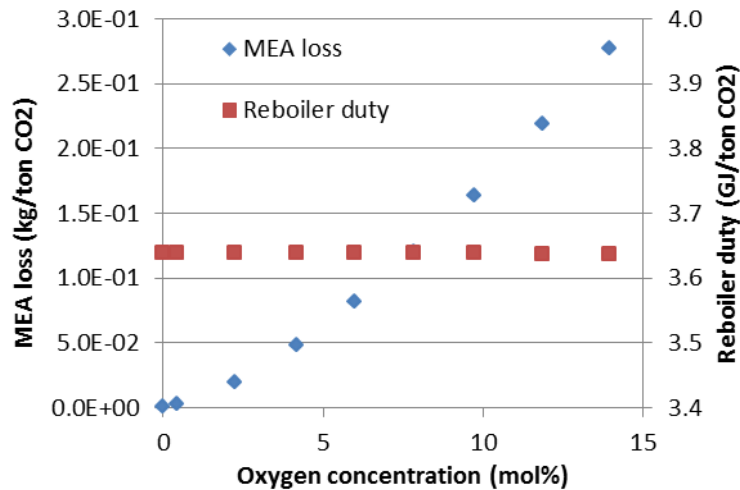


**Figure 3.32: influence of the oxygen concentration in the flue gas on the process energy and environmental penalties**

Figure 3.33 confirms that the higher O<sub>2</sub> content in the flue gas enhances the oxidative degradation of MEA, thus leading to a global increase of the MEA loss. The different slopes of the MEA, ammonia and HEPO curves are related to the stoichiometry of the oxidative degradation (equation 3.36).

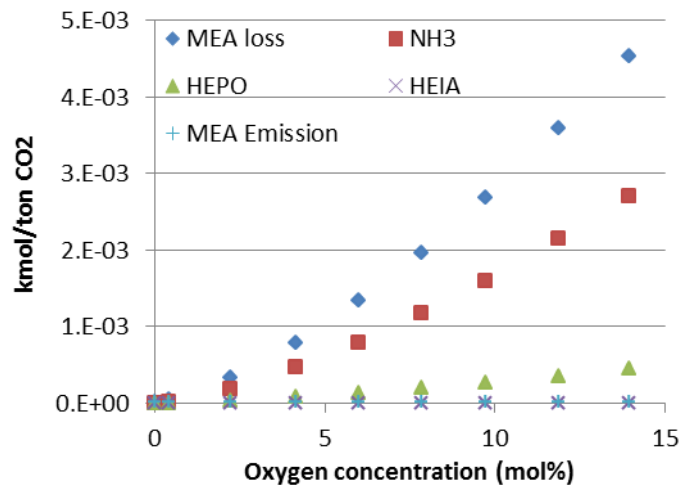


**Figure 3.33: influence of the oxygen concentration on the MEA loss**

#### MEA concentration

As mentioned in section 4.1, a higher solvent concentration increases the driving force for the CO<sub>2</sub> absorption and thus reduces the process thermal energy requirement. However, if we consider that oxygen also undergoes a reactive absorption like CO<sub>2</sub>, we can describe the O<sub>2</sub> mass transfer using an enhancement factor and the MEA concentration is also implied in the expression of this enhancement factor. As a consequence, the oxygen transfer is accelerated and the degradation increases at higher MEA concentrations as represented in figure 3.34. It appears that increasing the MEA concentration from 30 wt% to 40 wt% approximately doubles the MEA loss from 0.082 up to 0.175 kg/ton CO<sub>2</sub> while the reboiler heat duty is decreased by 4 % from 3.64 to 3.49 GJ/ton CO<sub>2</sub>.



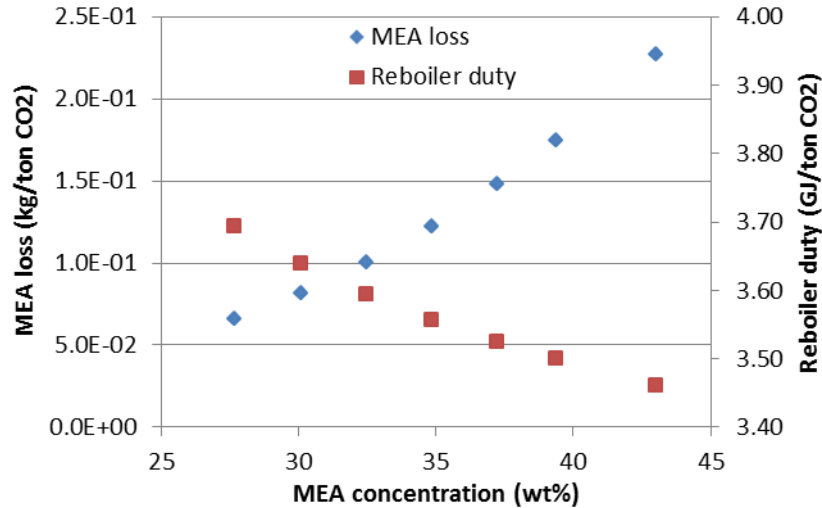


**Figure 3.34: influence of the MEA concentration on the process energy and environmental penalties**

As a consequence, concentrated MEA is not an advantageous solvent except if oxidative degradation inhibitors are added as proposed by Lemaire et al. (2011). Finally, no significant effect due to the concentration has been observed on the MEA thermal degradation or the MEA emission as represented in figure 3.35.

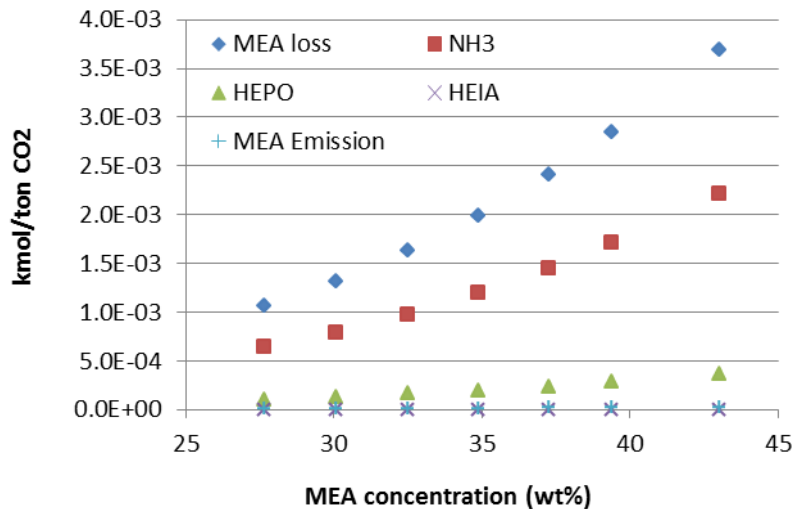


**Figure 3.35: influence of the MEA concentration on the degradation products**

#### *Stripper pressure*

Increasing the stripper pressure leads to a higher temperature and thus to an exponential increase of the MEA degradation in the stripper as presented in figure 3.36. The increase of the HEIA concentration indicates that thermal degradation with CO<sub>2</sub> becomes clearly the main degradation pathway in the stripper.

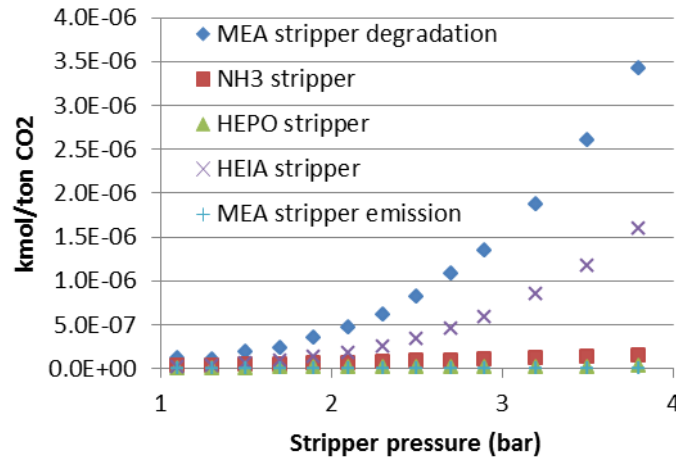


**Figure 3.36: influence of the stripper pressure on stripper degradation products**

However, the influence of the stripper pressure on the MEA loss over the entire process is limited as represented in figure 3.37 since the amount of degraded MEA in the stripper ( $\sim 1\text{e-}5$  kg/ton CO<sub>2</sub>) remains a few orders of magnitude lower than the MEA loss over the entire process ( $8.2\text{e-}2$  kg/ton CO<sub>2</sub>). Finally, the influence of the stripper pressure on the reboiler heat duty suggests that high stripping pressures are advantageous for CO<sub>2</sub> capture with MEA. For instance, increasing the stripper pressure from 1.1 to 1.7 bar decreases the reboiler heat duty by 12% from 4.13 to 3.64 GJ/ton CO<sub>2</sub>. The MEA loss is almost not affected since it varies between 8.0 and 8.2 kg/ton CO<sub>2</sub>.

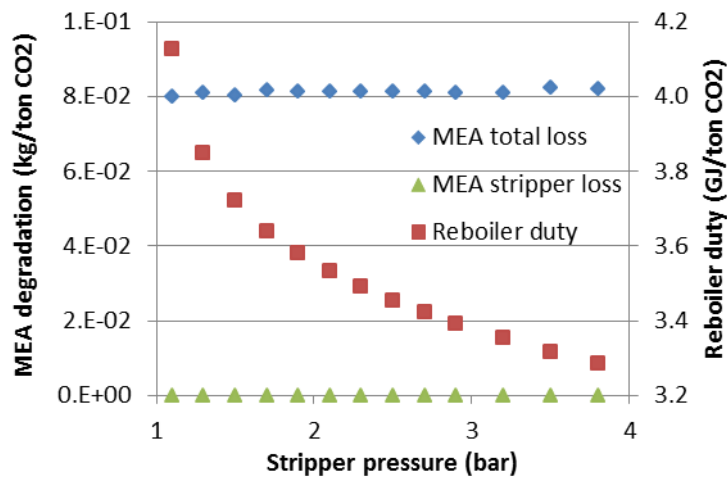


**Figure 3.37: influence of the stripper pressure on the process energy and environmental penalties**

### *Alternative flowsheet configurations*

Besides sensitivity studies, the modeling of alternative process configurations is a useful tool to explore potential energy savings. In the present section, the impact of two flowsheet modifications is evaluated: the absorber intercooling and the lean vapor compression.

#### *Absorber intercooling*

Since the absorption is an exothermic reaction, reducing the average absorption temperature improves the process efficiency as discussed in section 2.3. To simulate the intercooling, the

whole solvent flow has been cooled down to 40°C between two absorber stages. Figure 3.38 confirms that it is possible to decrease the process energy consumption by about 3% (from 3.64 to 3.54 GJ/ton CO<sub>2</sub>), depending on the location of the intercooler.

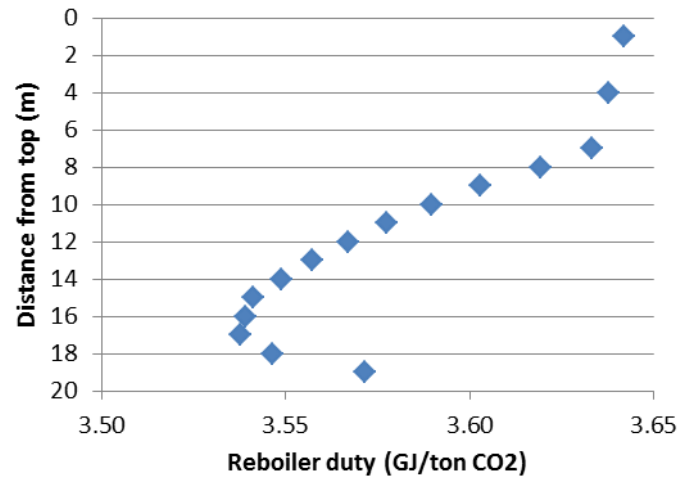


**Figure 3.38: influence of the intercooler location on the process thermal energy requirement**

It appears that the best process efficiency is reached when the intercooler is located in the lower third of the column. This is explained by the fact that the largest part of the absorption occurs at the absorber inlet due to the high CO<sub>2</sub> partial pressure in the gas phase at that place. Finally, the effect of absorber intercooling on solvent degradation may also be studied. It appears that the presence of an intercooler optimally located slightly reduces the rate of MEA degradation, from 8.2e-2 down to 7.8e-2 kg/ton CO<sub>2</sub>. This small improvement may be due to a globally lower absorber temperature, and thus to a lower rate of oxidative degradation.

#### *Lean vapor compression*

As described in section 2.3, the lean vapor compression (LVC) consists in partially evaporating the regenerated solvent at the stripper exit in order to recover energy from the hot solvent. The generated vapor in the flash tank is composed of approximately 90 wt% water and 10 wt% CO<sub>2</sub>. This vapor is compressed and recycled to the stripper where it acts as auxiliary stripping steam and thus allows a reduction of the reboiler duty. Some water is added to the generated vapor flow to desuperheat it, so that the vapor temperature does not exceed 125°C after compression. This flowsheet modification is represented in figure 3.39.

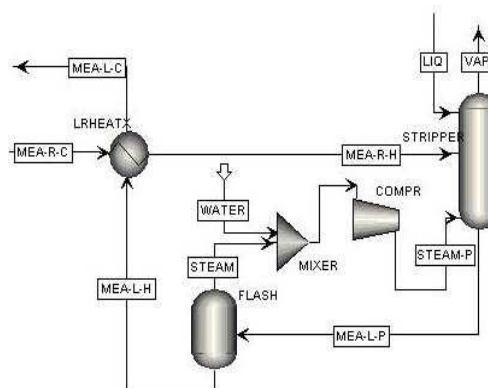


**Figure 3.39: flowsheet of the lean vapor compression**

The influence of the flash tank pressure on the reboiler heat duty and on the process exergy requirement has been studied as represented in figure 3.40. Indeed, an additional energy requirement for the vapor compression must be considered since the lower the flash tank pressure, the higher the compression cost. If the flash tank is operated at 1.1 bar, the reboiler heat duty is reduced by 13% from 3.64 to 3.17 GJ/ton CO<sub>2</sub>. But based on an exergetic comparison<sup>41</sup>, the process exergy requirement is reduced by 9% from 1.28 down to 1.16 GJ/ton CO<sub>2</sub>. During this study, the stripper pressure has been kept constant at 1.7 bar and the generated lean vapor has been compressed to the stripper pressure, whatever the flash pressure. The case at 1.7 bar thus corresponds to the base case with no LVC.

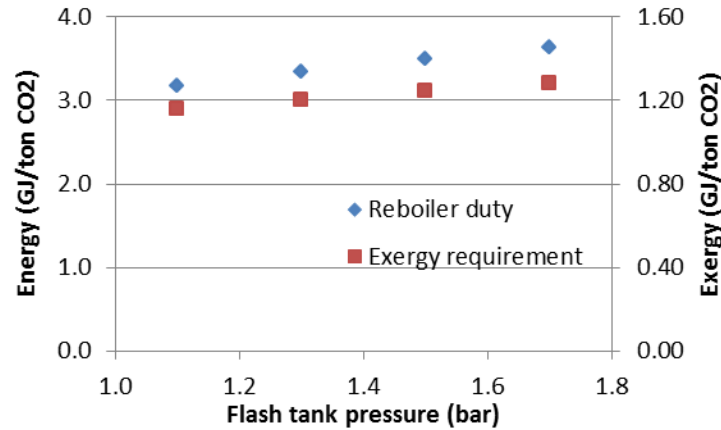


**Figure 3.40: influence of the flash tank pressure for lean vapor compression on the process energy requirement**

Finally, the lean vapor compression shows a small influence on the degradation of MEA since the MEA consumption varies from 8.2e-2 kg/ton CO<sub>2</sub> (base case) to 8.1 e-2 kg/ton CO<sub>2</sub> (LVC with flash pressure at 1.1 bar).

### *Optimal operating conditions*

According to the sensitivity analysis, the optimal conditions for the CO<sub>2</sub> capture process would be the following:

- Concentrated MEA solvent: 40 wt% MEA (if degradation inhibitors are available).
- Optimized solvent flow rate: 24 m<sup>3</sup>/h in the simulated configuration.
- Low oxygen concentration in the flue gas: 0% O<sub>2</sub>.
- High stripper pressure: 4 bar.
- Equipment for absorber intercooling and lean vapor compression.

<sup>41</sup> The exergy is defined as the maximum work that can be produced during a process when the system is brought to equilibrium with its thermodynamic reference state (atmospheric pressure, 288.15°K). This thermodynamic variable is used to compare heat and work streams based on  $1 W_{ex} = 1 W_{el} = 1 W_{th} \cdot \eta^{-1}$  where  $\eta$  is the Carnot efficiency:  $\eta = 1 - T_c/T_h$ . We assume a steam temperature ( $T_h$ ) of 443°K in the reboiler, while  $T_c = 288.15°K$ .

Unfortunately, these conditions are not realistic in a real capture plant. For instance, the oxygen concentration is determined by the operation of the power plant<sup>42</sup> and removing oxygen from the flue gas would further increase the CO<sub>2</sub> capture costs. Thus, an intermediate configuration is proposed with following characteristics:

- The concentration of the MEA solvent is kept equal to 30 wt%. If efficient oxidative degradation inhibitors are available, the concentration could be increased to 40 wt%.
- The stripper pressure is set at 1.7 bar.
- The solvent flow rate is optimized depending on design data of the CO<sub>2</sub> capture plant (24 m<sup>3</sup>/h in the present case).
- The oxygen concentration is equal to 6 mol%.

These specifications have been used for the base case degradation model described previously, which was already the result of an optimization process. Then, the process can be further improved by adding the two flowsheet modifications that have been tested. Figure 3.41 compares the energy requirement and the solvent losses for four different configurations:

- The base case process.
- The base case with absorber intercooling (IC).
- The base case with lean vapor compression (LVC).
- The optimum configuration, combining intercooling and lean vapor compression.

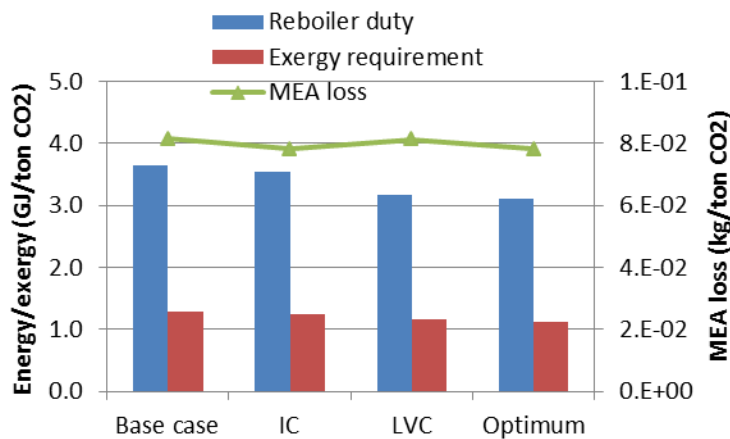


**Figure 3.41: comparison of different process configurations for optimal CO<sub>2</sub> capture**

Finally, it appears that combining the absorber intercooling with the lean vapor compression decreases the reboiler duty by 15% from 3.64 to 3.10 GJ/ton CO<sub>2</sub> while the MEA loss slightly decreases from 8.2e-2 to 7.8e-2 kg/ton CO<sub>2</sub>. The reduction of the reboiler duty is mainly due to the lean vapor compression, while the reduction of the MEA loss seems to be related to the absorber intercooling that decreases the mean absorber temperature. Overall, the process exergy requirement decreases by 12%, from 1.28 GJ/ton CO<sub>2</sub> in the base case configuration to 1.13 GJ/ton CO<sub>2</sub> in the best configuration.

<sup>42</sup> In gas-fired power plants, the oxygen concentration of the flue gas may be decreased down to 2 vol%.

## 5. Conclusions

Most existing models of the CO<sub>2</sub> capture process have been developed to evaluate the process energy requirement in order to reduce the cost of the technology. However, solvent degradation has been identified as a major issue in CO<sub>2</sub> capture plants due to the emission of environmentally harmful degradation products. Thus, the objective of this chapter was to integrate the experimental results of solvent degradation previously presented into a global process model of the CO<sub>2</sub> capture. The purpose of this model is to bring a better understanding of the interactions between the process operating conditions and the solvent degradation, so that solvent degradation may also be considered during the design of CO<sub>2</sub> capture units, which is particularly relevant for the large-scale deployment of the CO<sub>2</sub> capture technology.

Before all, the main modeling aspects of the CO<sub>2</sub> capture process with MEA have been detailed and discussed. The Electrolyte NRTL model has been selected to evaluate fluid properties. This model has the particularity of considering electrostatic forces due to dissolved ions in amine solutions. Two main approaches have been tested for modeling the reactive absorption of CO<sub>2</sub> in mass transfer columns. The first one assumes equilibrium stages in the columns and neglects mass transfer limitations and chemical kinetics (equilibrium assumption). The second approach performs rigorous calculations of the reactive absorption based on experimental data for packing hydrodynamics and chemical kinetics (rate-based assumption).

The simulation studies have been performed based on design data from two different pilot plants: the Mobile Pilot Unit for which our industrial partner Laborelec has collaborated to the design and the Esbjerg Pilot Plant developed in the framework of European CCS projects. All models have been developed using the simulation tool Aspen Plus. In the first part of the simulation study, two models have been developed based on the Mobile Pilot Unit to compare the equilibrium and the rate-based assumptions. This has been done by studying the influence of key operating parameters on the process thermal energy requirement. It appears that both models lead to globally similar results, but the equilibrium model systematically predicts a higher process efficiency since it neglects the mass transfer limitations and the reaction kinetics (it assumes instantaneous chemical equilibria). Moreover, the rate-based model better predicts column temperature profiles.

Then, the second part of the simulation study explores the potential of dynamic simulations for describing the behavior of the process in transient regimes. The control of the process water balance is improved compared to published dynamic models and the stability of the control strategy is evaluated for different process disturbances. The process response in case of reduced steam availability in the power plant is simulated for two different scenarios. The scenario in which the flue gas and the solvent flow rates are kept constant at lower CO<sub>2</sub> capture rate seems to give better results than the scenario in which the flue gas and the solvent flow rates are decreased in the capture plant.

The third part of the modeling study is the main innovation of the present work. A global process model has been developed that includes degradation reactions based on the experimental results detailed in Chapter II. Oxidative and thermal degradations are represented by two apparent degradation reactions with corresponding kinetics. Moreover, solvent emissions are quantified before and after the absorber and stripper washing sections. The degradation model confirms that oxidative degradation in the absorber is by far the

dominant cause for MEA loss in CO<sub>2</sub> capture units. It also confirms pilot plant observations that reported high NH<sub>3</sub> emissions at the absorber outlet as the major emission of degradation products to the environment.

Moreover, the degradation model predicts solvent consumption rates in the same order of magnitude but slightly lower (0.082 kg/ton CO<sub>2</sub>) than those observed in pilot plants (0.284 kg/ton CO<sub>2</sub>). The lower predicted values can be explained by the modeling assumptions so that further potential model refinements are identified:

- Consideration of SO<sub>x</sub> and NO<sub>x</sub>-induced degradation.
- Development of a better estimation for the oxygen solubility and transfer in amine solutions.
- Consideration of the influence of dissolved metals on the degradation rate.

Using this degradation model, the influence on solvent degradation of different key operating variables and alternative flowsheet configurations is studied. It appears that:

- An optimum value for the solvent flow rate can be identified to minimize the reboiler heat duty. Moreover, increasing the solvent flow rate by 4 m<sup>3</sup>/h leads to a slight increase of the MEA loss (about 1e-2 kg/ton CO<sub>2</sub>).
- An increased O<sub>2</sub> concentration in the flue gas from 6 mol% to 12 mol% increases the MEA loss from 0.08 to 0.22 kg/ton CO<sub>2</sub> while no effect on the reboiler heat duty is observed.
- Increasing the MEA solvent concentration from 30 wt% to 40 wt% doubles the solvent consumption rate from 0.082 up to 0.175 kg/ton CO<sub>2</sub> while the reboiler heat duty is decreased by 4 % from 3.64 to 3.49 GJ/ton CO<sub>2</sub>.
- Increasing the stripper pressure from 1.1 to 1.7 bar reduces the reboiler duty by 12% with no significant increase of the MEA consumption.
- The absorber intercooling and the lean vapor compression both reduce the total process energy requirement, by 3% and 9% respectively. Moreover, they do not significantly influence the solvent degradation.

Finally, the degradation model proposes a first approach for considering degradation reactions as a part of the optimal design of the CO<sub>2</sub> capture process. A methodology implying experimental degradation studies and process modeling tools has been proposed based on the benchmark solvent 30wt% MEA and further model improvements have been identified.

## **Chapter IV**

# **Conclusions and perspectives**

*“If you do not change direction, you may end up where you are heading.”*  
*Lao Tzu*



## 1. Conclusions

Environmental concerns have received an increased attention in the last few decades as the scientific community has warned about the effects of anthropogenic greenhouse gas emissions on the environment. In this context, CO<sub>2</sub> capture and storage technologies are proposed as one of the potential contributions to a decarbonated energy mix. Their objective is to capture the CO<sub>2</sub> emitted during the combustion of fossil fuels and to re-use it or to store it underground.

In the present work, the post-combustion CO<sub>2</sub> capture with amine solvents is studied. It is the most mature CO<sub>2</sub> capture technology for large-scale applications like coal or natural gas-fired power plants. Moreover, this technique can be used to retrofit existing plants by treating the flue gas after combustion. However, two main drawbacks slow down the development of post-combustion capture from a technical point of view:

- The high energy requirement of the process for regenerating the amine solvent that has absorbed CO<sub>2</sub>.
- The environmental impact related to the emission of amine solvents and degradation products into the atmosphere.

Both of these aspects are usually studied separately. In the present work, they are combined in a multi-disciplinary approach. Indeed, a methodology is developed to simultaneously evaluate the influence of process operating parameters on the process energy requirement and on the degradation of amine solvents. This study considers an aqueous solution of monoethanolamine (MEA), which is the benchmark solvent for post-combustion CO<sub>2</sub> capture.

In a first phase, the influence of several process operating parameters on the solvent degradation is quantified. The two main degradation pathways of MEA are studied experimentally, i.e. the oxidative degradation is studied using an experimental degradation test rig with continuous gas flow and the thermal degradation with CO<sub>2</sub> is studied in batch degradation cylinders. Moreover, appropriate analytical techniques are developed to characterize solvent degradation by quantifying the amine content and the formation of liquid and vapor degradation products. The principal conclusions of this experimental study are:

- Similar degradation pathways and products are observed in the degradation test rig compared with CO<sub>2</sub> capture pilot plants.
- Solvent degradation in CO<sub>2</sub> capture plants is essentially caused by the oxidative degradation of MEA.
- The rate of oxidative degradation is determined by the oxygen mass transfer between the flue gas and the liquid solvent. Different factors affect the oxygen mass transfer, and thus the rate of oxidative degradation. These factors are the agitation rate, the oxygen concentration in the flue gas, the presence of CO<sub>2</sub> in the amine, and the temperature.
- Dissolved metals catalyze the oxidative degradation but show no influence on the thermal degradation with CO<sub>2</sub>.

- Inhibitors of the oxidative degradation may successfully prevent MEA degradation.
- The rate of thermal degradation with CO<sub>2</sub> is affected by the temperature and the presence of CO<sub>2</sub>. Moreover, some oxidative degradation inhibitors decrease the thermal stability of amine solutions.

In a second phase, a simulation model of the process has been developed using the software package Aspen Plus. Different modeling approaches are considered for the post-combustion CO<sub>2</sub> capture with MEA. The main results of this modeling study are listed below:

- The limitations of a simplified model that assumes ideal mass transfer and instantaneous chemical reactions have been evidenced, especially for the prediction of column temperature profiles. This model is compared with a rigorous rate-based model by studying the influence of different process parameters on the reboiler duty.
- The potential of dynamic modeling for predicting the behavior of the CO<sub>2</sub> capture process in transient operating mode has been evidenced. An efficient control strategy has been developed and two scenarios for a rapid reduction of the energy requirement of the capture plant have been studied.

Finally, a kinetic model of solvent degradation considering oxidative and thermal degradation of MEA with CO<sub>2</sub> has been developed based on the results of degradation experiments. This model has been included into a global model of the CO<sub>2</sub> capture process using a rate-based approach for the calculation of mass transfer and chemical reactions. The main observations reported for this model are the following:

- The model confirms that oxidative degradation in the absorber is the main cause for solvent loss in CO<sub>2</sub> capture plants. It also confirms that ammonia emissions at the absorber outlet are one of the major environmental issues.
- The influence of process operating variables on the energy and the environmental penalties of the CO<sub>2</sub> capture process is quantified. The solvent flow rate and concentration, the stripper pressure and the oxygen concentration in the flue gas are varied. The largest energy savings are observed by increasing the stripper pressure and the solvent concentration, while the most significant increases of the MEA consumption are due to the increased oxygen concentration in the flue gas and to the higher solvent concentration.
- Two process improvements have been tested. The absorber intercooling and the lean vapor compression both reduce the total process energy requirement with no significant influence on solvent degradation. Combining these two improvements allows a reduction of the process energy requirement by 12%.

In conclusion, an important step towards the consideration of solvent degradation in the design of CO<sub>2</sub> capture plants has been achieved. Indeed, degradation models similar to that proposed in the present work could and should be used when developing CO<sub>2</sub> capture units to consider not only the process energy penalty, but also its environmental penalty, which is particularly relevant for large-scale applications.

## 2. Perspectives

In the framework of this new research subject, different experimental and modeling tools have been developed at the University of Liège. However, numerous questions have been raised during the present study that would require further investigations. Similarly, many assumptions have been made for modeling solvent degradation in a first approach, and there is room for significant improvements of the resulting degradation model. Among others, following assumptions could be refined:

- The influence of dissolved metals on MEA degradation has been observed, but the kinetic models have been developed based on metal-free solutions. Studying the influence of process operating parameters in the presence of dissolved metals should lead to a more precise modeling of solvent degradation.
- The calculation of dissolved oxygen concentrations in the amine solutions is based on the assumption of oxygen saturation. However, experimental results evidence that oxidative degradation is limited by the oxygen transfer. Thus, a better description of the oxygen solubility would certainly improve the precision of the model.
- The influence of flue gas contaminants like  $\text{SO}_x$  and  $\text{NO}_x$  on the degradation of MEA has not been considered. This could be the object of further experimental and modeling works.
- The influence of the MEA concentration on solvent degradation has been neglected. This assumption could be verified by experimental tests in the degradation test rig.
- The activation energy of the oxidative degradation has been measured in the presence of  $\text{CO}_2$ . Measurements of the oxidative degradation rate at different temperatures and in the absence of  $\text{CO}_2$  could refine the estimation of the activation energy for the oxidative degradation of MEA.
- The model describing the thermal degradation of MEA with  $\text{CO}_2$  is very basic. It could be refined by using the degradation kinetics proposed by Davis (2009). Alternatively, more tests could be performed in batch cylinders in order to get more experimental data for the model development.
- The influence of  $\text{CO}_2$  has been considered in a basic way, assuming that the amines solutions were either loaded with  $\text{CO}_2$  or unloaded. Studying the effect of process operating parameters at various solvent loading could improve the comprehension of the  $\text{CO}_2$  inhibiting effect. However, an analytic method should be developed for that specific purpose since the loading of degraded amine solutions cannot be determined precisely by available analytical methods.
- The proposed degradation model has not been validated against pilot plant data. This could be a further improvement of the model in order to precisely evaluate the process energy requirement and the emissions of amine solvent and degradation products.

- The potential of dynamic simulations has been evidenced with an equilibrium model. Further developments could include a rate-based approach for the mass transfer calculations in dynamic mode.

However, the most important development proposed in this work is not the degradation model on itself, but rather the methodology that has been applied to develop this model. The experimental, analytic and modeling procedures that have been presented in the present study can be easily transposed to other solvent systems since many studies focus on developing alternative solvent to MEA. For instance, piperazine appears as a promising solvent for post-combustion CO<sub>2</sub> capture, so that a process model including solvent degradation could be developed for piperazine. Solvent blends also offer interesting perspectives, as well as demixing solvents.

Finally, a further important improvement would be to consider the impact of solvent degradation on solvent properties, and thus on the operation of the CO<sub>2</sub> capture process. For instance, preliminary tests performed at the University of Liège have shown that the viscosity of a degraded MEA solution increases by about 5% compared to the fresh solvent. Other solvent properties may also be influenced by the presence of degradation products so that the performances of the CO<sub>2</sub> capture process may be significantly affected. This is also the case for the corrosivity of the solvent solution, which increases in the presence of degradation products. As a consequence, quantifying the effects of degradation on solvent properties would help to reduce the technology drawbacks and further contribute to the large-scale development of the CO<sub>2</sub> capture.

## Bibliography

Abanades J., Anthony E., Lu D., Salvador C., Alvarez D., 2004. Capture of CO<sub>2</sub> from combustion gases in a fluidized bed of CaO. *AiCHE Journal* 50 (7), 1614-1622.

Abu-Zahra M., Schneiders L., Niederer J., Feron P., Versteeg G., 2007a. CO<sub>2</sub> capture from power plants. Part I. A parametric study of the technical performance based on monoethanolamine. *International Journal of Greenhouse Gas Control* 1, 37-46.

Abu-Zahra M., Schneiders L., Niederer J., Feron P., Versteeg G., 2007b. CO<sub>2</sub> capture from power plants. Part II. A parametric study of the economical performance based on monoethanolamine. *International Journal of Greenhouse Gas Control* 1, 135-142.

Abu-Zahra M., 2009. Carbon dioxide capture from flue gas. PhD Thesis at the Technical University of Delft, The Netherlands.

ADEME, 2010. Panorama des voies de valorisation du CO<sub>2</sub>. Agence de l'Environnement et de la Maîtrise de l'Energie, France.

Ahmadi A., 2011. Modélisation de l'absorption réactive multiconstituant : application au traitement des gaz acides par des solvants aux alcanolamines. PhD Thesis at the University of Toulouse (INP Toulouse), France.

Aroonwilas V., 2005. Evaluation of split-flow scheme for CO<sub>2</sub> absorption process using mechanistic mass-transfer and hydrodynamic model. *Proceedings of the 7th International Conference on Greenhouse Gas Control Technologies* 5, 1841-1844.

Aspentech, 2008. Rate-based model of the CO<sub>2</sub> capture process by MEA using Aspen Plus. Aspen Plus V7.0 support files.

Aspentech, 2012. Rate-based model of the CO<sub>2</sub> capture process by MEA using Aspen Plus. Aspen Plus V8.0 support files.

Astarita G., Savage D., Bisio A., 1983. Gas treating with chemical solvents. Wiley, New York.

Austgen D., 1989. A model of vapor-liquid equilibria for acid gas-alkanolamine-water systems. PhD Thesis at the University of Texas at Austin, USA.

Austgen D., Rochelle G., Peng X., Chen C.-C., 1989. Model of vapor-liquid equilibria for aqueous acid gas-alkanolamine systems using the electrolyte-NRTL equation. *Ind. Eng. Chem. Res.* 28, 1060-1073.

Bailey D., Feron P., 2005. Post-combustion decarbonisation processes. *Oil & Gas Science and Technology* 60 (3), 461-474.

Barchas R., Davis R., 1992. The Kerr-McGee/ABB Lummus Crest Technology for the recovery of CO<sub>2</sub> from stack gases. *Energy Conversion Management*, 33 (5-8), 333-340.

Barker D., Turner S., Napier-Moore P., Clark M., Davison J., 2009. CO<sub>2</sub> Capture in the cement industry. *Energy Procedia* 1, 87-94.

Bascougnano M., 2012. Développement d'une méthode analytique pour l'étude de la dégradation de la 2-éthanolamine dans le cadre d'un procédé de capture de CO<sub>2</sub>. Internship report. University of Liège, Belgium.

Bedell S., 2009. Oxidative degradation mechanisms for amine in flue gas capture. *Energy Procedia* 1, 771-778.

Bedell S., 2011. Amine autoxidation in flue gas CO<sub>2</sub> capture – Mechanistic lessons learned from other gas treating processes. *International Journal of Greenhouse Gas Control* 5, 1-6.

Bello A., Idem R., 2005. Pathways for the formation of products of the oxidative degradation of CO<sub>2</sub>-loaded concentrated aqueous monoethanolamine solutions during CO<sub>2</sub> absorption from flue gases. *Ind. Eng. Chem. Res.* 44, 945-969.

Bello A., Idem R., 2006. Comprehensive study of the kinetics of the oxidative degradation of CO<sub>2</sub> loaded and concentrated aqueous monoethanolamine (MEA) with and without sodium metavanadate during CO<sub>2</sub> absorption from flue gases. *Ind. Eng. Chem. Res.* 45, 2569-2579.

Bellona, 2007. Factsheet : CO<sub>2</sub> capture. The Bellona Foundation. [www.bellona.org](http://www.bellona.org), accessed in March 2013.

Bellona, 2013. CO<sub>2</sub> capture. Bellona environmental CCS team. [www.bellona.org](http://www.bellona.org), accessed in March 2013.

Benson H., McCrea D., 1979. Removal of acid gases from hot gas mixtures. US Patent 4160810.

Billet R., Schultes M., 1993. Predicting mass transfer in packed columns. *Chemical Engineering and Technology* 16, 1-9.

Billet R., Schultes M., 1999. Prediction of mass transfer columns with dumped and arranged packings. Updated summary of the calculation method of Billet and Schultes. *Chem. Eng. Res. Des.* 77, 498-504.

Blachly C., Ravner H., 1965a. The stabilization of monoethanolamine solutions for submarine carbon dioxide scrubbers. Report 6189, U.S. Naval Research Laboratory.

Blachly C., Ravner H., 1965b. Studies of submarine carbon dioxide scrubber operation: effect of an additive package for the stabilization of monoethanolamine solutions. Report 1598, U.S. Naval Research Laboratory.

Bollas G., Chen C.-C., Barton P., 2008. Refined electrolyte-NRTL model: activity coefficient expressions for application to multi-electrolyte systems. *AIChE Journal* 54 (6), 1608-1624.

Bosoaga A., Masek O., Oakey J., 2009. CO<sub>2</sub> capture technologies for cement industry. *Energy Procedia* 1, 133-140.

- Bravo J., Fair J., 1982. Generalized correlation for mass transfer in packed distillation columns. *Ind. Eng. Chem. Process Des. Dev.* 21, 162-170.
- Bravo J., Rocha J., Fair J., 1985. Mass-transfer in Gauze packings. *Hydrocarbon Process* 64, 91-95.
- Bravo J., Rocha J., Fair J., 1992. A comprehensive model for the performance of columns containing structured packings. *ICHEME. Symp. Ser.* 128, A439.
- Brüder P., Svendsen H., 2012. Capacity and kinetics of solvents for post-combustion CO<sub>2</sub> Capture. *Energy Procedia* 23, 45-54.
- Captech, 2007. Advanced solvents: openbaareindrapport Captech jaar 1 (2006-2007). [www.co2-captech.nl](http://www.co2-captech.nl), accessed in January 2010.
- Carrette P.-L., Delfort B., 2009a. Absorbing solution containing a sulphurated organic degradation inhibitor and method for limiting the degradation of an absorbent solution. International Patent WO2009/156622 A1.
- Carrette P.-L., Delfort B., 2009b. Absorbing solution containing a degradation sulphur-containing inhibitor having a carboxyl group and method for limiting the degradation of an absorbent solution. International Patent WO2009/156621 A1.
- Carrette P.-L., Delfort B., 2009c. Absorbing solution containing a thiadiazole-derived degradation inhibitor and method for limiting the degradation of an absorbing solution. International Patent WO2009/156619 A2.
- Carrette P.-L., Delfort B., 2010. Absorbing solution containing a sulphur-containing degradation inhibitor derived from an amino-acid and method for limiting the degradation of an absorbent solution. International Patent WO2010/004119 A1.
- Carrette P.-L., Delfort B., 2011. Absorbing solution containing a degradation inhibitor derived from a triazole or from a tetrazole and process for the absorption of acid compounds contained in a gaseous effluent. International Patent WO2011/012777 A1.
- Cato, 2012. Dutch national research and development program for CO<sub>2</sub> capture, transport and storage. [www.co2-cato.org](http://www.co2-cato.org), accessed in February 2012.
- Cesar, 2012. CO<sub>2</sub> enhanced separation and recovery. Project co-founded by the 7<sup>th</sup> framework program of the European Commission. [www.co2cesar.eu](http://www.co2cesar.eu), accessed in February 2012.
- Chakma A., 1997. CO<sub>2</sub> capture processes – Opportunities for improved energy efficiencies. *Energy Conversion Management* 38, 51-56.
- Challis B., Challis J., 1982. N-nitrosamines and N-nitrosimines. In: Patai, S., ed., *The chemistry of amino, nitroso and nitro compounds and their derivatives*, Wiley, New York, 1151-1223.

- Chanchev A., Saiwan C., Supap T., Idem R., Tontiwachwuthikul P., 2011. Off-gas emission in CO<sub>2</sub> capture process using aqueous monoethanolamine solution. *Energy Procedia* 4, 504-511.
- Chapel D., Mariz C., Ernest J., 1999. Recovery of CO<sub>2</sub> from flue gases: commercial trends. Presentation at the Canadian Society of Chemical Engineers annual meeting, Saskatchewan, Canada.
- Chen C.-C., Britt H., Boston J., Evans L., 1982. Local compositions model for excess Gibbs energy of electrolyte systems: Part I: Single solvent, single completely dissociated electrolyte systems. *AIChE Journal* 28 (4), 588-596.
- Chen C.-C., Evans L., 1986. A local composition model for the excess Gibbs energy of aqueous electrolyte systems. *AIChE Journal* 32 (3), 444-454.
- Chen C.-C., 2006. Toward development of activity coefficient models for process and product design of complex chemical systems. *Fluid Phase Equilibria* 241, 103-112.
- Chi S., Rochelle G., 2001. Oxidative degradation of monoethanolamine. Master Thesis at the University of Texas at Austin, USA.
- Chi S., Rochelle G., 2002. Oxidative degradation of monoethanolamine. *Ind. Eng. Chem. Res.* 41, 4178-4186.
- Ciferno J., Di Pietro P., Tarka T., 2005. An economic scoping study for CO<sub>2</sub> capture using aqueous ammonia. Final Report - DOE/NETL.
- CO<sub>2</sub> capture project, 2008. Three basic methods to separate gases. [www.co2captureproject.org/pdfs/3\\_basic\\_methods\\_gas\\_separation.pdf](http://www.co2captureproject.org/pdfs/3_basic_methods_gas_separation.pdf), accessed in April 2013.
- CO<sub>2</sub> capture project, 2013. CO<sub>2</sub> Storage: operation - injecting CO<sub>2</sub> underground [www.co2captureproject.org/operation.html](http://www.co2captureproject.org/operation.html), accessed in April 2013.
- Cook P., 2009. Demonstration and deployment of carbon dioxide capture and storage in Australia. *Energy Procedia* 1, 3859-3866.
- Cooper C. on behalf of the CO<sub>2</sub> capture project, 2009. A technical basis for carbon dioxide storage. *Energy Procedia* 1, 1727-1733.
- Cousins A., Wardhaugh L., Feron P., 2011. Preliminary analysis of process flow sheet modifications for energy efficient CO<sub>2</sub> capture from flue gases using chemical absorption. *Chemical Engineering Research and Design* 89, 1237-1251.
- CSLF, 2011. In focus: what is carbon utilization. Carbon sequestration leadership forum. [www.cslforum.org](http://www.cslforum.org), accessed in April 2013.
- Cummings A., Smith G., Nelsen D., 2007. Advances in amine reclaiming - Why there's no excuse to operate a dirty amine system. Proceedings of the Laurance Reid gas conditioning conference, 227-244.



- Danckwerts A., 1951. Significance of liquid film coefficient in gas absorption. *Ind. Eng. Chem.* 43, 1460-1467.
- Danckwerts P., 1979. The reaction of CO<sub>2</sub> with ethanolamines. *Chem. Eng. Sci.* 34 (4), 443-446.
- Davis J., 2009. Thermal degradation of aqueous amines used for carbon dioxide capture. PhD Thesis at the University of Texas at Austin, USA.
- Davis J., Rochelle G., 2009. Thermal degradation of monoethanolamine at stripper conditions. *Energy Procedia* 1, 327-333.
- de Koeijer G., Enge Y., Sanden K., Graff O., Falk-Pedersenc O., Amundsen T., Overå S., 2011. CO<sub>2</sub> Technology Centre Mongstad – Design, functionality and emissions of the amine plant. *Energy Procedia* 4, 1207-1213.
- Delfort B., Carrette P.-L., 2009a. Absorbent solution containing a degradation inhibitor having a thiocarbonyl functional group and method for limiting the degradation of an absorbent solution. International Patent WO2009/156618 A1.
- Delfort B., Carrette P.-L., 2009b. Absorbent solution containing a degradation inhibitor of the family of dithiophosphates and method for limiting the degradation of an absorbent solution. International Patent WO2010/004118 A1.
- Delfort B., Carrette P.-L., Bonnard L., 2011. MEA 40% with improved oxidative stability for CO<sub>2</sub> capture in post-combustion. *Energy Procedia* 4, 9-14.
- Deshmukh R., Mather A., 1981. A mathematical model for equilibrium solubility of hydrogen sulfide and carbon dioxide in aqueous alkanolamine solutions. *Chemical Engineering Science* 36, 355-362.
- Dow, 2003. Material safety data sheet for ethanolamines. [http://msdssearch.dow.com/PublishedLiteratureDOWCOM/dh\\_017d/0901b8038017d302.pdf](http://msdssearch.dow.com/PublishedLiteratureDOWCOM/dh_017d/0901b8038017d302.pdf), accessed in April 2013.
- Dubois L., 2013. Etude de la capture du CO<sub>2</sub> en postcombustion par absorption dans des solvants aminés : application aux fumées issues de cimenteries. PhD thesis at the University of Mons, Belgium.
- Dugas R., Alix P., Lemaire E., Broutin P., Rochelle G., 2009. Absorber model for CO<sub>2</sub> capture by monoethanolamine – application to CASTOR pilot results. *Energy Procedia* 1, 103-107.
- Eide-Haugmo I., Lepaumier H., Einbu A., Vernstad K., Falck da Silva E., Svendsen H., 2011. Chemical stability and biodegradability of new solvents for CO<sub>2</sub> capture. *Energy Procedia* 4, 1631-1636.

- Endo T., Kajiya Y., Nagayasu H., Iijima M., Ohishi T., Tanaka H., Mitchell R., 2011. Current status of MHI's CO<sub>2</sub> recovery technology and optimization of CO<sub>2</sub> recovery plant with a PC fired power plant. *Energy Procedia* 4, 1513-1519.
- Engebo A., Ahmed N., Rose E., Helle K., Hage L., 2012. Report activity 5: CO<sub>2</sub> transport. Det Norske Veritas, Report No 2012-0076 for Gassnova SF.
- Epp B., Fahlenkamp H., Vogt M., 2011. Degradation of solutions of monoethanolamine, diglycolamine and potassium glycinate in view of tail-end CO<sub>2</sub> absorption. *Energy Procedia* 4, 75-80.
- Faramarzi L., Kontogeorgis G., Michelsen M., Thosen K., Stenby E., 2010. Absorber model for CO<sub>2</sub> capture by monoethanolamine. *Ind. Eng. Chem. Res.* 49, 3751-3759.
- Faucher J., 1989. Process for inhibiting mono and diethanolamine degradation. US Patent 4840777.
- Figueroa J., Fout T., Plasynski S., McIlvried H., Srivastava R., 2008. Advances in CO<sub>2</sub> capture technology – The U.S. Department of Energy's Carbon Sequestration Program. *International Journal of Greenhouse Gas Control* 2, 9-20.
- Fluxys, 2013. Stockage de gas naturel: le site de Loenhout. [www.fluxys.be](http://www.fluxys.be) accessed in February 2013.
- Fostås B., Gangstad A., Nenseter B., Pedersen S., Sjøvoll M., Sorensen A., 2011. Effects of NO<sub>x</sub> in the flue gas degradation of MEA. *Energy Procedia* 4, 1566-1573.
- Fouad W., Berrouk A., Peters C., 2012. Improved Kent-Eisenberg models for predicting H<sub>2</sub>S and CO<sub>2</sub> solubilities in aqueous TEA solutions. *Proceedings of the 3<sup>rd</sup> International Gas Processing Symposium*, Qatar.
- Freguia S., Rochelle G., 2003. Modeling of CO<sub>2</sub> capture by aqueous monoethanolamine. *AIChE Journal* 49 (7), 1676-1686.
- Fürst W., Renon H., 1993. Representation of excess properties of electrolyte solutions using a new equation of state. *AIChE Journal* 39 (2), 335-343.
- Gabrielsen J., Michelsen M., Stenby E., Kontogeorgis G., 2005. A model for estimating CO<sub>2</sub> solubility in aqueous alkanolamines. *Ind. Eng. Chem. Res.* 44, 3348-3354.
- Gaspar J., Cormos A-M., 2012. Dynamic modeling and absorption capacity assessment of CO<sub>2</sub> capture process. *International Journal of Greenhouse Gas Control* 8, 45-55.
- Goff G., Rochelle G., 2003. Oxidative degradation of aqueous monoethanolamine in CO<sub>2</sub> capture systems under absorber conditions. *Greenhouse Gas Control Technologies* 1, 115-120.
- Goff G., Rochelle G., 2004. Monoethanolamine degradation: O<sub>2</sub> mass transfer effects under CO<sub>2</sub> capture conditions. *Ind. Eng. Chem. Res.* 43, 6400-6408.

- Goff G., 2005. Oxidative degradation of aqueous MEA in CO<sub>2</sub>-capture processes: iron and copper catalysis, inhibition and O<sub>2</sub> mass transfer. PhD Thesis at the University of Texas at Austin, USA.
- Goff G., Rochelle G., 2006. Oxidation inhibitors for copper and iron catalyzed degradation of monoethanolamine in CO<sub>2</sub> capture processes. *Ind. Eng. Chem. Res.* 45, 2513-2521.
- Gross J., Sadowski G., 2001. Perturbed-Chain SAFT: an equation of state based on a perturbation theory for chain molecules. *Ind. Eng. Chem. Res.* 40, 1244-1260.
- Guggenheim E., 1935. The specific thermodynamic properties of aqueous solutions of strong electrolytes. *Phil. Mag.* 19, 588-643.
- Harun N., Douglas P., Ricardez-Sandoval L., Croiset E., 2011. Dynamic simulation of MEA absorption processes for CO<sub>2</sub> capture from fossil fuel power plant. *Energy Procedia* 4, 1478-1485.
- Heldebrant D., Yonker C., Jessop P., Phan L., 2009. CO<sub>2</sub>-binding organic liquids (CO<sub>2</sub>BOLs) for post-combustion CO<sub>2</sub> Capture. *Energy Procedia* 1, 1187-1195.
- Hessen E., Haug-Warberg T., Svendsen H., 2010. The refined e-NRTL model applied to CO<sub>2</sub>-H<sub>2</sub>O-alkanolamine systems. *Chemical Engineering Science* 65, 3638-3648.
- Higbie R., 1935. The rate of absorption of a pure gas into a still liquid during short periods of exposure. *Trans. Am. Inst. Chem. Eng.* 31, 365-389.
- Hikita H., Asai S., Ishikawa H., Honda M., 1977. The kinetics of reactions of carbon dioxide with monoethanolamine, diethanolamine, and triethanolamine by a rapid mixing method. *Chemical Engineering Journal* 13 (1), 7-12.
- Hoff K., Juliussen O., Falk-Pedersen O., Svendsen H., 2004. Modeling and experimental study of carbon dioxide absorption in aqueous alkanolamine solutions using a membrane contactor. *Ind. Eng. Chem. Res.* 43, 4908-4921.
- Huizeling E., van der Weijde G., 2011. ROAD Maasvlakte CCS Project C.V., Non-confidential FEED study report – Special report for the Global Carbon Capture and Storage Institute. [www.globalccsinstitute.com](http://www.globalccsinstitute.com), accessed in February 2013.
- Idem R., Wilson M., Tontiwachwuthikul P., Chakma A., Veawab A., Aroonwilas A., Gelowitz D., 2006. Pilot plant studies of the CO<sub>2</sub> capture performance of aqueous MEA and mixed MEA/MDEA solvents at the University of Regina CO<sub>2</sub> Capture Technology Development Plant and the Boundary Dam CO<sub>2</sub> Capture Demonstration Plant. *Ind. Eng. Chem. Res.* 45, 2414-2420.
- IEA, 2008. CO<sub>2</sub> capture and storage: a key carbon abatement option. International Energy Agency, 2008.
- IEO, 2011. International energy outlook 2011. US Energy Information Administration. [www.eia.gov/forecasts/ieo](http://www.eia.gov/forecasts/ieo), accessed in 2012.

IPCC, 2005. IPCC special report on carbon dioxide capture and storage. Prepared by working group III of the Intergovernmental Panel on Climate Change. Cambridge university press, Cambridge, NY, USA.

Jamal A., Meisen A., Lim C., 2006. Kinetics of carbon dioxide absorption and desorption in aqueous alkanolamine solutions using a novel hemispherical contactor – I. Experimental apparatus and mathematical modeling. *Chemical Engineering Science* 61, 6571-6589.

Jassim M., Rochelle G., 2006. Innovative absorber/stripper configurations for CO<sub>2</sub> capture by aqueous monoethanolamine. *Ind. Eng. Chem. Res.* 45, 2465-2472.

Jockenhövel T., Schneider R., Rode H., 2009a. Development of an economic post-combustion carbon capture process. *Energy Procedia* 1, 1043-1050.

Jockenhövel T., Schneider R., Sandell M., Schlüter L., 2009b. Optimal power plant integration of post-combustion CO<sub>2</sub> capture. POWER-GEN Europe 2009, Cologne, Germany.

Johnson W., McElwain R., 1964. Stabilization of aqueous alkanolamines solutions in gas treating processes. US Patent 3137654.

Jou F., Mather A., Otto F., 1982. Solubility of hydrogen sulfide and carbon dioxide in aqueous methyldiethanolamine solutions. *Ind. Eng. Chem. Process Des. Dev.* 21 (4), 539-544.

Jou F., Carroll J., Mather A., Otto F., 1993a. Solubility of mixtures of hydrogen sulfide and carbon dioxide in aqueous N-methyldiethanolamine solutions. *J. Chem. Eng. Data* 38 (1), 75-77.

Jou F., Carroll J., Mather A., Otto F., 1993b. The solubility of carbon dioxide and hydrogen sulfide in a 35 wt% aqueous solution of methyldiethanolamine. *The Canadian Journal of Chemical Engineering* 71 (2), 264-268.

Kale C., Tönnies I., Hasse H., Górak A., 2011. Simulation of reactive absorption: model validation for CO<sub>2</sub>-MEA system. *Computer Aided Chemical Engineering* 29, 61-65.

Kaminski M., Jastrzebski D., Przyjazny A., Kartanowicz R., 2002. Determination of the amount of wash amines and ammonium ion in desulfurization products of process gases and results of related studies. *J. Chromatogr. A* 947, 217-225.

Karimi M., Hillestad M., Svendsen H., 2011a. Investigation of intercooling effect in CO<sub>2</sub> capture energy consumption. *Energy Procedia* 4, 1601-1607.

Karimi M., Hillestad M., Svendsen H., 2011b. Capital costs and energy considerations of different alternative stripper configurations for post combustion CO<sub>2</sub> capture. *Chemical Engineering Research and Design* 89, 1229-1236.

Karimi M., Hillestad M., Svendsen H., 2012. Investigation of the dynamic behavior of different stripper configurations for post-combustion CO<sub>2</sub> capture. *International Journal of Greenhouse Gas Control* 7, 230-239.

- Kenig E., Schneider R., Górak A., 2001. Reactive absorption: optimal process design via optimal modelling. *Chemical engineering science* 56, 343-350.
- Kent R., Eisenberg B, 1976. Better data for amine treating. *Hydrocarbon Processing* 55 (2), 87-90.
- Knudsen J., Jensen J., Vilhelmsen P., Biede O., 2007. First year operation experience with a 1 t/h CO<sub>2</sub> absorption pilot plant at Esbjerg coal-fired power plant. *Proceedings of the European Congress of Chemical Engineering (ECCE-6)*, Copenhagen, Denmark.
- Knudsen J., Vilhelmsen P., Jensen J., Biede O., 2009. Experience with CO<sub>2</sub> capture from coal flue gas in pilot scale. *Energy Procedia* 1, 783-790.
- Knudsen J., Andersen J., Jensen J., Biede O., 2011. Evaluation of process upgrades and novel solvents for the post combustion CO<sub>2</sub> capture process in pilot-scale. *Energy Procedia* 4, 1558-1565.
- Krishna R., Standart G., 1976. A multicomponent film model incorporating a general matrix method of solution to the Maxwell-Stefan equations. *AIChE Journal* 22 (2), 383-389.
- Kucka L., Richter J., Kenig E., Górak A., 2003. Determination of gas-liquid reaction kinetics with a stirred cell reactor. *Sep. Purif. Technol.* 31, 163-175.
- Kumar A., 1982. Kinetics of complexation and oxidation of ethanolamine and diols by silver (II). *J. Phys. Chem.* 86, 1674-1678.
- Kvamsdal H., Jakobsen J., Hoff K., 2009. Dynamic modeling and simulation of a CO<sub>2</sub> absorber column for post-combustion CO<sub>2</sub> capture. *Chemical Engineering and Processing* 48, 135-144.
- Kvamsdal H., Hetland J., Haugen G., Svendsen H., Major F., Kårstad V., Tjellander G., 2010. Maintaining a neutral water balance in a 450MWe NGCC-CCS power system with post-combustion carbon dioxide capture aimed at offshore operation. *International Journal of Greenhouse Gas Control* 4, 613-622.
- Kvamsdal H., Haugen G., Svendsen H., 2011a. Flue-gas cooling in post-combustion capture plants. *Chemical Engineering Research and Design* 89, 1544-1552.
- Kvamsdal H., Haugen G., Svendsen H., Tobiesen A., Mangalapally H., Hartono A., Mejdell T., 2011b. Modelling and simulation of the Esbjerg Pilot Plant using the Cesar 1 solvent. *Energy Procedia* 4, 1644-1651.
- Laborelec, 2009. Discussions with the industrial partner. Sustainable Process Technologies group.
- Lam M., Lee K., Mohamed A., 2012. Current status and challenges on microalgae-based carbon capture. *International Journal of Greenhouse Gas Control* 10, 456-469.

Lawal A., Idem R., 2005. Effects of operating variables on the product distribution and reaction pathways in the oxidative degradation of CO<sub>2</sub>-loaded aqueous MEA-MDEA blends during CO<sub>2</sub> absorption from flue gas streams. *Ind. Eng. Chem. Res.* 44, 986-1003.

Lawal A., Bello A., Idem R., 2005. The role of methyl diethanolamine (MDEA) in preventing the oxidative degradation of CO<sub>2</sub> loaded and concentrated aqueous monoethanolamine (MEA)-MDEA blends during CO<sub>2</sub> absorption from flue gases. *Ind. Eng. Chem. Res.* 44, 1874-1896.

Lawal A., Idem R., 2006. Kinetics of the oxidative degradation of CO<sub>2</sub> loaded and concentrated aqueous MEA-MDEA blends during CO<sub>2</sub> absorption from flue gas streams. *Ind. Eng. Chem. Res.* 45, 2601-2607.

Lawal A., Wang M., Stephenson P., 2011. Investigating the dynamic response of CO<sub>2</sub> chemical absorption process in enhanced-O<sub>2</sub> coal power plant with post-combustion CO<sub>2</sub> capture. *Energy Procedia* 4, 1035-1042.

Lemaire E., Bouillon P.A., Gomez A. Kittel J., Gonzales S., Carrette P.-L., Delfort B., Ougin P., Alix P., Normand L., 2011. New IFP optimized first generation process for post-combustion CO<sub>2</sub> capture: HiCapt+<sup>TM</sup>. *Energy Procedia* 4, 1361-1368.

Lemoine R., Fillion B., Behkish A., Smith A., Morsi B., 2003. Prediction of the gas-liquid volumetric mass transfer coefficients in surface-aeration and gas-inducing reactors using neural networks. *Chemical Engineering and Processing* 42, 621-643.

Léonard G., 2009. Modeling of a pilot plant for the CO<sub>2</sub>-reactive absorption in amine solvents for power plant flue gases. Diploma thesis at the University of Liège, Belgium.

Léonard G., Heyen G., 2011a. Modeling post-combustion CO<sub>2</sub> capture with amine solvents. *Computer Aided Chemical Engineering* 29, 1768-1772.

Léonard G., Heyen G., 2011b. Optimisation du procédé de captage de CO<sub>2</sub> dans des solvants aminés. *Récents Progrès en Génie des Procédés*, 101.

Léonard G., Mogador Cabeza B., Belletante S., Heyen G., 2013. Dynamic modeling and control of a pilot plant for post-combustion capture. *Computer Aided Chemical Engineering* 32, 451-456.

Lepaumier H., 2008. Etude des mécanismes de dégradation des amines utilisées pour le captage du CO<sub>2</sub> dans les fumées. PhD thesis at the University of Savoie, France.

Lepaumier H., Picq D., Carrette P., 2009a. Degradation study of new solvents for CO<sub>2</sub> capture in post combustion. *Energy Procedia* 1, 893-900.

Lepaumier H., Picq D., Carrette P., 2009b. New amines for CO<sub>2</sub> capture. I. Mechanisms of amine degradation in the presence of CO<sub>2</sub>. *Ind. Eng. Chem. Res.* 48, 9061-9067.

Lepaumier H., Picq D., Carrette P., 2009c. New amines for CO<sub>2</sub> capture. II. Oxidative degradation mechanisms. *Ind. Eng. Chem. Res.* 48, 9068-9075.

- Lepaumier H., da Silva E., Einbu A., Grimstvedt A., Knudsen J., Vernstad K., Zahlse K., Svendsen H., 2010. Comparison of MEA degradation in pilot-scale and lab-scale experiments. Presentation at the 10<sup>th</sup> international conference on greenhouse gas technologies conference, Amsterdam, The Netherlands.
- Lepaumier H., da Silva E., Einbu A., Grimstvedt A., Knudsen J., Zahlse K., Svendsen H., 2011. Comparison of MEA degradation in pilot-scale with lab-scale experiments. *Energy Procedia* 4, 1652-1659.
- Lepaumier H., 2011. Informal discussion. Laborelec, Sustainable Process Technologies group.
- Lin Y-J., Wong D., Jang S-S., 2011. Control strategies for flexible operation of power plant with CO<sub>2</sub> capture plant. *AIChE Journal* 58 (9), 2697-2704.
- Luo X., Knudsen J., de Montigny D., Sanpasertparnich T., Idem R., Gelowitz D., Notz R., Hoch S., Hasse H., Lemaire E., Alix P., Tobiesen A., Juliussen O., Köpcke M., Svendsen H., 2009. Comparison and validation of simulation codes against sixteen sets of data from four different pilot plants. *Energy Procedia* 1, 1249-1256.
- Majer V., Sedlbauer J., Bergin G., 2008. Henry's law constant and related coefficients for aqueous hydrocarbons, CO<sub>2</sub> and H<sub>2</sub>S over a wide range of temperature and pressure. *Fluid Phase Equilibria* 272, 65-74.
- McCalley D., 2007. Is hydrophilic interaction chromatography with silica columns a viable alternative to reversed-phase liquid chromatography for the analysis of ionisable compounds? *Journal of Chromatography A* 1171, 46-55.
- McCullough J., Faucher J., Kubek D., Barr K., 1990. Alkanolamine gas treating composition and process. US Patent 4971718.
- McGlashan N., 2010. The thermodynamics of chemical looping combustion applied to the hydrogen economy. *International Journal of Hydrogen Energy* 35, 6465-6474.
- Mejdell T., Vassbotn T., Juliussen O., Tobiesen A., Einbu A., Knuutila H., Hoff K., Andersson V., Svendsen H., 2011. Novel full height pilot plant for solvent development and model validation. *Energy Procedia* 4, 1753-1760.
- Meldon J., Morales-Cabrera M., 2011. Analysis of carbon dioxide absorption in and stripping from aqueous monoethanolamine. *Chemical Engineering Journal* 171, 753-759.
- Meng L., 2004. Development of an analytical method for distinguishing ammonium bicarbonate from the products of an aqueous ammonia CO<sub>2</sub> scrubber and the characterization of ammonium bicarbonate. Master Thesis at the Western Kentucky University.
- Mertens J., Knudsen J., Thielens M.-L., Andersen J., 2012. On-line monitoring and controlling emissions in amine post combustion carbon capture: a field test. *International Journal of Greenhouse Gas Control* 6, 2-11.

- Mertens J., Lepaumier H., Desagher D., Thielens M.-L., 2013. Understanding ethanolamine (MEA) and ammonia emissions from amine based post combustion carbon capture: Lessons learned from field tests. *International Journal of Greenhouse Gas Control* 13, 72-77.
- MHI, 2012. World's First Integrated CCS of Coal-fired Power Plant Emissions Begins 500 tons/day Joint Demonstration Project with Southern Company. Press Information, Mitsubishi Heavy Industries. [www.mhi.co.jp/en/news/story/1209141573.html](http://www.mhi.co.jp/en/news/story/1209141573.html), accessed in April 2013.
- Mimura T., Shimojo S., Suda T., Iijima M., Mitsuoka S., 1995. Research and development on energy saving technology for flue gas carbon dioxide recovery and steam system in power plant. *Energy Conversion Management* 36 (6-9), 397-400.
- Moser P., Schmidt S., Sieder G., Garcia H., Stoffregen T., Stamatov V., 2011a. The post-combustion capture pilot plant Niederaussem – Results of the first half of the testing programme. *Energy Procedia* 4, 1310-1316.
- Moser P., Schmidt S., Stahl K., 2011b. Investigation of trace elements in the inlet and outlet streams of a MEA-based post-combustion capture process – Results from the test programme at the Niederaussem pilot plant. *Energy Procedia* 4, 473-479.
- Moser P., Schmidt S., Sieder G., Garcia H., Stoffregen T., 2011c. Performance of MEA in a long-term test at the post-combustion capture pilot plant in Niederaussem. *International Journal of Greenhouse Gas Control* 5, 620-627.
- NETL, 2013. CO<sub>2</sub> Utilization focus area. US National Energy Technology Laboratory, Department of Energy. [www.netl.doe.gov/technologies/carbon\\_seq/corerd/co2utilization.html](http://www.netl.doe.gov/technologies/carbon_seq/corerd/co2utilization.html) accessed in April 2013.
- Nguyen T., Hilliard M., Rochelle G., 2010. Amine volatility in CO<sub>2</sub> capture. *International Journal of Greenhouse Gas Control* 4, 707-715.
- Notz R., Asprien N., Clausen I., Hasse H., 2007. Selection and pilot plant tests of new absorbents for post-combustion carbon dioxide capture. *Chem. Eng. Res. Des.* 85, 510-515.
- Notz R., 2009. CO<sub>2</sub>-Abtrennung aus Kraftwerksabgasen mittels Reaktivabsorption. PhD Thesis at the University of Stuttgart, Germany.
- Øi L., 2007. Aspen HYSYS Simulation of CO<sub>2</sub> Removal by Amine Absorption from a Gas Based Power Plant. Proceedings of the SIMS2007 Conference, Göteborg, Sweden.
- Øi L., 2012. Removal of CO<sub>2</sub> from exhaust gas. PhD thesis at the Telemark University College, Norway.
- Olujic Z., 1999. Effect of column diameter on pressure drop of a corrugated sheet structured packing. *Chemical Engineering Research and Design* 77, 505-510.
- Onda K., Takeuchi H., Okumoto Y., 1968. Mass transfer coefficients between gas and liquid phases in packed columns. *J. Chem. Eng. Jpn.* 1, 56-62.



- Oyenekan B., Rochelle G., 2007. Alternative stripper configurations for CO<sub>2</sub> capture by aqueous amines. *AIChE Journal* 53 (12), 3144-3154.
- Panahi M., Skogestad S., 2011. Economically efficient operation of CO<sub>2</sub> capturing process. Part II. Design of control layer. *Chemical Engineering and Processing* 52, 112-124.
- Peng D., Robinson D., 1976. A new two-constant equation-of-state. *Ind. Eng. Chem. Fundam.* 15, 59-64.
- Piessens K., Baele J.-M., De Weireld G., Dreesen R., Dusar M., Laenen B., Mathieu P., Swennen R., 2010. CO<sub>2</sub> Capture and Storage: Inevitable for a climate friendly Belgium. Royal Belgian Academy Council of Applied Science (BACAS).
- Pinsent B., Pearson L., Roughton F., 1956. The kinetics of combination of carbon dioxide with hydroxide ions. *Transactions of the Faraday Society* 52, 1512-1520.
- Pitzer K., 1973. Thermodynamics of electrolytes. I. Theoretical basis and general equations. *Journal of Physical Chemistry* 77 (2), 268-277.
- Plaza J., Van Wagener D., Rochelle G., 2009. Modeling CO<sub>2</sub> capture with aqueous monoethanolamine. *Energy Procedia* 1, 1171-1178.
- Plaza J., Van Wagener D., Rochelle G., 2010. Modeling CO<sub>2</sub> capture with aqueous monoethanolamine. *International Journal of Greenhouse Gas Control* 4, 161-166.
- Pröll K., Tummescheit H., Velut S., Åkesson J., 2011. Dynamic model of a post-combustion absorption unit for use in a non-linear model predictive control scheme. *Energy Procedia* 4, 2620-2627.
- Raynal L., Royon-Lebeaud A., 2007. A multi-scale approach for CFD calculations of gas-liquid flow within large size column equipped with structured packing. *Chemical Engineering Science* 62, 7196-7204.
- Raynal L., Ben Rayana F., Royon-Lebeaud A., 2009. Use of CFD for CO<sub>2</sub> absorbers optimum design : from local scale to large industrial scale. *Energy Procedia* 1, 917-924.
- Raynal L., Alix P., Bouillon P.-A., Gomez A., le Febvre de Nailly M., Jacquin M., Kittel J., di Lella A., Mougin P., Trapy J., 2011. The DMX™ process: an original solution for lowering the cost of post-combustion carbon capture. *Energy Procedia* 4, 779-786.
- Razi N., Bolland O., Svendsen H., 2012. Review of design correlations for CO<sub>2</sub> absorption into MEA using structured packings. *International Journal of Greenhouse Gas Control* 9, 193-219.
- Redlich O., Kwong J., 1949. On the thermodynamics of solutions. V. An equation of state. Fugacities of gaseous solutions. *Chemical Reviews* 44 (1), 233-244.
- Rehfeldt S., Stichlmair J., 2006. Wärme- und Stoffübertragung. Teil II: Stoffübertragung. Lecture script, winter semester 2006-2007. Technical University of Munich, Germany.

- Rehfeldt S., Stichlmair J., 2007. Measurement and calculation of multicomponent diffusion coefficients in liquids. *Fluid Phase Equilibria* 256, 99-104.
- Renon H., Prausnitz J., 1968. Local compositions in thermodynamic excess functions for liquid mixtures. *AIChE Journal* 14 (1), 135-144.
- Renon H., 1996. Models for excess properties of electrolyte solutions: molecular bases and classification, needs and trends for new developments. *Fluid Phase Equilibria* 116, 217-224.
- Rochelle G., Seibert F., Cullinane T., Jones T., 2003. CO<sub>2</sub> Capture by absorption with potassium carbonate. Quarterly progress report, DOE Award #: DE-FC26-02NT41440.
- Rochelle G., Chen E., Freeman S., Van Wagener D., Xu Q., Voice A., 2011. Aqueous piperazine as the new standard for CO<sub>2</sub> capture technology. *Chemical Engineering Journal* 171, 725-733.
- Rooney P., Daniel D., 1998. Oxygen solubility in various alkanolamine/water mixtures. *Petroleum Technology Quarterly* 3 (1), 97-101.
- Rubin E., Mantripragada H., Marks A., Versteeg P., Kitchin J., 2012. The outlook for improved carbon capture technology. *Progress in Energy and Combustion Science* 38, 630-671.
- Saiwan C., Chanchey A., Supap T., Iden R., Tontiwachwuthikul P., 2013. Ammonia emission kinetics of monoethanolamine (MEA) based CO<sub>2</sub> absorption process. *International Journal of Greenhouse Gas Control* 12, 333-340.
- Sander R., 1999. Compilation of Henry's law constants for inorganic and organic species of potential importance in environmental chemistry. Air Chemistry Department, Max-Planck Institute for Chemistry. [www.henrys-law.org](http://www.henrys-law.org), accessed in April 2013.
- Seibert F., Chen E., Perry M., Briggs S., Montgomery R., Rochelle G., 2001. UT/SRP CO<sub>2</sub> Capture Pilot Plant – Operating experience and procedures. *Energy Procedia* 4, 1616-1623.
- Sexton A., Rochelle G., 2006. Oxidation products of amines in CO<sub>2</sub> capture. [www.che.utexas.edu/rochelle\\_group/Pubs/Pubs/SextonGHGT8.pdf](http://www.che.utexas.edu/rochelle_group/Pubs/Pubs/SextonGHGT8.pdf), accessed in December 2009.
- Sexton A., 2008. Amine oxidation in CO<sub>2</sub> capture processes. PhD Thesis at the University of Texas at Austin, Texas, USA.
- Sexton A., Rochelle G., 2009. Catalysts and inhibitors for oxidative degradation of monoethanolamine. *International Journal of Greenhouse Gas Control* 3, 704-711.
- Sexton A., Rochelle G., 2011. Reaction products from the oxidative degradation of monoethanolamine. *Ind. Eng. Chem. Res.* 50, 667-673.
- Shao R., Stangeland A., 2009. Amine used in CO<sub>2</sub> capture – Health and environmental impacts. Bellona report. [www.bellona.org](http://www.bellona.org), accessed in October 2011.

Sintef, 2013. CO<sub>2</sub> capture. [www.sintef.no](http://www.sintef.no), website accessed in February 2013.

Simon L., Elias Y., Puxty G., Artanto Y., Hungerbuhler K., 2011. Rate based modeling and validation of a carbon-dioxide pilot plant absorption column operating on monoethanolamine. *Chemical Engineering Research and Design* 89, 1684-1692.

Skogestad S., 2006. Tuning for smooth PID control with acceptable disturbance rejection. *Ind. Eng. Chem. Res.* 45, 7817-7822.

Singh K., 1970a. Method of stabilizing a monoethanolamine solution by adding a trialkanolamine. US Patent 3535260.

Singh K., 1970b. Ethanolamine solutions stabilized with an aldonic acid or an aldonate. US Patent 3535263.

Song Y., Chen C.-C., 2009. Symmetric electrolyte nonrandom two-liquid activity coefficient model. *Ind. Eng. Chem. Res.* 48, 7788-7797.

Sridhar N., Hill D., 2011. Carbon dioxide utilization, electrochemical conversion of CO<sub>2</sub>, opportunities and challenges. Det Norske Veritas, Position paper 07-2011.

Stanwell, 2012. Post-combustion capture pilot project: fact sheet January 2012. Stanwell Corporation Limited. [www.stanwell.com](http://www.stanwell.com), accessed in April 2013.

Stichlmair J., Bravo J., Fair J., 1989. General model for prediction of pressure drop and capacity of countercurrent gas/liquid packed columns. *Gas Separation and Purification* 3 (1), 19-28.

Strazisar B., Anderson R., White C., 2003. Degradation pathways for monoethanolamine in a CO<sub>2</sub> capture facility. *Energy Fuels* 17, 1034-1039.

Supap T., Idem R., Veawab A., Aroonwilas A., Tontiwachwuthikul P., Chakma A., Kybett B., 2001. Kinetics of the oxidative degradation of aqueous monoethanolamine in a flue gas treating unit. *Ind. Eng. Chem. Res.* 40, 3445-3450.

Supap T., Idem R., Tontiwachwuthikul P., Saiwan C., 2006. Analysis of monoethanolamine and its oxidative degradation products during CO<sub>2</sub> absorption from flue gases: a comparative study of GC-MS, HPLC-RID, and CE-DAD analytical techniques and possible optimum combinations. *Ind. Eng. Chem. Res.* 2006 (45), 2437-2451.

Supap T., Idem R., Tontiwachwuthikul P., Saiwan C., 2009. Kinetics of sulfur dioxide- and oxygen-induced degradation of aqueous monoethanolamine solution during CO<sub>2</sub> absorption from power plant flue gas streams. *International Journal of greenhouse gas control* 3, 133-142.

Supap T., Idem R., Tontiwachwuthikul P., Saiwan C., 2011a. Investigation of degradation inhibitors on CO<sub>2</sub> capture process. *Energy Procedia* 4, 583-590.

- Supap T., Idem R., Tontiwachwuthikul P., 2011b. Mechanism of formation of heat stable salts (HSSs) and their roles in further degradation of monoethanolamine during CO<sub>2</sub> capture from flue gas streams. *Energy Procedia* 4, 591-598.
- Svendsen H., Essen E., Mejdell T., 2011. Carbon dioxide capture by absorption, challenges and possibilities. *Chemical Engineering Journal* 171, 718-724.
- Taylor R., Krishna R., 1993. Multicomponent mass transfer. Wiley Series in Chemical Engineering. New York.
- TCM, 2012. Technology Centre Mongstad. Joint venture between Gassnova (on behalf of the Norwegian state), Statoil, Shell and Sasol. [www.tcnda.com](http://www.tcnda.com), accessed in February 2012.
- Thitakamol B., Veawab A., 2008. Foaming behavior in CO<sub>2</sub> absorption process using aqueous solutions of single and blended alkanolamines. *Ind. Eng. Chem. Res.* 47, 216-225.
- Thong D., Dave N., Feron P., Azzi M., 2012. Estimated emissions to the atmosphere from amine based PCC processes for a black coal fired power station based on literature and modelling. Deliverable 3.1 for Australian National Low Emissions Coal Research and Development, Environmental Impact of Amine-based CO<sub>2</sub> Post-combustion Capture (PCC) Process. CSIRO - Advanced Coal Technology Portfolio. [www.csiro.au](http://www.csiro.au), accessed in September 2012.
- Tobiesen A., Juliussen O., Svendsen H., 2007. Experimental validation of a rigorous absorber model for CO<sub>2</sub> postcombustion capture. *AIChE Journal* 53 (4), 846-865.
- Tobiesen A., Juliussen O., Svendsen H., 2008. Experimental validation of a rigorous desorber model for CO<sub>2</sub> post-combustion capture. *Chemical Engineering Science* 63, 2641-2656.
- Tobiesen A., Schumann-Olsen H., 2011. Obtaining optimum operation of CO<sub>2</sub> absorption plants. *Energy Procedia* 4, 1745-1752.
- Tönnies I., Mangalapally H., Hasse H., 2011. Sensitivity study for the rate-based simulation of the reactive absorption of CO<sub>2</sub>. *Energy Procedia* 4, 533-540.
- Tönnies I., 2011. Informal discussion. Chair for Thermodynamics, Technical University of Kaiserslautern, Germany.
- ULCOS, 2013. [www.ulcos.org](http://www.ulcos.org), accessed in April 2013.
- Uyanga I., Idem R., 2007. Studies of SO<sub>2</sub>- and O<sub>2</sub>-induced degradation of aqueous MEA during CO<sub>2</sub> capture from power plant flue gas streams. *Ind. Eng. Chem. Res.* 46, 2558-2566.
- van Elk E., Arendsen A., Versteeg G., 2009. A new flowsheeting tool for flue gas treating. *Energy Procedia* 1, 1481-1488.
- van Krevelen D., Hoftijzer P., 1948. Kinetics of gas-liquid reactions. Part I. General theory. *Rec. Trav. Chim.* 67, 563-586.

- Van Wagener D., Rochelle G., 2011. Stripper configurations for CO<sub>2</sub> capture by aqueous monoethanolamine. *Chemical Engineering Research and Design* 89, 1639-1646.
- Versteeg G., Van Swaaij W., 1988. On the kinetics between CO<sub>2</sub> and Alkanolamines both in aqueous and non-aqueous solutions – I. primary and secondary amines. *Chem. Eng. Sci.* 43 (3), 573-585.
- Vevelstad S., Eide-Haugmo I., Falck da Silva E., Svendsen H., 2011. Degradation of MEA: a theoretical study. *Energy Procedia* 4, 1608-1615.
- Voice A., Rochelle G., 2011a. Oxidation of amines at absorber conditions for CO<sub>2</sub> capture from flue gas. *Energy Procedia* 4, 171-178.
- Voice A., Rochelle G., 2011b. MEA oxidation in CO<sub>2</sub> capture, inhibitor screening with hot gas FTIR. Presentation at Luminant Carbon Management Program. UT Austin, Texas, USA.
- Voice A., Rochelle G., 2011c. Catalysts and inhibitors of monoethanolamine oxidation. Presentation at the 1st Post Combustion Capture Conference. UT Austin, Texas, USA.
- Voice A., Wei D., Rochelle G., 2012. Sequential degradation of aqueous monoethanolamine for CO<sub>2</sub> capture. *Recent advances in post-combustion CO<sub>2</sub> capture chemistry*, chapter 13, 249-263.
- Voice A., Rochelle G., 2013. Products and process variables in oxidation of monoethanolamine for CO<sub>2</sub> capture. *International Journal of Greenhouse Gas Control* 12, 472-477.
- Weiland R., Dingman J., Cronin D., Browning G., 1998. Density and viscosity of some partially carbonated aqueous alkanolamine solutions and their blends. *J. Chem. Eng. Data* 43, 378-382.
- WEO, 2012. World energy outlook 2012, executive summary. International Energy Agency. [www.worldenergyoutlook.org](http://www.worldenergyoutlook.org), accessed in February 2013.
- Withman W., 1923. A preliminary confirmation of the two film theory of gas absorption. *Chem. Met. Eng.* 29 (4), 146-148.
- Xu Q., Rochelle G., 2009. Solvent reclaiming by crystallization of potassium sulfate. *Energy Procedia* 1, 1205-1212.
- Yara, 2013. Utilization of carbon dioxide dry ice. [www.yara.com/products\\_services/industrial\\_solutions/carbon\\_dioxide\\_dry\\_ice](http://www.yara.com/products_services/industrial_solutions/carbon_dioxide_dry_ice), accessed in April 2013.
- Zemaitis J., Clark D., Rafal M., Scrivner N., 1986. Handbook of aqueous electrolyte thermodynamics. American Institute of Chemical Engineers Inc., New York.
- ZEP, 2011. The costs of CO<sub>2</sub> transport. European Technology Platform for Zero Emission Fossil Fuel Power Plants. [www.zeroemissionsplatform.eu](http://www.zeroemissionsplatform.eu), accessed in April 2013.

ZERO, 2013a. Transport of CO<sub>2</sub>. Zero Emissions Resource Organisation. [www.zeroco2.no/transport](http://www.zeroco2.no/transport), accessed in April 2013.

ZERO, 2013b. CCS projects database. Zero Emissions Resource Organisation. [www.zeroco2.no/projects](http://www.zeroco2.no/projects), accessed in April 2013.

Zhang Y., Chen H., Chen C.-C., Plaza J., Dugas R., Rochelle G., 2009. Rate-based process modeling of CO<sub>2</sub> capture with aqueous monoethanolamine solution. *Ind. Eng. Chem. Res.* 48, 9233-9246.

Zhang Y., Que H., Chen C., 2011. Thermodynamic modeling for CO<sub>2</sub> absorption in aqueous MEA solution with electrolyte NRTL model. *Fluid Phase Equilibria* 311, 67-75.

Ziaii S., Rochelle G., Edgar T., 2011. Optimum design and control of amine scrubbing in response to electricity and CO<sub>2</sub> prices. *Energy Procedia* 4, 1683-1690.

Zuo G., Hirsch A., 2008. The trial of the top gas recycling blast furnace at LKAB's EBF and scale-up. Proceedings of the 4<sup>th</sup> ULCOS seminar, Essen, Germany.

## Figure index

### Chapter I

|   |    |
|---|----|
| Figure 1.1: growth in world energy generation and total delivered energy consumption, 1990-2035 (index 1990=1) (IEO, 2011)..... | 3  |
| Figure 1.2: world net electricity generation by fuel in trillion kWh, 2008-2035 (IEO, 2011)...                                  | 4  |
| Figure 1.3: typically used alkanolamines for chemical absorption of CO <sub>2</sub> .....                                       | 6  |
| Figure 1.4: comparison between chemical and physical absorption (Bailey and Feron, 2005).                                       | 7  |
| Figure 1.5: different methods for CO <sub>2</sub> capture (IPCC, 2005) .....  | 8  |
| Figure 1.6: simplified flowsheet of the post-combustion capture (Bellona, 2007).....  | 9  |
| Figure 1.7: simplified flowsheet of the pre-combustion capture (Bellona, 2007) .....  | 9  |
| Figure 1.8: simplified flowsheet of the CO <sub>2</sub> capture by oxyfuel combustion (Bellona, 2007)                           | 10 |
| Figure 1.9: simplified flowsheet of a chemical looping process (McGlashan, 2010).....   | 11 |
| Figure 1.10: calcium looping cycle for CO <sub>2</sub> capture (Abanades et al., 2004) .....                                    | 13 |
| Figure 1.11: potential reuse routes for captured CO <sub>2</sub> (NETL, 2013).....  | 14 |
| Figure 1.12: monitoring techniques for CO <sub>2</sub> storage (CO <sub>2</sub> capture project, 2013).....                     | 16 |
| Figure 1.13: flowsheet of the chemical absorption process (Sintef, 2013).....   | 17 |
| Figure 1.14: Major contributions to the cost of avoided CO <sub>2</sub> (Abu-Zahra, 2009).....                                  | 20 |

### Chapter II

|   |    |
|---|----|
| Figure 2.1: degradation products of MEA .....   | 28 |
| Figure 2.2: oxazolidinone formation mechanism from MEA carbamate (R <sup>1</sup> =H).....   | 28 |
| Figure 2.3: imidazolidinone formation from oxazolidinone .....  | 29 |
| Figure 2.4: free radical chain reaction for MEA (Delfort et al., 2011) .....  | 30 |
| Figure 2.5: MEA degradation reactions with organic acids.....   | 30 |
| Figure 2.6: formation of HEPO.....  | 31 |
| Figure 2.7: formation of HEI (Voice et al., 2012).....  | 31 |
| Figure 2.8: comparison of GC-MS spectra: lab and pilot degraded MEA samples (Lepaumier et al., 2011).....   | 32 |
| Figure 2.9: decomposition of hydroperoxides by catalytic action of metals .....   | 37 |
| Figure 2.10: flowsheet of the degradation test rig.....   | 47 |
| Figure 2.11: cylinder for thermal degradation with CO <sub>2</sub> .....  | 49 |
| Figure 2.12: FTIR analyzer .....  | 51 |
| Figure 2.13: TG-DSC spectrum of a crystal sample .....  | 52 |
| Figure 2.14: XRD spectrum compared with different ammonium salts .....  | 53 |
| Figure 2.15: HPLC unit.....   | 54 |
| Figure 2.16: absorbance range of MEA (pure MEA diluted 1:10,000 in water) .....   | 55 |
| Figure 2.17: gas chromatograph.....   | 56 |
| Figure 2.18: GC spectrum of MEA and some degradation products .....   | 57 |
| Figure 2.19: GC calibration curve for component HEPO .....  | 59 |
| Figure 2.20: GC comparison of the base case degradation (300 g, 30 wt% CO <sub>2</sub> loaded MEA, 120°C, 4 barg, 600 rpm, 160 Nml/min gas feed, 5% O <sub>2</sub> /15% CO <sub>2</sub> /80% N <sub>2</sub> , 1 week) with pilot plant degradation..... | 63 |
| Figure 2.21: nitrogen balance of the base case experiment (300 g, 30 wt% CO <sub>2</sub> loaded MEA, no additives, 120°C, 4 barg, 600 rpm, 160 Nml/min gas feed, 5% O <sub>2</sub> /15% CO <sub>2</sub> /80% N <sub>2</sub> , 1 week) .....             | 64 |

|  |    |
|--|----|
| Figure 2.22: distribution of identified nitrogen-containing degradation products in the base case experiment (300 g, 30 wt% CO <sub>2</sub> loaded MEA, no additives, 120°C, 4 barg, 600 rpm, 160 Nml/min gas feed, 5% O <sub>2</sub> /15% CO <sub>2</sub> /80% N <sub>2</sub> , 1 week) ..... | 65 |
| Figure 2.23: nitrogen balance of the base case experiments (300 g, 30 wt% CO <sub>2</sub> loaded MEA, no additives, 600 rpm, 120°C, 4 barg, 160 Nml/min gas feed, 5% O <sub>2</sub> /15% CO <sub>2</sub> /80% N <sub>2</sub> , 1 week) .....   | 65 |
| Figure 2.24: influence of the gas feed composition on MEA degradation and NH <sub>3</sub> emission (300 g, 30 wt% CO <sub>2</sub> loaded MEA, 120°C, 4 barg, 600 rpm, 160 Nml/min gas feed, 1 week) .....  | 66 |
| Figure 2.25: influence of the gas feed composition on organic degradation products (300 g, 30 wt% CO <sub>2</sub> loaded MEA, 120°C, 4 barg, 600 rpm, 160 Nml/min gas feed, 1 week)....  | 67 |
| Figure 2.26: influence of the gas feed composition on organic acids, nitrites and nitrates (left) and dissolved metal concentrations (right) (300 g, 30 wt% CO <sub>2</sub> loaded MEA <sup>21</sup> , 120°C, 4 barg, 600 rpm, 160 Nml/min gas feed, 5% O <sub>2</sub> , 1 week) .....         | 67 |
| Figure 2.27: influence of the CO <sub>2</sub> concentration in the gas feed on MEA degradation and NH <sub>3</sub> emission (300 g, 30 wt% CO <sub>2</sub> loaded MEA, 120°C, 4 barg, 600 rpm, 160 Nml/min gas feed, 5% O <sub>2</sub> , 1 week).....  | 68 |
| Figure 2.28: influence of the CO <sub>2</sub> concentration in the gas feed on organic degradation products (300 g, 30 wt% CO <sub>2</sub> loaded MEA, 120°C, 4 barg, 600 rpm, 160 Nml/min gas feed, 5% O <sub>2</sub> , 1 week).....  | 69 |
| Figure 2.29: influence of the O <sub>2</sub> concentration in the gas feed on MEA degradation and NH <sub>3</sub> emission (300 g, 30 wt% CO <sub>2</sub> loaded MEA, 120°C, 4 barg, 600 rpm, 160 Nml/min gas feed, 15% CO <sub>2</sub> , 1 week).....   | 69 |
| Figure 2.30: influence of the O <sub>2</sub> concentration in the gas feed on organic degradation products (300 g, 30 wt% CO <sub>2</sub> loaded MEA, 120°C, 4 barg, 600 rpm, 160 Nml/min gas feed, 15% CO <sub>2</sub> , 1 week) .....  | 70 |
| Figure 2.31: influence of the agitation rate on MEA degradation (300 g, 30 wt% CO <sub>2</sub> loaded MEA, 120°C, 4 barg, 5% O <sub>2</sub> , 160Nml/min gas feed, 1 week).....  | 71 |
| Figure 2.32: influence of the agitation rate on NH <sub>3</sub> emission (300 g, 30 wt% unloaded MEA, 120°C, 4 barg, 160Nml/min gas feed, 5% O <sub>2</sub> /95% N <sub>2</sub> , 1 week).....   | 71 |
| Figure 2.33: influence of the agitation rate on organic degradation products (300 g, 30 wt% CO <sub>2</sub> loaded MEA, 120°C, 4 barg, 160Nml/min gas feed, 5% O <sub>2</sub> , 1 week) .....  | 72 |
| Figure 2.34: GC comparison of the degradation at high agitation rate (300 g, 30 wt% CO <sub>2</sub> loaded MEA, 120°C, 4 barg, 1380 rpm, 160 Nml/min gas feed, 5% O <sub>2</sub> /15% CO <sub>2</sub> /80% N <sub>2</sub> , 1 week) with pilot plant degradation.....                          | 72 |
| Figure 2.35: influence of the agitation rate on the organic acids, nitrites and nitrates (300 g, 30 wt% CO <sub>2</sub> loaded MEA, 120°C, 4 barg, 160Nml/min gas feed, 1 week) .....  | 73 |
| Figure 2.36: influence of the agitation rate on dissolved metal concentrations (300 g, 30 wt% CO <sub>2</sub> loaded MEA <sup>27</sup> , 120°C, 4 barg, 160 Nml/min gas feed, 5% O <sub>2</sub> /15% CO <sub>2</sub> /80% N <sub>2</sub> , 1 week) .....                                       | 73 |
| Figure 2.37: influence of the temperature on MEA degradation and NH <sub>3</sub> emission (300 g, 30 wt% CO <sub>2</sub> loaded MEA, 600 rpm, 4 barg, 160 Nml/min gas feed, 5% O <sub>2</sub> /15% CO <sub>2</sub> /80% N <sub>2</sub> , 1 week).....  | 74 |
| Figure 2.38: influence of the temperature on organic degradation products (300 g, 30 wt% CO <sub>2</sub> loaded MEA, 600 rpm, 4 barg, 160 Nml/min gas feed, 5% O <sub>2</sub> /15% CO <sub>2</sub> /80% N <sub>2</sub> , 1 week).....  | 76 |
| Figure 2.39: influence of the temperature on organic acids, nitrite and nitrate (300 g, 30 wt% CO <sub>2</sub> loaded MEA, 600 rpm, 4 barg, 160 Nml/min gas feed, 5% O <sub>2</sub> /15% CO <sub>2</sub> /80% N <sub>2</sub> , 1 week) .....   | 77 |



|   |    |
|---|----|
| Figure 2.40: influence of the temperature on dissolved metal concentrations (300 g, 30 wt% CO <sub>2</sub> loaded MEA, 600 rpm, 4 barg, 160 Nml/min gas feed, 5% O <sub>2</sub> /15% CO <sub>2</sub> /80% N <sub>2</sub> , 1 week) .....                      | 77 |
| Figure 2.41: evolution of the MEA concentration with time (300 g, 30 wt% CO <sub>2</sub> loaded MEA, 120°C, 4 barg, 160 Nml/min gas feed, 5% O <sub>2</sub> /30% CO <sub>2</sub> /65% N <sub>2</sub> , 1 week) .....  | 78 |
| Figure 2.42: evolution of the organic degradation products with time (300 g, 30 wt% CO <sub>2</sub> loaded MEA, 120°C, 4 barg, 160 Nml/min gas feed, 5% O <sub>2</sub> /30% CO <sub>2</sub> /65% N <sub>2</sub> , 1 week) .....                               | 79 |
| Figure 2.43: influence of dissolved metals on MEA degradation and NH <sub>3</sub> emission (300 g, 30 wt% CO <sub>2</sub> loaded MEA, 600 rpm, 120°C, 4 barg, 160 Nml/min gas feed, 5% O <sub>2</sub> /15% CO <sub>2</sub> /80% N <sub>2</sub> , 1 week)..... | 80 |
| Figure 2.44: influence of dissolved metals on organic degradation products (300 g, 30 wt% CO <sub>2</sub> loaded MEA, 600 rpm, 120°C, 4 barg, 160 Nml/min gas feed, 5% O <sub>2</sub> /15% CO <sub>2</sub> /80% N <sub>2</sub> , 1 week).....                 | 80 |
| Figure 2.45: influence of dissolved metals on organic acids, nitrite and nitrate (300 g, 30 wt% CO <sub>2</sub> loaded MEA, 600 rpm, 120°C, 4 barg, 160 Nml/min gas feed, 5% O <sub>2</sub> /15% CO <sub>2</sub> /80% N <sub>2</sub> , 1 week).....           | 81 |
| Figure 2.46: influence of inhibitors on MEA degradation and NH <sub>3</sub> emission (300 g, 30 wt% CO <sub>2</sub> loaded MEA, 600 rpm, 120°C, 4 barg, 160 Nml/min gas feed, 5% O <sub>2</sub> /15% CO <sub>2</sub> /80% N <sub>2</sub> , 1 week).....       | 82 |
| Figure 2.47: influence of inhibitors on organic degradation products (300 g, 30 wt% CO <sub>2</sub> loaded MEA, 600 rpm, 120°C, 4 barg, 160 Nml/min gas feed, 5% O <sub>2</sub> /15% CO <sub>2</sub> /80% N <sub>2</sub> , 1 week) .....                      | 83 |
| Figure 2.48: influence of inhibitors on organic acids, nitrite and nitrate (300 g, 30 wt% CO <sub>2</sub> loaded MEA, 600 rpm, 120°C, 4 barg, 160 Nml/min gas feed, 5% O <sub>2</sub> /15% CO <sub>2</sub> /80% N <sub>2</sub> , 1 week) .....                | 83 |
| Figure 2.49: comparison of MEA batch degradation in cylinders (100 g, 30 wt% CO <sub>2</sub> loaded MEA, no gas feed, 140°C, 3 weeks) and in the DTR (300 g, 30 wt% CO <sub>2</sub> loaded MEA, 400 rpm, 120°C, 20 barg, no gas feed, 2 weeks) .....          | 84 |
| Figure 2.50: influence of CO <sub>2</sub> and dissolved metals on MEA thermal degradation with CO <sub>2</sub> (100 g, 30 wt% MEA, no gas feed, 140°C, 3 weeks).....  | 85 |
| Figure 2.51: influence of CO <sub>2</sub> on thermal degradation products (100 g, 30 wt% MEA, no gas feed, 140°C, 3 weeks) .....  | 85 |
| Figure 2.52: formation of degradation product over time in the case of loaded MEA (left) and loaded MEA with metal mix (right) (100 g, 30 wt% CO <sub>2</sub> loaded MEA, no gas feed, 140°C, 3 weeks) .....  | 86 |
| Figure 2.53: influence of the temperature on MEA thermal degradation with CO <sub>2</sub> (100 g, 30 wt% CO <sub>2</sub> loaded MEA, no gas feed, 3 weeks).....   | 87 |
| Figure 2.54: influence of temperature on thermal degradation products (100 g, 30 wt% CO <sub>2</sub> loaded MEA, no gas feed, 3 weeks).....   | 87 |
| Figure 2.55: thermal stability of loaded MEA solutions with degradation inhibitors (100 g, 30 wt% CO <sub>2</sub> loaded MEA, no gas feed, 140°C, 3 weeks) .....  | 88 |
| Figure 2.56: influence of inhibitors on thermal degradation products (100 g, 30 wt% CO <sub>2</sub> loaded MEA, no gas feed, 140°C, 3 weeks).....   | 89 |
| Figure 2.57: batch degraded samples with degradation inhibitors.....  | 89 |
| Figure 2.58: influence of inhibitors on GC thermal degradation products (100 g, 30 wt% CO <sub>2</sub> loaded MEA, no gas feed, 140°C, 3 weeks).....  | 90 |
| Figure 2.59: influence of metals and inhibitors on MEA thermal degradation (100 g, 30 wt% CO <sub>2</sub> loaded MEA, no gas feed, 140°C, 3 weeks).....   | 90 |

### Chapter III

|  |     |
|--|-----|
| Figure 3.1: schematic view of a column stage, RateSep model (Zhang et al., 2009) .....   | 101 |
| Figure 3.2: interface concentration profiles in the film model.....  | 105 |
| Figure 3.3: interface concentration profiles of the Higbie penetration model .....   | 106 |
| Figure 3.4: influence of the enhancement factor expression on the absorption performance<br>(Faramarzi et al., 2010) .....                                     | 110 |
| Figure 3.5: model complexity for the simulation of reactive absorption (Kenig et al., 2001).....   | 113 |
| Figure 3.6: flowsheet of the absorber intercooling (Cousins et al., 2011) .....  | 117 |
| Figure 3.7: flowsheet of the lean vapor compression (Cousins et al., 2011) .....   | 118 |
| Figure 3.8: flowsheet of the split-flow configuration (Karimi et al., 2011b).....  | 118 |
| Figure 3.9: flowsheet of the stripper interheating (Van Wagener and Rochelle, 2011) .....  | 119 |
| Figure 3.10: flowsheet of the double matrix configuration (Van Wagener and Rochelle, 2011)<br>.....  | 120 |
| Figure 3.11: main degradation products considered by Davis (2009) for modeling the MEA<br>thermal degradation.....   | 123 |
| Figure 3.12: model predictions (curves) and experimental results (points) for 35 wt% MEA, at<br>135°C and 0.4 mol CO <sub>2</sub> /mol MEA (Davis, 2009) ..... | 123 |
| Figure 3.13: influence of the stripper pressure on the process energy and MEA costs .....  | 124 |
| Figure 3.14: flowsheet of the Mobile Pilot Unit .....  | 127 |
| Figure 3.15: steady-state model flowsheet of the Esbjerg Pilot Plant.....  | 132 |
| Figure 3.16: dynamic model flowsheet of the Esbjerg Pilot Plant.....   | 134 |
| Figure 3.17: model agreement with observed degradation rates for the oxidative degradation<br>of MEA.....  | 138 |
| Figure 3.18: model agreement with observed degradation rates for the oxidative degradation<br>of MEA.....  | 140 |
| Figure 3.19: flowsheet of the CO <sub>2</sub> capture model with solvent purge and make-up .....   | 144 |
| Figure 3.20: influence of the solvent flow rate on the process thermal energy requirement .  | 147 |
| Figure 3.21: influence of the MEA concentration on the process thermal energy requirement<br>.....   | 148 |
| Figure 3.22: influence of the stripper pressure on the process thermal energy requirement .  | 148 |
| Figure 3.23: liquid temperature profiles of the absorber (left) and the stripper (right).....  | 149 |
| Figure 3.24: temperature profiles of the absorber (left) and the stripper (right) as reported by<br>Abu-Zahra, 2009 .....                                      | 149 |
| Figure 3.25: effect of simulated process disturbances on the liquid levels.....  | 151 |
| Figure 3.26: effect of simulated process disturbances on the CO <sub>2</sub> capture rate.....   | 151 |
| Figure 3.27: effect of simulated process disturbances on the process thermal energy<br>requirement.....  | 152 |
| Figure 3.28: two scenarios for reducing the process energy requirement over 12 minutes ...   | 153 |
| Figure 3.29: effect of a CO <sub>2</sub> capture rate decrease down to 10% capture on the stripper liquid<br>level .....                                       | 153 |
| Figure 3.30: influence of the solvent flow rate on the process energy and environmental<br>penalties.....  | 157 |
| Figure 3.31: influence of the solvent flow rate on the degradation products.....   | 157 |
| Figure 3.32: influence of the oxygen concentration in the flue gas on the process energy and<br>environmental penalties.....                                   | 158 |
| Figure 3.33: influence of the oxygen concentration on the MEA loss.....  | 158 |
| Figure 3.34: influence of the MEA concentration on the process energy and environmental<br>penalties.....  | 159 |

|   |     |
|---|-----|
| Figure 3.35: influence of the MEA concentration on the degradation products .....                                   | 159 |
| Figure 3.36: influence of the stripper pressure on stripper degradation products.....                               | 160 |
| Figure 3.37: influence of the stripper pressure on the process energy and environmental penalties.....              | 160 |
| Figure 3.38: influence of the intercooler location on the process thermal energy requirement .....                  | 161 |
| Figure 3.39: flowsheet of the lean vapor compression.....   | 161 |
| Figure 3.40: influence of the flash tank pressure for lean vapor compression on the process energy requirement..... | 162 |
| Figure 3.41: comparison of different process configurations for optimal CO <sub>2</sub> capture.....                | 163 |

## Appendix

|   |     |
|---|-----|
| Figure A.1: effect of Fe <sup>2+</sup> and Fe <sup>3+</sup> on NH <sub>3</sub> evolution (Chi and Rochelle, 2002).....                      | 199 |
| Figure A.2: effect of Iron on NH <sub>3</sub> evolution (Blachly and Ravner, 1965a).....  | 200 |
| Figure A.3: influence of the iron concentration (Chi and Rochelle, 2002).....   | 200 |
| Figure A.4: influence of the Fe <sup>2+</sup> concentration (Goff and Rochelle, 2004).....  | 201 |
| Figure A.5: influence of Cu <sup>2+</sup> concentration at rich (left) and lean CO <sub>2</sub> loading (right) .....                       | 201 |
| Figure A.6: effect of Cu <sup>2+</sup> concentration on NH <sub>3</sub> evolution (Blachly and Ravner, 1965a) ...                           | 202 |
| Figure A.7: effect of Ni <sup>2+</sup> on NH <sub>3</sub> evolution .....   | 202 |
| Figure A.8: effect of V <sup>5+</sup> on MEA oxidative degradation rate (Bello and Idem, 2006) .....  | 203 |
| Figure A.9: profile of NH <sub>3</sub> production after KMnO <sub>4</sub> addition in MEA (Goff and Rochelle, 2004).....                    | 204 |
| Figure A.10: combined effect of Fe <sup>2+</sup> and Cu <sup>2+</sup> in presence of inh. A.....  | 205 |
| Figure A.11: comparison of the effects of Fe <sup>2+</sup> , Cu <sup>2+</sup> and Mn <sup>2+</sup> (Voice, 2011b).....                      | 205 |
| Figure A.12: comparison of metal effect in presence of EDTA .....   | 206 |
| Figure A.13: effect of V <sup>5+</sup> on MEA degradation with CO <sub>2</sub> (Bello and Idem, 2006) .....                                 | 207 |
| Figure A.14: influence of NaVO <sub>3</sub> on the MEA-H <sub>2</sub> O-O <sub>2</sub> -SO <sub>2</sub> system (Uyanda et Idem, 2007) ..... | 208 |
| Figure A.15: effect of bicine in presence of 56 ppm Fe <sup>2+</sup> (Chi and Rochelle, 2002) .....   | 209 |
| Figure A.16: effect of EDTA and Bicine on MEA oxidative degradation without (left) and with metals (right) .....                            | 210 |
| Figure A.17: effect of EDTA concentration on O <sub>2</sub> -SO <sub>2</sub> induced degradation .....                                      | 211 |
| Figure A.18: comparison of blended potassium-sodium tartarate/Na <sub>2</sub> SO <sub>3</sub> with other inhibitors .....                   | 212 |
| Figure A.19: screening of new inhibitors (Voice and Rochelle, 2011b).....   | 212 |
| Figure A.20: effect of formaldehyde on NH <sub>3</sub> evolution rate (Goff and Rochelle, 2006) .....                                       | 213 |
| Figure A.21: effect of Na <sub>2</sub> SO <sub>3</sub> on NH <sub>3</sub> evolution rate (Goff and Rochelle, 2006) .....                    | 214 |
| Figure A.22: effect of Na <sub>2</sub> SO <sub>3</sub> concentration on NH <sub>3</sub> evolution rate (Supap et al., 2011a) ..             | 214 |
| Figure A.23: effect of oxidation state for inhibitor A (Goff and Rochelle, 2006) .....  | 215 |
| Figure A.24: effect of inhibitor A on Fe <sup>2+</sup> and Cu <sup>2+</sup> catalyzed degradation .....                                     | 215 |
| Figure A.25: effect of temperature and Inhibitor A concentration on NH <sub>3</sub> evolution .....   | 216 |

## Table index

### Chapter I

|   |    |
|---|----|
| Table 1.1: impact of the CO <sub>2</sub> capture method on the power plant efficiency ..... | 11 |
| Table 1.2: chronologic listing of the main CO <sub>2</sub> capture installations .....      | 19 |

### Chapter II

|  |    |
|--|----|
| Table 2.1: degradation products detected by GC (Lepaumier et al., 2011) .....  | 32 |
| Table 2.2: research interests and operating parameters at the University of Regina, Canada<br>(n.a.: not applicable; n.s.: not specified) .....  | 33 |
| Table 2.3: research interests and operating parameters at the University of Texas at Austin<br>(n.a.: not applicable; n.s.: not specified) ..... | 34 |
| Table 2.4: research interests and operating parameters of other research groups (n.a.: not<br>applicable; n.s.: not specified) .....             | 35 |
| Table 2.4: continued (n.a.: not applicable; n.s.: not specified) .....   | 36 |
| Table 2.5: studies about metal effects on MEA degradation .....  | 38 |
| Table 2.6: studies about degradation inhibitors (effective inhibitors are in bold letters).....  | 42 |
| Table 2.7: analytical methods for characterizing amine solutions .....   | 50 |
| Table 2.8: method parameters for FTIR analysis .....   | 51 |
| Table 2.9: elements of the HPLC unit .....   | 53 |
| Table 2.10: characteristics of tested HPLC columns .....   | 54 |
| Table 2.11: characteristics of the OPTIMA-35 MS GC column.....   | 56 |
| Table 2.12: main peaks identified in GC spectra of degraded MEA samples .....  | 58 |
| Table 2.13: base case conditions for semi-batch degradation experiments .....  | 62 |
| Table 2.14: metal concentrations in amine solution.....  | 79 |
| Table 2.15: oxidative degradation inhibitors tested in batch reactors .....  | 88 |

### Chapter III

|   |     |
|---|-----|
| Table 3.1: main correlations for hydrodynamic and transfer parameters .....                                   | 103 |
| Table 3.2: different expressions of the enhancement factor.....   | 109 |
| Table 3.3: main modeling software packages for the CO <sub>2</sub> capture process .....                      | 113 |
| Table 3.4: dynamic modeling studies of the CO <sub>2</sub> capture process.....                               | 121 |
| Table 3.5: objectives and drawbacks of published degradation models .....                                     | 125 |
| Table 3.6: design characteristics of the MPU .....  | 127 |
| Table 3.7: parameters used for the determination of equilibrium constants in the equilibrium<br>model.....    | 129 |
| Table 3.8: packing characteristics and parameters for rate-based calculations.....                            | 130 |
| Table 3.9: reactions and rate parameters in the MEA-CO <sub>2</sub> -H <sub>2</sub> O system .....            | 131 |
| Table 3.10: Vessel geometries for dynamic simulations.....  | 133 |
| Table 3.11: Heat exchanger geometries for dynamic simulations .....   | 133 |
| Table 3.12: kinetics parameters of the oxidative degradation of MEA .....                                     | 136 |
| Table 3.13: experiments for determining the kinetics of MEA oxidative degradation.....                        | 137 |
| Table 3.14: kinetics parameters of the thermal degradation of MEA with CO <sub>2</sub> .....                  | 139 |
| Table 3.15: experiments for determining the kinetics of MEA thermal degradation with CO <sub>2</sub><br>..... | 140 |
| Table 3.16: comparison of kinetics parameters for oxidative degradation .....                                 | 141 |
| Table 3.17: comparison of kinetics parameters for the formation of HEIA .....                                 | 142 |
| Table 3.18: reactions and rate parameters in the MEA-CO <sub>2</sub> -H <sub>2</sub> O system .....           | 145 |

|   |     |
|---|-----|
| Table 3.19: simulated disturbances for the evaluation of the process strategy stability ..... | 150 |
| Table 3.20: degradation and emission results of the base case model .....                     | 155 |

**Appendix**

|   |     |
|---|-----|
| Table A.1: influence of Fe and Fe/Cu on degradation products (Sexton and Rochelle, 2006)<br>..... | 207 |
| Table A.2: sulfur-containing inhibitors patented by IFPEN .....                                   | 216 |
| Table A.3: reported NH <sub>3</sub> concentrations for a calibration NH <sub>3</sub> sample ..... | 229 |
| Table A.4: relative standard deviations of the HPLC quantification of MEA.....                    | 230 |
| Table A.5: relative standard deviations for GC quantified components .....                        | 230 |

## Abbreviation list

|        |  |
|--------|--|
| AC     | Anion chromatography   |
| AEHEIA | <i>N</i> -(2-aminoethyl)- <i>N'</i> -(2-hydroxyethyl)imidazolidinone |
| AMP    | 2-amino-2-methylpropanol   |
| B.C.   | Base Case  |
| BHEOX  | <i>N,N'</i> -bis(2-hydroxyethyl)oxalamide                            |
| CC     | Cation chromatography  |
| CCS    | Carbon Capture and Storage   |
| CCUS   | Carbon Capture, Utilization and Storage                              |
| CE     | Capillary Electrophoresis  |
| CFD    | Computational Fluid Dynamics   |
| DEA    | Diethanolamine   |
| DMTD   | dimercaptothiadiazone  |
| Dept   | Department   |
| DTR    | Degradation Test Rig   |
| EDA    | Ethyabblenediamine   |
| eNRTL  | Electrolyte NonRandom Two Liquid                                     |
| ETP-W  | EcoTechnoPole Wallonie   |
| 1FGD   | Flue Gas Desulfurization   |
| FID    | Flame Ionization Detector  |
| FTIR   | Fourier Transform Infra-Red spectroscopy                             |
| GC     | Gas Chromatography   |
| Gt     | Gigatonnes   |
| HEA    | <i>N</i> -(2-hydroxyethyl)acetamide                                  |
| HEDP   | Hydroxyethylidene diphosphonic acid                                  |
| HEEDA  | 2-(2-aminoethylamino)ethanol   |
| HEF    | <i>N</i> -(2-hydroxyethyl)formamide                                  |
| HEHEAA | <i>N</i> -(2-hydroxyethyl)-2-(2-hydroxyethylamino)acetamide          |
| HEI    | 1-(2-hydroxyethylimidazole)  |
| HEIA   | 1-(2-hydroxyethyl)-2-imidazolidinone                                 |
| HEPO   | 4-(2-hydroxyethyl)-piperazin-2-one                                   |
| HHEA   | 2-hydroxy- <i>N</i> -(2-hydroxyethyl)acetamide                       |
| HILIC  | Hydrophilic Interaction Chromatography                               |
| HPLC   | High Performance Liquid Chromatography                               |
| HSS    | Heat Stable Salts  |
| Ibid.  | Latin “ibidem”: the same   |
| IC     | Ionic chromatography   |
| ICP    | Inductively coupled plasma   |
| i.e.   | Latin “id est”: that is  |
| IFPEN  | Institut Français du Pétrole - Energies Nouvelles                    |
| Inh. A | Inhibitor A  |
| IR     | Infra Red  |
| KF     | Karl Fischer   |
| LC     | Liquid Chromatography  |
| L/G    | Liquid over gas ratio  |
| LNG    | Liquefied natural gas  |
| LPG    | Liquefied petroleum gas  |
| LVC    | Lean Vapor Compression   |
| M      | Manometer  |

|                 |   |
|-----------------|---|
| MDEA            | Methyldiethanolamine  |
| MEA             | Monoethanolamine  |
| MF              | Mass Flow meter   |
| MFC             | Mass Flow Controller  |
| MS              | Mass Spectrometry   |
| Mt              | Megatonnes  |
| n.a.            | not applicable  |
| NDELA           | Nitrosodiethanolamine   |
| NDMA            | nitrosodimethylamine  |
| Nml             | normal milliliter (Normal state: 0°C; 1.013 bar)  |
| NMOR            | nitrosomorpholine   |
| NMR             | Nuclear magnetic resonance  |
| NO <sub>x</sub> | Nitrogen oxides (NO, NO <sub>2</sub> , N <sub>2</sub> O <sub>3</sub> , N <sub>2</sub> O <sub>4</sub> and HNO <sub>2</sub> ) |
| n.s.            | not specified   |
| NTNU            | Norwegian University of Science and Technology  |
| OECD            | Organisation for Economic Co-operation and Development  |
| OZD             | 2-Oxazolidinone   |
| P               | Pressure / Pressure transducer  |
| PTFE            | Polytetrafluoroethylene (Teflon <sup>®</sup> )  |
| PZ              | Piperazine  |
| Resp.           | Respectively  |
| RID             | Refractive Index Detector   |
| RPM             | Revolutions Per Minute  |
| SCR             | Selective Catalytic Reduction   |
| SO <sub>x</sub> | Sulfur oxides (mainly SO <sub>2</sub> , SO <sub>3</sub> )   |
| T               | Temperature / Thermocouple  |
| TC              | Total Carbon  |
| TCD             | Thermal Conductivity Detector   |
| TG-DSC          | Thermogravimetric Differential Scanning Calorimetry   |
| TIC             | Total Inorganic Carbon  |
| TN              | Total Nitrogen  |
| TOC             | Total Organic Carbon  |
| TriHEIA         | Cyclic Urea of MEA trimer   |
| ULg             | University of Liege   |
| URegina         | University of Regina  |
| UT Austin       | University of Texas at Austin   |
| UV              | Ultra Violet  |
| VOC             | Volatile Organic Compounds  |
| Wt%             | weight percentage   |
| XRD             | X-Ray Diffraction   |

## **Appendices**

1. Literature review: influence of dissolved metals on MEA solvent degradation.
2. Literature review: influence of degradation inhibitors on MEA solvent degradation.
3. Risk analysis for the degradation test rig.
4. Error analysis for the main analytical techniques.
5. Detailed results of the solvent degradation experiments.



## Appendix 1: Influence of dissolved metals on MEA degradation

In this section, we will mainly address oxidative degradation. The effect of each metal will be described separately, as well as the effect of the metal concentration for iron and copper, the effect of combined metals and the metal influence on the observed degradation products. Finally, the effect of metals on other types of degradation will briefly be evocated.

### A.1.1 Effect of iron

Iron is the main component of stainless steel, so that its presence cannot be prevented during CO<sub>2</sub> capture. In solution, iron can be present under the form of Fe<sup>2+</sup> or Fe<sup>3+</sup> (it can respectively be added as FeSO<sub>4</sub> or FeCl<sub>3</sub>). It seems from Chi and Rochelle (2002) that Fe<sup>2+</sup> has a larger catalytic effect on MEA degradation than Fe<sup>3+</sup>. The higher catalytic effect of Fe<sup>2+</sup> compared to Fe<sup>3+</sup> is represented in figure A.1 at both CO<sub>2</sub> lean and rich loading. The production of NH<sub>3</sub> is used as tracer for the oxidative degradation of MEA.

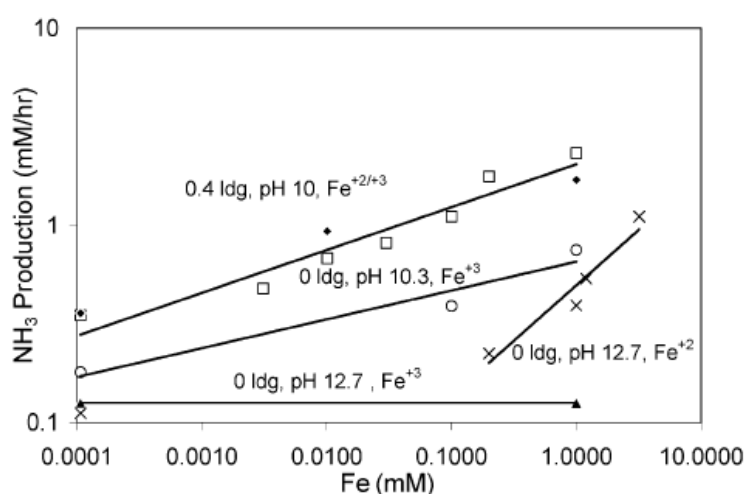


**Figure A.1: effect of Fe<sup>2+</sup> and Fe<sup>3+</sup> on NH<sub>3</sub> evolution (Chi and Rochelle, 2002)**

Explanation for the higher influence of Fe<sup>2+</sup> compared to Fe<sup>3+</sup> may come from the Fe<sup>2+</sup>-catalyzed pathway for hydroperoxide formation proposed by Bedell (2009) and presented in chapter II, section 2.3.

Although Blachly and Ravner (1965a) have performed all their experiments with degradation inhibitors, they have also stated that Fe<sup>2+</sup> has a larger catalytic effect on NH<sub>3</sub> production than Fe<sup>3+</sup> (figure A.2). Moreover, in the presence of degradation inhibitors, bulk iron has no impact on NH<sub>3</sub> production.

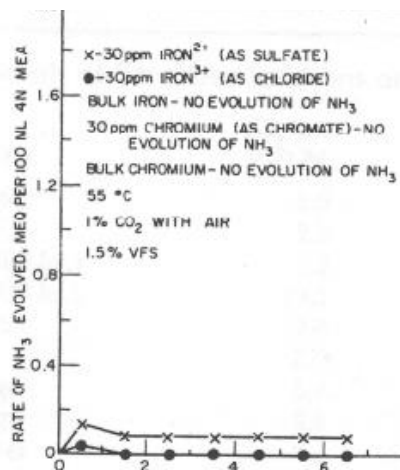


**Figure A.2: effect of Iron on NH<sub>3</sub> evolution (Blachly and Ravner, 1965a)**

All the authors that have studied the influence of Fe<sup>2+</sup> have confirmed its catalytic effect on the oxidative degradation of MEA. Chi and Rochelle (2002) have also evidenced (figure A.3) that a higher metal concentration induces a higher oxidative degradation, both with Fe<sup>2+</sup> (dissolved FeSO<sub>4</sub>, left chart) and Fe<sup>3+</sup> (dissolved FeCl<sub>3</sub>, right chart).

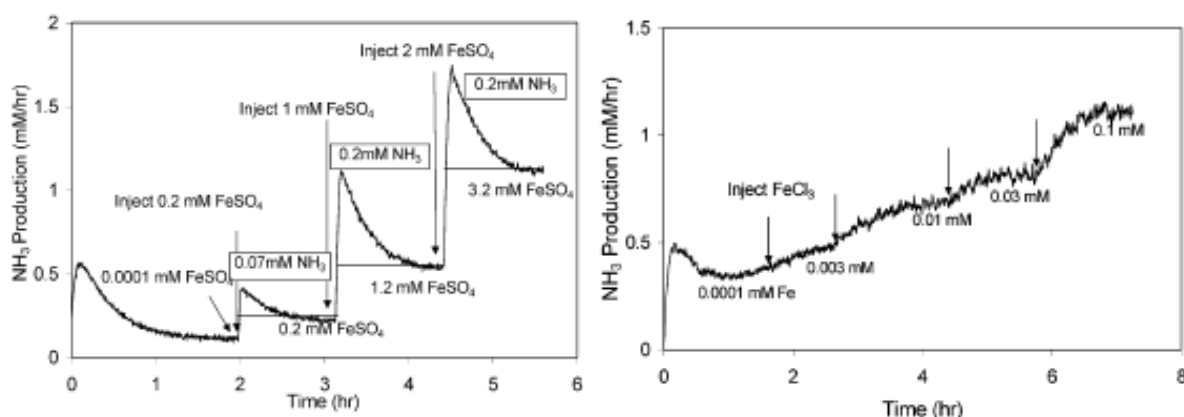


**Figure A.3: influence of the iron concentration (Chi and Rochelle, 2002)**

Only one other work (Goff and Rochelle, 2004) has studied the impact of varying Fe<sup>2+</sup> concentration, with similar evidence of a NH<sub>3</sub> production increasing when the metal concentration is increased (figure A.4). However, the authors have stated that the degradation rate dependence on iron concentration was much lower than first order. They attribute this to the limiting O<sub>2</sub> mass transfer due to insufficient agitation rate during their experiment.

Furthermore, figure A.4 shows that CO<sub>2</sub> loading has an impact on the MEA degradation rate. Diverging from previous results of Chi and Rochelle (2002, see also figure A.1), they have shown that the degradation rate was higher in case of unloaded solutions (Goff and Rochelle, 2004). This latest result has been confirmed in the case of metal-free solutions as well as in presence of vanadium catalyst (Bello and Idem, 2006). The reason for this lower degradation rate would be a decrease of O<sub>2</sub> solubility in loaded MEA solutions.

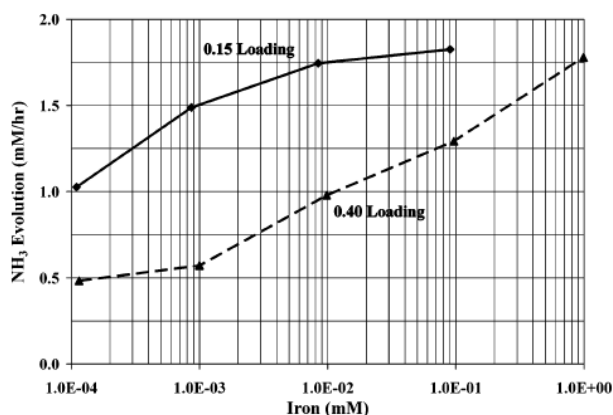


**Figure A.4: influence of the Fe<sup>2+</sup> concentration (Goff and Rochelle, 2004)**

Finally, according to Chi and Rochelle (2002), the CO<sub>2</sub>-loading has a further effect on MEA oxidation since only Fe<sup>2+</sup> presents a catalytic effect in unloaded solutions. This may be due to an influence of the solution pH. Unloaded solutions are more basic, so that Fe<sup>3+</sup> may precipitate under the form of Fe(OH)<sub>3</sub>, which could however not be confirmed visually.

### A.1.2 Effect of copper

Since 1966, the large catalytic effect of Cu<sup>2+</sup> on the oxidative degradation of MEA has been evidenced (Blachly and Ravner, 1965a). This has been later confirmed by several studies (Goff and Rochelle, 2003, 2004; Voice and Rochelle, 2011c).

Goff and Rochelle (2003, see figure 6) have evidenced the influence of Cu<sup>2+</sup> on NH<sub>3</sub> production rate at both rich (left chart) and lean CO<sub>2</sub> loading (right chart). They have found that the NH<sub>3</sub> production rate first increases with the Cu<sup>2+</sup> concentration, and then decreases, so that a maximal NH<sub>3</sub> production rate is achieved. However, like for Iron, the rate dependency on Cu<sup>2+</sup> concentration was lower than first order, also due to O<sub>2</sub> mass transfer limitations in the bulk liquid.

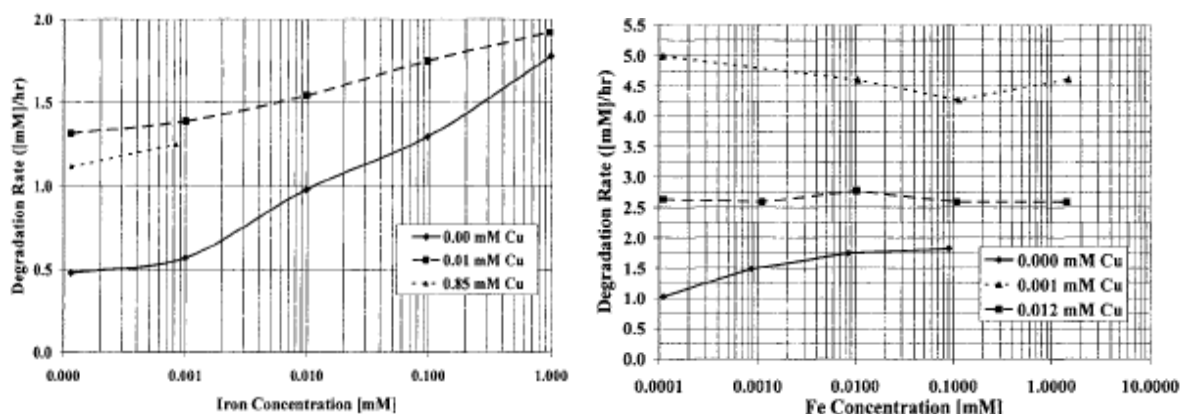


**Figure A.5: influence of Cu<sup>2+</sup> concentration at rich (left) and lean CO<sub>2</sub> loading (right)**

In the presence of bicine (tradename VFS), a degradation inhibitor, Blachly and Ravner (1965a) have shown that the Cu<sup>2+</sup> concentration has a large influence on the oxidative degradation. Even at 1ppm Cu, figure A.6 shows an effect on MEA degradation in presence of bicine. However, they did not report about a maximal NH<sub>3</sub> production rate.

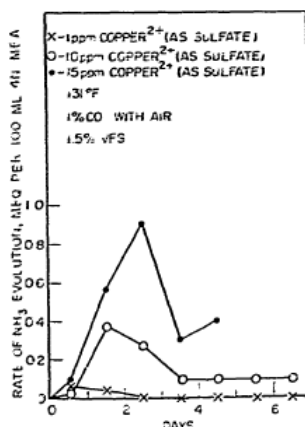


Figure A.6: effect of  $\text{Cu}^{2+}$  concentration on  $\text{NH}_3$  evolution (Blachly and Ravner, 1965a)

### A.1.3 Effect of nickel

Blachly and Ravner (1965a) have studied the effect of nickel in presence of degradation inhibitor bicine (VFS). Their study has been performed at 55°C. Bulk nickel rapidly corroded, inducing severe amine degradation. Dissolved nickel ( $\text{Ni}^{2+}$  dissolved from  $\text{NiCl}_2$ ) at low concentration (3.7ppm) had no effect but larger amount (37ppm) induced perceptible degradation as observed in figure A.7.

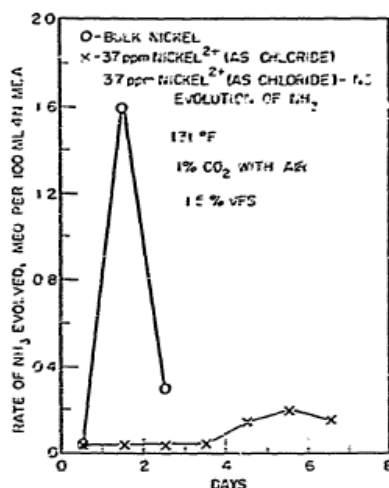


Figure A.7: effect of  $\text{Ni}^{2+}$  on  $\text{NH}_3$  evolution

However, in a more recent study, Voice and Rochelle (2011b) indicate that  $\text{Ni}^{43}$  has no significant effect on MEA oxidative degradation at 70°C.

### A.1.4 Effect of chromium

Voice and Rochelle (2011b and c) have evidenced a mild catalytic effect of chromium. According to Blachly and Ravner (1965a), chromium has no effect on MEA oxidative degradation when bicine is present, neither under the form of bulk chromium nor under the form of chromate. However, a mild effect has been observed when the inhibitor is EDTA.

<sup>43</sup> Oxidation state not reported

### A.1.5 Effect of vanadium

Vanadium may be present in MEA solutions under the form of  $\text{NaVO}_3$ , a corrosion inhibitor. Bello and Idem (2006) have tested the effect of  $\text{V}^{5+}$  (from dissolved  $\text{NaVO}_3$ ) at 55 and 120°C as represented in Figure A.8. In both cases, the addition of  $\text{V}^{5+}$  induced higher oxidative degradation rates.

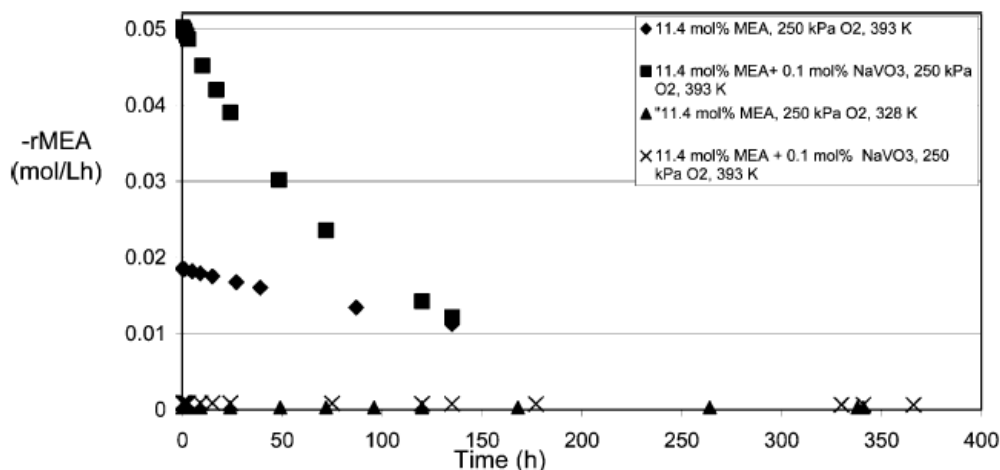


Figure A.8: effect of  $\text{V}^{5+}$  on MEA oxidative degradation rate (Bello and Idem, 2006)

The catalytic effect of  $\text{V}^{5+}$  ( $\text{NaVO}_3$ ) has been confirmed by Sexton and Rochelle (2006). Uyanga and Idem (2007) have also confirmed an effect on MEA degradation in presence of both  $\text{O}_2$  and  $\text{SO}_2$ . Voice and Rochelle (2011b) have reported a mild catalyst effect of vanadium<sup>44</sup>, but in a second publication (2011c), they have presented vanadium ( $\text{VO}_4^-$ ) as an inhibitor. This point must be considered with care since vanadium does not exist at the oxidation state 7+.

### A.1.6 Effect of manganese

Chi and Rochelle (2002) have tested the influence of  $\text{Mn}^{7+}$  ( $\text{KMnO}_4$ ) as a potential oxidant of MEA. The presence of this metal induced a rapid MEA degradation. They have also stated that the production rate of  $\text{NH}_3$  was  $1 \text{ mol NH}_3/\text{mol KMnO}_4$ , which would mean a linear variation of MEA degradation with the  $\text{Mn}^{7+}$  concentration. Goff and Rochelle (2004) confirmed the catalytic effect of manganese. They have studied the impact of  $\text{Mn}^{2+}$  ( $\text{MnSO}_4$ ) and  $\text{Mn}^{7+}$  ( $\text{KMnO}_4$ ) and observed that both oxidation states seriously increased the MEA oxidative degradation. However, they have supposed that Mn was reacting in a different way than Fe or Cu since the  $\text{NH}_3$  evolution rate was varying with time differently than other metals as shown in Figure A.9 (to compare with figure A.3, left chart).

This profile has been confirmed by Voice and Rochelle (2011b) (see also figure A.11). In a second paper, Voice and Rochelle (2011c) have confirmed the catalytic effect of Mn, making though a distinction between  $\text{Mn}^{2+}$ , rather a degradation inhibitor and  $\text{Mn}^{7+}$ , a serious oxidant. They have supposed that  $\text{Mn}^{2+}$  changes its oxidation state at stripper temperatures, without giving any further details.

<sup>44</sup>Oxidation state not reported

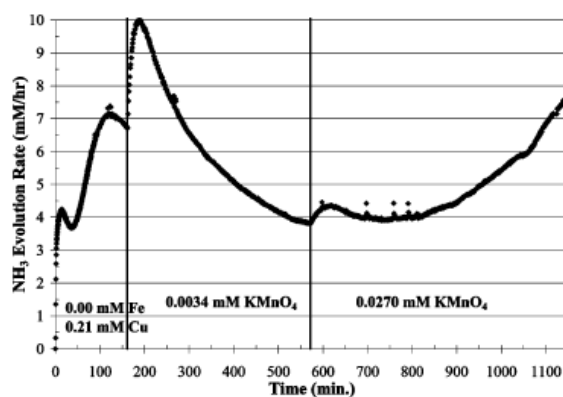


**Figure A.9: profile of NH<sub>3</sub> production after KMnO<sub>4</sub> addition in MEA (Goff and Rochelle, 2004)**

### *A.1.7 Effect of silver*

Kumar (1982) has studied the effect of silver on the oxidation of low amounts of MEA. He has reported that Ag<sup>2+</sup> oxidizes MEA. MEA first forms a complex with the metal ions. The MEA oxidation proceeds by an intramolecular electron transfer within the complex.

### *A.1.8 Effect of other metals*

Voice and Rochelle (2011b) have performed a large screening of metal effects on MEA oxidative degradation. Besides the results already described, they have also tested Ti, Mo, Co, Se, Ce, Sn and Zn<sup>45</sup>. None of these metals showed significant catalytic effect on MEA degradation.

### *A.1.9 Effect of combined metals*

- *Fe<sup>2+</sup> and Cu<sup>2+</sup>:*

Goff and Rochelle (2003, 2004) have tested the effect of both Fe<sup>2+</sup> and Cu<sup>2+</sup> on MEA oxidation (see figure A.5). It seems that the concentration of Cu<sup>2+</sup> has a larger influence than the Fe<sup>2+</sup> concentration on the NH<sub>3</sub> evolution, especially at lean CO<sub>2</sub> loading.

While testing the effect of Inhibitor A, Goff and Rochelle (2006) observed that it was more difficult to inhibit the degradation when both Fe and Cu were in solution in comparison with only one metal in solution. This can be observed in figure A.10. Sexton and Rochelle (2009) have confirmed the combined effect of Cu<sup>2+</sup> and Fe<sup>2+</sup>. They described the influence of the metal combination on the observed degradation products.

<sup>45</sup> Oxidation state not reported

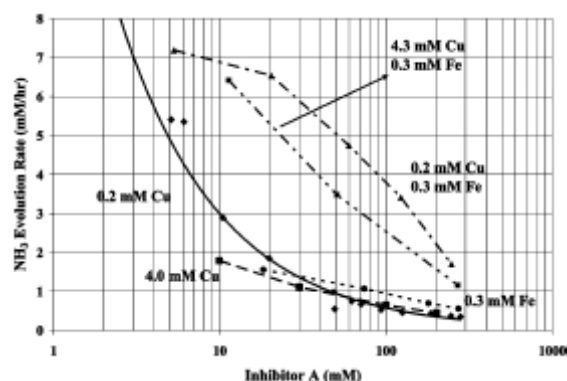


**Figure A.10: combined effect of  $\text{Fe}^{2+}$  and  $\text{Cu}^{2+}$  in presence of inh. A**

- $\text{Cr}^{3+}$  and  $\text{Ni}^{2+}$

Sexton and Rochelle (2009) have tested the combination of  $\text{Cr}^{3+}$  and  $\text{Ni}^{2+}$ . They observed a higher catalytic effect on MEA degradation rate than with  $\text{Fe}^{2+}$  alone. This was not expected from discussions in Sections A.1.3 and A.1.4 describing the rather low activity of separate metals.

#### A.1.10 Comparison of the different metals: Degradation rate

In the absence of degradation inhibitor, Goff and Rochelle (2004) have shown that Cu presents a higher catalytic effect than Fe. This has been evidenced by Voice and Rochelle (2011b) in figure A.10 when comparing  $\text{Fe}^{2+}$ ,  $\text{Cu}^{2+}$ , as well as  $\text{Mn}^{2+}$  at equal molar concentrations (1mM, respectively 56, 63.5 and 55ppm). According to the authors, Cr and V only show a mild effect, while the other metals tested (Ti, Co, Mo, Ni, Sn, Se, Ce, Zn) don't show any significant effect.

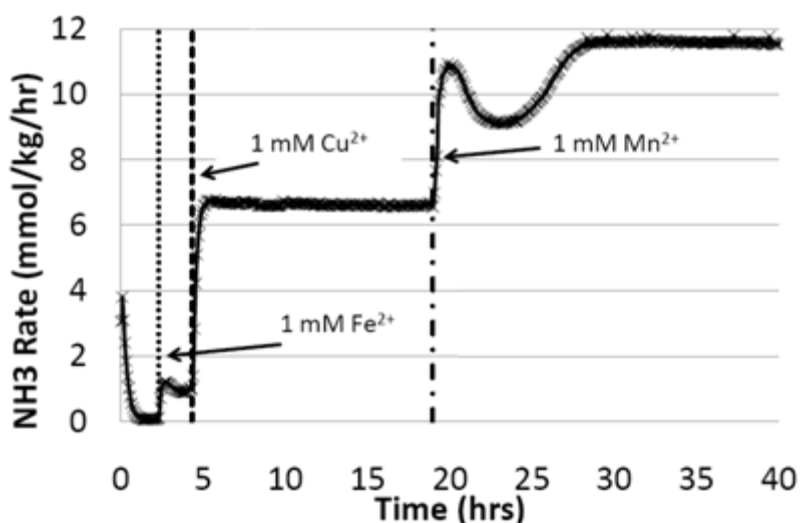


**Figure A.11: comparison of the effects of  $\text{Fe}^{2+}$ ,  $\text{Cu}^{2+}$  and  $\text{Mn}^{2+}$  (Voice, 2011b)**

In a second study (Voice and Rochelle, 2011c), the catalytic effect decreases as following:  $\text{Mn}^{x+} > \text{Cu}^{2+} > \text{Fe}^{2+} > \text{Cr}^{3+}$ . The exact oxidation state of  $\text{Mn}^{x+}$  has not been defined. The oxidation state has an effect but this effect for Mn is still unclear in the literature. In this study,  $\text{Mn}^{2+}$  and  $\text{VO}^{4+}$  are presented as having rather a strong respectively mild inhibiting effect on MEA oxidation. In the case of  $\text{Mn}^{2+}$ , this is in direct contradiction with the results presented in figure A.11 where there may be confusion between  $\text{Mn}^{2+}$  and  $\text{Mn}^{x+}$ .

Sexton and Rochelle (2009) list the metal with decreasing oxidative degradation potential as following:  $\text{Cu}^{2+}$  (or  $\text{Fe}^{2+}/\text{Cu}^{2+}$ ) >  $\text{Cr}^{3+}/\text{Ni}^{2+}$  >  $\text{Fe}^{2+}$  >  $\text{V}^{5+}$ .

According to Blachly and Ravner (1965a), the most serious oxidative degradation of MEA in presence of the inhibitor EDTA is observed with  $\text{Fe}^{2+}$  (30ppm) (Figure A.12). The catalytic activity of  $\text{Cu}^{2+}$  is neutralized by EDTA.  $\text{Cr}^{3+}$  (10ppm) and  $\text{Ni}^{2+}$  (30ppm) also influence the degradation but in a much lower extent than  $\text{Fe}^{2+}$ . This evidences that the classification of the respective catalytic effect of metals depends on the degradation conditions.

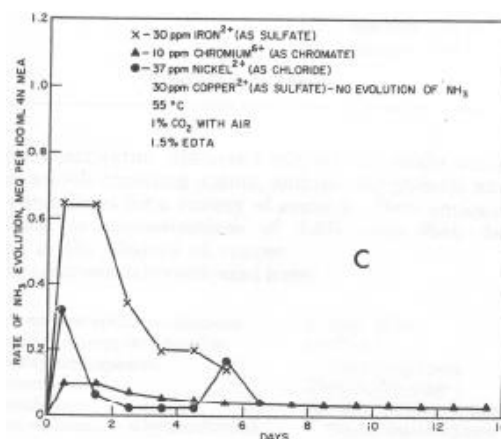


**Figure A.12: comparison of metal effect in presence of EDTA**

So it is possible to summarize these studies with the following decreasing order of oxidation potential:

$\text{Mn}^{7+} > \text{Fe}^{2+}/\text{Cu}^{2+} \geq \text{Cu}^{2+} > \text{Cr}^{3+}/\text{Ni}^{2+} > \text{Fe}^{2+} > \text{Fe}^{3+} > \text{Cr}^{3+} > \text{V}^{5+} \gg \text{Ti}, \text{Co}, \text{Mo}, \text{Ni}, \text{Sn}, \text{Se}, \text{Ce}, \text{Zn}$

Moreover, the combination of different metals may increase their respective effect.  $\text{Mn}^{2+}$  is not listed since it is considered as a degradation inhibitor. The effect of  $\text{Ag}^{2+}$  has not been compared to other metals.

#### **A.1.11 Comparison of the different metals: products observed**

Most studies relate the evolution of  $\text{NH}_3$  in the experiment flue gas to the degradation rate of MEA. However, some studies also performed liquid phase analysis and related the results to the metal added to the solution. This was the case for Sexton and Rochelle (2006 and 2009). In their first paper, they observed that more formate and glycolate were formed when both Fe and Cu were in solution compared to only Cu (oxidation states not specified). In the same way, more  $\text{NO}_2$  and  $\text{NO}_3$  were produced, as represented in Table A.1.

Those assumptions seem to confirm the larger oxidation potential of Cu/Fe compared to Cu only. Indeed, the ratio Formate over Acetate/Glycolate (their respective peaks could not be separated) increases when Fe is present, and formate is a more oxidized degradation product. The same argument can be applied to the ratio  $\text{NO}_3/\text{NO}_2$ .



**Table A.1: influence of Fe and Fe/Cu on degradation products (Sexton and Rochelle, 2006)**

| Experiment                | 12/2004   | 09/2005          |
|---------------------------|-----------|------------------|
| Distinguishing Conditions | 0.2 mM Cu | 0.2 mM Cu and Fe |
| Acetate/Glycolate (mM/hr) | 0.26      | 0.34             |
| Formate (mM/hr)           | 0.33      | 0.64             |
| Oxalate (mM/hr)           | 0.03      | 0.03             |
| Nitrate (mM/hr)           | 0.07      | 0.20             |
| Nitrite (mM/hr)           | 0.18      | 0.26             |
| EDA (mM/hr)               | N/A       | N/A              |

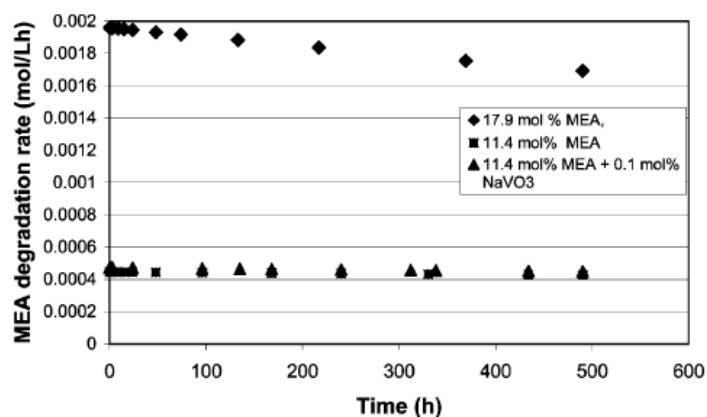
This behavior is confirmed in Sexton and Rochelle (2009). The presence of  $\text{Fe}^{2+}$  multiplies by 3 the amount of formate, HEI (1-(2-HydroxyEthyl)Imidazole) and HEF (N-(2-HydroxyEthyl)Formamide) produced compared to  $\text{Cu}^{2+}$  only. However, when the metal catalyst is  $\text{V}^{5+}$  instead of  $\text{Fe}^{2+}$ , less formate and HEI is produced, but more oxamide.

*To summarize, degradation products may be observed in different proportions according to the metal catalyst. Degradation pathways must be further studied.*

#### A.1.12 Effect of metals on $\text{CO}_2$ degradation

Only little research has been performed to study the effect of metals on the MEA degradation when the solution is only loaded with  $\text{CO}_2$  (no  $\text{O}_2$ ). Chi and Rochelle (2002) have observed no  $\text{NH}_3$  production at  $55^\circ\text{C}$  when the gas feed only contains  $\text{N}_2$  and  $\text{CO}_2$ , whether Fe had been added to the solution or not. The only exception was the production of  $\text{NH}_3$  when  $\text{Mn}^{7+}$  ( $\text{KMnO}_4$ ) was added. The stoichiometry between  $\text{NH}_3$  production and  $\text{KMnO}_4$  addition was 0.97.

The second study performed on this subject showed no influence of  $\text{V}^{5+}$  ( $\text{NaVO}_3$ ) on MEA degradation when only  $\text{CO}_2$  was present in the reactor gas feed (Figure A.13). This study was performed at  $120^\circ\text{C}$  by Bello and Idem (2006).

**Figure A.13: effect of  $\text{V}^{5+}$  on MEA degradation with  $\text{CO}_2$  (Bello and Idem, 2006)**

Davis (2009) has spiked CO<sub>2</sub> loaded MEA at 150°C with 100mM of Fe, Cr, Ni, Cu, V<sup>46</sup> (respectively 5600, 5200, 5900, 6350 and 5100ppm). No degradation could be observed.

#### A.1.13 Effect of metals on MEA thermal degradation

No research could be retrieved on the effect of metals on MEA thermal degradation in the absence of CO<sub>2</sub> and O<sub>2</sub>.

#### A.1.14 Effect of metals on SO<sub>x</sub> and NO<sub>x</sub> degradation

Pure SO<sub>2</sub> degradation has not been studied in presence of metals. However, Uyanga et Idem (2007) have studied the influence of V<sup>5+</sup> (NaVO<sub>3</sub>) on the MEA-H<sub>2</sub>O-O<sub>2</sub>-SO<sub>2</sub> system. They observed an increase of the degradation due to NaVO<sub>3</sub> as presented in figure A.14. However, they did not distinguish between SO<sub>2</sub> and O<sub>2</sub> degradation, so that no conclusion can be made.

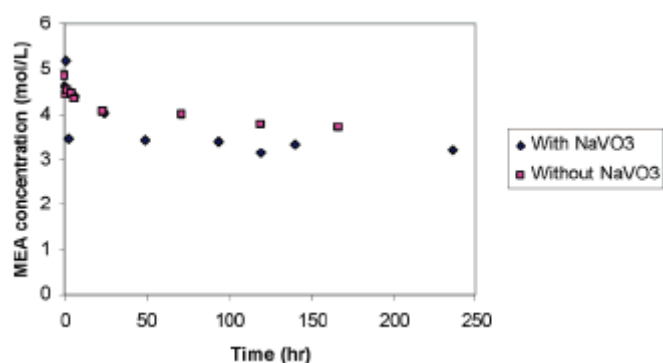
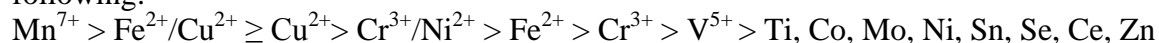


**Figure A.14: influence of NaVO<sub>3</sub> on the MEA-H<sub>2</sub>O-O<sub>2</sub>-SO<sub>2</sub> system (Uyanga et Idem, 2007)**

No research has been made on the influence of metals on NO<sub>x</sub> degradation.

#### A.1.15 Conclusions on metal effect

The influence of metals on MEA degradation has only been studied for the case of oxidative degradation and degradation with CO<sub>2</sub>. The influence of metal catalysts on oxidative degradation has clearly been established. The oxidation potential of metals can be listed as following:



Mn<sup>2+</sup> is not listed since it is considered as a degradation inhibitor. It has also been evidenced that the combination of different metals may increase their respective effect.

Moreover, degradation products may be observed in different proportions according to the metal catalyst. This highlights the fact that degradation pathways still have to be studied.

Finally, different studies have evidenced that the presence of metal has no influence on degradation with CO<sub>2</sub>. The influence of metals on MEA degradation with temperature only, SO<sub>x</sub> and NO<sub>x</sub> has not been studied so far.

<sup>46</sup> Oxidation state not reported

## Appendix 2: Influence of degradation inhibitors for the MEA solvent

As mentioned in chapter II, section 2.4, the large majority of studies about degradation inhibitors concern oxidative degradation. Oxidative degradation inhibitors may be separated into two main categories (Bedell, 2009):

- Chelating agents. They form a complex with dissolved metals, inhibiting their catalytic activity and stopping the initiation/propagation steps of the chain reaction.
- Radical and O<sub>2</sub> scavengers. As presented in chapter II, section 2.1, dissolved O<sub>2</sub> forms peroxides in water. Radical scavengers react with the peroxides to form stable products and stop the chain reaction. They are also called O<sub>2</sub> scavengers since they stoichiometrically react with the dissolved O<sub>2</sub>. Disadvantage of many radical scavengers is that they are consumed during the reaction and must be renewed.

A third category has been tested by Goff and Rochelle (2006). Stable salts like KCl, KBr or KCOOH increase the ionic strength of water, so that the solubility of gases in the solvent decreases. However, these salts appeared to be poor inhibitors, decreasing the NH<sub>3</sub> production by only 15% in the best case. They will not be further considered.

### A.2.1 Chelating agents

#### Bicine

*N,N*-diethanolglycine, also called bicine or VFS (Dow Chemical trade name, Versene Fe-3 Specific), is a metal complexant. Johnson and McElwain (1964) reported in a patent that the addition of bicine reduced the emitted amount of air contaminant (supposed to be NH<sub>3</sub>) by 95% over 48 hours at 55°C. No metal had been added to the solution. Blachly and Ravner (1965a) tested bicine in metal-free solutions for 6 weeks at 55°C without observing any degradation.

In the presence of metals, Chi and Rochelle (2002) showed that bicine reduces the NH<sub>3</sub> production rate by 50% in the presence of 56ppm Fe<sup>2+</sup> at both lean and rich loading (figure A.15).

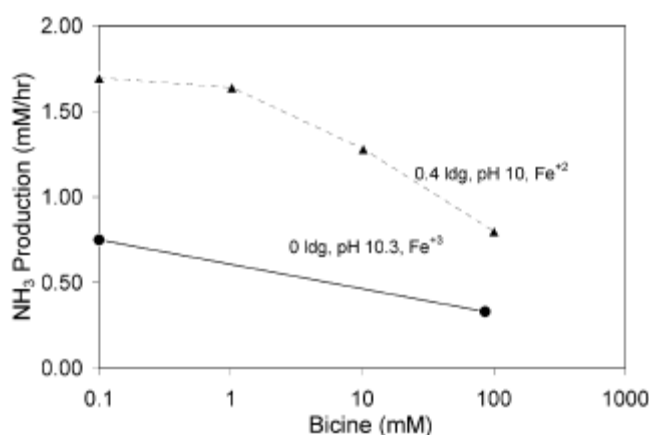


Figure A.15: effect of bicine in presence of 56 ppm Fe<sup>2+</sup> (Chi and Rochelle, 2002)

However, Blachly and Ravner (1965a) noted that 100 mM bicine (1,5 wt%) was not effective in presence of Cu<sup>2+</sup> at concentrations varying from 1 to 15ppm. Finally, Goff and Rochelle

(2003) tested bicine but listed it as an ineffective degradation inhibitor when  $\text{Fe}^{2+}$  and  $\text{Cu}^{2+}$  were both present in solution.

### EDTA

EDTA (EthylenDiamine TetraAcetic Acid) is a well-known chelating agent for metals. Johnson and McElwain (1964) reported that the addition of EDTA reduced the emitted amount of air contaminant (supposed to be  $\text{NH}_3$ ) by 75% over 48 hours at  $55^\circ\text{C}$ .

Chi and Rochelle (2002) have confirmed a mild inhibition effect of EDTA in loaded MEA (20-40% reduction of the  $\text{NH}_3$  formation) at  $55^\circ\text{C}$ . Goff and Rochelle (2003) also observed a reduction by approximately 50% of the  $\text{NH}_3$  production rate at  $55^\circ\text{C}$ .

Blachly and Ravner (1965a) reported that EDTA was only mildly effective (less effective than bicine) into inhibiting MEA oxidation at  $98^\circ\text{C}$  in metal-free solution (Figure A.16, left), as well as in  $\text{Fe}^{2+}$ -spiked solutions. Sexton and Rochelle (2009) showed however that at higher EDTA concentrations (3 wt% instead of 1.5 wt%), MEA oxidative degradation due to  $\text{Fe}^{2+}$  could be completely inhibited.

In the presence of several metals including both  $\text{Fe}^{2+}$  and  $\text{Cu}^{2+}$ , EDTA induced a reduction of the  $\text{NH}_3$  production rate that could not be achieved with bicine alone (Figure A.16, right). The efficient inhibition of  $\text{Cu}^{2+}$ -catalyzed (in comparison with  $\text{Fe}^{2+}$ -catalyzed) degradation has also been observed by Goff and Rochelle (2003, 2004).

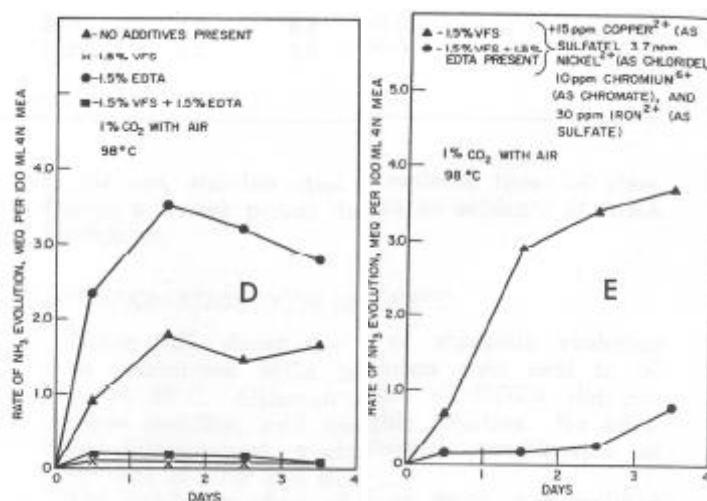


**Figure A.16: effect of EDTA and Bicine on MEA oxidative degradation without (left) and with metals (right)**

According to Chi and Rochelle (2002), EDTA did not show any inhibiting effect in unloaded MEA. Furthermore, Goff and Rochelle (2004) reported that the effect of EDTA decreased with time probably due to EDTA oxidation. According to Sexton and Rochelle (2009), due to continuous corrosion, the endless supply of  $\text{Fe}^{2+}$  may saturate all the EDTA active sites, so that the Fe-EDTA complexes will have to be regularly reclaimed or fresh EDTA will have to be regularly fed to the amine solution.

According to Supap et al. (2011a), the optimal EDTA concentration for inhibiting  $\text{O}_2$  and  $\text{SO}_2$ -induced degradation was 0,07 wt% in metal-free solutions, reducing the MEA degradation rate by 68% in presence of 6ppm  $\text{SO}_2$ . Higher EDTA concentrations induced

more degradation with O<sub>2</sub> and SO<sub>2</sub> as represented in figure A.17. Both CO<sub>2</sub> loaded and unloaded solutions degraded slower under SO<sub>2</sub> and O<sub>2</sub> with EDTA.

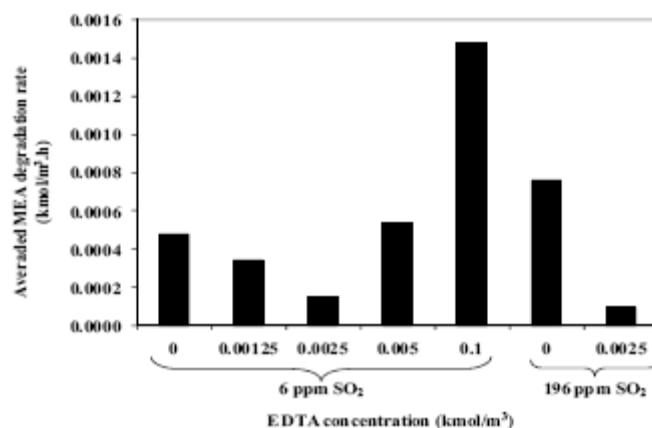


**Figure A.17: effect of EDTA concentration on O<sub>2</sub>-SO<sub>2</sub> induced degradation**

#### *HEDTA*

HEDTA (*N*-HydroxyEthylDiamine TriAcetic acid, trade name Versenol 120) has only been tested by Johnson and McElwain (1964). They reported that HEDTA reduced the emitted amount of air contaminant (supposed to be NH<sub>3</sub>) by 90% over 48hours at 55°C.

#### *TEA*

TriEthanolAmine (TEA) has been patented as a degradation inhibitor for H<sub>2</sub>S and CO<sub>2</sub> degradation by Singh (1970a). The authors observed that at 150°C, the MEA degradation rate over 4 hours was reduced by 85% in presence of TEA. However, no test was performed in the presence of O<sub>2</sub>. An advantage of TEA is that this tertiary amine can absorb CO<sub>2</sub>.

#### *Gluconate*

Singh (1970b) has patented gluconate as degradation inhibitor for H<sub>2</sub>S and CO<sub>2</sub> degradation. He observed that at 150°C, the MEA degradation rate over 4 hours was reduced by 85% in presence of sodium gluconate. However, no test was performed in the presence of O<sub>2</sub>.

#### *Potassium-sodium tartarate*

Supap et al. (2011a) have tested potassium-sodium tartarate (KNaC<sub>4</sub>H<sub>4</sub>O<sub>6</sub>.4H<sub>2</sub>O) in presence of O<sub>2</sub> and SO<sub>2</sub>. In CO<sub>2</sub>-loaded (respectively unloaded) solutions, the MEA degradation rate decreases by 83% (resp. 91%). They also reported that the blending of potassium-sodium tartarate with Na<sub>2</sub>SO<sub>3</sub> produced the best inhibiting results compared to other inhibitors (see figure A.18).

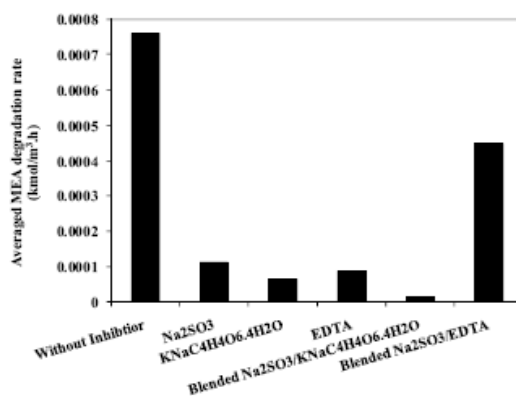


**Figure A.18: comparison of blended potassium-sodium tartarate/Na<sub>2</sub>SO<sub>3</sub> with other inhibitors**

*HEDP, DTPA, DTPMP, citric acid, NTA*

Voice and Rochelle (2011b) screened various inhibitors but they have not published the detailed results of their studies yet (Figure A.19). They have classified the inhibiting potential of chelating agents as following:

DTPA (DiethyleneTriaminePentaAcetic acid) >> EDTA >> NTA (NitriloTriAcetic acid)

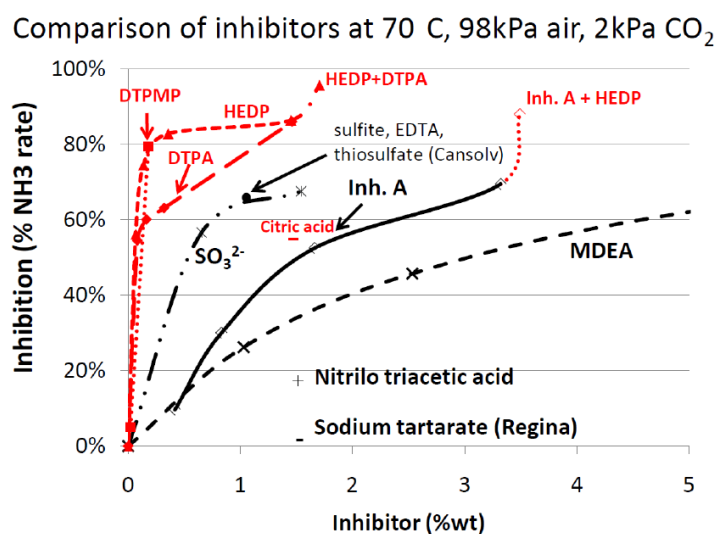


**Figure A.19: screening of new inhibitors (Voice and Rochelle, 2011b)**

On the other side, they also reported HEDP (Etidronic acid, 1-hydroxyethane 1,1-diphosphonic acid), DTPMP (diethylenetriamine penta(methylene phosphonic acid)) and citric acid as promising chelating agents for inhibiting MEA oxidative degradation.

*Conclusion about chelating agents*

Many chelating agents have been studied. First generation ligands have shown their limits:

- Bicine is not stable with Cu<sup>2+</sup>
- EDTA is slowly oxidized with Fe<sup>2+</sup>
- HEDTA, TEA, gluconate still require more studies

Second generation ligands may prove interesting inhibiting effects (Figure A.19):

- Potassium-sodium tartarate presents very interesting properties, especially in combination with  $\text{Na}_2\text{SO}_3$ . This has to be confirmed by further studies.
- HEDP also seems very promising, especially in combination with DTPA.
- Citric acid and NTA seem less interesting

### A.2.2 Radical and $\text{O}_2$ scavengers

#### MDEA

Faucher (1989) first patented the use of MDEA (methylDiEthanolAmine) blended with MEA for inhibiting MEA degradation. Under oxidative conditions, MDEA preferentially reacts with  $\text{O}_2$  to protect MEA, so that the MEA degradation rate is reduced by about 80% (Lawal et al., 2005). To achieve a 90% reduction of the  $\text{NH}_3$  production rate, Voice and Rochelle (2011b) have shown that the MDEA concentration must be equal or higher than 20 wt%. This is much more than conventional inhibitors evocated so far, but it shall be noted that MDEA has the capacity of absorbing  $\text{CO}_2$ . According to McCullough et al. (1990), the combined use of MDEA with Antimony is used to inhibit both corrosion and degradation. Antimony is a rather toxic element that is used in this context as corrosion inhibitor.

MDEA has many disadvantages:

- The amount of degradation products remains high, these products resulting from MDEA degradation (Lawal et al., 2005).
- MEA degradation is slowed down but not stopped (Voice et Rochelle, 2011b).
- The protective effect of MDEA is only active at temperature  $>100^\circ\text{C}$ . At absorber temperatures, MEA degrades more than MDEA (Lawal et al., 2005).

#### Formate and formaldehyde

Formate and formaldehyde are degradation products of MEA oxidative degradation. According to Goff and Rochelle (2006), degradation products may compete with MEA for available oxygen to further react. Chi and Rochelle (2002) and Goff and Rochelle (2004) have not observed a large inhibition effect due to formaldehyde. However, Goff and Rochelle (2006) have observed the inhibition effect of formaldehyde, this effect being larger in presence of  $\text{Cu}^{2+}$  than  $\text{Fe}^{2+}$  (Figure A.20).

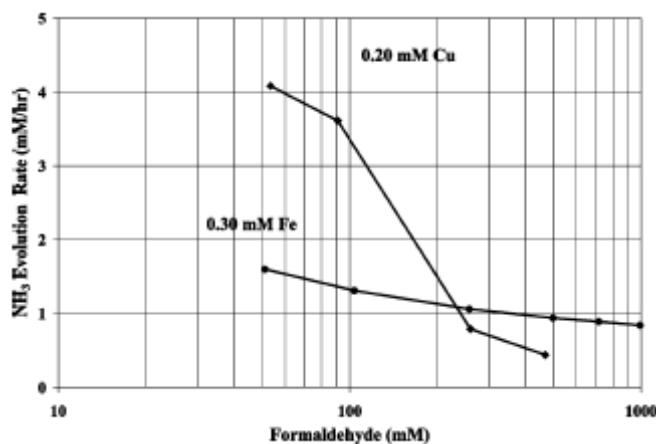
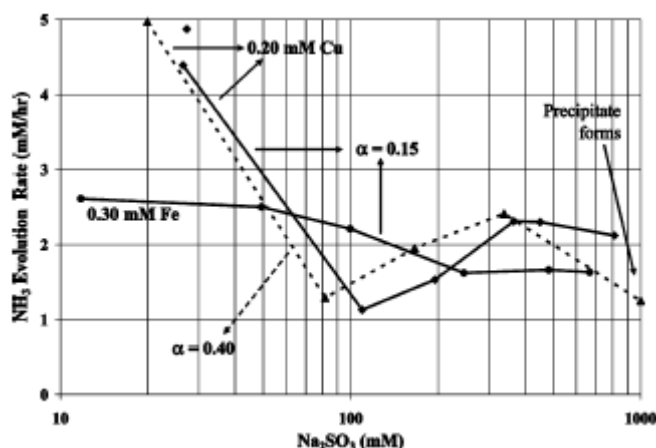


Figure A.20: effect of formaldehyde on  $\text{NH}_3$  evolution rate (Goff and Rochelle, 2006)

However, Sexton and Rochelle (2009) could not confirm those results. They stated that the addition of formaldehyde increased the MEA loss rate by 30%. Similarly, the presence of formate increased the MEA loss rate by 20%.

### $Na_2SO_3$

According to Goff and Rochelle (2006), sulfite (obtained by adding  $Na_2SO_3$ ) is rapidly oxidized into sulfate, competing with MEA for the available  $O_2$ . Goff and Rochelle (2006) have shown in figure A.21 that sulfite can reduce the  $NH_3$  production rate in systems catalyzed by  $Cu^{2+}$  and  $Fe^{2+}$ , achieving a better reduction with  $Cu^{2+}$  systems. However, above a limit concentration ( $\sim 1000mM$ ),  $Na_2SO_3$  is not soluble anymore and precipitates.



**Figure A.21: effect of  $Na_2SO_3$  on  $NH_3$  evolution rate (Goff and Rochelle, 2006)**

Even if sulfite is not very efficient as a degradation inhibitor in comparison to inhibitor A for instance, it would be a cheap degradation inhibitor since it can be derived from  $SO_2$  contained in power plant flue gas (Goff and Rochelle, 2006). Supap et al. (2011a) confirm the benefic effect observed with sulfite on  $O_2$  and  $SO_2$ -induced degradation. They determine the optimal sulfite concentration at  $0.05kmol/m^3$ , i.e. 50mM (Figure A.22).

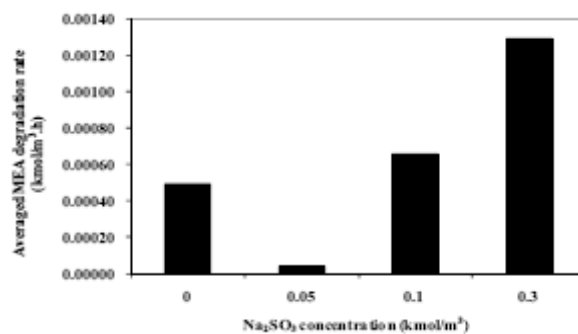


**Figure A.22: effect of  $Na_2SO_3$  concentration on  $NH_3$  evolution rate (Supap et al., 2011a)**

However, Sexton and Rochelle (2009) did not observe any inhibition effect for  $Na_2SO_3$ . They showed that the addition of 100mM sulfite increased the MEA loss rate by 30% in comparison to  $Fe^{2+}$ -catalyzed system.



*NH<sub>2</sub>OH*

NH<sub>2</sub>OH (hydroxylamine) has been tested by Supap et al. (2011a) which propose 25mM as an optimal inhibitor concentration for inhibiting O<sub>2</sub> and SO<sub>2</sub> degradation. No other study has been performed using this interesting inhibitor.

*Inhibitor A*

Inhibitor A is an inorganic additive developed at the University of Texas (Goff and Rochelle, 2006). Inhibitor A possesses at least three different oxidation states, but the reduced oxidation states clearly appear to be more effective (Figure A.23).

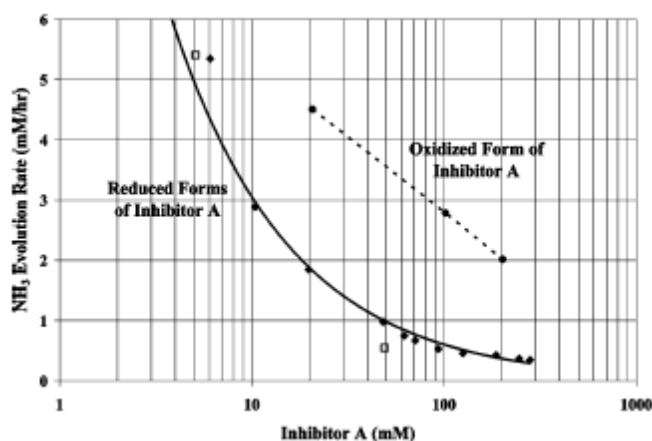


**Figure A.23: effect of oxidation state for inhibitor A (Goff and Rochelle, 2006)**

According to Goff and Rochelle (2006), inhibitor A is very stable at absorber conditions, so that it is not consumed with time. This has been confirmed by Voice and Rochelle (2011b). Goff and Rochelle (2006) described it as a radical scavenger effectively inhibiting MEA oxidative degradation caused by both Fe<sup>2+</sup> and Cu<sup>2+</sup> (Figure A.24). A higher concentration of inhibitor A induces a lower NH<sub>3</sub> evolution rate in all systems.

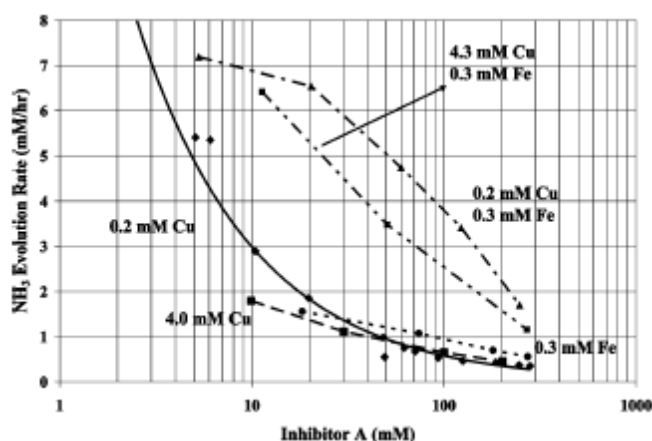


**Figure A.24: effect of inhibitor A on Fe<sup>2+</sup> and Cu<sup>2+</sup> catalyzed degradation**

According to Sexton and Rochelle (2009), the presence of inhibitor A in a Cr<sup>3+</sup>/Ni<sup>2+</sup>-catalyzed system decreased the formation of degradation products by 99%. The MEA losses decreased by 87.5%, approaching the detection limits of the MEA quantification analysis.

In the presence of Fe and Cu, Sexton and Rochelle (2006) observed that proportionally more glycolate was formed in MEA solutions inhibited with inhibitor A, but the amount of carboxylic acid formed is much lower than in inhibitor-free systems.

However, according to Voice and Rochelle (2011a) the inhibiting effect of inhibitor A decreases at higher temperatures in the presence of  $\text{Fe}^{2+}$ ,  $\text{Cr}^{3+}$  and  $\text{Ni}^{2+}$  (Figure A.25), whatever the inhibitor concentration. At  $70^\circ\text{C}$ , steady state in the production rate of  $\text{NH}_3$  was not often observed, even after several days.

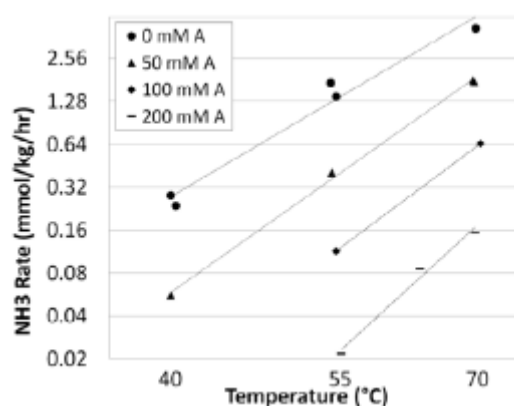


**Figure A.25: effect of temperature and Inhibitor A concentration on  $\text{NH}_3$  evolution**

#### *Inhibitor B*

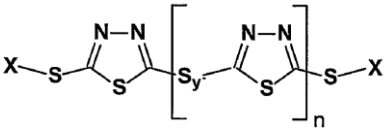
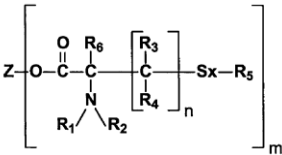
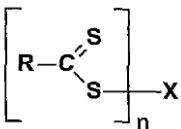
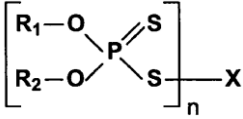
Sexton and Rochelle (2009) have presented inhibitor B as an effective inhibitor for preventing MEA oxidative degradation since it decreased the MEA losses by 75% at  $55^\circ\text{C}$  in  $\text{Fe}^{2+}$ -catalyzed systems. However, it could not reach the efficiency of inhibitor A.

#### *Various sulfur containing products*

IFPEN has patented various sulfur containing inhibitors at  $80^\circ\text{C}$  (Carrette and Delfort, 2009a-b-c; Carrette and Delfort, 2010; Carrette and Delfort, 2011; Delfort and Carrette, 2009a-b). Those inhibitors are listed in Table A.2, as well as their general formula. Based on the formate production rate compared to the uninhibited system, the best inhibitor of each family is presented.

**Table A.2: sulfur-containing inhibitors patented by IFPEN**

| Reference                   | Formula   | Best inhibitor           | Formate reduction |
|-----------------------------|---|--------------------------|-------------------|
| Carrette and Delfort, 2009a | $\text{R}_1 - \left[ \begin{array}{c} \text{R}_3 \\   \\ \text{C} \\   \\ \text{R}_4 \end{array} \right]_n - \text{S}_x - \left[ \begin{array}{c} \text{R}_5 \\   \\ \text{C} \\   \\ \text{R}_6 \end{array} \right]_m - \text{R}_2$  | 2-2'-thiodiethanol       | 99,7%             |
| Carrette and Delfort, 2009b | $\text{R}_1 - \text{C} \begin{array}{c} \text{O} \\    \\ \text{C} \end{array} - \left[ \begin{array}{c} \text{R}_3 \\   \\ \text{C} \\   \\ \text{R}_4 \end{array} \right]_n - \text{S}_x - \left[ \begin{array}{c} \text{R}_5 \\   \\ \text{C} \\   \\ \text{R}_6 \end{array} \right]_m - \text{R}_2$ | 3-3-dithiopropionic acid | 99,8%             |

|   |   |  |                        |
|---|---|--|------------------------|
| Carrette and Delfort, 2009c             |  | DMTD<br>(Dimercaptho-thiadiazole)            | 99,1%                  |
| Carrette and Delfort and Carrette, 2010 |  | Sodium L-Cysteine                            | 82,8%                  |
| Carrette and Delfort, 2011              | Triazole and tetrazole  | All tested inhibitors produced equal results | No MEA losses observed |
| Delfort and Carrette, 2009a             |  | O-O'-Diisopropyl dithiobis(thioformate)      | 98,1%                  |
| Delfort and Carrette, 2009b             |  | ammonium-O,O'-diethyldithiophosphate         | 98,4%                  |

Among the inhibitors presented in Table A.2, only DMTD (Dimercaptho-thiadiazole) has been tested in another study. Voice and Rochelle (2011b) identified DMTD as one of the best inhibitors tested, but they note that it requires additional testing.

#### *Conclusion about radical and O<sub>2</sub> scavenger*

First generation radical scavengers have shown their limits:

- MDEA does not completely prevent MEA degradation
- Formaldehyde, formate and sulfite increased the MEA losses
- Inhibitor A seems to become less effective at higher temperatures (70°C)

Second generation scavengers, especially sulfur containing inhibitors patented by IFP seem however very promising, reducing the amount of degradation products by more than 99%.

#### **A.2.3 Conclusion about degradation inhibitors**

Chelating agents and radical/O<sub>2</sub> scavengers are the two main types of degradation inhibitors. Depending on the operating conditions, both seem to be very promising inhibitors. Combinations of different inhibitors may also lead to excellent inhibition effect.

Chelating agent HEDP (Hydroxyethylidene diphosphonic acid) may advantageously be combined with radical scavengers Inhibitor A or DTPA (diethylenetriamine pentaacetic acid) to decrease the emission of NH<sub>3</sub> at 70°C. Good results were also achieved for DTPMP (diethylenetriamine pentamethylene phosphoric acid), less stable but which can also be used as a corrosion inhibitor and DMTD (dimercaptho-thiadiazole) even if this latest requires more tests.

### *Appendix 3: Risk analysis for the degradation test rig.*

This section describes in French the risk analysis that has been performed for the degradation test rig.

#### **A.3.1 Les locaux et zones de travail**

Le banc de dégradation des solvants CCS construit dans le cadre de la thèse de doctorat de G. Léonard en collaboration avec l'entreprise Laborelec se situe à la Halle de Chimie Appliquée (figure 1) à l'adresse suivante :

Halle de Chimie Appliquée,  
B17, P35, Grande traverse  
4000 Liège Sart-Tilman.  
Tel. : 04/366 44 62

L'accès à la Halle se fait par une porte sur laquelle un affichage indique clairement que l'accès est réservé aux seules personnes autorisées ou accompagnées. En dehors des heures d'ouvertures, cette porte est fermée à clé et une alarme est activée à l'intérieur du bâtiment.



Fig. 1 : B17, Halle de chimie appliquée



Fig. 2 : Porte d'accès à la Halle

Les activités de la halle concernent le génie chimique et génie des procédés. Les principales activités sont les suivantes : études hydrodynamiques de cuves agitées et de colonnes à empilage, tomographie rayons X, isothermes d'adsorption de polluants, séchage de boues d'épuration, ...

Le réacteur de dégradation se situe à l'intérieur d'un local ventilé fermé, lui-même à l'intérieur d'une pièce ouverte sur la Halle (voir plan ci-dessous, figure 3). Il y a 2 entrées / sorties à la Halle, et les flèches rouges sur la figure 3 symbolisent les voies d'évacuation du bâtiment.

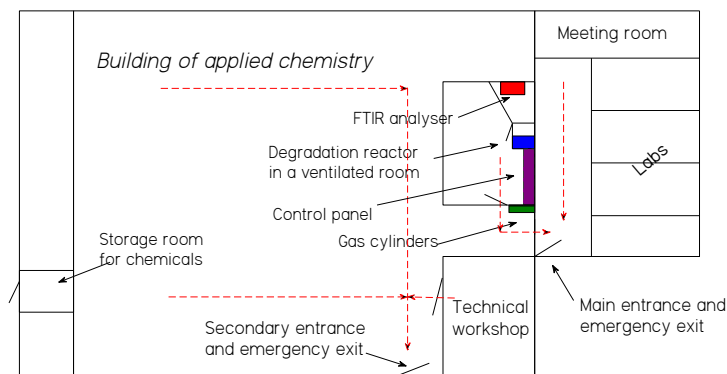


Fig. 3 : Plan de la halle de chimie appliquée

### A.3.2 L'organisation technique entre postes de travail

L'installation de dégradation est composée de quatre parties principales (figures 4 à 7) :

- un local ventilé où se trouvent le réacteur et ses auxiliaires (figure 4)
- dans un deuxième local ventilé voisin de celui où se trouve le réacteur : l'analyseur FTIR (figure 5)
- à côté du local ventilé où se trouve le réacteur : le poste de contrôle, l'analyseur HPLC et les lignes d'arrivée du gaz (figure 6)
- à l'entrée de la pièce ouverte, côté Halle : les bouteilles de gaz et leur centrale de détente (figure 7).



Fig. 4 : local ventilé



Fig. 5 : Analyseur FTIR

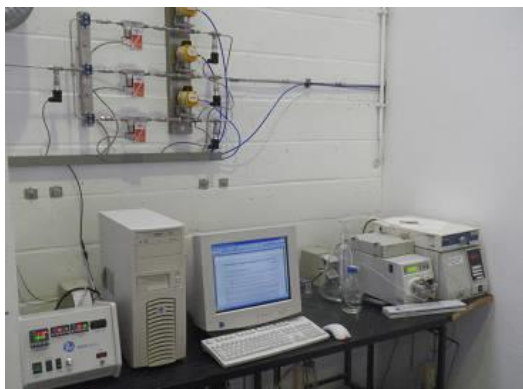


Fig. 6 : Poste de contrôle



Fig. 7 : Rack à bouteilles

Le local ventilé où se situe le réacteur de dégradation peut accueillir une personne qui manipule l'installation. Ce local doit être fermé durant les manipulations entre les expériences ainsi que lors des expériences.

La pièce dans laquelle se situe ce local ventilé est partagée entre deux utilisateurs réguliers. Le premier utilisateur régulier travaille sur l'installation située dans le même local ventilé que l'analyseur FTIR. Le deuxième utilisateur régulier est l'opérateur du banc de dégradation. Occasionnellement, d'autres utilisateurs pénètrent dans cette pièce pour avoir accès aux machines qui s'y trouvent (étuve, centrifugeuse).

Cette pièce a une seule porte d'accès, tout comme le local ventilé. Les voies de circulation dans la pièce sont clairement délimitées. L'accès aux zones de travail se fait sans problème. L'encombrement devra être limité au strict nécessaire, et des rangements réguliers (une fois tous les mois au minimum) seront prévus pour éviter l'accumulation de matériel dans les locaux et zones de travail.

### ***A.3.3 Prévention des accidents de travail***

Les équipements de protection individuelle nécessaires sont disponibles à la halle : tabliers de laboratoires, lunettes de protection, gants adaptés à la manipulation de solutions aminées.

Ils se trouvent dans une armoire située à côté de la porte d'entrée de la pièce ouverte sur la Halle (figure 8). Dans cette armoire se trouve également un flacon de produit nettoyant pour rincer les yeux en cas de contact avec un produit non désirable. La durée de validité de ce produit est contrôlée régulièrement.



Fig. 8 : Equipements de protection individuelle

La boîte de premiers soins se trouve près des toilettes, à côté de la salle de réunion.

La procédure à appliquer en cas d'accident est celle applicable de manière générale dans les laboratoires de l'ULg. Cette procédure est à suivre en cas d'urgence lors d'un fonctionnement défectueux de l'installation de dégradation et dans le cas où les alarmes automatiques ne se seraient pas déclenchées. Cette procédure se trouve en première page de la farde accompagnant l'installation et qui se trouve près du panneau de contrôle.

Le fonctionnement défectueux du banc d'essai est constaté lorsque :

- une fuite importante de gaz ou de liquide audible ou observable par le hublot fixé sur la porte du local ventilé ou sur la ligne de gaz en dehors du local ventilé permet de conclure que l'installation n'est pas dans un mode de fonctionnement habituel ou prévu par l'opérateur, entraînant l'apparition d'un danger potentiel pour le personnel ou le matériel à proximité.
- Une valeur anormale d'un capteur de température ou de pression est constatée, entraînant l'apparition d'un danger potentiel pour le personnel ou le matériel à proximité.
- Un bruit anormal lié à l'installation permet de conclure que l'installation n'est pas dans un mode de fonctionnement habituel ou prévu par l'opérateur, entraînant l'apparition d'un danger potentiel pour le personnel ou le matériel à proximité.
- tout autre élément significatif amenant à cette même conclusion.

La procédure à suivre en cas d'urgence est dès lors la suivante :

1. Arrêt immédiat de l'installation au moyen du bouton d'arrêt d'urgence situé sur la cloison extérieure du local ventilé
2. Arrêt du chauffage du réacteur sur le poste de contrôle situé juste à coté du local ventilé.
3. Fermeture manuelle des vannes de sécurité commandant l'arrivée de gaz au niveau des détendeurs
4. Fermeture manuelle des vannes sur les bouteilles de gaz
5. Si quelqu'un est présent dans le local ventilé où se trouve le réacteur, évacuer ce local en refermant bien la porte
6. Si la ventilation du local ventilé n'est pas activée, mise en route de la ventilation au moyen de l'interrupteur situé sur la cloison extérieure de ce local
7. En cas de danger persistant, évacuer le bâtiment en s'assurant que tout le personnel présent à l'intérieur de la halle est évacué
8. Contacter le service d'urgence au 100 (Service médical d'urgence et pompiers) ou au 112 (numéro d'appel européen en cas d'accident ou d'agression)
9. Contacter le Central d'alarme de l'ULg au numéro 04/366 44 44 (44 44 si appel interne)
10. Contacter le personnel responsable de l'installation au numéro suivant : 04/366 95 92 ou 0487/47 11 35 (GSM Grégoire Léonard).

#### ***A.3.4 Les risques électriques***

L'installation électrique a été effectuée par le personnel qualifié en suivant les normes en vigueur. Différentes protections ont été prévues pour limiter les conséquences de tout dysfonctionnement électrique. Entre-autres :

- un différentiel 30mA protège l'installation et ses utilisateurs en coupant l'alimentation lorsque des courants de fuite sont détectés,
- un fusible coupe le courant en cas de court-circuit ou de surintensité du courant à l'installation

- une prise de terre est établie selon les normes en vigueur et toute l'installation y est électriquement reliée.

L'appareillage électrique se situe dans un coffret facile d'accès à l'intérieur du local ventilé (figure 9). Ce coffret est fermé à clef, mais la clef est facilement accessible en cas de besoin. Un bloc mural de quatre prises électriques est également disponible dans le local ventilé en dessous du coffret électrique. Il convient de prendre garde à ne pas renverser de liquide sur le bloc ou le coffret. Pour limiter ce risque, ces deux éléments ont été placés plus haut que le plan de travail.

Le bouton d'arrêt d'urgence dont il a déjà été question est directement relié au coffret électrique et permet d'en couper l'alimentation simplement et rapidement, sans pour autant couper l'aération du local ventilé qui n'est pas branchée sur le même coffret. Un interrupteur supplémentaire avec voyant lumineux se situe sur la porte du coffret. Ce voyant étant visible à travers le hublot de la porte (figure 10), il est possible de déterminer si l'installation est sous tension ou non sans devoir pénétrer dans le local ventilé.

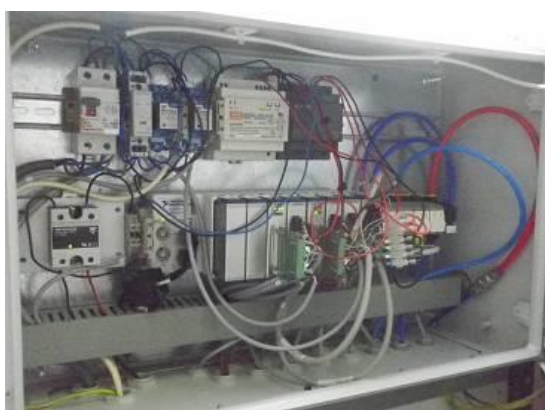


Fig. 9 : Coffret électrique



Fig. 10 : vue du coffret à travers le hublot

### A.3.5 Les risques liés au gaz

Quatre bonbonnes de gaz sont fixées au mur extérieur de la pièce où se trouve le local ventilé. Il s'agit de bouteilles d'air comprimé, d'azote, de dioxyde de carbone et d'oxygène. Les fiches de sécurité relatives à ces gaz sont disponibles dans la farde accompagnant l'installation. Grâce à une identification appropriée (code couleur et plaque signalisatrice), un simple coup d'œil permet de savoir directement quel gaz est contenu dans chacune des bonbonnes. Cette même signalisation est clairement repérable sur chacune des lignes de gaz partant des bonbonnes. De plus, un affichage au-dessus des bouteilles signale les risques liés au gaz de manière explicite (figure 11). Le code couleur est repris dans le tableau ci-dessous et se trouve également dans la farde de l'installation:

| Couleur | Gaz             |
|---------|-----------------|
| Noir    | N <sub>2</sub>  |
| Gris    | CO <sub>2</sub> |
| Blanc   | O <sub>2</sub>  |
| Vert    | Air comprimé    |

Les gaz sont stockés sous forme gazeuse à 200 bars sauf le CO<sub>2</sub> qui est sous forme biphasique à 50 bars. Les bouteilles sont attachées par des chaînes à une armature métallique



(rack) fixée au mur. Une chaîne supplémentaire retenant toutes les bouteilles est sécurisée par un cadenas (figure 12). Les bouteilles se situent à proximité de zones de passage de piétons uniquement, il n'y a pas de risque de passage de transpalette à cet endroit.



Fig. 11 : Affichage du rack à bouteilles



Fig. 12 : Chaîne de sécurité et cadenas

Le transport des bonbonnes se fait avec toutes les précautions d'usage : le capuchon de protection de la valve doit être fixé pour protéger la valve en cas de chute de la bonbonne, le déplacement se fait au moyen d'un diable conçu spécialement pour le transport de bouteilles. Les précautions à appliquer concernant la manipulation des bouteilles de gaz comprimé sont reprises à la fiche 28 p125 de la brochure sur la gestion des risques professionnels (stratégie Sobane) qui se trouve dans la farde de l'installation.

Le cas de fuites de gaz doit être également envisagé. Aucun détecteur n'est prévu car les volumes contenus dans les bouteilles sont faibles et la halle de chimie appliquée est d'un volume assez grand et continuellement aéré, ce qui limite le risque d'accumulation locale de gaz en cas de fuite importante d'un gaz. Les risques d'asphyxie sont très réduits car le volume total de gaz asphyxiant est de 27m<sup>3</sup> (bouteilles de N<sub>2</sub> et CO<sub>2</sub>) et que le volume de la halle est d'approximativement 3400m<sup>3</sup>.

Les fuites d'oxygène ne présentent pas non plus un risque exagéré car aucun élément susceptible de déclencher une étincelle ou d'enflammer le gaz de fuite ne se trouve à proximité immédiate des bonbonnes. Les bouteilles sont éloignées de toute source de chaleur. La température maximale ne doit pas dépasser les 50°C, valeur qui n'est jamais atteinte dans la halle, même en été. De plus, le volume d'oxygène qui serait ajouté à l'atmosphère de la halle en cas de fuite de tout l'oxygène présent de la bouteille ne modifierait la concentration en oxygène de la halle que de 0,3%, n'augmentant pas significativement le risque d'explosion du bâtiment.



Fig. 13 : Centrale de détente azote

La détente des gaz se fait au moyen de centrales de détentes constituée d'une vanne d'arrivée, d'un détendeur, d'une vanne de purge, d'une soupape de sécurité ainsi que d'une vanne de sécurité (figure 13). L'échappement des soupapes de sécurité n'est pas canalisé car la probabilité que ces soupapes soient appelées à fonctionner est très faible. De plus, si une fuite par ces soupapes survenait, celle-ci n'entraînerait pas de danger excessif au vu du paragraphe précédent. Dans le cas de la bouteille d'oxygène, la clé permettant la fixation de la bouteille à la centrale de détente a été enlevée afin d'éviter tout manipulation non autorisée.

La procédure en cas d'urgence en cas de fuite importante de gaz dans le local ventilé a été décrite au point 3. En cas de fuite de gaz en dehors du local ventilé, la procédure d'arrêt d'urgence est identique. En fonction de l'endroit de la fuite, l'ordre des points peut varier.

D'autres protections programmées dans le logiciel de commande renforcent encore la sécurité. Ainsi, la pression sur les lignes de gaz est mesurée en plusieurs endroits et directement communiquée à l'ordinateur qui actionne l'arrêt d'urgence de l'installation en cas de fonctionnement en dehors des limites de sécurité prescrites par l'opérateur. Des dispositifs de purge et de relâchement manuel et/ou automatique de pression sont prévus partout où cela pourrait s'avérer nécessaire :

- soupape de sécurité et vanne de purge sur chacun des détendeurs
- soupape de sécurité et vanne de purge sur l'humidificateur de gaz
- disque de rupture sur le réacteur
- déverseur régulant la pression maximale du réacteur et évacuant le trop-plein de pression vers le conduit d'évacuation des gaz
- soupape de sécurité sur la ligne de gaz en aval du réacteur en protection de l'analyseur FTIR

Avant la mise en service de l'installation, les lignes de gaz sont contrôlées sous pression afin de repérer d'éventuelles fuites. Egalement avant la mise en service, les différents éléments de l'installation (réacteur et humidificateur de gaz) sont éprouvés sous haute pression (30bar) pour s'assurer de leur bonne tenue en cas de dépassement de la pression de consigne (fixée à 25bar au maximum). Ce contrôle pourra être renouvelé tous les ans si le besoin le justifie. Les épreuves sous pression sont décrites dans des fichiers qui seront joints à la présente analyse dès que les tests auront été effectués.

### ***A.3.6 Les risques incendie et explosion***

Les risques d'incendie et d'explosion ont déjà été partiellement abordés aux points 3 et 5. Aucune source de feu ne se trouve directement à proximité des bouteilles. Les risques d'inflammabilité de l'oxygène sont réduits par un nettoyage préalable à l'acétone des conduites et éléments en contact avec l'oxygène. En cas d'incendie dans les bâtiments, la procédure d'arrêt d'urgence de l'installation est celle qui a été décrite au point 3. Un extincteur est disponible dans le couloir d'entrée de la halle, à proximité immédiate de l'installation. La lance incendie la plus proche se trouve dans l'atelier des techniciens et a une longueur suffisante pour atteindre l'installation de dégradation et ses auxiliaires.

En cas de surpression dans le réacteur de dégradation ou sur les lignes de gaz périphériques au réacteur, le risque d'explosion ne peut être négligé. En fonctionnement normal, la pression maximale du réacteur est régulée par un déverseur qui évacue le trop-plein de pression vers le conduit d'évacuation des gaz. Lors des expériences, la pression est mesurée en continu dans le réacteur et à différents endroits des lignes de gaz. En cas de dépassement des valeurs limites de sécurité prescrites par l'opérateur, le système informatique coupe automatiquement l'arrivée de gaz au réacteur. Pour diminuer encore le risque lié à une défaillance informatique ou mécanique, diverses précautions ont été prises :

- Manomètres placés sur le réacteur et sur le saturateur de gaz visibles à travers le hublot depuis l'extérieur du local ventilé.
- Disque de rupture sur le réacteur calibré à 200 bars, dirigé vers le mur en cas de fuite
- Soupape de sécurité calibrée à 2.5 bars sur la ligne gaz en aval du réacteur pour protéger l'analyseur FTIR. La sortie est redirigée vers un conduit d'aération en cas de dépassement de la pression maximale admissible au FTIR.
- Soupape de sécurité calibrée à 40 bars sur le saturateur de gaz et dont la sortie est dirigée vers le mur.

### ***A.3.7 Le stockage des produits chimiques ou biologiques***

La commande des produits chimiques se fait par l'intermédiaire du magasin de produits chimiques de l'ULg. Les produits une fois arrivés sont stockés dans un endroit approprié pour éviter toute dégradation de leur qualité. Le stockage et le transport des produits chimiques se font en conservant l'emballage original de transport.

Selon les cas, le stockage se fait dans un frigo à proximité de l'installation ou dans une pièce ventilée prévue à cet effet en dehors de la halle de chimie appliquée. La présence de produits chimiques en dehors des lieux de stockage est limitée au strict nécessaire. La pièce ventilée prévue pour le stockage des produits chimiques ne disposant pas d'un système d'aération performant, il convient de patienter une à deux minutes entre l'ouverture de la porte de cette pièce et l'entrée dans la pièce.

Les produits chimiques concernés ne présentent pas de risques particuliers lors de leur stockage. Ils sont stockés par famille de risques. Leurs fiches de sécurité se trouvent dans la farde de l'installation. Il n'y a pas manipulation de produits biologiques.

### ***A.3.8 Le matériel de travail, les outils, les machines***

Les surfaces de travail sont en bois traité de type « paillasse de laboratoire » et ne présentent pas de risque de réaction avec les produits manipulés. Les outils de travail sont rangés dans l'atelier des techniciens dans la halle de chimie appliquée. Leur état est régulièrement contrôlé et les travailleurs sont suffisamment formés à leur utilisation.

### ***A.3.9 Les commandes et signaux***

Le panneau de contrôle de l'installation se situe juste à l'extérieur du local ventilé où se trouve le réacteur de dégradation. L'ordinateur permet l'acquisition de données ainsi que le contrôle des lignes de gaz. Un boîtier de contrôle fourni avec le réacteur permet l'acquisition de données ainsi que le contrôle du réacteur. Le panneau de contrôle peut être relié à internet

de sorte que les données lues en direct puissent être consultables par un accès sécurisé depuis n'importe quel ordinateur connecté à internet.

En cas de fonctionnement de l'installation en dehors des limites de sécurité prescrites par l'opérateur, le système informatique coupe automatiquement l'alimentation en gaz du réacteur. Le système de chauffe du réacteur est coupé automatiquement en cas de dépassement des valeurs consignes de température et de pression au sein du réacteur.

#### ***A.3.10 Les positions de travail***

L'installation étant prévue pour pouvoir fonctionner automatiquement, les principales manipulations manuelles auront lieu entre les expériences. Lors du remplissage de l'humidificateur de gaz au moyen d'eau distillée, il conviendra d'utiliser systématiquement un entonnoir pour éviter de renverser de l'eau à proximité de l'installation et des fils électriques environnants. Le réservoir de l'humidificateur sera toujours entièrement vidé avant remplissage et le volume de remplissage sera toujours le même afin d'éviter tout débordement d'eau. La fréquence de remplissage ne dépassera pas une fois tous les trois mois.

#### ***A.3.11 Les efforts et les manutentions***

Pas d'effort ni de manutention spécifiques.

#### ***A.3.12 L'éclairage***

L'éclairage du local ventilé se fait par lumière naturelle au travers d'une plaque de plastique translucide au plafond du local. Un tube lumineux est également prévu, son interrupteur se trouve en dehors du local ventilé, au-dessus de l'interrupteur pour l'aération. En dehors du local ventilé, l'éclairage de la halle est suffisant pour le poste de contrôle.

En cas de coupure brusque de courant, un éclairage de secours situé à proximité de l'installation prend le relais et éclaire le chemin vers la sortie. L'état de charge de cet éclairage secondaire fonctionnant sur batterie est contrôlé régulièrement. De plus, une lampe de poche se trouve dans l'atelier des techniciens dans un endroit facilement accessible dans le noir.

#### ***A.3.13 Le bruit***

Les principaux bruits sont ceux de la ventilation du local et de l'agitateur du réacteur. Ils sont largement en-dessous des limites autorisées. En cas d'arrêt d'urgence de l'installation, les vannes pneumatiques relâchent brusquement de l'air comprimé, laissant entendre un bruit semblable à une détonation d'arme à feu. Afin d'éviter cela, des silencieux d'échappement ont été rajoutés.

#### ***A.3.14 Les ambiances thermiques***

La température est celle de la Halle de Chimie Appliquée. Un système de chauffage est prévu pour l'hiver mais ne fonctionne qu'en mode anti-gel en dehors des heures d'ouverture de la Halle. Il n'y a pas de climatisation en été, mais si nécessaire, les portes de la halle sont maintenues ouvertes pour permettre une circulation supplémentaire d'air. Aucun problème lié à l'humidité n'a été constaté.

### ***A.3.15 Les risques d'exposition aux radiations***

Les radiations infrarouges émises par l'analyseur FTIR sont confinées et l'analyseur dispose de tous les équipements de sécurité nécessaires pour empêcher les radiations en dehors de la cellule d'analyse. Aucune autre source de radiation dangereuse ne se trouve à proximité.

### ***A.3.16 Les risques chimiques***

La liste des produits chimiques utilisés ainsi que les fiches de sécurité associées sont disponibles dans la farde de l'installation, à proximité immédiate du panneau de contrôle de celle-ci.

La manipulation de produits chimiques et la préparation de solutions se fait principalement dans les laboratoires attenants à la halle de chimie appliquée, ainsi que dans le local ventilé pour ce qui concerne la préparation des échantillons pour l'analyse HPLC. Les équipements de travail adéquats sont disponibles dans ces laboratoires. Les produits utilisés sont bien étiquetés et les procédures de préparation des produits chimiques (principalement la préparation d'amines à étudier et d'éluant pour les analyses chromatographiques) sont clairement établies.

Les manipulations de produits chimiques se font en local fermé, sous hotte dans les laboratoires (figure 14), ou en local ventilé quand il s'agit du local où se trouve le réacteur de dégradation. La ventilation mise en place dans ce local fonctionne par aspiration et envoi l'air aspiré directement à l'atmosphère. Cette aération a été testée à plusieurs reprises de manière concluante.

Les équipements de protection individuels sont systématiquement portés (gants et lunettes de protection, blouse de laboratoire). Ces équipements de protection individuelle sont disponibles à proximité de l'installation (voir point 3).

Les déchets chimiques sont triés selon les normes en vigueur à l'ULg, dans des bidons prévus exclusivement à cet effet et clairement annotés (figure 15). Une fois remplis, ils sont déposés sur les lieux de collecte spécifique en échange de récipients neufs.



Fig. 14 : Hotte de laboratoire



Fig. 15 : bidons pour les déchets

### ***A.3.17 Les risques biologiques (bactéries, virus, liquides corporels...)***

Aucun produit biologique n'est utilisé.

### ***A.3.18 Le contenu du travail***

Les procédures de travail sont clairement décrites dans la farde accompagnant l'installation. Ne sont autorisés à travailler sur l'installation de dégradation que l'opérateur principal ou les opérateurs ayant reçu une formation spécifique.

### ***A.3.19 L'organisation du travail***

L'organisation du travail se fait selon les normes en vigueur à l'ULg.

### ***A.3.20 Les contraintes de temps***

L'installation est prévue pour fonctionner en continu, en ce compris les nuits et les week-ends. Concernant le programme de travail, celui-ci est déterminé d'un commun accord entre l'ULg et Laborelec. Ce programme est régulièrement discuté et mis à jour en fonction des résultats intermédiaires.

### ***A.3.21 Les relations de travail au sein du personnel et avec la hiérarchie***

Les décisions se prennent collégalement.

### ***A.3.22 L'environnement psychosocial***

Les conditions de vie et d'environnement psychosocial sont en accord avec les normes en vigueur à l'ULg.



Fig. 16 : installation de dégradation des solvants CCS

Analyse lue et approuvée en janvier 2011 par

Pr. G. Heyen, Promoteur de thèse

M. F. Blandina, Laborelec

M. F. Fyon, Technicien ULg

Mme. A. Grogna, Conseillère en prévention ULg

M. G. Léonard, Doctorant

### Appendix 4: Error analysis

Analytical methods have been evaluated regarding the method uncertainty. For this purpose and when it was possible, the error has been evaluated by measuring seven times the same sample.

#### *FTIR error*

The same NH<sub>3</sub> calibration sample has been analyzed 32 times in two days. The resulting ammonia concentrations are reported in table A.3. The calculated relative standard deviation equals 0.17%.

**Table A.3: reported NH<sub>3</sub> concentrations for a calibration NH<sub>3</sub> sample**

| Day 1                       | Day 2  |
|-----------------------------|--------|
| 174.4                       | 180.3  |
| 175.1                       |        |
| 174.8                       | 180.5  |
| 174.2                       |        |
| 175.2                       | 179.3  |
| 175.3                       |        |
| 174.5                       | 177.7  |
| 175.9                       |        |
| 176.1                       | 176.8  |
| 175.3                       |        |
| 176.5                       | 175.3  |
| 176.3                       |        |
| 176.1                       | 175.7  |
| 176.5                       |        |
| 177.3                       | 175.2  |
| 176.8                       |        |
| 175.7                       | 174.6  |
| 177.3                       |        |
| 176.5                       | 173.7  |
| 175.8                       |        |
| 176.7                       | 172.7  |
| Mean value                  | 176.07 |
| Variancy                    | 2.89   |
| Standard deviation          | 0.3003 |
| Relative standard deviation | 0.0017 |

**HPLC error**

Seven samples of a same solution have been analyzed. The analysis of one of those samples has been repeated 5 times. The resulting relative standard deviation equals 0.5%.

**Table A.4: relative standard deviations of the HPLC quantification of MEA**

| 7 different samples of the same solution | 5 analyses of the same sample |
|--|-------------------------------|
| 30.22                                    | 29.06                         |
| 28.38                                    | 28.13                         |
| 29.43                                    | 28.98                         |
| 29.65                                    | 29.24                         |
| 29.26                                    | 29.38                         |
| 29.43                                    |                               |
| 29.30                                    |                               |
| Mean value                               | 29.21                         |
| Variancy                                 | 0.299                         |
| Standard deviation                       | 0.158                         |
| Relative Standard deviation              | 0.0054                        |

**GC error**

The same sample has been analyzed seven times to determine the relative standard deviations for each component quantified in GC.

**Table A.5: relative standard deviations for GC quantified components**

| Compound | Mean concentration (wt%) | Standard deviation (wt%) | Relative error (%) |
|----------|--------------------------|--------------------------|--------------------|
| HEEDA    | 5.85E-02                 | 7.15E-05                 | 0.12               |
| OZD      | 5.13E-02                 | 9.61E-04                 | 1.87               |
| HEI      | 8.54E-02                 | 2.01E-03                 | 2.36               |
| HEIA     | 5.67E-02                 | 6.65E-04                 | 1.17               |
| HEPO     | 2.94E-01                 | 7.06E-03                 | 2.40               |
| BHEOX    | 3.58E-02                 | 4.30E-03                 | 12.02              |



## Appendix 5: Experimental results

In this section, the detailed amounts of degradation products and residual MEA are reported. The figures presented in Chapter 2 are based on the present results. Missing analyses have been marked with a hyphen.

### A.5.1 Repetition experiments

Two repetition experiments have been performed: one at 100°C and one at 120°C.

| Parameter           | Unit     | 100°C   | 100°C   | 120°C   | 120°C   |
|---------------------|----------|---------|---------|---------|---------|
| Temperature         | °C       | 100     | 100     | 120     | 120     |
| Pressure            | barg     | 4       | 4       | 4       | 4       |
| Agitation rate      | rpm      | 600     | 600     | 600     | 600     |
| Gas feed flow rate  | mNml/min | 160     | 160     | 160     | 160     |
| O2 concentration    | mol %    | 5       | 5       | 5       | 5       |
| CO2 concentration   | mol %    | 15      | 15      | 15      | 15      |
| N2 concentration    | mol %    | 80      | 80      | 80      | 80      |
| Experiment duration | hours    | 168     | 168     | 168     | 168     |
| Initial MEA content | mol      | 1.47    | 1.47    | 1.47    | 1.47    |
| <b>mol T1w</b>      |          |         |         |         |         |
| MEA                 | mol      | 1.4176  | 1.3685  | 1.1594  | 1.1357  |
| HEEDA               | mol      | 0.0000  | 0.0000  | 0.0000  | 0.0017  |
| OZD                 | mol      | 0.0011  | 0.0008  | 0.0016  | 0.0021  |
| HEI                 | mol      | 0.0097  | 0.0104  | 0.0043  | 0.0055  |
| HEIA                | mol      | 0.0000  | 0.0000  | 0.0012  | 0.0000  |
| HEPO                | mol      | 0.0011  | 0.0011  | 0.0051  | 0.0073  |
| BHEOX               | mol      | 0.0000  | 0.0007  | 0.0005  | 0.0012  |
| Total NH3 emission  | mol      | 0.0000  | 0.0332  | 0.1351  | 0.1195  |
| NH4+                | mol      | 0.0000  | 0.0000  | 0.0023  | 0.0000  |
| NO2                 | mol      | 0.0000  | 0.0000  | 0.0000  | 0.0000  |
| NO3                 | mol      | 0.0000  | 0.0000  | 0.0003  | 0.0000  |
| Glycolate           | mol      | 0.0000  | 0.0000  | 0.0000  | 0.0000  |
| Acetate             | mol      | 0.0000  | 0.0000  | 0.0000  | 0.0000  |
| Formate             | mol      | 0.0000  | 0.0000  | 0.0001  | 0.0000  |
| Oxalate             | mol      | 0.0000  | 0.0000  | 0.0001  | 0.0000  |
| H2O                 | mol      | 11.4898 | 11.5040 | 12.9021 | 12.3501 |
| Total N             | mol      | 1.2279  | 1.2377  | 1.2389  | 1.1923  |
| Total C             | mol      | 3.4606  | 3.3415  | 3.3013  | 3.2041  |
| Densité             | kg/L     | 1.10    | 1.09    | 1.08    | 1.08    |
| Fe                  | ppm      | 6.42    | 3.20    | 2.83    | 6.73    |
| Cr                  | ppm      | 1.38    | 1.40    | 1.03    | 1.45    |
| Ni                  | ppm      | 0.79    | 0.71    | 0.34    | 1.24    |
| Mn                  | ppm      | 0.20    | 0.21    | 0.13    | 0.15    |

**A.5.2 Influence of the flue gas composition**

| Parameter                      | Unit    | N <sub>2</sub> | CO <sub>2</sub> - N <sub>2</sub> | O <sub>2</sub> - N <sub>2</sub> | O <sub>2</sub> - CO <sub>2</sub> - N <sub>2</sub> |
|--------------------------------|---------|----------------|----------------------------------|---------------------------------|---|
| Temperature                    | °C      | 120            | 120                              | 120                             | 120   |
| Pressure                       | barg    | 20             | 4                                | 4                               | 4   |
| Agitation rate                 | rpm     | 400            | 600                              | 600                             | 600   |
| Gas feed flow rate             | Nml/min | 200            | 160                              | 160                             | 160   |
| O <sub>2</sub> concentration   | mol %   | 0              | 0                                | 5                               | 5   |
| CO <sub>2</sub> concentration  | mol %   | 0              | 15                               | 0                               | 15  |
| N <sub>2</sub> concentration   | mol %   | 100            | 85                               | 95                              | 80  |
| Experiment duration            | hours   | 216            | 168                              | 168                             | 168   |
| Initial MEA content            | mol     | 1.47           | 1.47                             | 1.47                            | 1.47  |
| <b>Final products amount</b>   |         |                |                                  |                                 |   |
| MEA                            | mol     | 1.4419         | 1.6553                           | 0.9274                          | 1.1594  |
| HEEDA                          | mol     | 0.0000         | 0.0000                           | 0.0000                          | 0.0000  |
| OZD                            | mol     | 0.0000         | 0.0019                           | 0.0005                          | 0.0016  |
| HEI                            | mol     | 0.0000         | 0.0000                           | 0.0128                          | 0.0043  |
| HEIA                           | mol     | 0.0000         | 0.0000                           | 0.0000                          | 0.0012  |
| HEPO                           | mol     | 0.0008         | 0.0000                           | 0.0017                          | 0.0051  |
| BHEOX                          | mol     | 0.0000         | 0.0000                           | 0.0000                          | 0.0005  |
| Total NH <sub>3</sub> emission | mol     | -              | 0.0000                           | 0.2293                          | 0.1351  |
| NH <sub>4</sub> <sup>+</sup>   | mol     | -              | -                                | 0.0015                          | 0.0023  |
| NO <sub>2</sub>                | mol     | -              | -                                | 0.0000                          | 0.0000  |
| NO <sub>3</sub>                | mol     | -              | -                                | 0.0005                          | 0.0003  |
| Glycolate                      | mol     | 0.0001         | -                                | 0.0008                          | 0.0000  |
| Acetate                        | mol     | 0.0000         | -                                | 0.0001                          | 0.0000  |
| Formate                        | mol     | 0.0000         | -                                | 0.0000                          | 0.0001  |
| Oxalate                        | mol     | 0.0000         | -                                | 0.0002                          | 0.0001  |
| H <sub>2</sub> O               | mol     | 10.7074        | 12.3094                          | 13.3990                         | 12.9021   |
| Total N                        | mol     | -              | 1.2811                           | 1.1034                          | 1.2389  |
| Total C                        | mol     | -              | 3.3761                           | 2.8837                          | 3.3013  |
| Density                        | kg/L    | -              | 1.09                             | 1.04                            | 1.08  |
| Fe                             | ppm     | 0.14           | 1.68                             | 0.87                            | 2.83  |
| Cr                             | ppm     | 2.39           | 0.51                             | 1.13                            | 1.03  |
| Ni                             | ppm     | 0.51           | 0.43                             | 0.50                            | 0.34  |
| Mn                             | ppm     | -              | 0.03                             | 0.12                            | 0.13  |

*A.5.3 Influence of the CO<sub>2</sub> concentration*

| Parameter                      | Unit    | 0% CO <sub>2</sub> | 7.5% CO <sub>2</sub> | 15% CO <sub>2</sub> | 30% CO <sub>2</sub> |
|--------------------------------|---------|--------------------|----------------------|---------------------|---------------------|
| Temperature                    | °C      | 120                | 120                  | 120                 | 120                 |
| Pressure                       | barg    | 4                  | 4                    | 4                   | 4                   |
| Agitation rate                 | rpm     | 600                | 600                  | 600                 | 600                 |
| Gas feed flow rate             | Nml/min | 160                | 160                  | 160                 | 160                 |
| O <sub>2</sub> concentration   | mol %   | 5                  | 5                    | 5                   | 5                   |
| CO <sub>2</sub> concentration  | mol %   | 0                  | 7.5                  | 15                  | 30                  |
| N <sub>2</sub> concentration   | mol %   | 95                 | 87.5                 | 80                  | 65                  |
| Experiment duration            | hours   | 168                | 168                  | 168                 | 168                 |
| Initial MEA content            | mol     | 1.47               | 1.47                 | 1.47                | 1.47                |
| <b>Final products amount</b>   |         |                    |                      |                     |                     |
| MEA                            | mol     | 0.9274             | 1.1410               | 1.1594              | 1.1187              |
| HEEDA                          | mol     | 0.0000             | 0.0017               | 0.0000              | 0.0017              |
| OZD                            | mol     | 0.0005             | 0.0019               | 0.0016              | 0.0026              |
| HEI                            | mol     | 0.0128             | 0.0063               | 0.0043              | 0.0067              |
| HEIA                           | mol     | 0.0000             | 0.0011               | 0.0012              | 0.0012              |
| HEPO                           | mol     | 0.0017             | 0.0060               | 0.0051              | 0.0068              |
| BHEOX                          | mol     | 0.0000             | 0.0006               | 0.0005              | 0.0017              |
| Total NH <sub>3</sub> emission | mol     | 0.2293             | 0.1435               | 0.1351              | 0.1286              |
| NH <sub>4</sub> <sup>+</sup>   | mol     | 0.0015             | -                    | 0.0023              | -                   |
| NO <sub>2</sub>                | mol     | 0.0000             | -                    | 0.0000              | -                   |
| NO <sub>3</sub>                | mol     | 0.0005             | -                    | 0.0003              | -                   |
| Glycolate                      | mol     | 0.0008             | -                    | 0.0000              | -                   |
| Acetate                        | mol     | 0.0001             | -                    | 0.0000              | -                   |
| Formate                        | mol     | 0.0000             | -                    | 0.0001              | -                   |
| Oxalate                        | mol     | 0.0002             | -                    | 0.0001              | -                   |
| H <sub>2</sub> O               | mol     | 13.3990            | 12.4477              | 12.9021             | 11.2065             |
| Total N                        | mol     | 1.1034             | 1.1433               | 1.2389              | 1.1569              |
| Total C                        | mol     | 2.8837             | 3.1061               | 3.3013              | 3.2204              |
| Densité                        | kg/L    | 1.04               | 1.07                 | 1.08                | 1.09                |
| Fe                             | ppm     | 0.87               | 6.13                 | 2.83                | 3.96                |
| Cr                             | ppm     | 1.13               | 1.46                 | 1.03                | 1.62                |
| Ni                             | ppm     | 0.50               | 1.48                 | 0.34                | 1.06                |
| Mn                             | ppm     | 0.12               | 0.07                 | 0.13                | 0.23                |

*A.5.4 Influence of the O<sub>2</sub> concentration*

| Parameter                      | Unit    | 0% O <sub>2</sub> | 5% O <sub>2</sub> | 7.5% O <sub>2</sub> | 10% O <sub>2</sub> |
|--------------------------------|---------|-------------------|-------------------|---------------------|--------------------|
| Temperature                    | °C      | 120               | 120               | 120                 | 120                |
| Pressure                       | barg    | 4                 | 4                 | 4                   | 4                  |
| Agitation rate                 | rpm     | 600               | 600               | 600                 | 600                |
| Gas feed flow rate             | Nml/min | 160               | 160               | 160                 | 160                |
| O <sub>2</sub> concentration   | mol %   | 0                 | 5                 | 7.5                 | 10                 |
| CO <sub>2</sub> concentration  | mol %   | 15                | 15.0              | 15                  | 15                 |
| N <sub>2</sub> concentration   | mol %   | 85                | 80.0              | 77.5                | 75                 |
| Experiment duration            | hours   | 168               | 168               | 168                 | 168                |
| Initial MEA content            | mol     | 1.47              | 1.47              | 1.47                | 1.47               |
| <b>Final product amount</b>    |         |                   |                   |                     |                    |
| MEA                            | mol     | 1.6553            | 1.1594            | 0.9284              | 0.6603             |
| HEEDA                          | mol     | 0.0000            | 0.0000            | 0.0016              | 0.0000             |
| OZD                            | mol     | 0.0019            | 0.0016            | 0.0021              | 0.0021             |
| HEI                            | mol     | 0.0000            | 0.0043            | 0.0134              | 0.0370             |
| HEIA                           | mol     | 0.0000            | 0.0012            | 0.0011              | 0.0000             |
| HEPO                           | mol     | 0.0000            | 0.0051            | 0.0058              | 0.0048             |
| BHEOX                          | mol     | 0.0000            | 0.0005            | 0.0010              | 0.0003             |
| Total NH <sub>3</sub> emission | mol     | 0.0000            | 0.1351            | 0.2514              | 0.3005             |
| NH <sub>4</sub> <sup>+</sup>   | mol     | 0.0000            | 0.0023            | 0.0000              | 0.0000             |
| NO <sub>2</sub>                | mol     | 0.0000            | 0.0000            | 0.0000              | 0.0000             |
| NO <sub>3</sub>                | mol     | 0.0000            | 0.0003            | 0.0000              | 0.0000             |
| Glycolate                      | mol     | 0.0000            | 0.0000            | 0.0000              | 0.0000             |
| Acetate                        | mol     | 0.0000            | 0.0000            | 0.0000              | 0.0000             |
| Formate                        | mol     | 0.0000            | 0.0001            | 0.0000              | 0.0000             |
| Oxalate                        | mol     | 0.0000            | 0.0001            | 0.0000              | 0.0000             |
| H <sub>2</sub> O               | mol     | 12.3094           | 12.9021           | 10.7193             | 12.2341            |
| Total N                        | mol     | 1.2811            | 1.2389            | 1.0174              | 0.9640             |
| Total C                        | mol     | 3.3761            | 3.3013            | 3.0402              | 2.9092             |
| Densité                        | kg/L    | 1.09              | 1.08              | 1.09                | 1.07               |
| Fe                             | ppm     | 1.68              | 2.83              | 7.82                | 6.44               |
| Cr                             | ppm     | 0.51              | 1.03              | 2.98                | 1.87               |
| Ni                             | ppm     | 0.43              | 0.34              | 1.28                | 1.60               |
| Mn                             | ppm     | 0.03              | 0.13              | 0.13                | 0.30               |

A.5.5 Influence of the agitation rate, with and without CO<sub>2</sub>

| Parameter                                 | Unit    | 400 rpm        | 600 rpm        | 1000 rpm       | 400 rpm                         | 600 rpm                         | 1380 rpm                        |
|---|---------|----------------|----------------|----------------|---------------------------------|---------------------------------|---------------------------------|
|   |         | O <sub>2</sub> | O <sub>2</sub> | O <sub>2</sub> | O <sub>2</sub> -CO <sub>2</sub> | O <sub>2</sub> -CO <sub>2</sub> | O <sub>2</sub> -CO <sub>2</sub> |
| Temperature                               | °C      | 120            | 120            | 120            | 120                             | 120                             | 120                             |
| Pressure                                  | barg    | 4              | 4              | 4              | 4                               | 4                               | 4                               |
| Agitation rate                            | rpm     | 400            | 600            | 1 000          | 400.00                          | 600.00                          | 1 380.00                        |
| Gas feed flow rate                        | Nml/min | 160            | 160            | 160            | 160                             | 160                             | 160                             |
| O <sub>2</sub> concentration              | mol %   | 5              | 5              | 5              | 5                               | 5                               | 5                               |
| CO <sub>2</sub> concentration             | mol %   | 0              | 0              | 0              | 15                              | 15                              | 15                              |
| N <sub>2</sub> concentration              | mol %   | 95             | 95             | 95             | 80                              | 80                              | 80                              |
| Experiment duration                       | hours   | 336            | 168            | 336            | 336                             | 168                             | 336                             |
| Initial MEA content                       | mol     | 1.48           | 1.47           | 1.47           | 1.47                            | 1.47                            | 1.48                            |
| <b>Product amount T1week</b>              |         |                |                |                |                                 |                                 |                                 |
| MEA                                       | mol     | 1.1719         | 0.9274         | 0.2091         | 1.3600                          | 1.1594                          | 0.2297                          |
| HEEDA                                     | mol     | 0.0000         | 0.0000         | 0.0000         | 0.0000                          | 0.0000                          | 0.0000                          |
| OZD                                       | mol     | 0.0002         | 0.0005         | 0.0061         | 0.0017                          | 0.0016                          | 0.0043                          |
| HEI                                       | mol     | 0.0023         | 0.0128         | 0.0920         | 0.0005                          | 0.0043                          | 0.1109                          |
| HEIA                                      | mol     | 0.0000         | 0.0000         | 0.0000         | 0.0013                          | 0.0012                          | 0.0000                          |
| HEPO                                      | mol     | 0.0011         | 0.0017         | 0.0019         | 0.0056                          | 0.0051                          | 0.0014                          |
| BHEOX                                     | mol     | 0.0000         | 0.0000         | 0.0002         | 0.0006                          | 0.0005                          | 0.0000                          |
| Total NH <sub>3</sub> emission            | mol     | 0.1917         | 0.2293         | 0.6694         | 0.0257                          | 0.1351                          | -                               |
| <b>Product amount T2week</b>              |         |                |                |                |                                 |                                 |                                 |
| MEA                                       | mol     | 9.9E-01        | -              | 2.2E-01        | 1.2E+00                         | -                               | 2.0E-01                         |
| HEEDA                                     | mol     | 0.0E+00        | -              | 0.0E+00        | 0.0E+00                         | -                               | 0.0E+00                         |
| OZD                                       | mol     | 3.6E-04        | -              | 1.1E-02        | 1.8E-03                         | -                               | 4.8E-03                         |
| HEI                                       | mol     | 3.5E-03        | -              | 1.2E-01        | 9.7E-04                         | -                               | 1.1E-01                         |
| HEIA                                      | mol     | 0.0E+00        | -              | 1.6E-03        | 1.5E-03                         | -                               | 0.0E+00                         |
| HEPO                                      | mol     | 3.0E-03        | -              | 1.9E-03        | 1.2E-02                         | -                               | 1.4E-03                         |
| BHEOX                                     | mol     | 4.1E-05        | -              | 2.0E-03        | 1.7E-03                         | -                               | 0.0E+00                         |
| Total NH <sub>3</sub> emission            | mol     | 0.3723         | -              | 0.6752         | 0.0515                          | -                               | -                               |
| <b>Product amount T_end (1 or 2 week)</b> |         |                |                |                |                                 |                                 |                                 |
| NH <sub>4</sub> <sup>+</sup>              | mol     | 0.0005         | 0.0015         | 0.0095         | 0.0008                          | 0.0023                          | 0.0114                          |
| NO <sub>2</sub>                           | mol     | 0.0000         | 0.0000         | 0.0000         | 0.0000                          | 0.0000                          | 0.0000                          |
| NO <sub>3</sub>                           | mol     | 0.0003         | 0.0005         | 0.0000         | 0.0002                          | 0.0003                          | 0.0000                          |
| Glycolate                                 | mol     | 0.0009         | 0.0008         | 0.0004         | 0.0003                          | 0.0000                          | 0.0003                          |
| Acetate                                   | mol     | 0.0000         | 0.0001         | 0.0017         | 0.0000                          | 0.0000                          | 0.0012                          |
| Formate                                   | mol     | 0.0020         | 0.0000         | 0.0118         | 0.0005                          | 0.0001                          | 0.0122                          |
| Oxalate                                   | mol     | 0.0002         | 0.0002         | 0.0024         | 0.0001                          | 0.0001                          | 0.0029                          |
| H <sub>2</sub> O                          | mol     | 12.9882        | 13.3990        | 13.2146        | 13.3731                         | 12.9021                         | 14.6046                         |
| Total N                                   | mol     | 1.1027         | 1.1034         | 0.7674         | 1.2155                          | 1.2389                          | 0.8426                          |
| Total C                                   | mol     | 2.9088         | 2.8837         | 2.4174         | 3.3062                          | 3.3013                          | 2.3536                          |
| Density                                   | kg/L    | 1.039          | 1.04           | 1.06           | 1.09                            | 1.08                            | 1.08                            |
| Fe  | ppm     | 1.43           | 0.87           | 15.2           | 1.40                            | 2.83                            | 37.3                            |
| Cr  | ppm     | 1.26           | 1.13           | 5.29           | 1.26                            | 1.03                            | 7.38                            |
| Ni  | ppm     | 0.52           | 0.50           | 3.57           | 0.44                            | 0.34                            | 4.31                            |
| Mn  | ppm     | 0.12           | 0.12           | 0.80           | 0.20                            | 0.13                            | 0.51                            |

***A.5.6 Influence of the experiment duration***

| Parameter                     | Unit    | 5% O <sub>2</sub> /30% CO <sub>2</sub> | 5% O <sub>2</sub> /15% CO <sub>2</sub> |
|-------------------------------|---------|--|--|
| Temperature                   | °C      | 120                                    | 120                                    |
| Pressure                      | barg    | 4                                      | 4                                      |
| Agitation rate                | rpm     | 600                                    | 600                                    |
| Gas feed flow rate            | Nml/min | 160                                    | 160                                    |
| O <sub>2</sub> concentration  | mol %   | 5                                      | 5                                      |
| CO <sub>2</sub> concentration | mol %   | 30                                     | 15                                     |
| N <sub>2</sub> concentration  | mol %   | 65                                     | 80                                     |
| Experiment duration           | hours   | 168                                    | 168                                    |
| Initial MEA content           | mol     | 1.47                                   | 1.47                                   |

| 5% O <sub>2</sub> /30% CO <sub>2</sub> |     | T=0h  | T=72h  | T=144h  | T=168h |
|--|-----|-------|--------|---------|--------|
| MEA                                    | mol | 1.47  | 1.4667 | 1.1085  | 1.1793 |
| MEA                                    | wt% | 30.00 | 28.28  | 22.2300 | 22.74  |
| HEEDA                                  | mol | 0     | 0.0000 | 0.0000  | 0.0017 |
| OZD                                    | mol | 0     | 0.0019 | 0.0028  | 0.0027 |
| HEI                                    | mol | 0     | 0.0026 | 0.0063  | 0.0071 |
| HEIA                                   | mol | 0     | 0.0000 | 0.0000  | 0.0012 |
| HEPO                                   | mol | 0     | 0.0032 | 0.0064  | 0.0072 |
| BHEOX                                  | mol | 0     | 0.0003 | 0.0016  | 0.0018 |
| 5% O <sub>2</sub> /15% CO <sub>2</sub> |     |       |        |         |        |
| MEA                                    | wt% | 30.34 | 28.09  | -       | 22.67  |

*A.5.7 Influence of the temperature*

| Parameter                   | Unit    | 55°C    | 100°C   | 120°C   | 140°C   |
|-----------------------------|---------|---------|---------|---------|---------|
| Temperature                 | °C      | 55      | 100     | 120     | 140     |
| Pressure                    | barg    | 4       | 4       | 4       | 4       |
| Agitation rate              | rpm     | 600     | 600     | 600     | 600     |
| Gas feed flow rate          | Nml/min | 160     | 160     | 160     | 160     |
| O2 concentration            | mol %   | 5       | 5       | 5       | 5       |
| CO2 concentration           | mol %   | 15      | 15      | 15      | 15      |
| N2 concentration            | mol %   | 80      | 80      | 80      | 80      |
| Experiment duration         | hours   | 168     | 168     | 168     | 168     |
| Initial MEA content         | mol     | 1.47    | 1.47    | 1.47    | 1.47    |
| <b>Final product amount</b> |         |         |         |         |         |
| MEA                         | mol     | 1.5161  | 1.3685  | 1.1594  | 0.9703  |
| HEEDA                       | mol     | 0.0000  | 0.0000  | 0.0000  | 0.0019  |
| OZD                         | mol     | 0.0004  | 0.0008  | 0.0016  | 0.0010  |
| HEI                         | mol     | 0.0003  | 0.0104  | 0.0043  | 0.0009  |
| HEIA                        | mol     | 0.0012  | 0.0000  | 0.0012  | 0.0019  |
| HEPO                        | mol     | 0.0006  | 0.0011  | 0.0051  | 0.0190  |
| BHEOX                       | mol     | 0.0000  | 0.0007  | 0.0005  | 0.0011  |
| Total NH3 emission          | mol     | 0.0060  | 0.0332  | 0.1351  | 0.1674  |
| NH4+                        | mol     | 0.0025  | 0.0000  | 0.0023  | 0.0011  |
| NO2                         | mol     | 0.0000  | 0.0000  | 0.0000  | 0.0000  |
| NO3                         | mol     | 0.0000  | 0.0000  | 0.0003  | 0.0004  |
| Glycolate                   | mol     | 0.0003  | 0.0000  | 0.0000  | 0.0003  |
| Acetate                     | mol     | 0.0000  | 0.0000  | 0.0000  | 0.0001  |
| Formate                     | mol     | 0.0000  | 0.0000  | 0.0001  | 0.0009  |
| Oxalate                     | mol     | 0.0000  | 0.0000  | 0.0001  | 0.0001  |
| H2O                         | mol     | 12.7871 | 11.5040 | 12.9021 | 12.7208 |
| Total N                     | mol     | 1.4472  | 1.2377  | 1.2389  | 1.0940  |
| Total C                     | mol     | 3.7044  | 3.3415  | 3.3013  | 2.9917  |
| Densité                     | kg/L    | 1.11    | 1.09    | 1.08    | 1.06    |
| Fe                          | ppm     | 0.71    | 3.20    | 2.83    | 2.52    |
| Cr                          | ppm     | 0.51    | 1.40    | 1.03    | 1.79    |
| Ni                          | ppm     | 0.09    | 0.71    | 0.34    | 0.88    |
| Mn                          | ppm     | 0.05    | 0.21    | 0.13    | 0.22    |

*A.5.8 Influence of dissolved metals*

| Parameter                     | Unit    | Base case |                       |         |         |
|-------------------------------|---------|-----------|-----------------------|---------|---------|
|                               |         | Base case | Base case with metals | Pilot 1 | Pilot 2 |
| Temperature                   | °C      | 120       | 120                   | -       | -       |
| Pressure                      | barg    | 4         | 4                     | -       | -       |
| Agitation rate                | rpm     | 600       | 600                   | -       | -       |
| Gas feed flow rate            | Nml/min | 160       | 160                   | -       | -       |
| O2 concentration              | mol %   | 5         | 5                     | -       | -       |
| CO2 concentration             | mol %   | 15        | 15                    | -       | -       |
| N2 concentration              | mol %   | 80        | 80                    | -       | -       |
| Experiment duration           | hours   | 168       | 168                   | -       | -       |
| Initial MEA content           | mol     | 1.47      | 1.47                  | -       | -       |
| <b>Final products amounts</b> |         |           |                       |         |         |
| MEA                           | mol     | 1.1594    | 0.9861                | 0.5377  | 1.4710  |
| HEEDA                         | mol     | 0.0000    | 0.0000                | 0.0017  | 0.0017  |
| OZD                           | mol     | 0.0016    | 0.0025                | 0.0013  | 0.0018  |
| HEI                           | mol     | 0.0043    | 0.0145                | 0.0038  | 0.0024  |
| HEIA                          | mol     | 0.0012    | 0.0000                | 0.0012  | 0.0013  |
| HEPO                          | mol     | 0.0051    | 0.0068                | 0.0089  | 0.0063  |
| BHEOX                         | mol     | 0.0005    | 0.0014                | 0.0012  | 0.0006  |
| Total NH3 emission            | mol     | 0.1351    | 0.1967                | -       | -       |
| NH4+                          | mol     | 0.0023    | 0.0029                | 0.0007  | 0.0015  |
| NO2                           | mol     | 0.0000    | 0.0000                | 0.0000  | 0.0000  |
| NO3                           | mol     | 0.0003    | 0.0005                | 0.0022  | 0.0012  |
| Glycolate                     | mol     | 0.0000    | 0.0004                | 0.0004  | 0.0004  |
| Acetate                       | mol     | 0.0000    | 0.0000                | 0.0000  | 0.0000  |
| Formate                       | mol     | 0.0001    | 0.0011                | 0.0031  | 0.0026  |
| Oxalate                       | mol     | 0.0001    | 0.0002                | 0.0000  | 0.0000  |
| H2O                           | mol     | 12.9021   | 13.0381               | 13.6306 | 10.7757 |
| Total N                       | mol     | 1.2389    | 1.0903                | 0.8326  | 1.5301  |
| Total C                       | mol     | 2.8297    | 2.7390                | 2.3737  | 3.8573  |
| Densité                       | kg/L    | 1.08      | 1.08                  | 1.07    | 1.08    |
| Fe                            | ppm     | 2.83      | 21                    | 564     | 361     |
| Cr                            | ppm     | 1.03      | 5.745                 | 136.52  | 61.9    |
| Ni                            | ppm     | 0.34      | 5.68                  | 68.1    | 36.5    |
| Mn                            | ppm     | 0.13      | 2.985                 | 11.825  | 7.01    |



*A.5.9 Influence of degradation inhibitors*

| Parameter                     | Unit    | B.C. with metals |         |              |         |         |
|-------------------------------|---------|------------------|---------|--------------|---------|---------|
|                               |         | Inh. A           | DMTD    | Inh. A/ HEDP | HEDP    |         |
| Temperature                   | °C      | 120              | 120     | 120          | 120     | 120     |
| Pressure                      | barg    | 20               | 4       | 4            | 4       | 4       |
| Agitation rate                | rpm     | 400              | 600     | 600          | 600     | 600     |
| Gas feed flow rate            | Nml/min | 200              | 160     | 160          | 160     | 160     |
| O2 concentration              | mol %   | 5                | 5       | 5            | 5       | 5       |
| CO2 concentration             | mol %   | 15               | 15      | 15           | 15      | 15      |
| N2 concentration              | mol %   | 80               | 80      | 80           | 80      | 80      |
| Experiment duration           | hours   | 168              | 168     | 168          | 168     | 168     |
| Initial MEA content           | mol     | 1.47             | 1.47    | 1.47         | 1.47    | 1.48    |
| <b>Final products amounts</b> |         |                  |         |              |         |         |
| MEA                           | mol     | 0.9861           | 1.5278  | 1.4547       | 1.4257  | 1.0147  |
| HEEDA                         | mol     | 0.0000           | 0.0000  | 0.0000       | 0.0000  | 0.0000  |
| OZD                           | mol     | 0.0025           | 0.0014  | 0.0045       | 0.0016  | 0.0020  |
| HEI                           | mol     | 0.0145           | 0.0000  | 0.0000       | 0.0000  | 0.0160  |
| HEIA                          | mol     | 0.0000           | 0.0000  | 0.0013       | 0.0000  | 0.0000  |
| HEPO                          | mol     | 0.0068           | 0.0025  | 0.0013       | 0.0039  | 0.0062  |
| BHEOX                         | mol     | 0.0014           | 0.0000  | 0.0001       | 0.0000  | 0.0005  |
| Total NH3 emission            | mol     | 0.1967           | 0.0032  | 0.0038       | 0.0065  | 0.1577  |
| NH4+                          | mol     | 0.0029           | 0.0000  | 0.0010       | 0.0004  | 0.0035  |
| NO2                           | mol     | 0.0000           | 0.0000  | 0.0000       | 0.0000  | 0.0000  |
| NO3                           | mol     | 0.0005           | 0.0000  | 0.0001       | 0.0003  | 0.0005  |
| Glycolate                     | mol     | 0.0004           | 0.0005  | 0.0002       | 0.0004  | 0.0003  |
| Acetate                       | mol     | 0.0000           | 0.0000  | 0.0002       | 0.0000  | 0.0001  |
| Formate                       | mol     | 0.0011           | 0.0001  | 0.0001       | 0.0007  | 0.0010  |
| Oxalate                       | mol     | 0.0002           | 0.0000  | 0.0000       | 0.0001  | 0.0002  |
| H2O                           | mol     | 13.0381          | 13.0185 | 11.8792      | 11.8362 | 12.5850 |
| Total N                       | mol     | 1.0903           | 1.2558  | 1.2933       | 1.2660  | 1.1232  |
| Total C                       | mol     | 3.1955           | 3.3649  | 3.3970       | 3.2758  | 3.1330  |
| Densité                       | kg/L    | 1.08             | 1.09    | 1.08         | 1.09    | 1.08    |
| Fe                            | ppm     | 21               | 29.5    | 42.2         | 50.7    | 50.9    |
| Cr                            | ppm     | 5.745            | 3.11    | 3.29         | 2.38    | 5.12    |
| Ni                            | ppm     | 5.68             | 5.13    | 5.47         | 5.92    | 5.80    |
| Mn                            | ppm     | 2.985            | 1.07    | 1.60         | 2.52    | 2.17    |

*A.5.10 Influence of CO<sub>2</sub> loading and metals in batch experiments*

| Parameter               | Unit | MEA     | MEA-CO <sub>2</sub> | MEA-metal mix | MEA-CO <sub>2</sub> -metal mix |
|-------------------------|------|---------|---------------------|---------------|--------------------------------|
| Temperature             | °C   | 140     | 140                 | 140           | 140                            |
| CO <sub>2</sub> loading | -    | no      | yes                 | no            | yes                            |
| <b>T0</b>               |      |         |                     |               |                                |
| MEA                     | mol  | 0.49    | 0.45                | 0.50          | 0.44                           |
| HEEDA                   | mol  | 0.0E+00 | 0.0E+00             | 0.0E+00       | 0.0E+00                        |
| OZD                     | mol  | 0.0E+00 | 0.0E+00             | 0.0E+00       | 0.0E+00                        |
| HEI                     | mol  | 0.0E+00 | 0.0E+00             | 0.0E+00       | 0.0E+00                        |
| HEIA                    | mol  | 0.0E+00 | 0.0E+00             | 0.0E+00       | 0.0E+00                        |
| HEPO                    | mol  | 0.0E+00 | 0.0E+00             | 0.0E+00       | 0.0E+00                        |
| BHEOX                   | mol  | 0.0E+00 | 0.0E+00             | 0.0E+00       | 0.0E+00                        |
| <b>T=1week</b>          |      |         |                     |               |                                |
| MEA                     | mol  | 0.48    | 0.39                | 0.49          | 0.38                           |
| HEEDA                   | mol  | 0.0E+00 | 5.4E-03             | 0.0E+00       | 6.5E-03                        |
| OZD                     | mol  | 0.0E+00 | 1.2E-03             | 0.0E+00       | 1.5E-03                        |
| HEI                     | mol  | 0.0E+00 | 0.0E+00             | 0.0E+00       | 0.0E+00                        |
| HEIA                    | mol  | 0.0E+00 | 8.5E-03             | 0.0E+00       | 8.5E-03                        |
| HEPO                    | mol  | 0.0E+00 | 0.0E+00             | 0.0E+00       | 0.0E+00                        |
| BHEOX                   | mol  | 0.0E+00 | 0.0E+00             | 0.0E+00       | 0.0E+00                        |
| <b>T=2weeks</b>         |      |         |                     |               |                                |
| MEA                     | mol  | 0.47    | 0.33                | 0.49          | 0.32                           |
| HEEDA                   | mol  | 8.2E-04 | 5.3E-03             | 0.0E+00       | 9.1E-03                        |
| OZD                     | mol  | 0.0E+00 | 1.2E-03             | 0.0E+00       | 1.1E-03                        |
| HEI                     | mol  | 0.0E+00 | 0.0E+00             | 0.0E+00       | 0.0E+00                        |
| HEIA                    | mol  | 0.0E+00 | 1.8E-02             | 0.0E+00       | 1.9E-02                        |
| HEPO                    | mol  | 0.0E+00 | 0.0E+00             | 0.0E+00       | 0.0E+00                        |
| BHEOX                   | mol  | 9.1E-05 | 0.0E+00             | 0.0E+00       | 0.0E+00                        |
| <b>T=3weeks</b>         |      |         |                     |               |                                |
| MEA                     | mol  | 0.47    | 0.28                | 0.46          | 0.28                           |
| HEEDA                   | mol  | 6.7E-04 | 4.7E-03             | 0.0E+00       | 7.1E-03                        |
| OZD                     | mol  | 0.0E+00 | 8.0E-04             | 0.0E+00       | 7.6E-04                        |
| HEI                     | mol  | 0.0E+00 | 0.0E+00             | 0.0E+00       | 0.0E+00                        |
| HEIA                    | mol  | 3.9E-04 | 2.6E-02             | 3.8E-04       | 2.7E-02                        |
| HEPO                    | mol  | 0.0E+00 | 0.0E+00             | 0.0E+00       | 0.0E+00                        |
| BHEOX                   | mol  | 1.0E-05 | 0.0E+00             | 0.0E+00       | 0.0E+00                        |
| Fe                      | ppm  | 4.88    | 23.6                | 66.9          | 53.6                           |
| Cr                      | ppm  | 2.37    | 9.13                | 8.75          | 7.37                           |
| Ni                      | ppm  | 2.83    | 6.7                 | 11.3          | 8.6                            |
| Mn                      | ppm  | 0.11    | 0.9                 | 2.12          | 1.89                           |

*A.5.11 Influence of temperature and oxidative degradation products in batch experiments*

| Parameter               | Unit | Fresh MEA<br>120°C | Fresh MEA<br>140°C | Degraded MEA<br>120°C | Degraded MEA<br>140°C |
|-------------------------|------|--------------------|--------------------|-----------------------|-----------------------|
| Temperature             | °C   | 120                | 140                | 120                   | 140                   |
| CO <sub>2</sub> loading | -    | yes                | yes                | yes                   | yes                   |
| <b>T0</b>               |      |                    |                    |                       |                       |
| MEA                     | mol  | 0.45               | 0.45               | 0.46                  | 0.46                  |
| HEEDA                   | mol  | 0.0E+00            | 0.0E+00            | 0.0E+00               | 0.0E+00               |
| OZD                     | mol  | 0.0E+00            | 0.0E+00            | 2.9E-04               | 3.0E-04               |
| HEI                     | mol  | 0.0E+00            | 0.0E+00            | 6.4E-04               | 6.6E-04               |
| HEIA                    | mol  | 0.0E+00            | 0.0E+00            | 0.0E+00               | 0.0E+00               |
| HEPO                    | mol  | 0.0E+00            | 0.0E+00            | 1.4E-03               | 1.4E-03               |
| BHEOX                   | mol  | 0.0E+00            | 0.0E+00            | 2.2E-04               | 2.9E-04               |
| <b>T=1week</b>          |      |                    |                    |                       |                       |
| MEA                     | mol  | 0.44               | 0.39               | 0.43                  | 0.41                  |
| HEEDA                   | mol  | 7.3E-04            | 5.4E-03            | 0.0E+00               | 1.2E-03               |
| OZD                     | mol  | 7.2E-04            | 1.2E-03            | 7.8E-04               | 7.4E-04               |
| HEI                     | mol  | 0.0E+00            | 0.0E+00            | 6.9E-04               | 5.9E-04               |
| HEIA                    | mol  | 0.0E+00            | 8.5E-03            | 3.9E-04               | 2.7E-03               |
| HEPO                    | mol  | 0.0E+00            | 0.0E+00            | 1.3E-03               | 1.0E-03               |
| BHEOX                   | mol  | 0.0E+00            | 0.0E+00            | 8.3E-04               | 1.5E-03               |
| <b>T=2weeks</b>         |      |                    |                    |                       |                       |
| MEA                     | mol  | 0.44               | 0.33               | 0.44                  | 0.37                  |
| HEEDA                   | mol  | 1.0E-03            | 5.3E-03            | 6.8E-04               | 3.6E-03               |
| OZD                     | mol  | 7.0E-04            | 1.2E-03            | 5.6E-04               | 7.7E-04               |
| HEI                     | mol  | 0.0E+00            | 0.0E+00            | 5.6E-04               | 6.5E-04               |
| HEIA                    | mol  | 7.8E-04            | 1.8E-02            | 5.7E-04               | 1.1E-02               |
| HEPO                    | mol  | 0.0E+00            | 0.0E+00            | 1.2E-03               | 1.5E-03               |
| BHEOX                   | mol  | 0.0E+00            | 0.0E+00            | 1.1E-03               | 1.6E-03               |
| <b>T=3weeks</b>         |      |                    |                    |                       |                       |
| MEA                     | mol  | 0.43               | 0.28               | 0.43                  | 0.32                  |
| HEEDA                   | mol  | 3.2E-03            | 4.7E-03            | 1.3E-03               | 3.5E-03               |
| OZD                     | mol  | 7.4E-04            | 8.0E-04            | 7.3E-04               | 4.8E-04               |
| HEI                     | mol  | 0.0E+00            | 0.0E+00            | 7.3E-04               | 5.2E-04               |
| HEIA                    | mol  | 1.6E-03            | 2.6E-02            | 1.0E-03               | 1.0E-02               |
| HEPO                    | mol  | 0.0E+00            | 0.0E+00            | 1.6E-03               | 1.3E-03               |
| BHEOX                   | mol  | 0.0E+00            | 0.0E+00            | 1.3E-03               | 9.1E-04               |
| Fe                      | ppm  | 11.5               | 23.6               | 1220                  | 431                   |
| Cr                      | ppm  | 2.57               | 9.13               | 283                   | 66.1                  |
| Ni                      | ppm  | 1.84               | 6.7                | 251                   | 45.3                  |
| Mn                      | ppm  | 0.35               | 0.9                | 27.8                  | 7.72                  |

**A.5.12 Influence of degradation inhibitors in batch experiments**

| Parameter               | Unit | No inhibitor | Inh. A  | HEDP    | DMTD    | TDE     | DTPA    | DTDP    | Inh.A/HEDP | HEDP + metals | Inh. A + metals |
|-------------------------|------|--------------|---------|---------|---------|---------|---------|---------|------------|---------------|-----------------|
| Temperature             | °C   | 140          | 140     | 140     | 140     | 140     | 140     | 140     | 140        | 140           | 140             |
| CO <sub>2</sub> loading | -    | yes          | yes     | yes     | yes     | yes     | yes     | yes     | yes        | yes           | yes             |
| <b>T0</b>               |      |              |         |         |         |         |         |         |            |               |                 |
| MEA                     | mol  | 0.45         | 0.45    | 0.44    | 0.45    | 0.45    | 0.45    | 0.45    | 0.45       | 0.44          | 0.45            |
| HEEDA                   | mol  | 0.0E+00      | 0.0E+00 | 0.0E+00 | 0.0E+00 | 0.0E+00 | 0.0E+00 | 0.0E+00 | 0.0E+00    | 0.0E+00       | 0.0E+00         |
| OZD                     | mol  | 0.0E+00      | 0.0E+00 | 0.0E+00 | 0.0E+00 | 0.0E+00 | 0.0E+00 | 0.0E+00 | 0.0E+00    | 0.0E+00       | 0.0E+00         |
| HEI                     | mol  | 0.0E+00      | 0.0E+00 | 0.0E+00 | 0.0E+00 | 0.0E+00 | 0.0E+00 | 0.0E+00 | 0.0E+00    | 0.0E+00       | 0.0E+00         |
| HEIA                    | mol  | 0.0E+00      | 0.0E+00 | 0.0E+00 | 0.0E+00 | 0.0E+00 | 0.0E+00 | 0.0E+00 | 0.0E+00    | 0.0E+00       | 0.0E+00         |
| HEPO                    | mol  | 0.0E+00      | 0.0E+00 | 0.0E+00 | 0.0E+00 | 0.0E+00 | 0.0E+00 | 0.0E+00 | 0.0E+00    | 0.0E+00       | 0.0E+00         |
| BHEOX                   | mol  | 0.0E+00      | 0.0E+00 | 0.0E+00 | 0.0E+00 | 0.0E+00 | 0.0E+00 | 0.0E+00 | 0.0E+00    | 0.0E+00       | 0.0E+00         |
| <b>T=1week</b>          |      |              |         |         |         |         |         |         |            |               |                 |
| MEA                     | mol  | 0.39         | 0.40    | 0.40    | 0.36    | 0.40    | 0.34    | 0.36    | 0.38       | 0.37          | 0.40            |
| HEEDA                   | mol  | 5.4E-03      | 5.5E-03 | 5.1E-03 | 7.6E-03 | 5.8E-03 | 7.4E-03 | 6.8E-03 | 6.6E-03    | 5.6E-03       | 6.5E-03         |
| OZD                     | mol  | 1.2E-03      | 1.4E-03 | 9.8E-04 | 1.1E-03 | 1.2E-03 | 7.1E-04 | 9.7E-04 | 6.8E-04    | 1.1E-03       | 8.6E-04         |
| HEI                     | mol  | 0.0E+00      | 0.0E+00 | 0.0E+00 | 1.4E-04 | 0.0E+00 | 0.0E+00 | 0.0E+00 | 0.0E+00    | 0.0E+00       | 0.0E+00         |
| HEIA                    | mol  | 8.5E-03      | 8.2E-03 | 6.0E-03 | 1.3E-02 | 6.4E-03 | 1.2E-02 | 9.1E-03 | 8.4E-03    | 7.5E-03       | 5.5E-03         |
| HEPO                    | mol  | 0.0E+00      | 0.0E+00 | 0.0E+00 | 2.9E-04 | 0.0E+00 | 0.0E+00 | 2.4E-04 | 0.0E+00    | 0.0E+00       | 2.1E-04         |
| BHEOX                   | mol  | 0.0E+00      | 0.0E+00 | 0.0E+00 | 0.0E+00 | 0.0E+00 | 2.5E-04 | 0.0E+00 | 1.1E-04    | 0.0E+00       | 0.0E+00         |
| <b>T=2weeks</b>         |      |              |         |         |         |         |         |         |            |               |                 |
| MEA                     | mol  | 0.33         | 0.34    | 0.34    | 0.28    | 0.33    | 0.29    | 0.29    | 0.31       | 0.33          | 0.33            |
| HEEDA                   | mol  | 5.3E-03      | 5.2E-03 | 5.5E-03 | 7.0E-03 | 7.8E-03 | 7.2E-03 | 6.9E-03 | 6.8E-03    | 6.1E-03       | 8.2E-03         |
| OZD                     | mol  | 1.2E-03      | 8.4E-04 | 1.5E-03 | 5.3E-04 | 1.2E-03 | 7.2E-04 | 7.4E-04 | 6.1E-04    | 1.3E-03       | 7.7E-04         |
| HEI                     | mol  | 0.0E+00      | 0.0E+00 | 0.0E+00 | 2.1E-04 | 0.0E+00 | 0.0E+00 | 1.2E-04 | 0.0E+00    | 0.0E+00       | 7.5E-05         |
| HEIA                    | mol  | 1.8E-02      | 1.6E-02 | 1.3E-02 | 2.2E-02 | 1.5E-02 | 1.8E-02 | 1.8E-02 | 1.5E-02    | 1.9E-02       | 1.4E-02         |
| HEPO                    | mol  | 0.0E+00      | 0.0E+00 | 0.0E+00 | 2.6E-04 | 2.1E-04 | 2.1E-04 | 2.0E-04 | 2.2E-04    | 0.0E+00       | 2.5E-04         |
| BHEOX                   | mol  | 0.0E+00      | 0.0E+00 | 0.0E+00 | 0.0E+00 | 0.0E+00 | 0.0E+00 | 0.0E+00 | -3.5E-06   | 0.0E+00       | 0.0E+00         |

| Parameter               | Unit | No inhibitor | Inh. A  | HEDP    | DMTD    | TDE     | DTPA    | DTDP    | Inh.A/HEDP | HEDP + metals | Inh. A + metals |
|-------------------------|------|--------------|---------|---------|---------|---------|---------|---------|------------|---------------|-----------------|
| Temperature             | °C   | 140          | 140     | 140     | 140     | 140     | 140     | 140     | 140        | 140           | 140             |
| CO <sub>2</sub> loading | -    | yes          | yes     | yes     | yes     | yes     | yes     | yes     | yes        | yes           | yes             |
| <b>T=3weeks</b>         |      |              |         |         |         |         |         |         |            |               |                 |
| MEA                     | mol  | 0.28         | 0.28    | 0.29    | 0.24    | 0.27    | 0.24    | 0.23    | 0.27       | 0.29          | 0.28            |
| HEEDA                   | mol  | 4.7E-03      | 5.1E-03 | 5.6E-03 | 5.7E-03 | 6.4E-03 | 6.0E-03 | 6.0E-03 | 5.9E-03    | 5.3E-03       | 6.5E-03         |
| OZD                     | mol  | 8.0E-04      | 6.6E-04 | 8.2E-04 | 6.5E-04 | 1.0E-03 | 5.9E-04 | 5.3E-04 | 5.8E-04    | 7.0E-04       | 5.1E-04         |
| HEI                     | mol  | 0.0E+00      | 0.0E+00 | 0.0E+00 | 3.9E-04 | 0.0E+00 | 0.0E+00 | 1.7E-04 | 0.0E+00    | 1.9E-04       | 0.0E+00         |
| HEIA                    | mol  | 2.6E-02      | 2.2E-02 | 2.7E-02 | 3.1E-02 | 1.9E-02 | 2.2E-02 | 2.0E-02 | 1.9E-02    | 2.7E-02       | 1.6E-02         |
| HEPO                    | mol  | 0.0E+00      | 0.0E+00 | 0.0E+00 | 2.9E-04 | 2.0E-04 | 2.0E-04 | 2.4E-04 | 3.0E-04    | 1.9E-04       | 2.0E-04         |
| BHEOX                   | mol  | 0.0E+00      | 0.0E+00 | 0.0E+00 | 0.0E+00 | 0.0E+00 | 0.0E+00 | 0.0E+00 | 1.2E-08    | 0.0E+00       | 0.0E+00         |
| Fe                      | ppm  | 23.6         | 14.5    | 5.11    | 40.8    | 33.1    | 1020    | 39.3    | 7.90       | 45.0          | 47.8            |
| Cr                      | ppm  | 9.13         | 4.65    | 1.48    | 7.83    | 6.39    | 75.07   | 7.79    | 1.64       | 5.17          | 5.03            |
| Ni                      | ppm  | 6.7          | 3.03    | 0.65    | 6.2     | 5.91    | 96.9    | 6.82    | 1.19       | 4.59          | 7.02            |
| Mn                      | ppm  | 0.9          | 0.5     | 0.25    | 1.17    | 0.87    | 13.4    | 1.09    | 0.27       | 1.67          | 2.42            |

## List of publications

### Publications

Léonard G., Toye D., Heyen G., 2013. Optimal conception of a post-combustion CO<sub>2</sub> capture unit with assessment of solvent degradation, to be submitted for publication in International Journal for Greenhouse Gas Control.

Léonard G., Mogador Cabeza B., Belletante S., Toye D., Heyen G., 2013. Modeling amine solvent degradation for post-combustion CO<sub>2</sub> capture. *Récents Progrès en Génie des Procédés*, 103.

Léonard G., Mogador Cabeza B., Belletante S., Heyen G., 2013. Dynamic modeling and control of a pilot plant for post-combustion capture. *Computer Aided Chemical Engineering* 32, 451-456.

Léonard G., Heyen G., 2011. Optimization of the CO<sub>2</sub> capture process in amine solvents. *Récents Progrès en Génie des Procédés* 101.

Leonard G., Heyen G., 2011. Modeling post-combustion CO<sub>2</sub> capture with amine solvents. *Computer Aided Chemical Engineering* 29, 1768-1772.

### Oral presentations

Léonard G., Mogador Cabeza B., Belletante S., Toye D., Heyen G., 2013. Modeling amine solvent degradation for post-combustion CO<sub>2</sub> capture. Oral presentation at the 14<sup>th</sup> congress of the French Society for Process Engineering (SFGP), Lyon, France.

Léonard G., Toye D., Heyen G., 2012. Study of 2-ethanolamine degradation. Oral presentation at the "First University of Texas conference on CO<sub>2</sub> capture and storage", Austin, USA.

Léonard G., Heyen G., 2011. Optimisation du procédé de captage de CO<sub>2</sub> dans des solvants aminés. Oral presentation at the "XIIIème Congrès de la Société Française de Génie des Procédés", Lille, France.

Léonard G., Heyen G., 2010. Modeling post-combustion CO<sub>2</sub> capture with amine solvents. Oral presentation at the "Computer Aided Process Engineering Forum", Aachen, Germany.

### Poster presentations

Léonard G., Toye D., Heyen G., 2013. Optimal conception of a CO<sub>2</sub> capture unit with assessment of solvent degradation. Poster presented at the 2<sup>nd</sup> Post-Combustion Capture Conference, Bergen, Norway.

Léonard G., Mogador Cabeza B., Belletante S., Heyen G., 2013. Dynamic modeling and control of a pilot plant for post-combustion capture. Poster presentation at the 23<sup>rd</sup> European Symposium on Computer Aided Process Engineering, Lappeenranta, Finland.

Leonard G., Lepaumier H., Thielens M.-L., Toye D., Heyen G., 2012. CO<sub>2</sub> capture in power plants: process simulation and solvent degradation. Poster presentation at a Ph.D. meeting, Louvain-la-Neuve, Belgium.

Leonard G., Lepaumier H., Blandina F., Thielens M.-L., Toye D., Heyen G., 2012. Post-combustion CO<sub>2</sub> capture: global process simulation and solvent degradation. Poster presentation at a Ph.D. meeting, Gembloux, Belgium. *3<sup>rd</sup> Best Poster Award*.

Leonard G. and Heyen G., 2011. Modeling post-combustion CO<sub>2</sub> capture with amine solvents. Poster presentation at the 21<sup>st</sup> European Symposium on Computer Aided Process Engineering, Chalkidiki, Greece.

Léonard G. and Heyen G., 2010. Modeling post-combustion CO<sub>2</sub> capture with amine solvents. Poster presentation at the Computer Aided Process Engineering Forum, Aachen, Germany.

